Water binding and water release by plant-based meat analogues

Steven H.V. Cornet

Propositions

1. The effect of bath pH and ionic strength on the water holding capacity of meat analogues can be captured entirely by the 'intra-gellular' pH.
   (this thesis)

2. The development of better meat analogues cannot do without mechanistic modeling.
   (this thesis)

3. By embracing the variability and instability of food ingredients, the relevance of research findings can be improved.

4. In applied fields of study, the intimate interaction between universities and companies ensures the fast adoption of novel technologies.

5. Widespread adoption of meat analogues requires what Tesla is for the electric car industry: a cool and flashy product that outperforms the original.

6. Working from home for long periods of time is a threat to mental well-being.

Propositions belonging to the thesis, entitled

Water binding and water release by plant-based meat analogues

Steven H. V. Cornet
Wageningen, 26 March 2021

Water binding and water release by plant-based meat analogues

Steven H.V. Cornet

Thesis committee

Promotors
Prof. Dr Atze Jan van der Goot
Personal chair at the Laboratory of Food Process Engineering
Wageningen University & Research

Prof. Dr Ruud G. M. van der Sman
Special Professor at the Laboratory of Food Process Engineering
Wageningen University & Research

Other members
Prof. Dr Erik van der Linden, Wageningen University & Research
Prof. Dr John van Duynhoven, Unilever, Wageningen
Prof. Dr Jacques M. Huyghe, University of Limerick, Limerick, Ireland
Dr Lieke van Riemsdijk, Fromageries Bel, Schoonrewoerd

Water binding and water release by plant-based meat analogues

Steven H.V. Cornet

Summary

The sustainability of the human diet could be improved by lowering meat consumption and offering consumers plant-based meat substitutes as an alternative. Consumers are thought to prefer meat substitutes with a high similarity to real meat. Therefore, meat *analogues* that accurately mimic the different textural properties of real meat are being developed. Recent advancements in high-moisture extrusion cooking and shear cell processing have enabled the production of fibrous, meat-like products from plant-based ingredients. This has resulted in a wider research scope, which includes other textural properties such as the juiciness. For meat, the juiciness is associated with the water holding capacity (WHC). We have aimed to better understand the uptake, distribution, and release of water of meat analogues. Since these properties relate to the water holding capacity (WHC), this work could help the development of juicier meat analogues.

Meat analogues were simplified to gels consisting of two protein phases, such as soy protein isolate (SPI) and gluten. In **Chapter 2** we studied the WHC of two-phase gels with different ratio's between SPI and gluten. The WHC of single-phase SPI gels as a function of applied pressure could be described adequately with Flory–Rehner theory. The WHC of gluten gels was very low and could not be described with Flory–Rehner theory as the WHC did not depend on the applied pressure. Therefore, the WHC of gluten was approximated as a constant when describing the WHC of the two-phase gels. The WHC of SPI gels was found to depend on the polymer content at gelation. This was accounted for by determining the water partitioning before gelation using Flory–Rehner theory. The WHC of SPI in the two-phase gels decreased as gluten content increased. This was explained as the result of a mechanical interaction by which the continuous gluten network lowers the WHC of the entrapped SPI phase. In **Chapter 3** the effect of gluten on the WHC was further studied using protein

isolates from soy, pea and fababean (SPI, PPI, FPI resp.). Gels made from these protein isolates differed in terms of WHC, with SPI having the highest WHC and FPI the lowest. When combined with gluten, the relative reduction in WHC as a function of gluten content was the same for all three proteins. This suggested that the interaction between gluten and leguminous proteins is universal. A reduction in WHC with increasing gluten content was also observed after thermo-mechanical processing in a shear cell, albeit to a lesser degree. Visual inspection of the structures obtained after thermo-mechanical processing indicated that gluten should contribute $\geq 50\%$ to the total protein content to obtain fibrous structures. Since fibres were also obtained after processing hydrated gluten, we hypothesized that gluten is primarily responsible for fibre formation. The second protein might merely act as a filler and could be easily replaced. The WHC experiments suggested that a continuous gluten network could form already at low gluten contents. Since no fibres were observed at low gluten contents it was suggested that the fraction of gluten should be high enough for them to be observed as fibres.

In **Chapter 4** we studied whether the WHC of meat analogues could be controlled during post-processing by varying the pH and ionic strength of the marinade, or by altering the cross-link density. Our experiments showed that the WHC can be increased by lowering the ionic strength or increasing the pH of the marinade. Lowering the cross-link density also led to an increase of the WHC. Similar results were obtained from qualitative simulations using a model based on Flory–Rehner and an extension to account for charge effects. The simulations showed that the difference between the iso-electric point (pI) and the internal pH of the meat analogue strongly affects the WHC. At low ionic strengths, the meat analogue's internal pH can deviate from the pH of the marinade due to the buffering effect of proteins and the requirement of electro-neutrality inside and outside the protein network. The results showed that marinade pH and ionic strength offer control over the WHC and that low-salt marinades might improve juiciness.

The release of water during mastication is considered essential to the perception of juiciness. In **Chapter 5** we developed a confined compression cell to measure the dynamics of juice release for SPI gels and meat analogues. The release rates for SPI gels were in good agreement with model simulations based on Flory–Rehner theory and Darcy's law. The release rates for meat analogues were greatly underestimated by the model, especially for low applied pressures. Time domain nuclear magnetic resonance (TD-NMR) results indicated the presence of water–filled cavities within the meat analogue. This water was expelled at a lower pressure than the water

inside the protein matrix. The water-filled cavities can provide a path of low resistance, which explains the higher measured water release rates. The porous structure of meat analogues, therefore, appears to be important for their water release properties. Control over the porous structure of meat analogues could, therefore, offer an additional tool to control the juiciness.

Since the WHC of meat analogues is related to their structure, control over the WHC, and presumably the juiciness, will require a good understanding of their production process. Meat analogues are most commonly produced through thermo-mechanical processing with high moisture extrusion cooking (HMEC) or with a shear cell. In **Chapter 6** we reviewed these two processes by describing the physicochemical changes induced during the different processing steps. The processes consist of the same three steps: mixing and hydration, thermo-mechanical treatment, and cooling. Knowledge gaps were identified concerning the effect of thermo-mechanical treatment on protein–protein interactions and the formation of the fibrous structure. Filling these gaps will require more experimentation at process conditions and could improve control of the process and product. The use of food and non-food model systems could support this by allowing for more controlled experimentation.

In **Chapter 7** we reflect on our findings in a broader context. The different underlying assumptions of Flory–Rehner theory are discussed. Most assumptions are considered plausible for protein-based meat analogues, although the physical meaning of the model parameters might be limited. The use of physical models is expected to contribute to the development of better meat analogues in the future. Some suggestions are made on how to produce a juicy meat analogue under the assumption that the juiciness largely depends on the WHC. Although the relation between the WHC and the sensory juiciness is yet to be confirmed, we propose that juiciness could be considered a structure–function relationship. The juiciness is a complex sensory attribute with several contributing factors. Since we have only focused on the WHC, future research should explore the relative importance of the WHC as well as the other contributing factors, such as flavour, texture and salivating action. Given the interconnectedness of the different factors and the possibility of cross-modal perception, a high level of control over the product properties will be required. The level of control will largely depend on the level to which we understand the relations between ingredient properties, process parameters, and product properties.

Contents

Chapter 1

Introduction

1.1   Meat analogues as part of a sustainable diet

Global meat production is projected to increase by approximately 12 % over the next decade [1] despite the negative effect of meat production on the environment [2, 3]. The conversion of plant protein into animal protein can be considered inefficient [4], even when accounting for the use of co-products [5]. The production of plant protein generally requires less land and water and results in lower emissions than meat production [3, 4, 6–8]. Hence, the transition towards a diet rich in plant protein is considered inevitable when improving the sustainability of the human diet [6, 9]. A strategy towards achieving this goal is based on offering consumers sustainable plant-based meat substitutes [8]. However, consumer awareness of the negative environmental impact of meat production remains low [10]. Moreover, the environmental impact of plant-based meat substitutes was found to have only a minor effect on the purchase intent of omnivorous[*] and flexitarian[†] consumers [11]. By understanding the factors that determine food choices, more appealing sustainable products could be developed.

For plant-based meat substitutes, product price and taste are thought to be the factors most likely to encourage a purchase [11]. Similarly, the main drivers for omnivorous consumers to eat meat are related to habit and taste [12]. This contrasts with the main drivers for consumers to adopt a vegetarian diet[‡], which include perceived health benefits and animal welfare [13, 14]. Omnivorous consumers do expect to benefit from adopting a (semi-)vegetarian diet [15], but anticipate this diet to be inconvenient, expensive and not enjoyable [12, 15]. Repeated exposure to meat substitute products was shown to improve product liking among non-vegetarian consumers [16]. Hoek et al. [16] suggested that the willingness to try and repeatedly consume a product requires a positive first experience, underlining the need for enjoyable products. Aiking et al. [6] suggested that targeting omnivorous consumers is the most effective path towards mitigating the environmental impact of the human diet. Omnivorous consumers would prefer a meat substitute that closely resembles real meat in terms of taste, texture, smell, and appearance [17]. A meat *analogue* would, therefore, be most likely to persuade the omnivorous consumer to transition towards a more plant-based diet. It is to this end that food scientists can contribute by developing plant-based meat analogues that accurately mimic the properties of real meat. These properties include the fibrous structure, flavour and juicy mouthfeel of meat.

---

[*]Omnivore: a person whose diet includes both animal and vegetable substances
[†]Flexitarian: a person whose normally meatless diet occasionally includes meat or fish
[‡]Vegetarian: a person whose diet does not include meat

1.2   Development of fibrous structures

The food science community appears to have embraced the challenge of mimicking real meat with plant proteins by focusing primarily on replicating the fibrous structure of meat [18–21]. The first fibrous meat-like products were produced already in the 1970s using low-moisture extrusion cooking [22]. Extrusion still is the most commonly used technique for the production of meat analogues in industry today in the form of high moisture extrusion cooking. Despite the widespread use of extrusion cooking, the mechanisms governing the transformation of food ingredients into fibrous structures are still poorly understood [23, 24]. The high temperatures and pressures combined with the different flow patterns inside an extruder make it a challenge to accurately measure material properties during processing. The complex composition and behaviour of food materials further add to the challenge.

Compared to extrusion, shear cell technology offers a simpler way of structuring dense protein dispersions by making use of well-defined flow [23]. Shearing devices allow for the shear rate to be controlled independently from the throughput, which offers an advantage over extrusion cooking. Shearing devices were initially used to study food materials under flow [25–29] and were later identified as a method to create fibrous structures in their own right [30]. Since then, shearing devices have been used to create fibrous structures from various plant-based food polymers [20, 21, 31, 32]. All formulations that yielded fibrous textures consisted of at least two immiscible phases. Furthermore, the formation of a fibrous structure often coincided with the presence of an internal air phase, which can be deformed parallel to the shear-flow direction [21, 31, 33, 34]. Recent studies using shearing devices suggested that the phase behaviour of polymer mixtures is important for producing fibrous structures [33, 35, 36]. Since fibrous structures can be made from different combinations of proteins with different properties, the fibrous structure might be independent of the molecular composition and show some universality [37].

The advancements in shear cell processing show that meat analogues that accurately mimic the fibrous structure of real meat are within reach. Up-scaling efforts have already resulted in an increased production capacity by changing from a conical to a concentric cylinder or *Couette* design [38]. With fibrousness now under control, other important attributes come into view that could be improved, such as flavour [39] and juiciness.

1.3   Juiciness of meat and meat analogues

Juiciness is an important part of the sensory appeal of real meat [40] and should, therefore, be captured in a meat analogue [17]. However, unlike fibrousness, the juiciness of meat analogues has received little attention from the scientific community. The juiciness of real meat has been studied extensively [41–47] and could provide some guidance for our studies on the juiciness of meat analogues. Juiciness is a complex sensory attribute as there are several contributions to the overall sensation. This sensation is affected by intrinsic product properties, such as the release of meat juices and fat, and the presence of flavour compounds and ions. Extrinsic factors, such as salivation, also affect the perceived juiciness [48]. Furthermore, so-called cross-modal effects can alter the perceived juiciness through interactions between different sensory modalities. For example, a tender piece of meat could be perceived as juicier than a tough piece of meat [49]. Interestingly, high tenderness does not always improve the sensation of juiciness [50]. Given the different intrinsic, extrinsic, and cross-modal contributions to the sensation of juiciness, there is no single method available to accurately quantify a product's juiciness objectively. Instead, one can measure different product properties that are associated with juiciness.

The water holding capacity (WHC) is considered very important to the juiciness of meat [45, 47, 51]. Some investigators found positive correlations between the juiciness and the WHC or quality parameters associated with the WHC [48, 52, 53]. However, it must be noted that this relation is not always evident and can be obscured by variations in other sensory attributes [51]. The WHC can be measured by subjecting a sample to an external pressure for a period of time and determining the resulting change in composition. The pressure can be applied through gravity and can be increased by using weights or through centrifugation [41, 52, 54]. By subjecting a sample to a range of external pressures additional information on the WHC can be obtained. In this thesis, the term WHC is used to refer to the moisture content, or equivalently the polymer content, at a defined external pressure.

The sensation of juiciness is also associated with other properties of meat. Aaslyng et al. [48] suggested that the juiciness could be affected by the distribution of water in meat. The water distribution in meat has been studied extensively with time domain nuclear magnetic resonance (TD-NMR). TD-NMR can be used to differentiate between water populations based on their relaxation time, which is a measure for water mobility [55]. Bertram et al. [56] used TD-NMR to show that raw pig meat has three water populations. These populations were associated with either the

protein, the water inside the myofibrils, or water between the myofibrils; the latter population had the longest relaxation time. In a later study, Bertram et al. [57] showed that the cooking temperature affects the water mobility distribution, which they attributed to a change in the meat's structure. Furthermore, they concluded that the water mobility distribution correlates with sensory juiciness. Aaslyng et al. [48] suggested that cooking losses and the juiciness perceived during the first few chews both originate from the water between the myofibrils, while the sustained juiciness does not. The juice perceived during the different stages of chewing might, therefore, originate from different water populations.

The sensory properties of meat and meat analogue products can be enhanced through post-processing with a marinade [58, 59]. Marinades are solutions containing flavour compounds as well as ions and often have a specific pH. The pH can affect product properties as well as product stability. For example, marinades with a pH of around 4 are used to inhibit the growth of hazardous microbes [59]. Since proteins are polyampholytes, they can carry both positive and negative charges depending on the pH. The pH and ionic strength of the marinade will, therefore, affect the protein charge and probably also the WHC [60]. For chicken and beef, it was shown that the pH of the marinade affects the sensory juiciness [61, 62]. For beef, the increased juiciness was accompanied by an increase in WHC, which was attributed to the increased net charge on the meat proteins as the pH went below the iso-electric point at pH 5.1 [62]. The WHC of meat can also be improved by using marinades containing chloride ions. Chloride can disrupt the salt bridges that stabilize the myosin proteins in meat, which alters the meat's WHC [63]. Salt bridges are less important to the stability of plant protein gels [64], although the effect of salt and pH on the WHC of meat analogues remains to be investigated.

1.4 Theoretical tools to describe WHC and juiciness

While experimental observations provide a direct measure for a certain property, they often do not allow for direct identification of the mechanism responsible for the observation. Through analysis with a physical model, insight into the underlying mechanism can be obtained. Many food products can be approximated as cross-linked polymer networks. Hence we assume that their WHC can be described with the Flory–Rehner theory of swelling polymer networks [65]. Flory–Rehner theory states that at swelling equilibrium the externally applied pressure, Π_{ext}, is balanced by the

so-called swelling pressure, Π_{swell}:

$$\Pi_{ext} = \Pi_{swell} = \Pi_{mix} - \Pi_{elas} \tag{1.1}$$

The swelling pressure is a summation of the osmotic pressure, Π_{mix}, generated by the swelling polymers, and the elastic pressure, Π_{elas}, generated upon network deformation. Both Π_{mix} and Π_{elas} depend on the moisture content of the polymer network.

Van der Sman et al. used Flory–Rehner theory to simulate the WHC of meat and the migration of water in meat during cooking [42, 66, 67]. The change in WHC during cooking could be simulated well by taking into account the effect of heat-induced protein denaturation on the polymer–water affinity [67]. Meat can have internal channels commonly known as drip channels. These channels could facilitate moisture transport, but cannot be described with Flory–Rehner theory [67]. Flory–Rehner theory has also been used to describe the WHC of several plant-based foods, such as mushrooms [68, 69], broccoli [70], and carrots [69].

Given the different contributions to the sensation of juiciness, a combination of methods should be employed to improve our understanding and control of the juiciness of meat analogues. Therefore, the aim of this thesis is to develop a set of tools to better understand and control the uptake, distribution, and release of water by meat analogues composed of two protein phases. Tools from thermodynamics and soft matter will be employed to improve our understanding of the transformation of plant proteins into tasty, fibrous and juicy meat analogue products. An additional goal is to determine whether these tools can be applied to plant proteins in general. Earlier studies have demonstrated the ability of Flory–Rehner theory to describe the WHC of meat and several plant-based foods. Flory–Rehner theory might, therefore, also provide insight into the WHC of meat analogue products. The relatively complex structure of meat analogues poses several scientific challenges when applying Flory–Rehner theory. Flory–Rehner theory applies to homogeneous polymer networks, while meat analogues consist of multiple phases with different compositions and properties [20, 32, 36]. Furthermore, Flory–Rehner theory considers neutral polymers, while proteins can carry a charge depending on the pH. Since charge effects can contribute to the WHC, an extension to the Flory–Rehner theory will need to be used to account for these effects [60, 71, 72]. Meat analogues can also contain internal air cavities [21, 31, 33], which cannot be described with Flory–Rehner theory.

1.5   Thesis outline

Here we present an outline of the different chapters that make up this thesis. Our initial scope was limited to the WHC of meat analogue in relation to juiciness, but as the project progressed we learned that the WHC has much broader implications. In **Chapter 2**, Flory–Rehner theory was introduced as a tool to describe the WHC of simplified meat analogues. Meat analogues most often contain two or more protein phases; here soy protein isolate (SPI) and gluten were used. The individual components were analysed by measuring the WHC of single-phase gels. The two-phase gels were then analysed based on the behaviour of the single-phase gels. Interactions between the SPI and gluten phases were studied by comparing the WHC of the single-phase and two-phase gels. In **Chapter 3** we further explored the effect of gluten on the WHC of protein isolates from soy, pea, and fababean (resp. SPI, PPI, FPI). Flory–Rehner theory was used to analyse the effect of gluten on the WHC of non-gluten proteins. The effect of gluten content on the formation of fibrous structures was also investigated. Parallels were drawn between the effect of gluten on the WHC and the formation of fibrous structures. In **Chapter 4**, a combination of experiments and simulations was used to study the effect of cross-link density, pH and ionic strength on the WHC of meat analogues. An extension of the Flory–Rehner theory was used to account for the effect of charge on swelling. In **Chapter 5** we developed a confined compression cell to study the rate of water release from soy protein gels and meat analogues. A numerical model based on Flory–Rehner theory was developed to simulate water release. The relation between the meat analogue's porous structure and the water release rate was studied using TD-NMR. In **Chapter 6** we reviewed the production of fibrous structures with a shear cell and high-moisture extrusion cooking. The two processes were broken down into their basic processing steps and described based on the physicochemical changes they induce in the hydrated protein. The current knowledge gaps and opportunities for future research were identified. In **Chapter 7** we connect the contents of **Chapters 2–6** through a general discussion. The underlying assumptions of Flory–Rehner theory are critically discussed in the context of protein-based meat analogues, and some suggestions for future research are made. Recommendations are made on applying the tools presented in this thesis for the production of juicier meat analogues.

References

[1] OECD/FAO. OECD-FAO Agricultural Outlook 2020-2029. Technical report, Rome/OECD Publishing, Paris, 2020.

[2] B. Notarnicola, G. Tassielli, P. Renzulli, V. Castellani, and S. Sala. Environmental impacts of food consumption in Europe. *Journal of Cleaner Production*, 140:753–765, 2017.

[3] H. Aiking. Future protein supply. *Trends in Food Science and Technology*, 22(2):112–120, 2011.

[4] D. Pimentel and M. Pimentel. Sustainability of meat-based and plant-based diets and the environment. *American Journal of Clinical Nutrition*, 78(3 SUPPL.), 2003.

[5] S. Wiedemann and M. Yan. Livestock meat processing : inventory data and methods for handling co-production for major livestock species and meat products Processing inventory data. In *Proceedings of the 9th International Conference LCA in the Agri-Food Sector*, 9, pages 1512–1520, 2014.

[6] H. Aiking, J. de Boer, and J. Vereijken, editors. *Sustainable Protein Production and Consumption: Pigs or Peas?*, volume 45. Springer, Dordrecht, 2006.

[7] P. Alexander, C. Brown, A. Arneth, C. Dias, J. Finnigan, D. Moran, and M. Rounsevell. Could consumption of insects, cultured meat or imitation meat reduce global agricultural land use? *Global Food Security*, 15:22–32, 2017.

[8] S. Smetana, A. Mathys, A. Knoch, and V. Heinz. Meat Alternatives – Life Cycle Assessment of Most Known Meat Substitutes. *The International Journal of Life Cycle Assessment*, 2050: 1254–1267, 2015.

[9] D. Leclère, M. Obersteiner, M. Barrett, and E. Al. Bending the curve of terrestrial biodiversity needs an integrated strategy. *Nature*, 2018(October 2018), 2020.

[10] C. Hartmann and M. Siegrist. Consumer perception and behaviour regarding sustainable protein consumption: A systematic review. *Trends in Food Science and Technology*, 61:11–25, 2017.

[11] J. Parry and R. Mitchell. Assessing the general population's implicit perceptions of the plant-based food category. Technical Report July, Good Food Institute, Washington D.C., 2019.

[12] A. Mullee, L. Vermeire, B. Vanaelst, P. Mullie, P. Deriemaeker, T. Leenaert, S. De Henauw, A. Dunne, M. Gunter, P. Clarys, and I. Huybrechts. Vegetarianism and meat consumption: A comparison of attitudes and beliefs between vegetarian, semi-vegetarian, and omnivorous subjects in Belgium. *Appetite*, 114:299–305, 2017.

[13] N. Fox and K. Ward. Health, ethics and environment: A qualitative study of vegetarian motivations. *Appetite*, 50(2-3):422–429, 2008.

[14] A. Hoek, P. Luning, A. Stafleu, and C. De Graaf. Food-related lifestyle and health attitudes of Dutch vegetarians, non-vegetarian consumers of meat substitutes, and meat consumers. *Appetite*, 42(3):265–272, 2004.

[15] C. Bryant. We can't keep meating like this: Attitudes towards vegetarian and vegan diets in the United Kingdom. *Sustainability (Switzerland)*, 11(23):1–17, 2019.

[16] A. Hoek, J. Elzerman, R. Hageman, F. Kok, P. Luning, and C. de Graaf. Are meat substitutes liked better over time? A repeated in-home use test with meat substitutes or meat in meals.

Food Quality and Preference, 28(1):253–263, 2013.

[17] A.C. Hoek, P.A. Luning, P. Weijzen, W. Engels, F.J. Kok, and C. de Graaf. Replacement of meat by meat substitutes. A survey on person- and product-related factors in consumer acceptance. *Appetite*, 56(3):662–673, jun 2011.

[18] J. Cheftel, M. Kitagawa, and C. Queguiner. New Protein Texturization Processes by Extrusion Cooking at High Moisture Levels. *Food Reviews International*, 8(2):235–275, 1992.

[19] J.H. Chiang, S.M. Loveday, A.K. Hardacre, and M.E. Parker. Effects of soy protein to wheat gluten ratio on the physicochemical properties of extruded meat analogues. *Food Structure*, 19 (September 2018):100102, 2019.

[20] B.L. Dekkers, C.V. Nikiforidis, and A.J. van der Goot. Shear-induced fibrous structure formation from a pectin/SPI blend. *Innovative Food Science and Emerging Technologies*, 36:193–200, aug 2016.

[21] F.K.G. Schreuders, B.L. Dekkers, I. Bodnár, P. Erni, R.M. Boom, and A.J. van der Goot. Comparing structuring potential of pea and soy protein with gluten for meat analogue preparation. *Journal of Food Engineering*, 261(May):32–39, 2019.

[22] G. Puski and A.H. Konwinski. Process of making a soy-based meat substitute, 1976.

[23] J.M. Manski, A.J. van der Goot, and R.M. Boom. Advances in structure formation of anisotropic protein-rich foods through novel processing concepts. *Trends in Food Science and Technology*, 18(11):546–557, 2007.

[24] J.L. Sandoval Murillo, R. Osen, S. Hiermaier, and G. Ganzenmüller. Towards understanding the mechanism of fibrous texture formation during high-moisture extrusion of meat substitutes. *Journal of Food Engineering*, 242(November 2019):8–20, 2019.

[25] R.M. Van Den Einde, A.J. Van Der Goot, and R.M. Boom. Understanding Molecular Weight Reduction of Starch during Heating-shearing Processes. *Journal of Food Science*, 68(8): 2396–2404, 2003.

[26] S.H. Peighambardoust, A.J. van der Goot, R.J. Hamer, and R.M. Boom. A New Method to Study Simple Shear Processing of Wheat Gluten-Starch Mixtures. *Cereal Chemistry*, 81(6):714, 2004.

[27] S.H. Peighambardoust, A.J. Van Der Goot, T. Van Vliet, R.J. Hamer, and R.M. Boom. Microstructure formation and rheological behaviour of dough under simple shear flow. *Journal of Cereal Science*, 43(2):183–197, 2006.

[28] S.H. Peighambardoust, R.J. Hamer, R.M. Boom, and A.J. van der Goot. Migration of gluten under shear flow as a novel mechanism for separating wheat flour into gluten and starch. *Journal of Cereal Science*, 48(2):327–338, 2008.

[29] E. Habeych, B. Dekkers, A.J. van der Goot, and R. Boom. Starch-zein blends formed by shear flow. *Chemical Engineering Science*, 63(21):5229–5238, 2008.

[30] J.M. Manski, A.J. van der Goot, and R.M. Boom. Formation of fibrous materials from dense calcium caseinate dispersions. *Biomacromolecules*, 8(4):1271–1279, 2007.

[31] K.J. Grabowska, S. Tekidou, R.M. Boom, and A.J. van der Goot. Shear structuring as a new method to make anisotropic structures from soy-gluten blends. *Food Research International*, 64:743–751, 2014.

[32] K.J. Grabowska, S. Zhu, B.L. Dekkers, N.C.A. De Ruijter, J. Gieteling, and A.J. van der Goot. Shear-induced structuring as a tool to make anisotropic materials using soy protein concentrate. *Journal of Food Engineering*, 188:77–86, 2016.

[33] B.L. Dekkers, R. Hamoen, R.M. Boom, and A.J. van der Goot. Understanding fiber formation in a concentrated soy protein isolate - Pectin blend. *Journal of Food Engineering*, 222:84–92, 2018.

[34] B. Tian, Z. Wang, A.J. van der Goot, and W.G. Bouwman. Air bubbles in fibrous caseinate gels investigated by neutron refraction, X-ray tomography and refractive microscope. *Food Hydrocolloids*, 83:287–295, 2018.

[35] B.L. Dekkers, D.W. de Kort, K.J. Grabowska, B. Tian, H. Van As, and A.J. van der Goot. A combined rheology and time domain NMR approach for determining water distributions in protein blends. *Food Hydrocolloids*, 60:525–532, 2016.

[36] F. Schreuders, I. Bodnár, P. Erni, R. Boom, and A. van der Goot. Water redistribution determined by time domain NMR explains rheological properties of dense fibrous protein blends at high temperature. *Food Hydrocolloids*, 101, 2020.

[37] R.G.M. van der Sman and A.J. van der Goot. The science of food structuring. *Soft Matter*, pages 1147–1150, 2008.

[38] G.A. Krintiras, J. Gadea Diaz, A.J. Van Der Goot, A.I. Stankiewicz, and G.D. Stefanidis. On the use of the Couette Cell technology for large scale production of textured soy-based meat replacers. *Journal of Food Engineering*, 169:205–213, 2016.

[39] Z. Guo, F. Teng, Z. Huang, B. Lv, X. Lv, O. Babich, W. Yu, Y. Li, Z. Wang, and L. Jiang. Effects of material characteristics on the structural characteristics and flavor substances retention of meat analogs. *Food Hydrocolloids*, 105(February), 2020.

[40] R. Miller. The Eating Quality of Meat: V-Sensory Evaluation of Meat. In F. Toldra, editor, *Lawrie's Meat Science*, chapter 15, pages 461–499. Elsevier Ltd, eighth edition, 2017.

[41] K. Honikel. Reference methods for the assessment of physical characteristics of meat. *Meat Science*, 49(4):447–457, 1998.

[42] R.G.M. van der Sman. Moisture transport during cooking of meat: An analysis based on Flory-Rehner theory. *Meat Science*, 76(4):730–738, 2007.

[43] H. Bertram, I. Straadt, J. Jensen, and M. Aaslyng. Relationship between water mobility and distribution and sensory attributes in pork slaughtered at an age between 90 and 180 days. *Meat Science*, 77(2):190–195, 2007.

[44] E. Puolanne and M. Halonen. Theoretical aspects of water-holding in meat. *Meat Science*, 86 (1):151–165, 2010.

[45] K.L. Pearce, K. Rosenvold, H.J. Andersen, and D.L. Hopkins. Water distribution and mobility in meat during the conversion of muscle to meat and ageing and the impacts on fresh meat quality attributes - A review. *Meat Science*, 89(2):111–124, 2011.

[46] E. Puolanne and J. Peltonen. The effects of high salt and low pH on the water-holding of meat. *Meat Science*, 93(2):167–170, 2013.

[47] R.D. Warner. Chapter 14 – The Eating Quality of Meat—IV Water-Holding Capacity and Juiciness. In F. Toldra, editor, *Lawrie´s Meat Science*, pages 419–459. Woodhead Publishing Limited, eighth edition, 2017. ISBN 9780081006948.

[48] M.D. Aaslyng, C. Bejerholm, P. Ertbjerg, H.C. Bertram, and H.J. Andersen. Cooking loss and juiciness of pork in relation to raw meat quality and cooking procedure. *Food Quality and Preference*, 14(4):277–288, 2003.

[49] E. Huff-Lonergan, T.J. Baas, M. Malek, J.C. Dekkers, K. Prusa, and M.F. Rothschild. Correlations among selected pork quality traits. *Journal of Animal Science*, 80(3):617–627, 2002.

[50] S. Cover, J. Ritchey, and R.L. Hostetler. Tenderness of Beef. II. Juiciness and the Softness Components of Tenderness. *Journal of Food Science*, 27(5):476–482, 1962.

[51] A. Pearson and Dutson, editors. *Quality attributes and their measurement in meat, poultry and fish*. Springer Science+Business Media, Dordrecht, 1 edition, 1994.

[52] M.J. Van Oeckel, N. Warnants, and C.V. Boucqué. Comparison of different methods for measuring water holding capacity and juiciness of pork versus on-line screening methods. *Meat Science*, 51(4):313–320, 1999.

[53] L.W. Lucherk, T.G. O'Quinn, J.F. Legako, R.J. Rathmann, J.C. Brooks, and M.F. Miller. Assessment of objective measures of beef steak juiciness and their relationships to sensory panel juiciness ratings. *Journal of Animal Science*, 95(6):2421–2437, 2017.

[54] P.N. Kocher and E.A. Foegeding. Microcentrifuge-Based Method for Measuring Water-Holding of Protein Gels. *Journal of Food Science*, 58(5):1040–1046, 1993.

[55] F. Mariette. Investigations of food colloids by NMR and MRI. *Current Opinion in Colloid and Interface Science*, 14(3):203–211, 2009.

[56] H. Bertram, P. Purslow, and H. Andersen. Relationship between meat structure, water mobility, and distribution: A low-field nuclear magnetic resonance study. *Journal of Agricultural and Food Chemistry*, 50(4):824–829, 2002.

[57] H.C. Bertram, M.D. Aaslyng, and H.J. Andersen. Elucidation of the relationship between cooking temperature, water distribution and sensory attributes of pork - A combined NMR and sensory study. *Meat Science*, 70(1):75–81, 2005.

[58] I. Gómez, F. Ibañez, and M. Beriain. Physicochemical and sensory properties of sous vide meat and meat analog products marinated and cooked at different temperature-time combinations. *International Journal of Food Properties*, 22(1):1693–1708, 2019.

[59] C. Alvarado and S. Mckee. Marination to Improve Functional Properties. *Journal of Applied Poultry Research*, 16(1):113–120, 2007.

[60] A.E. English, S. Mafé, J.A. Manzanares, X. Yu, A.Y. Grosberg, and T. Tanaka. Equilibrium swelling properties of polyamapholytic hydrogels. *Journal of Chemical Physics*, 104(21): 8713–8720, 1996.

[61] S.M. Yusop, M.G. O'Sullivan, J.F.P. Kerry, and J.F.P. Kerry. Effect of marinating time and low pH on marinade performance and sensory acceptability of poultry meat. *Meat Science*, 85 (4):657–663, 2010.

[62] R.M. Burke and F.J. Monahan. The tenderisation of shin beef using a citrus juice marinade. *Meat Science*, 63(2):161–168, 2003.

[63] E. Puolanne. Developments in our understanding of water-holding capacity. In P.P. Purslow, editor, *New Aspects of Meat Quality*, chapter 8, pages 77–113. Woodhead Publishing Limited, 2017.

[64] V.L. Pietsch, J.M. Bühler, H.P. Karbstein, and M.A. Emin. High moisture extrusion of soy protein concentrate: Influence of thermomechanical treatment on protein-protein interactions and rheological properties. *Journal of Food Engineering*, 251(August 2018):11–18, 2019.

[65] P.J. Flory and J. Rehner. Statistical Mechanics of Cross-Linked Polymer Networks II. Swelling. *The Journal of Chemical Physics*, 11(11):521–526, 1943.

[66] R.G.M. van der Sman. Thermodynamics of meat proteins. *Food Hydrocolloids*, 27(2):529–535, 2012.

[67] R.G.M. van der Sman. Modeling cooking of chicken meat in industrial tunnel ovens with the Flory-Rehner theory. *Meat Science*, 95(4):940–957, 2013.

[68] E. Paudel, R.M. Boom, and R.G.M. van der Sman. Change in Water-Holding Capacity in Mushroom with Temperature Analyzed by Flory-Rehner Theory. *Food and Bioprocess Technology*, 8(5):960–970, 2015.

[69] R. van der Sman, E. Paudel, A. Voda, and S. Khalloufi. Hydration properties of vegetable foods explained by Flory–Rehner theory. *Food Research International*, 54(1):804–811, nov 2013.

[70] X. Jin, R.G.M. van der Sman, J.F.C. van Maanen, H.C. van Deventer, G. van Straten, R.M. Boom, and A.J.B. van Boxtel. Moisture Sorption Isotherms of Broccoli Interpreted with the Flory-Huggins Free Volume Theory. *Food Biophysics*, 9(1):1–9, 2014.

[71] R.G.M. van der Sman, S. Houlder, S.H.V. Cornet, and A. Janssen. Physical chemistry of gastric digestion of proteins gels. *Current Research in Food Science*, 2:45–60, 2020.

[72] H. Li, L. Zhao, X.D. Chen, and R. Mercadé-Prieto. Swelling of whey and egg white protein hydrogels with stranded and particulate microstructures. *International Journal of Biological Macromolecules*, 83:152–159, 2016.

Chapter 2

Effect of mechanical interaction on the hydration of mixed soy protein and gluten gels

Abstract

Mixed gels of plant proteins are being investigated for use as meat analogues. Juiciness is an important characteristic for the acceptability of meat analogues. The juiciness is assumed to be governed by the hydration properties, or water holding capacity, of the gel (WHC). We analyse the WHC of single-phase gels of respectively soy protein and gluten by applying Flory–Rehner theory. This enabled us to describe the WHC of more the complex mixed gels. The WHC of mixed soy protein - gluten gels is shown not to be a linear combination of their constituents. At high volume fractions, soy forms a continuous network and swells similarly to pure soy without being hindered by gluten. However, increasing gluten content leads to a gradual decrease in soy swelling. This is due to the mechanical interaction between soy and gluten. We propose that gluten-rich gels have a continuous gluten network that entraps soy and hinders its swelling. The elastic moduli of the gluten network were extracted from WHC data, and are in reasonable agreement with experimentally determined moduli. A better understanding of the effect of mixed gel composition on WHC is valuable for the development of the next generation meat analogues.

2.1   Introduction

Technological advancements in high moisture extrusion and shear cell technology have enabled the production of fibrous structures from plant proteins [1–4]. These fibrous structures resemble the texture of muscle fibres but lack the juiciness found in real meat [5, 6]. The juiciness of meat is related to its water holding capacity (WHC) [7–10], and a similar relation is expected for meat analogues. The juice release from meat has a typical temporal profile. Some of the juice should be readily expelled, while the remainder should be more tightly bound to the matrix to prevent the sensation of dryness [11, 12]. Consumers demand a product similar to meat [13], and the lack of juiciness due to inadequate WHC and juice release profile is thus a hurdle for consumer acceptance.

Meat analogues are complex mixed gels, and often contain soy protein isolate (SPI), gluten, or a combination of both [1, 2, 14–16]. However, the physics governing the WHC of such mixed protein gels is still poorly understood. We apply the concept of Flory–Rehner theory in a phenomenological way to describe the WHC of single-phase and mixed gels as a function of pressure. We aim to improve our understanding of the WHC of such complex mixed systems.

It has been reported that water distributes unevenly between SPI and gluten [14, 17], which can be related to differences in polymer-water affinity and cross-link density between the two phases. The uneven distribution of water appears to be essential for obtaining a meat-like structure as the moisture content in the two phases affects their rheological properties [17]. Although the gluten network is known to be affected by the addition of soy in bread doughs [18], a recent study showed that heating mixtures of gluten proteins and soy glycinin, one of the main soy proteins, does not result in cross-linking between the different proteins [19]. This suggests that the two networks can coexist in mixed systems. Studying the mixed systems as well as the two phases separately could, therefore, provide valuable insights into the mixed system.

We investigate the WHC of mixed protein gels as a model system for meat analogues. To reduce the complexity of the system we first characterize the WHC of single-phase SPI and gluten gels before moving towards more complex mixed gels that could be regarded as a rudimentary meat analogue. As is the case for many foods, meat and meat analogues can be regarded as cross-linked polymer networks [20–24]. The WHC of polymer networks can be described using Flory–Rehner theory [21, 23–25], which describes the swelling of a cross-linked polymer network using two opposing contributions [26]. These contributions are the osmotic (mixing) pressure and the

elastic pressure due to network deformation. At equilibrium, the sum of these contributions is equal to the pressure exerted onto the network. As such, the theory can be used to describe the WHC (and thus moisture content) of a material as a function of the applied pressure.

Flory–Rehner theory has several underlying assumptions which might limit its application to (globular) protein gels. Globular proteins are innately non-linear given their secondary and tertiary structure, which for soy proteins persists after heating [27]. The assumption of linear Gaussian chains is therefore void. However, this does not mean the Flory–Rehner theorem is not applicable. The concept of a net swelling pressure as the result of opposing mixing and elastic pressures can still provide insight. In fact, Li et al. [28] showed that the swelling of fine-stranded (and predominantly globular) whey protein and egg white protein gels can be predicted with FR theory. Similarly, FR theory was used to describe the swelling of complex mixtures such as mushrooms [21]. The precise physical meaning of the different parameters may, however, be affected given that not all assumptions are met.

This paper is organized as follows. We study the WHC of single-phase SPI and gluten gels by applying an increasing load via centrifugation. Based on insights from the single-phase gels we describe the WHC of more complex mixed gels. By combining data from large strain compression experiments and data from the WHC experiments we hypothesize about the network structure of mixed SPI-gluten gels. We will briefly discuss the implications for the development of juicier meat analogues.

2.1.1 Flory–Rehner theory

The WHC of polymer gels is governed by their thermodynamics and can be analysed using Flory–Rehner theory [26, 29]. Flory–Rehner theory states that the amount of solvent retained by the polymer network depends on the external pressure, Π_{ext}. In our experiments, we will exert this pressure via centrifugation. Under equilibrium conditions the external pressure will be equal to the swelling pressure Π_{swell}:

$$\Pi_{ext} = \Pi_{swell} = \Pi_{mix} - \Pi_{elas} \tag{2.1}$$

The swelling pressure is composed of two independent contributions that account for the different interactions between water and polymer. These contributions are the mixing pressure, Π_{mix}, which accounts for the interaction between the polymer and the solvent, and the elastic pressure, Π_{elas}, which accounts for the elastic pressure exerted by the polymer network onto the solvent. Note that we assume the contribution of dissolved ions and polymer charges to the swelling pressure to be

constant, and of limited magnitude ($\Pi_{ion} = 0$). The theory assumes a homogeneous network of Gaussian chains that swells uniformly. van der Sman [30] showed that the behaviour of a range of bio-polymers can be captured with Flory–Rehner theory, and obey to the scaling laws from polymer physics.

The mixing pressure

Π_{mix} can be described with Flory–Huggins theory. We will use water sorption isotherms to estimate the governing parameter of the Flory–Huggins theory, namely the interaction parameter χ. However, as most bio-polymers undergo a glass transition during desorption, we will analyse the sorption isotherms with the Free Volume extension of Flory–Huggins theory, so-called FVFH theory, instead [31]. FVFH theory has already been successfully used to describe the water sorption of various food products such as vegetables [22], mushrooms [21], broccoli [20], meat [23], chicken [25], and various bio-polymer gels [30].

Note that FVFH theory includes an extra term, $F(\varphi)$, which is not found in the classical Flory–Huggins theory. $F(\varphi)$ is equal to zero above the glass transition temperature. Therefore, when describing WHC data, $F(\varphi)$ is equal to zero in our calculation of the mixing pressure. The mixing pressure is related to the water activity, a_w, and is taken as:

$$\frac{v_w \Pi_{mix}}{RT} = \ln(1 - \varphi) + \varphi(1 - \frac{1}{N}) + \chi \varphi^2 + F(\varphi) = \ln a_w \qquad (2.2)$$

where v_w is the molar volume of water, R is the universal gas constant, T is the absolute temperature, φ and $1 - \varphi$ are the volume fraction of polymer and water respectively, N is the ratio of the molar volume of water and polymer, and χ is the Flory–Huggins interaction parameter between water and polymer. Because of the relatively large size of a polymer, N becomes very large, allowing us to simplify the second term on the right hand side to φ. $F(\varphi)$ accounts for structural relaxation in the glassy state and the changes in hydrogen bonding between water and polymer in the semi-dilute regime [31, 32]. $F(\varphi)$ was calculated according to van der Sman et al. [22] as:

$$F(\varphi) = \begin{cases} 0 & \text{if } T \geq T_g \\ -M_w y_s^2 \frac{\Delta C_{p,w}}{RT} \frac{dT_g}{dy_s} \frac{T - T_g}{T_g} & \text{if } T \leq T_g \end{cases} \qquad (2.3)$$

with

$$\frac{dT_g}{dy_s} = -\frac{\Delta C_{p,s} \Delta C_{p,w}(T_{g,w} - T_{g,s})}{(y_w \Delta C_{p,w} + y_s \Delta C_{p,s})^2} \qquad (2.4)$$

T_g is calculated according to Couchman-Karasz [33]:

$$T_g = \frac{y_w \Delta C_{p,w} T_{g,w} + y_s \Delta C_{p,s} T_{g,s}}{y_w \Delta C_{p,w} + y_s \Delta C_{p,s}} \tag{2.5}$$

Here, M_w is the molar weight of water, $\Delta C_{p,i}$ is the change in heat capacity at the glass transition, and $T_{g,i}$ is the glass transition temperature in the dry state. y_i represents the weight fraction of polymer or water. We have used $\Delta C_{p,s} = 0.425$ kJ K^{-1}, which appears to be universal for bio-polymers [23, 32, 34].

As has been shown previously, the interaction parameter for bio-polymers and water is composition dependent and can be calculated as [32]:

$$\chi = \chi_0 + (\chi_1 - \chi_0)\,\varphi^2 \tag{2.6}$$

with χ_0 and χ_1 as the interaction parameters under dilute and concentrated conditions respectively. Water is a theta solvent for proteins at very low protein concentrations, and thus χ_0 is 0.5.

The elastic pressure

We take the elastic contribution to the swelling pressure as originally described in Flory–Rehner theory. It assumes a homogeneous polymer network that consists of linear Gaussian chains that swell isotropically. The *Young's* modulus E of such gel networks can be described with the power law reported by Horkay and Zrínyi [35] as function of φ_0, which is based on the c^* theorem [36]:

$$E = a\varphi_0^\beta \tag{2.7}$$

in which β is 9/4 and a is a constant [35]. Higher values of β have also been reported for certain bio-polymers ($\beta \approx 2.3 - 2.7$, [30]. φ_0 is the φ for which $\Pi_{mix} = \Pi_{elas}$ and thus describes maximum swelling at $\Pi_{ext} = 0$. For incompressible materials, E is related to the *Shear* modulus, G, via:

$$E = 3G \tag{2.8}$$

For the elastic contribution we use the affine network model [30]:

$$\Pi_{elas} = G_{ref}\left[\tilde{\varphi}^{1/3} - \frac{\tilde{\varphi}}{2}\right] \tag{2.9}$$

G_{ref} is the *Shear* modulus in the reference state. G_{ref} is related to G via:

$$G = G_{ref}\tilde{\varphi}^{1/3} \tag{2.10}$$

$\tilde{\varphi}$ is defined as:

$$\tilde{\varphi} = \frac{\varphi}{\varphi_{ref}} \tag{2.11}$$

with φ_{ref} as the φ at which the polymer network is in the relaxed state and the chains experience zero stress. It must be noted that the conditions at which the reference state is determined differ greatly between studies [37], and the physical meaning of φ_{ref} is still under debate [37, 38]. For synthetic polymers, φ_{ref} is often defined as the φ at cross-linking, which often occurs in the dry state (thus $\varphi_{ref} = 1$). When cross-linking takes place in the presence of a solvent, as is the case for bio-polymers, the reference state is often chosen in a similar fashion [39, 40]. Khokhlov [38] argues that φ_{ref} should be chosen at theta-conditions at which the individual chains are unperturbed. However, since we apply the affine network model [30], polymer-solvent and polymer-polymer interaction are omnipresent [40]. van der Sman [30] showed that for many bio-polymer gels it holds that $\varphi_{ref} = 1.5\varphi_0$. Because of the ambiguous nature of φ_{ref}, we will determine it by fitting our WHC data with Equation 2.9.

2.2 Materials and methods

We have prepared single-phase gels from soy protein isolate (SPI) and gluten via heat-induced gelation. By varying the polymer weight fraction at cross-linking, gels with different cross-link densities were obtained. Gels were washed and swollen in water before their WHC as a function of pressure was determined using the centrifugation method [21, 41]. The WHC data was fitted with Flory–Rehner theory to obtain G_{ref} and φ_{ref}. Water sorption isotherms and glass transition temperatures were measured for the different bio-polymers before and after gelation to obtain χ_1 using FVFH theory. Based on the WHC of the single-phase gels we analysed the WHC of more complex mixed gels with different SPI : gluten ratios.

2.2.1 Materials

Soy protein isolate (Supro 500E IP) and vital wheat gluten were obtained from Solae (DuPont, St Louis, MO, USA) and Roquette (Lestrem, France) respectively. Some compositional data is presented in Table 2.1. Salt content was determined based on the conductivity of a 5 wt% protein dispersion and is expressed in NaCl equivalents. Mili-Q water was used in all experiments.

Table 2.1: Compositional information of the protein powders used. Dry matter content (DMC) as determined by drying at 105°C for 24 h, protein content according to the Dumas combustion method with Nx5.7 (see e.g. Berghout et al. [42]) and salt content of the powders based on the conductivity of 5 wt% dispersions (as NaCl equivalents).

	DMC (wt%)	Protein content (Nx5.7, wt%), n=3	Salt content (expressed as wt% NaCl), n=3
SPI	93.7±0.2	81.7±1.1	1.33±.01
Gluten	93.4±0.5	77.9±0.1	0.39±.01

2.2.2 Gel preparation

Soy gels

SPI gels were prepared by dispersing SPI powder in water, followed by vigorous mixing to achieve a final dry matter content of between approximately 25 and 35 wt%. SPI dispersions had an ionic strength of between 0.08 and 0.12 m and were not adjusted. Dispersions of SPI and gluten were of neutral pH and were not adjusted. Actual dry matter content of the dispersions was determined by drying at 105°C for 24 h. The obtained dispersions were placed in vacuum bags and exposed to a vacuum of 50 mbar for 15 s to remove any air bubbles. The dispersions were stored overnight at 4°C to ensure an even hydration of the protein. The hydrated dispersions were placed in cylindrical stainless steel gelation vessels with a radius of 12.5 mm and a height of 5 mm. The hermetically sealed vessels were submerged for 30 min in a shaking water bath (Julabo, Seelbach, Germany) preheated to 95°C. The vessels were cooled by submersion in water of 10°C for 15 min. After cooling, the gels were gently removed from their vessels.

Gel washing and swelling

Gel swelling and the removal of solutes was carried out simultaneously by washing in Mili-Q water. Gels were submerged in an excess of Mili-Q water (1/100 wt/wt) immediately after gelation and stored at 4°C for 24 h. The water was exchanged 3 times during the first 8 h at regular intervals. This was sufficient to reach a stable sample weight and constant conductivity of the washing liquid. These signs were taken as confirmation that equilibrium had been reached.

The maximum level of swelling is defined as the polymer volume fraction at maximum swelling and referred to as φ_0. φ_0 was determined based on the dry matter content as

determined by drying the swollen gels at 105°C for 24 h. Polymer and water densities were assumed to be 1330 $kg\,m^{-3}$ and 1000 $kg\,m^{-3}$ respectively.

Gluten gels

Gluten gels were prepared similarly to SPI gels, with some alterations to the protocol. The gel-like structures obtained after heating hydrated gluten were not uniform in shape and thus not suitable for uniaxial compression testing or centrifugation (for WHC). The use of ethanol can greatly improve the ease of handling of gluten [43, 44]. Gluten gels were, therefore, prepared in anhydrous ethanol (Sigma Aldrich, Steinheim, Germany) to study their strength and WHC. By mixing gluten with ethanol a particle dispersion is obtained. Gluten dispersions were transferred to the aforementioned gelation vessels, omitting the evacuation and hydration steps. Gelation and the subsequent washing and swelling was carried out as per the protocol for SPI gels. Three water changes were assumed to be sufficient to wash out all ethanol and solutes present. The range in which we could reproducibly prepare gluten gels was narrow ($y_{p,gluten}^{I} = 0.575 - 0.64$) due to issues such as gluten sedimentation and drainage within the gelation vessel.

Mixed gels

Mixed gels were prepared by dispersing SPI in water and vigorous mixing, followed by gluten addition and further mixing. Mixed gels had an ionic strength between 0.09 and 0.04 molal. The mixtures were freed from air, hydrated, and gelled according to the protocol for SPI gels. The overnight hydration at 4°C was assumed to be sufficient to reach an equilibrium water distribution.

2.2.3 Water holding capacity by centrifugation

WHC was determined by centrifugation at different relative centrifugal forces to apply a range of pressures to the equilibrated gels, similar to Kocher and Foegeding [41], and Paudel et al. [21]. Samples were gently taken from pre-swollen gels using a biopsy punch with a diameter of 4 mm. The samples were placed in centrifugal filters with a pore size of 0.2 μm (Pall Centrifugal Devices). An Eppendorf centrifuge with a swinging bucket rotor was used to ensure the pressure was applied perpendicularly to the surface of the sample. A centrifugation time of 1 h was found to be sufficient to reach a constant gel weight. During centrifugation, the expelled fluid was collected in the bottom compartment of the tube without being in contact with the sample, and the amount of water released was determined by weighing. Assuming a linear

gradient in φ and Π_{ext}, the relative centrifugal force can be converted to an average pressure applied on the sample as:

$$\Pi_{ext} = \frac{1}{2}\overline{\rho}g_{actual}H \tag{2.12}$$

$\overline{\rho}$ is the mean density of the sample, g_{actual} is the relative centrifugal force at the sample location, and H is the sample height. Since the amount of polymer is assumed to remain constant during centrifugation, the change in sample height as a result of the moisture loss can be calculated as:

$$\varphi_0 H_0 = \overline{\varphi}H \tag{2.13}$$

φ_0 is the polymer volume fraction at maximum swelling, H_0 is the initial sample height, and $\overline{\varphi}$ is the average polymer volume fraction.

2.2.4 Linear compression tests

Elastic *Young's* moduli, E, were determined by uniaxial compression of the swollen gels using an Instron texture analyser equipped with a 100 N load cell similar to Renkema et al. [45]. In short, gels prepared and swollen according to the protocol in Section 2.2.2 were trimmed to a radius of 12.5 mm using a cork borer and placed on the plate of the texture analyser. Gels were compressed at a rate of 1 mm s^{-1}. True Hencky strain was calculated as:

$$\epsilon = \ln \frac{H(t)}{H_0} \tag{2.14}$$

in which ϵ is the Hencky strain and H_0 and $H(t)$ are the initial height and height after deforming for a certain time t. The stress on the gel σ is calculated as:

$$\sigma = \frac{F(t)}{A(t)} \tag{2.15}$$

in which $F(t)$ is the force recorded by the texture analyser and $A(t)$ the contact area of the gel after deforming for a certain time t. We assume a constant sample volume during deformation, which enables us to calculate the sample area during deformation as:

$$A(t) = \frac{H_0}{H(t)}A_0 \tag{2.16}$$

in which A_0 is the initial cross-sectional area of the gel. E was determined as the slope of σ versus ϵ in the linear regime.

2.2.5 Dynamic vapour sorption

Water vapour sorption isotherms can be used to determine the interaction parameter χ with FVFH theory. Isotherms were determined at 25°C on a ProUmid SPSX-S3-EU01508. Measurements started by drying for 24 h at 0 %RH, after which the RH was increased with 10 % increments up to 90 % RH, and lowered again to 0 % RH in 10 % increments. Equilibrium was assumed when the weight change over a window of 10 min was less than 0.0005 % min^{-1} for a period of 120 min. A maximum step duration of 2000 min was used. Isotherms were determined in duplicate.

2.2.6 Determination of T_g

The glass transition temperature T_g is required to accurately fit sorption isotherms with FVFH theory. Values of T_g were determined using a TA Instruments DSC 250 (modulated Differential Scanning Calorimetry, mDSC). Samples with different moisture contents were prepared by exposing them to water vapour for different lengths of time after which the DSC sample pans were sealed hermetically. The samples were allowed to equilibrate inside of the sample pan for at least 1 week before being analysed. During thermal analysis, samples were equilibrated at -20°C after which a temperature modulation with an amplitude of 1.27°C with a period of 60 s was switched on. The temperature was raised to 120°C at a rate of 2 °C min^{-1} after which the samples cooled back to -20°C again, followed by a second heating cycle to 180°C. Glass transitions were identified from the shift in the baseline of the reversing heat flow signal of the second scan. Dry matter content of the samples was determined by puncturing the sample pan after measuring and drying at 105°C for 24 h.

2.2.7 Statistical analysis

Error bars indicate the 95 % confidence intervals of the mean value, as calculated from the standard error of the mean. n indicates the number of measurements. In the case of $n = 2$, error bars represent the absolute deviation from the mean. Fitted values are the result of fitting individual datasets, with error bars indicating the 95 % confidence interval of the mean of the fitted values. Where applicable, significant differences were tested with a one-way ANOVA and Tukey-test, with p indicating the significance level.

2.3 Results and discussion

2.3.1 T_g and water sorption isotherms

Glass transition temperatures of SPI and gluten were determined via mDSC for different levels of hydration and fitted with Couchman-Karasz with respect to T_g (Figure 2.1a). The fitted value for SPI (384 K) is in good agreement with the value reported by Morales and Kokini [46] for 7S soy globulins (387 K; [46, 47], which is remarkable as we used a crude commercial protein isolate. Values reported for the T_g of soy proteins deviate widely between references [46–49], possibly due to variations in experimental methodology, raw materials, and sample preparation. For the sake of consistency we will use our own determined values. The fitted T_g of gluten (428 K) is in good agreement with literature values [34, 50, 51], although higher values have also been reported [52].
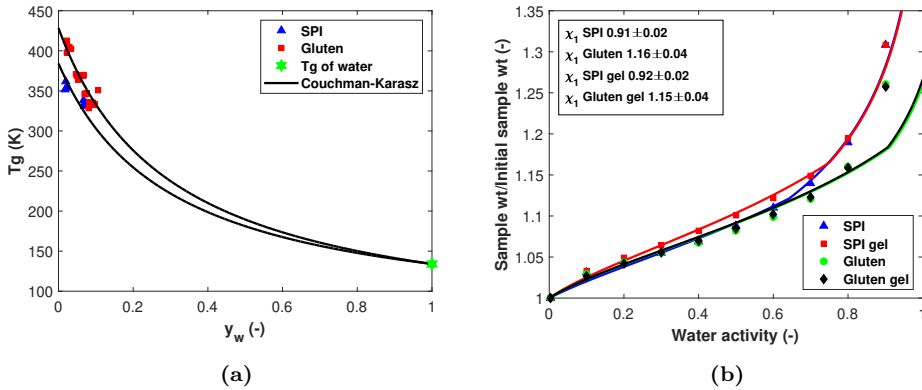

Figure 2.1: Glass transition temperatures of SPI and gluten protein at different moisture weight fractions, as determined via mDSC. Solid lines indicate best fits according to Couchman-Karasz (2.1a). Water sorption isotherms of SPI and gluten, before and after the gelation process. Error bars overlap with the markers (n=2). Solid lines indicate best fits with FVFH theory. Fitted values of χ_1 are presented in the insert (2.1b).

Water sorption isotherms of SPI and gluten were collected before and after the gelation process using dynamic vapour sorption (Figure 2.1b). Gels were lyophilized and ground to a fine powder before sorption analysis. The gelation process increased sorption by SPI at $a_w < 0.7$. Additional cross-linking can result in a higher glass

transition temperature [53] and, as follows from FVFH theory, increase sorption in the glassy regime. At a_w where $T > T_g$, the sorption of gelled and non-gelled SPI is identical. DSC analysis of the lyophilized gels did not reveal a clear glass transition. Therefore, a slightly higher T_g of 415 K was used, which coincides with the T_g of 11S soy glycinin as reported by Morales and Kokini [46]. Gluten sorption was not affected by the gelation process. Sorption isotherms were fitted using FVFH theory with respect to χ_1 (Equation 2.2). Best fits and fitted values for χ_1 are presented in Figure 2.1b. SPI has a lower χ_1 than gluten, indicating it has more attractive interactions with water compared to gluten.

2.3.2 Gel swelling and mechanical characterization

Soy protein gels

We will use $y_{p,j}^i$ as the polymer weight fraction at gelation of a single-phase ($i = I$) or two-phase ($i = II$) gel, made of polymer j, or of the gel as a whole ($j = gel$). Recall that φ_0 represents the polymer volume fraction at maximum swelling (when $\Pi_{ext} = 0$). Increasing $y_{p,SPI}^I$ resulted in a linear increase of φ_0 (Figure 2.2a). This indicates that varying $y_{p,SPI}^I$ is a controllable method to adjust maximum swelling. The elastic *Young's* moduli E of the swollen SPI gels were determined via uni-axial compression. E increased proportionally as φ_0 increased (Figure 2.2b); E thus also relates directly to $y_{p,SPI}^I$. The elastic modulus relates directly to the cross-link density of the gel [25]. An increased cross-link density results in a greater resistance to deformation (conform Equation 2.9), and explains the reduced swelling as $y_{p,SPI}^I$ is increased (Figure 2.2a). The moduli of the swollen gels as a function of φ_0 can be described with a power law with an exponent of 2.28 (Figure 2.2b). The apparent agreement with the theoretical exponent reported by Horkay and Zrínyi [35] for networks of Gaussian chains is most probably a deceptive coincidence as the majority of soy proteins are globular [54]. It is unlikely that the heat applied during gelation resulted in a complete loss of protein secondary structure [27].

Gluten gels

Wheat gluten proteins are more difficult to handle than soy proteins as they bind little water [2] and form a network upon hydration [55, 56]. Our swelling experiments revealed that non-heated gluten binds 2.1±0.1 g water g^{-1} protein, similar to Grabowska et al. [2] (1.9 g g^{-1}). Higher levels of swelling have also been reported (3.3 g g^{-1}, [57]). It must be noted that the strength of gluten networks depends on the temperature at hydration [58], which can affect swelling. In addition, the kneading
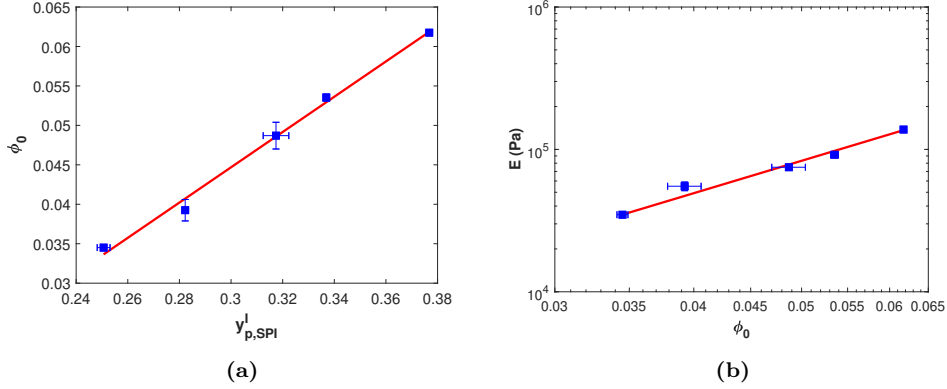
(a)   (b)

Figure 2.2: Maximum level of swelling, φ_0, of SPI gels as function of $y_{p,SPI}^{I}$ (solid line $0.224y_p - 0.0224$, $R^2 = 0.99$; Figure 2.2a), and elastic *Young's* moduli of swollen SPI gels as function of φ_0 (solid line $a\varphi_0^{\beta}$ with $a = 7.59 \times 10^7$ and $\beta = 2.28$, $R^2 = 0.98$; Figure 2.2b). n=3 for $y_{p,SPI}^{I}$, n=2 for E, and n=3 for φ_0.

process can affect the gluten network structure in wheat flour doughs, by changing from a lumped to a strand-like structure [56, 59]. During preparation of our gluten doughs the gluten was only hydrated with water, and not kneaded as you would a bread dough, which may explain the difference in swelling.

Single-phase gluten gels were prepared in ethanol and swollen in water to study their swelling as function of $y_{p,gluten}^{I}$ (Figure 2.3 top). The gluten gels bind less water than hydrated gluten ($\sim$1.5 g g^{-1}). This could be due to additional cross-linking upon heating. The exposure to ethanol may have allowed for additional cross-linking as ethanol decreases the denaturation temperature of gluten [43] and may facilitate further protein unfolding. φ_0 increased slightly but significantly with increasing $y_{p,gluten}^{I}$. Elastic moduli of gluten gels swollen in water were not significantly different, which suggests similar cross-link densities. This is in line with the similar values of φ_0. A similarly limited dependence of swelling on the $y_{p,gluten}^{I}$ is expected for gels obtained from hydrated gluten.
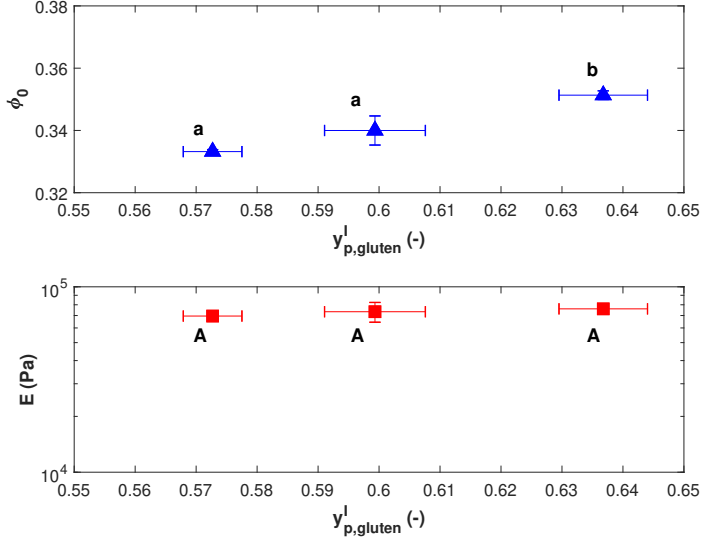
Figure 2.3: φ_0 (top) and elastic *Young's* moduli (bottom) of gluten gels prepared in ethanol and washed and swollen in water as function of $y^I_{p,gluten}$. Different letters indicate significant differences ($p < 0.01$; n=3).

2.3.3   WHC of single-phase protein gels during centrifugation

Soy protein gels

Swollen SPI gels were subjected to an increasing external pressure by centrifugation to determine their WHC as a function of applied pressure. The WHC data was fitted with Flory–Rehner theory (Figure 2.4). The mixing contribution to the swelling pressure was calculated using the interaction parameter, χ_1, as obtained from fitting the sorption isotherms with FVFH theory (Figure 2.1). This leaves only the *shear* modulus in the reference state, G_{ref}, and the polymer volume fraction in the reference state, φ_{ref}, as unknown parameters. Recall that the reference state refers to the relaxed state of the polymer. Defining φ_{ref} as φ at gelation did not match the observed swelling and de-swelling. φ_{ref} was therefore obtained through fitting. For some gels, gel collapse was observed at higher Π_{ext}, which affected the WHC. Data points where collapse occurred were therefore excluded from the fitting process (Figure 2.4, open symbols). Figure 2.4 shows a strong dependence of φ on the applied pressure
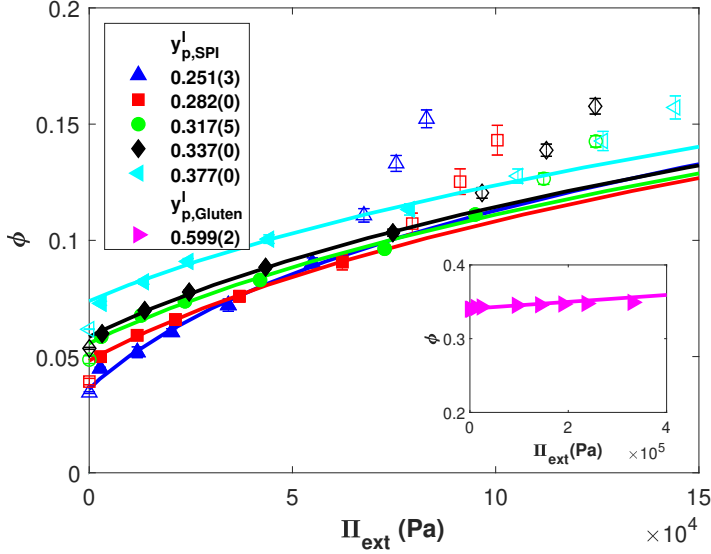
Figure 2.4: WHC of swollen SPI and gluten gels expressed as polymer volume fraction as a function of the applied pressure as determined via centrifugation. Open symbols were excluded from the fitting procedure due to gel collapse. Solid lines are best fits with Flory–Rehner ($R^2 \geq 0.97$). (n=8)

that can be described qualitatively with Flory–Rehner theory.

We compare the fitted values with E and φ_0 from Figure 2.2. Fitted values of φ_{ref} correlate linearly with the experimentally determined values of φ_0 (Figure 2.5a). However, the results deviate from the expected result of $\varphi_{ref} = 1.5\varphi_0$, as was found for various other bio-polymers [30]. The deviation could be the result of the globular (non-Gaussian) nature of soy protein network. Alternatively, it could be due to some inhomogeneity in the distribution of cross-links in the swollen gel. Hydrogel swelling depends on the local cross-link density, as was also addressed in the review by Hoffman [60, 61]. Areas of low cross-link density will swell to a higher level than high cross-link density areas, effectively increasing φ_0. Low cross-link density areas will exude more water at low Π_{ext}, after which a more homogeneous material is obtained. We have accounted for these inhomogeneities by excluding the first data point from the fits (Figure 2.4). A schematic representation of a possible gel structure is presented in Figure 2.6. The fitted elastic *shear* modulus in the reference state,
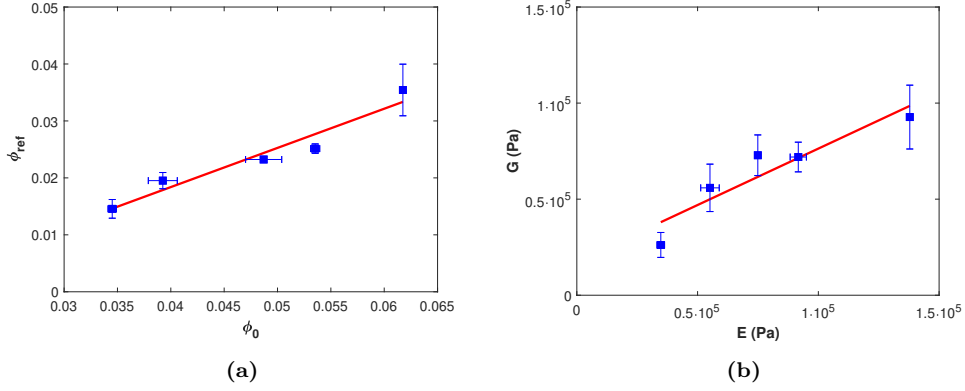
Figure 2.5: Fitted φ_{ref} as function of experimentally determined φ_0 (Slope: 0.69, $R^2 = 0.94$) (2.5a). Fitted elastic *Shear* moduli as function of experimentally determined elastic *Young's* moduli and $y_{p,SPI}^I$ (Slope: 0.59, $R^2 = 0.86$) (2.5b). Solid lines are the result of linear regression. n=3 for φ_0 and n=2 for E.

G_{ref}, is converted to the *Shear* modulus, G, using Equation 2.10. This enables direct comparison with the experimentally determined *Young's* modulus E. G correlates linearly with E (Figure 2.5b). For incompressible materials, a slope of 1/3 would be expected, while linear regression indicates a slope of 0.59. The deviation could be due to the globular nature of soy. Alternatively, inhomogeneities in cross-link density could account for this deviation. During relatively fast measurements (such as uni-axial compression), moisture losses are negligible and we measure the gel's bulk properties. During sustained deformation (such as during centrifugation) areas of lower cross-link density will exude more water until the higher cross-link density patches overlap (Figure 2.6b). The volume fraction of high cross-link density material increases, resulting in a higher modulus.

The physical meaning of the parameters obtained through fitting may be limited given that not all assumptions for Flory–Rehner theory are met. Still, they are practically usefulness when describing and predicting the WHC.

Gluten gels

Gluten gels prepared in ethanol were firm and showed no signs of collapse during centrifugation, even at the highest pressures applied. WHC as a function of pressure was similar for the different values of $y_{p,gluten}^I$; therefore, only $y_{p,gluten}^I = 0.60$ is shown
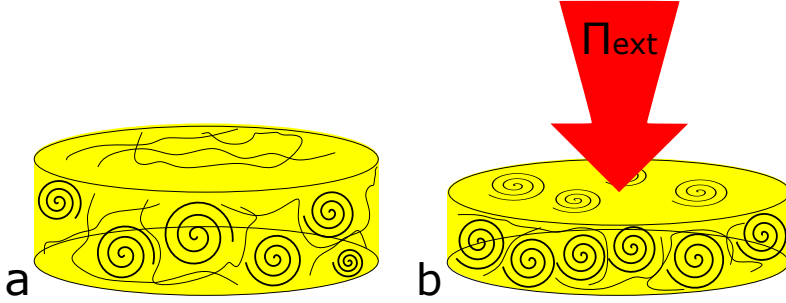
Figure 2.6: Schematic representation of the SPI gel network before (a) and after (b) the expulsion of water under external load (Π_{ext}). Sustained external pressure will induce the initial expulsion of water from the lower cross-link density areas. This results in a compaction of the network and allows for the higher cross-link density patches to overlap. This induces an increase in the elastic modulus of the gel after the exudation of water and a change in the effective φ_{ref}. Spirals represent patches with high cross-link density.

(Figure 2.4). Despite binding very little water, gluten gels (prepared in ethanol) bind water very tightly with negligible water losses in the relevant range of Π_{ext}. Similarly low losses were reported for hydrated gluten doughs [18] and we expect similar behaviour for gluten gels prepared in water. Gluten is an elastomer [56], and thus characterized by a high stretchability and limited polymer-solvent interaction. Although reasonable fits of Flory–Rehner theory could be made, the WHC of gluten gels is characterized by gluten's elastomeric behaviour as indicated by the limited interaction with the solvent.

2.3.4 WHC of mixed protein gels

Water distribution before gelation

We have prepared mixed gels with different SPI : gluten ratios while keeping the total dry matter content of the gel constant at $y_{p,gel}^{II} = 0.3$ to study the effect of the SPI : gluten ratio on the WHC. As was shown by Dekkers et al. [17], two separate phases of soy and gluten can be observed in similar mixed gels using confocal scanning laser microscopy. The two phases are thought to be relatively pure phases consisting of SPI or gluten [2, 14, 17], While gluten swelling shows only a limited dependence on $y_{p,gluten}^{I}$, the WHC of SPI depends strongly on $y_{p,SPI}^{I}$ (Figure 2.4). Knowledge of the water distribution between SPI and gluten before gelation is, therefore, required to understand the WHC of mixed gels.

Water distribution between polymers without cross-links, like our protein powders, should adhere to Flory–Huggins theory (Equation 2.2). However, gluten spontaneously cross-links upon hydration, which will limit its hydration. Therefore, the full Flory–Rehner theory is required to describe the water partitioning between SPI and gluten before gelation. An experimental study using Time Domain-NMR on the water distribution between SPI and gluten as a function of $y_{p,gel}^{II}$ and SPI : gluten ratio showed that SPI binds more water than gluten [14].

We define the partition coefficient P as the fraction of total water in the SPI phase; $(1 - P)$ is therefore the fraction in the gluten phase. Since SPI is not cross-linked, its swelling depends only on $\Pi_{mix,SPI}$. Gluten is cross-linked and its swelling depends on $\Pi_{mix,gluten}$ and $\Pi_{elas,gluten}$. Equilibrium is assumed when $-\Pi_{mix,SPI} = \Pi_{mix,gluten} - \Pi_{elas,gluten}$. $\Pi_{mix,i}$ depends on χ_1 from Figure 2.1b, and $\Pi_{elas,gluten}$ follows from fitting $G_{ref,gluten}$ and $\varphi_{ref,gluten}$ to the data from Dekkers et al. [14]. Predictions based on Flory–Rehner theory match the experimental data from Dekkers et al. [14] reasonably well (Figure 2.7). We calculate the polymer weight fraction of the hydrated SPI, $y_{p,SPI}^{II}$ before gelation, using the partition coefficient P:

$$y_{p,SPI}^{II} = \frac{wt_{p,2,SPI}}{(P \cdot wt_{w,2,gel}) + wt_{p,2,SPI}} \tag{2.17}$$

$wt_{p,2,SPI}$ is the weight of SPI and $wt_{w,2,gel}$ is the total weight of water in the mixture. We derive the expected level of swelling SPI in the mixed gel from $y_{p,SPI}^{II}$ and the relation between $y_{p,SPI}^{I}$ and φ_0 in Figure 2.2b.

WHC of mixed gels

Mixed gels with different SPI:gluten ratios were swollen until constant weight. We assume gluten to swell to 2 g water g^{-1} protein and derive the amount of water in the SPI phase of the mixed gel using a simple mass balance:

$$wt_{w,SPI}^{II} = wt_{w,gel}^{II} - \left[\left(\frac{1}{y_{p,gluten}^{II}} \right) - 1 \right] \cdot wt_{p,gluten}^{II} \tag{2.18}$$

where $y_{p,gluten}^{II}$ is equal to 0.33. From the result of Equation 2.18 we can derive φ using $y_{p,SPI}^{II}$ and the densities of polymer and water. Now that we have separated the contribution of gluten to the WHC from that of SPI we can study the WHC of SPI separately from gluten.

The swelling of the SPI phase strongly depends on the SPI:gluten ratio (Figure 2.8). Mixed gels containing primarily SPI (ratios 20:1, 10:1, 5:1) swell to a level similar
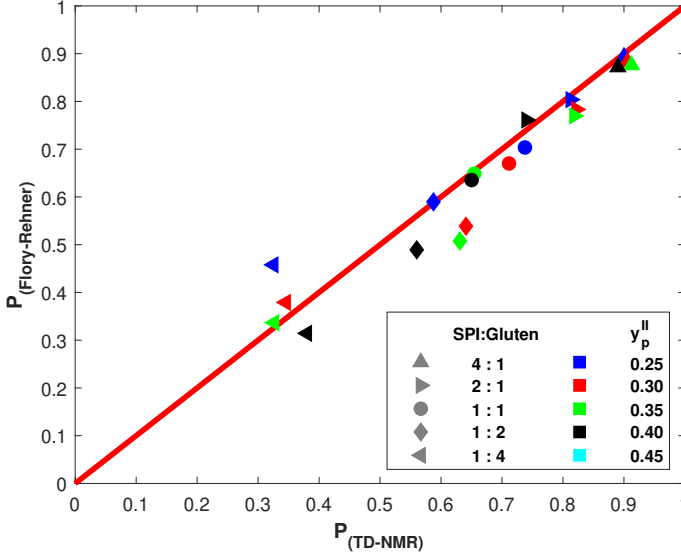
Figure 2.7: Prediction plot of the water partition coefficient, P, using TD-NMR data from Dekkers et al. [14], and as predicted with Flory–Rehner theory assuming $G_{ref,gluten} = 1.7e5$ Pa and $\varphi_{ref,gluten} = 0.023$. Average difference between experimental and predictions is ± 7.9 %.

to single-phase SPI gels, as indicated by the red line for a single-phase SPI gel with $y_{p,SPI}^{I} = 0.3$. The swelling of SPI decreased gradually as gluten content was increased. Because of the limited water uptake by gluten in the dough before gelation, more water will be available to hydrate SPI, causing $y_{p,SPI}^{II}$ before gelation to decrease. As was shown in Figure 2.2b, the maximum level of swelling increases with decreasing $y_{p,SPI}^{I}$ as a result of the decreased cross-link density. An increased level of swelling of SPI with increasing gluten content was therefore expected, while the opposite is observed. The swelling of mixed SPI-gluten gels is less than the weighted sum of the individual phases, indicating an interaction between SPI and gluten.

Mixed gel mechanics

To investigate the interaction between SPI and gluten in mixed gels, we have determined the elastic *Young's* moduli of swollen mixed gels via uni-axial compression (Figure 2.9). We express the modulus as a function of the volume fraction of the
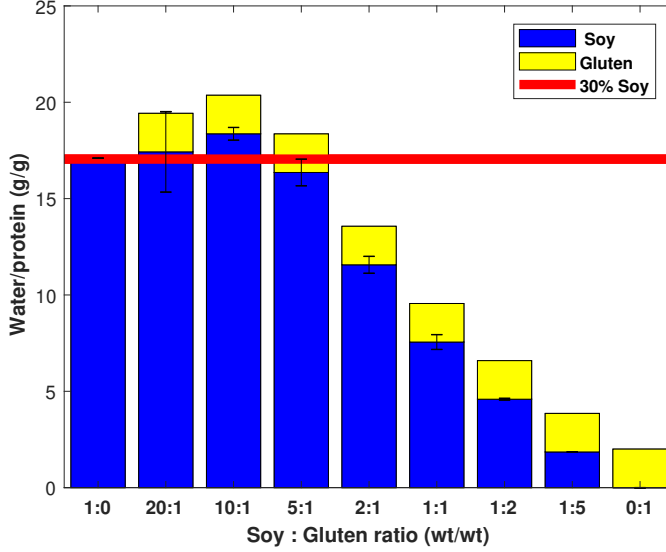
Figure 2.8: WHC of mixed SPI-gluten gels at $\Pi_{ext} = 0$ expressed as gram water per gram protein. Gluten is assumed to bind 2 grams of water per gram protein. Solid line indicates swelling of an SPI gel with $y_{p,SPI}^I = 0.3$ (n=3).

gluten phase in the mixed gel, Φ_{gluten}. Both single-phase SPI and gluten gels have a considerably higher modulus than mixed gels with low gluten fractions (SPI:gluten ratios 20:1, 10:1, 5:1). Since the modulus increases upon increasing the gluten content, it is unlikely that gluten acts as an inactive filler [62]. Gluten and soy proteins have recently been shown not to co-aggregate [19]. We hypothesize that the inclusion of gluten may have introduced defects in the SPI network, causing the observed weakening. The modulus of the mixed gels increases with Φ_{Gluten} and exceeds the modulus of neat gluten gels (ratios 1:1, 1:2). Gluten networks are known to be strain hardening [63]. For gels with a continuous gluten network, gluten may already be strained as a result of SPI swelling, and could consequently have a higher modulus. We hypothesise that mixed gels with low gluten fractions are SPI continuous (ratios 20:1, 10:1, 5:1). As the gluten content increases (ratios 2:1, 1:1, 1:2), a continuous gluten network forms that is either entrapping or co-continuous with the SPI network. The mechanism explaining the observed swelling of mixed SPI-Gluten gels is presented in Figure 2.10.
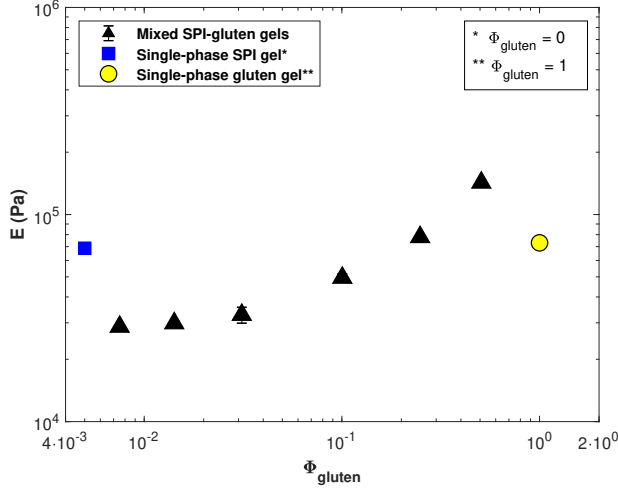
Figure 2.9: Elastic *Young's* moduli of swollen mixed gels with different SPI:gluten ratios as determined with uni-axial compression (n=2). Φ_{gluten} represents the volume fraction of the gluten phase in the swollen gel. Moduli of swollen single-phase SPI and gluten gels were added for comparison. Note that the single-phase SPI gel contains no gluten and thus $\Phi_{gluten} = 0$.

Mechanical interaction between SPI and gluten

The mechanism proposed in Figure 2.10 explains the reduced swelling of SPI based on confinement and compression by a continuous gluten network. To quantify this mechanical interaction between SPI and gluten, we analyse the WHC of the SPI phase in the mixed gel as a function of applied pressure. We derive the polymer volume fraction in the SPI phase by subtracting the contribution of gluten using Equation 2.18. We hypothesize that at higher gluten contents the gluten forms a continuous network and imposes a pressure on the SPI phase during swelling. This will limit SPI swelling, as schematically depicted in Figure 2.10. We will call this pressure Π_{gluten}, which is additive to the external pressure experienced by SPI as:

$$\Pi_{ext} + \Pi_{gluten} = \Pi_{swell} = \Pi_{mix,SPI} - \Pi_{elas,SPI} \quad (2.19)$$

Since Π_{gluten} is additive to Π_{ext}, we can determine Π_{gluten} as the difference in pressure between the freely swollen SPI gels and the SPI phase of the mixed gels at the same value of φ (Figure 2.11). We obtain the pressure dependence of φ for a freely swollen
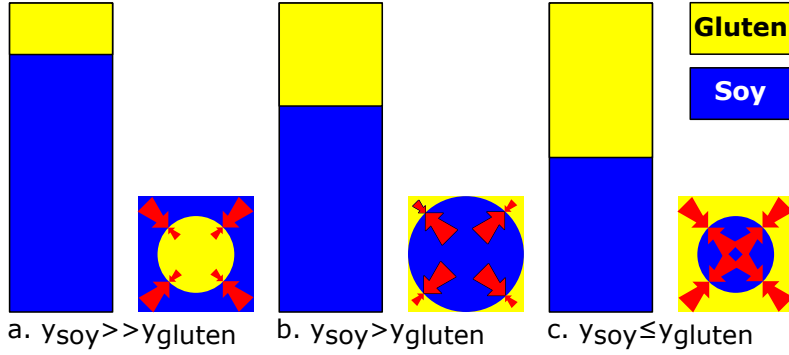
Figure 2.10: Proposed mechanism explaining the swelling of mixed SPI-gluten gels. SPI forms the continuous phase with gluten as a dispersed phase when $y_{SPI} >> y_{gluten}$ (2.10a). For intermediate ratios of SPI:Gluten ($y_{SPI} \approx y_{gluten}$; ratio$\sim 2-1$), gluten forms a continuous network and hinders SPI swelling (2.10b). Upon further increasing the amount of gluten the continuous gluten network becomes stronger, which further limits SPI swelling (2.10c). Here, y_i represents the fraction of polymer i of the total polymer content. Note that the depicted structure merely describes the interaction between gel phases and does not represent the proposed gel micro-structure.

SPI gel from $y^{II}_{p,SPI}$ and the relations for single-phase SPI gels between $y^{I}_{p,SPI}$ and G_{ref} and φ_{ref} (Figure 2.2b,2.5a), as indicated by the solid lines in Figure 2.11. The difference in Π_{ext} between experimental data points and the corresponding solid line indicates the value of Π_{gluten}:

$$\Pi_{gluten} = \Pi^{I}_{ext,SPI}(\varphi) - \Pi^{II}_{ext,SPI}(\varphi) \tag{2.20}$$

with Π_{gluten} as the pressure exerted by the gluten on the SPI phase in the mixed gel, $\Pi^{I}_{ext,SPI}$ as the external pressure associated with a certain φ for a single-phase SPI gel, and $\Pi^{II}_{ext,SPI}$ as the external pressure associated with that same φ for the SPI phase of the mixed gel. Dekkers et al. [14] showed that one cannot easily differentiate between iso-strain, iso-stress, and inter-penetrating networks for SPI-gluten mixtures as they provide similar outcomes over a wide range of sample compositions. The iso-strain model (Equation 2.14) should therefore provide a good indication of the strain on the network. By expressing Π_{gluten} as function of strain (ϵ), we effectively obtain the stress-strain relation for the gluten network. Two distinct regimes can be identified based on the SPI : Gluten ratios (Figure 2.12).

The first regime covers the gels low in gluten, which swell to a similar level as pure SPI
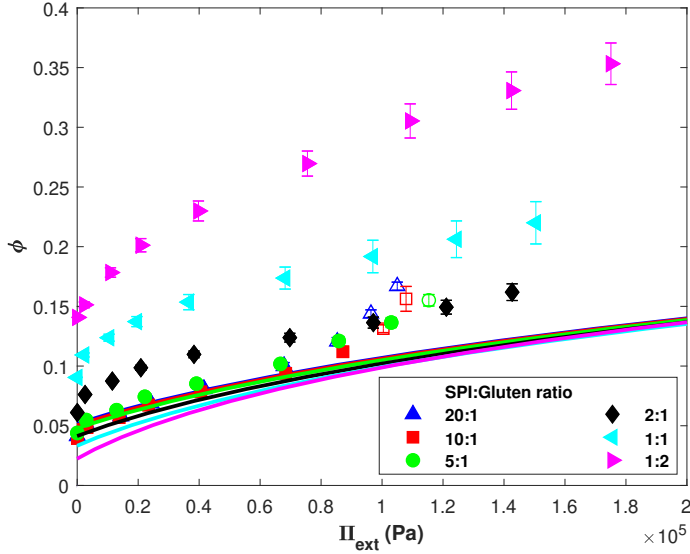
Figure 2.11: Water holding capacity as measured via centrifugation for mixed SPI-gluten gels, expressed for the SPI phase, assuming gluten binds 2 g water g^{-1} protein. Solid lines indicate the expected Π_{ext} dependence of φ based on the SPI phase composition according to Equation 2.17 . Open symbols indicate gel collapse (n=8).

(Figure 2.8, ratios 20:1, 10:1, 5:1). These gels have near-zero values of Π_{gluten} at low strains, indicating similarity in WHC to pure SPI. In line with our earlier hypothesis, SPI will be the continuous phase in gels as they swell and de-swell similarly to pure SPI, with the gluten present as inclusions. The increasingly positive pressures at high strain ($\epsilon \geq 1$) are the result of additional water loss associated with gel collapse (Figure 2.12, open symbols). The second regime covers the gels with higher gluten content, which show a gradual decrease in swelling as gluten content is increased (Figure 2.8, ratios 2:1, 1:1, 1:2). The markedly lower swelling of the SPI phase compared to pure SPI suggests gluten is a continuous phase. The ratio at which the second regime starts ($\sim$ 2:1) could be the ratio at which gluten starts forming a space-filling network. Π_{gluten} becomes higher as gluten content increases, indicating that the pressure exerted onto the SPI phase becomes higher. At higher strains, we observe an increase in Π_{gluten}. Gluten networks are strain hardening [64] which might explain the increasing slope of Π_{gluten} versus ϵ.
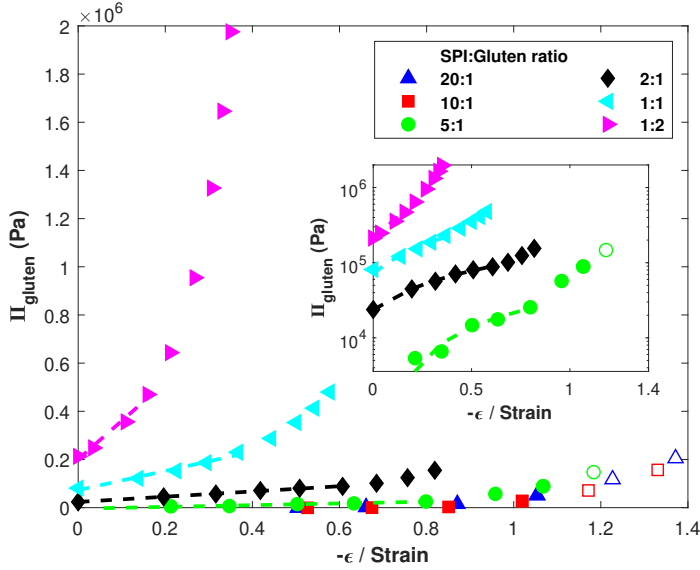
Figure 2.12: The pressure exerted by the gluten phase on the SPI phase, Π_{gluten}, as calculated with Equation 2.20, as function of the strain, ϵ. Dashed lines indicate the regime over which the elastic modulus was determined. Open symbols indicate gel collapse occurred during centrifugation. Insert shows the data for ratios 5:1, 2:1, 1:1 and 1:2 on a lin-log scale for clarity.

For the gluten-rich gels (ratios 2:1, 1:1, 1:2) we were able to calculate the elastic modulus of the gluten network as the slope in the linear regime in Figure 2.12. Naturally, a linear model cannot describe the observed strain hardening of gluten. However, the more sophisticated affine network model (similar to Equation 2.9) also failed to describe the observed non-linear behaviour, suggesting the observed strain hardening is real (fits not shown). The elastic modulus of the gluten phase increases with gluten volume fraction (Figure 2.13a), which is in line with the reduced swelling of SPI as the amount of gluten in the mixed gels is increased. To test the validity of the gluten moduli obtained from the WHC measurements, we use them to calculate the expected moduli of the mixed gels and compare the result with the experimentally determined moduli. An iso-strain or inter-penetrating network structure is most probable based on the hypothesized structure. The modulus

according to the iso-strain network model is given by Equation 2.21, [65]:

$$E_{gel}^{II,m} = (1 - \Phi_{Gluten})E_{SPI}^m + \Phi_{gluten}E_{gluten}^m \tag{2.21}$$

E_{gel}^{II} is the modulus of the mixed gel, and Φ_{Gluten}, $(1 - \Phi_{Gluten})$, and E_i are the volume fractions and moduli of the individual phases respectively. Exponent m taken as 1 for iso-strain behaviour. The modulus of an iso-tropic inter-penetrating network is given by [66]:

$$E_{gel}^{II} = (1 - a)^2 E_{SPI} + a^2 E_{Gluten} + 2a(1 - a)\left(\frac{(1 - a)}{E_{SPI}} + \frac{a}{E_{Gluten}}\right)^{-1} \tag{2.22}$$

where a is:

$$a = \left(1.5 - \frac{(9 - 4\Phi_{Gluten})^{\frac{1}{2}}}{2}\right)^{\frac{1}{2}} \tag{2.23}$$

We take the moduli of the SPI phase from the relation between $y_{p,SPI}^I$ and E_{SPI} from Figure 2.2b. We acknowledge that the modulus of SPI appears to be negatively affected by the addition of gluten. However, since the modulus of the composite is dominated by the elasticity of gluten in the relevant range of Φ_{gluten} the influence of the uncertainty in E_{SPI} on the modulus of the composite will be limited. Comparison of the moduli calculated for the mixed gels with our experimentally determined moduli shows a reasonable agreement, for both iso-strain and inter-penetrating models. Dekkers et al. [14] similarly reported that models describing the various network structures result in a similar modulus. Even though we cannot confirm the exact network structure, these findings support our hypothesis that at sufficiently high gluten contents a continuous network forms which is capable of limiting the swelling of SPI via a mechanical interaction.

The mechanical interaction between SPI and gluten in swollen mixed gels depends on the ratio between the two bio-polymers. Therefore, varying the ratio between SPI and gluten could be used to control the swelling and de-swelling of mixed gels, and possibly meat analogues. How the high shear processes commonly used to produce meat analogue products would affect these findings remains unclear.

2.3.5 General discussion

We have used Flory–Rehner theory to better understand the behaviour of mixed SPI-gluten gels. The parameters obtained through fitting of FR theory were not entirely consistent with theory, possibly due to the globular nature of soy protein.
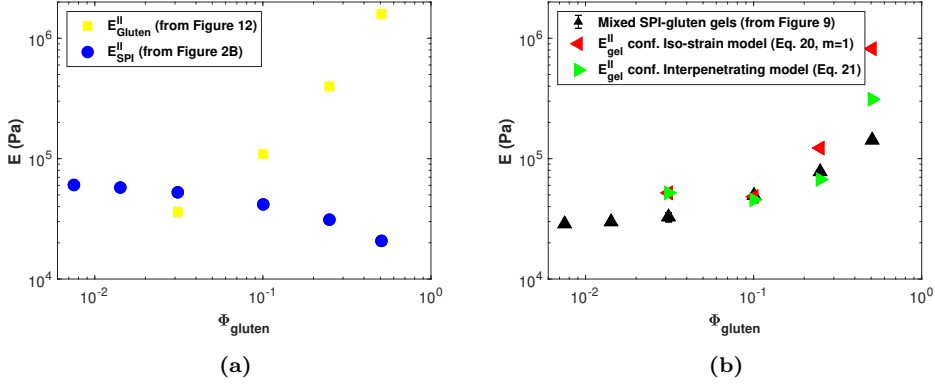
Figure 2.13: Elastic *Young's* moduli of the gluten and SPI phases in mixed gels (Figure 2.13a). Moduli of the mixed gels according to the iso-strain and inter-penetrating network models, and the experimental *Young's* moduli of mixed gels (Figure 2.13b). Φ_{gluten} represents the volume fraction of gluten in the swollen gel.

Nonetheless, using FR theory provided useful insights on the interaction between SPI and gluten. The results indicate that at sufficiently high gluten contents, a continuous gluten network forms. The gluten network both limits water uptake by SPI, and increases the modulus of the mixed gel. While the limited WHC might be detrimental to the juiciness of a meat analogue product, the improved texture could be beneficial to the product's 'bite'. Unfortunately, there is currently no experimental method capable of predicting juiciness accurately. The exact effect of SPI:gluten ratio on juiciness thus remains unclear. Interestingly, the SPI:gluten ratio at which gluten forms a continuous network coincides with the ratios at which fibrous materials can be made [2, 67], and suggests gluten continuity might be a prerequisite for making meat-like structures with shear-cell technology.

2.4   Conclusion

We have studied the WHC of single-phase and mixed SPI and gluten gels with Flory–Rehner theory to ultimately enhance the juiciness of meat analogues. WHC of single-phase SPI gels depends on the polymer weight fraction at gelation, $y^I_{p,SPI}$, and can be described with Flory–Rehner theory. WHC of mixed SPI - gluten gels is not a linear combination of the WHC of their constituents. Mixed gels low in gluten

exhibit similar behaviour to neat SPI gels, although their elastic moduli were lowered by gluten addition. This did not affect the WHC as a function of external pressure, as indicated by the near-zero values of Π_{gluten}. Increasing the gluten content results in the formation of a continuous gluten network, that limits SPI swelling via an apparent mechanical interaction with SPI. The pressure exerted on the SPI phase by the gluten network depends on the SPI:gluten ratio and the elastic modulus of the gluten network was extracted. The elastic modulus of the mixed gels could be approximated with the polymer blending law and the predicted moduli of soy and gluten. Understanding the interaction between the different phases in bio-polymer blends can help in improving their structuring potential, and aid the development of the next generation meat *analogues*. This work shows that the gel network structure can be controlled with the SPI-gluten ratio. Therefore, it can be an important tool to control both the WHC/juiciness and the mechanical properties of meat analogues.

Acknowledgements

References

[1] J.H. Chiang, S.M. Loveday, A.K. Hardacre, and M.E. Parker. Effects of soy protein to wheat gluten ratio on the physicochemical properties of extruded meat analogues. *Food Structure*, 19 (September 2018):100102, 2019.

[2] K.J. Grabowska, S. Tekidou, R.M. Boom, and A.J. van der Goot. Shear structuring as a new method to make anisotropic structures from soy-gluten blends. *Food Research International*, 64:743–751, 2014.

[3] B.L. Dekkers, C.V. Nikiforidis, and A.J. van der Goot. Shear-induced fibrous structure formation from a pectin/SPI blend. *Innovative Food Science and Emerging Technologies*, 36:193–200, aug 2016.

[4] K.J. Grabowska, S. Zhu, B.L. Dekkers, N.C.A. De Ruijter, J. Gieteling, and A.J. van der Goot. Shear-induced structuring as a tool to make anisotropic materials using soy protein concentrate. *Journal of Food Engineering*, 188:77–86, 2016.

[5] A.C. Hoek. *Will Novel Protein Foods beat meat? Consumer acceptance of meat substitutes - a multidisciplinary research approach*. PhD thesis, Wageningen UR, 2010.

[6] E. de Bakker and H. Dagevos. Vleesminnaars, vleesminderaars en vleesmijders - Duurzame eiwitconsumptie in een carnivore eetcultuur. Technical report, Wageningen UR, Den Haag, 2010.

[7] R.D. Warner. Chapter 14 – The Eating Quality of Meat—IV Water-Holding Capacity and Juiciness. In F. Toldra, editor, *Lawrie´s Meat Science*, pages 419–459. Woodhead Publishing Limited, eighth edition, 2017. ISBN 9780081006948.

[8] M.D. Aaslyng, C. Bejerholm, P. Ertbjerg, H.C. Bertram, and H.J. Andersen. Cooking loss and juiciness of pork in relation to raw meat quality and cooking procedure. *Food Quality and Preference*, 14(4):277–288, 2003.

[9] E. Puolanne. Developments in our understanding of water-holding capacity. In P.P. Purslow, editor, *New Aspects of Meat Quality*, chapter 8, pages 77–113. Woodhead Publishing Limited, 2017.

[10] K.L. Pearce, K. Rosenvold, H.J. Andersen, and D.L. Hopkins. Water distribution and mobility in meat during the conversion of muscle to meat and ageing and the impacts on fresh meat quality attributes - A review. *Meat Science*, 89(2):111–124, 2011.

[11] H.C. Bertram, M.D. Aaslyng, and H.J. Andersen. Elucidation of the relationship between cooking temperature, water distribution and sensory attributes of pork - A combined NMR and sensory study. *Meat Science*, 70(1):75–81, 2005.

[12] C. Yven, J. Culioli, and L. Mioche. Meat bolus properties in relation with meat texture and chewing context. *Meat Science*, 70(2):365–371, 2005.

[13] A.C. Hoek, P.A. Luning, P. Weijzen, W. Engels, F.J. Kok, and C. de Graaf. Replacement of meat by meat substitutes. A survey on person- and product-related factors in consumer acceptance. *Appetite*, 56(3):662–673, jun 2011.

[14] B.L. Dekkers, D.W. de Kort, K.J. Grabowska, B. Tian, H. Van As, and A.J. van der Goot. A combined rheology and time domain NMR approach for determining water distributions in protein blends. *Food Hydrocolloids*, 60:525–532, 2016.

[15] K.S. Liu and F.H. Hsieh. Protein-protein interactions in high moisture-extruded meat analogs and heat-induced soy protein gels. *JAOCS, Journal of the American Oil Chemists' Society*, 84 (8):741–748, 2007.

[16] H. Akdogan. High moisture food extrusion. *International Journal of Food Science and Technology*, 34(3):195–207, 1999.

[17] B.L. Dekkers, R. Hamoen, R.M. Boom, and A.J. van der Goot. Understanding fiber formation in a concentrated soy protein isolate - Pectin blend. *Journal of Food Engineering*, 222:84–92, 2018.

[18] P. Roccia, P.D. Ribotta, G.T. Pérez, and A.E. León. Influence of soy protein on rheological properties and water retention capacity of wheat gluten. *LWT - Food Science and Technology*, 42(1):358–362, 2009.

[19] M.A. Lambrecht, I. Rombouts, B. De Ketelaere, and J.A. Delcour. Prediction of heat-induced polymerization of different globular food proteins in mixtures with wheat gluten. *Food Chemistry*, 221:1158–1167, 2017.

[20] X. Jin, R.G.M. van der Sman, J.F.C. van Maanen, H.C. van Deventer, G. van Straten, R.M. Boom, and A.J.B. van Boxtel. Moisture Sorption Isotherms of Broccoli Interpreted with the Flory-Huggins Free Volume Theory. *Food Biophysics*, 9(1):1–9, 2014.

[21] E. Paudel, R.M. Boom, and R.G.M. van der Sman. Change in Water-Holding Capacity in Mushroom with Temperature Analyzed by Flory-Rehner Theory. *Food and Bioprocess Technology*, 8(5):960–970, 2015.

[22] R. van der Sman, E. Paudel, A. Voda, and S. Khalloufi. Hydration properties of vegetable foods explained by Flory–Rehner theory. *Food Research International*, 54(1):804–811, nov 2013.

[23] R.G.M. van der Sman. Thermodynamics of meat proteins. *Food Hydrocolloids*, 27(2):529–535, 2012.

[24] R.G.M. van der Sman. Moisture transport during cooking of meat: An analysis based on Flory-Rehner theory. *Meat Science*, 76(4):730–738, 2007.

[25] R.G.M. van der Sman. Modeling cooking of chicken meat in industrial tunnel ovens with the Flory-Rehner theory. *Meat Science*, 95(4):940–957, 2013.

[26] P.J. Flory and J. Rehner. Statistical Mechanics of Cross-Linked Polymer Networks II. Swelling. *The Journal of Chemical Physics*, 11(11):521–526, 1943.

[27] K.S. Kim, S. Kim, H.J. Yang, and D.Y. Kwon. Changes of glycinin conformation due to pH, heat and salt determined by differential scanning calorimetry and circular dichroism. *International Journal of Food Science and Technology*, 39(4):385–393, 2004.

[28] H. Li, L. Zhao, X.D. Chen, and R. Mercadé-Prieto. Swelling of whey and egg white protein hydrogels with stranded and particulate microstructures. *International Journal of Biological Macromolecules*, 83:152–159, 2016.

[29] P.J. Flory and J. Rehner. Effect of Deformation on the Swelling Capacity of Rubber. *The Journal of Chemical Physics*, 12(10):412, 1944.

[30] R.G.M. van der Sman. Biopolymer gel swelling analysed with scaling laws and Flory-Rehner theory. *Food Hydrocolloids*, 48:94–101, 2015.

[31] J.S. Vrentas and C.M. Vrentas. Sorption in Glassy Polymers. *Macromolecules*, 24(9):2404–2412,

1991.

[32] R.G.M. van der Sman and M.B.J. Meinders. Prediction of the state diagram of starch water mixtures using the Flory–Huggins free volume theory. *Soft Matter*, 7:429, 2011.

[33] P.R. Couchman and F.E. Karasz. A Classical Thermodynamic Discussion of the Effect of Composition on Glass-Transition Temperatures. *Macromolecules*, 11(1):117–119, 1978.

[34] M. Pouplin, A. Redl, and N. Gontard. Glass transition of wheat gluten plasticized with water, glycerol, or sorbitol. *Journal of Agricultural and Food Chemistry*, 47(2):538–543, 1999.

[35] F. Horkay and M. Zrínyi. Studies on the Mechanical and Swelling Behavior of Polymer Networks Based on the Scaling Concept. 4. Extension of the Scaling Approach to Gels Swollen to Equilibrium in a Diluent of Arbitrary Activity. *Macromolecules*, 15(5):1306–1310, 1982.

[36] P.G. De Gennes. *Scaling concepts in Polymer Physics*. Cornell University Press, Ithaca and London, 1979.

[37] M. Quesada-Pérez, J.A. Maroto-Centeno, J. Forcada, and R. Hidalgo-Alvarez. Gel swelling theories: the classical formalism and recent approaches. *Soft Matter*, 7(22):10536, 2011.

[38] A.R. Khokhlov. Swelling and collapse of polymer networks. *Polymer*, 21(4):376–380, 1980.

[39] T. Hino and J.M. Prausnitz. Swelling equilibria for heterogeneous polyacrylamide gels. *Journal of applied polymer science*, 62(1):1635–1640, 1996.

[40] M. Shibayama, Y. Shirotani, H. Hirose, and S. Nomura. Simple scaling rules on swollen and shrunken polymer gels. *Macromolecules*, 30(23):7307–7312, 1997.

[41] P.N. Kocher and E.A. Foegeding. Microcentrifuge-Based Method for Measuring Water-Holding of Protein Gels. *Journal of Food Science*, 58(5):1040–1046, 1993.

[42] J.A.M. Berghout, P. Venema, R.M. Boom, and A.J. van der Goot. Comparing functional properties of concentrated protein isolates with freeze-dried protein isolates from lupin seeds. *Food Hydrocolloids*, 51:346–354, 2015.

[43] M.A. Lambrecht, I. Rombouts, and J.A. Delcour. Denaturation and covalent network formation of wheat gluten, globular proteins and mixtures thereof in aqueous ethanol and water. *Food Hydrocolloids*, 57:122–131, 2016.

[44] M. Dahesh, A. Banc, A. Duri, M.H. Morel, and L. Ramos. Polymeric Assembly of Gluten Proteins in an Aqueous Ethanol Solvent Polymeric Assembly of Gluten Proteins in an Aqueous Ethanol Solvent. *Journal of Physical Chemistry B*, 118(38):11065–11076, 2014.

[45] J.M.S. Renkema, J.H.M. Knabben, and T. Van Vliet. Gel formation by beta-conglycinin and glycinin and their mixtures. *Food Hydrocolloids*, 15(4-6):407–414, 2001.

[46] A. Morales and J.L. Kokini. Glass transition of soy globulins using differential scanning calorimetry and mechanical spectrometry. *Biotechnology Progress*, 13(5):624–629, 1997.

[47] A. Morales and J.L. Kokini. State diagrams of soy globulins. *Journal of Rheology*, 43(2):315–325, 1999.

[48] A. Mizuno, M. Mitsuiki, and M. Motoki. Effect of transglutaminase treatment on the glass transition of soy protein. *Journal of Agricultural and Food Chemistry*, 48(8):3286–3291, 2000.

[49] C.S. Kealley, M.K. Rout, M.R. Dezfouli, E. Strounina, A.K. Whittaker, I.A.M. Appelqvist, P.J. Lillford, E.P. Gilbert, and M.J. Gidley. Structure and molecular mobility of soy glycinin in the solid state. *Biomacromolecules*, 9(10):2937–2946, 2008.

[50] M.T. Kalichevsky, E.M. Jaroszkiewicz, and J.M.V. Blanshard. Glass transition of gluten. 1: Gluten and gluten-sugar mixtures. *International Journal of Biological Macromolecules*, 14(5): 257–266, 1992.

[51] C.J. Verbeek and L.E. Van Den Berg. Extrusion processing and properties of protein-based thermoplastics. *Macromolecular Materials and Engineering*, 295(1):10–21, 2010.

[52] V. Micard and S. Guilbert. Thermal behavior of native and hydrophobized wheat gluten, gliadin and glutenin-rich fractions by modulated DSC. *International Journal of Biological Macromolecules*, 27(3):229–236, 2000.

[53] H. Stutz, K.H. Illers, and J. Mertes. A generalized theory for the glass transition temperature of crosslinked and uncrosslinked polymers. *Journal of Polymer Science Part B: Polymer Physics*, 28(9):1483–1498, 1990.

[54] H. de Jongh. Globular proteins. In W. Aalbersberg, R. Hamer, P. Jasperse, H. de Jongh, C. de Kruif, P. Walstra, and F. de Wolf, editors, *Industrial Proteins in Perspective*, volume 23, chapter III, pages 31–86. Elsevier Science B.V., 2003.

[55] G. Attenburrow, D.J. Barnes, A.P. Davies, and S.J. Ingman. Rheological properties of wheat gluten. *Journal of Cereal Science*, 12(1):1–14, 1990.

[56] T.S.K. Ng and G.H. McKinley. Power law gels at finite strains: The nonlinear rheology of gluten gels. *Journal of Rheology*, 52(2):417–449, 2008.

[57] M.E. Bárcenas, J. De la O-Keller, and C.M. Rosell. Influence of different hydrocolloids on major wheat dough components (gluten and starch). *Journal of Food Engineering*, 94(3-4):241–247, 2009.

[58] A. Farahnaky and S.E. Hill. The effect of salt , water and temperature on wheat dough rheology. *Journal of Texture Studies*, 38:499–510, 2007.

[59] F. Auger, M.H. Morel, J. Lefebvre, M. Dewilde, and A. Redl. A parametric and microstructural study of the formation of gluten network in mixed flour-water batter. *Journal of Cereal Science*, 48(2):349–358, 2008.

[60] A.S. Hoffman. Hydrogels for biomedical applications. *Advanced Drug Delivery Reviews*, 64 (SUPPL.):18–23, 2012.

[61] P.D. Drumheller and J.A. Hubbell. Densely crosslinked polymer networks of poly(ethylene glycol) in trimethylolpropane triacrylate for cell-adhesion-resistant surfaces. *Journal of Biomedical Materials Research*, 29(2):207–215, 1995.

[62] E. Dickinson and J. Chen. Heat-set whey protein emulsion gels: Role of active and inactive filler particles. *Journal of Dispersion Science and Technology*, 20(1-2):197–213, 1999.

[63] B.J. Dobraszczyk and M.P. Morgenstern. Rheology and the breadmaking process. *Journal of Cereal Science*, 38(3):229–245, 2003.

[64] S. Uthayakumaran, M. Newberry, N. Phan-Thien, and R. Tanner. Small and large strain rheology of wheat gluten. *Rheologica Acta*, 41(1):162–172, 2002.

[65] M. Takayanagi, H. Harima, and Y. Iwata. Viscoelastic behavior of polymer blends and its comparison with model experiments. *The society of Materials Science*, 12(116):389–394, 1963.

[66] X.Q. Feng, Y.W. Mai, and Q.H. Qin. A micromechanical model for interpenetrating multiphase composites. *Computational Materials Science*, 28(3-4 SPEC. ISS.):486–493, 2003.

[67] F.K.G. Schreuders, B.L. Dekkers, I. Bodnár, P. Erni, R.M. Boom, and A.J. van der Goot. Comparing structuring potential of pea and soy protein with gluten for meat analogue preparation. *Journal of Food Engineering*, 261(May):32–39, 2019.

Chapter 3

Apparent universality in swelling and fibre formation by mixtures of gluten and leguminous proteins

This chapter is based on:

Abstract

Fibrous meat analogues can be made through shear-induced structuring from gluten in combination with a second protein. A combination of swelling experiments and shear-cell structuring was used to investigate the relation between fibrousness and the presence of a continuous gluten network for mixtures containing gluten and either pea protein, fababean protein or soy protein. When the gluten content of the mixed gels increased, swelling of the other protein decreased proportionately. This suggested the presence of a continuous gluten network. Normalization of the swelling data resulted in an apparent master curve. The strain on the non-gluten protein was derived from the swelling data and increased with increasing gluten content. Structuring the protein mixtures in a shear cell resulted in fibrous structures at gluten contents ≥ 0.5 wt/wt. The effect of gluten on swelling and fibre formation is universal for the tested proteins. We, therefore, propose that in gluten-containing mixtures, a continuous gluten network is required for the formation of fibres, while the second protein acts merely as a filler and is replaceable.

3.1   Introduction

A number of technologies exist to produce fibrous meat-like structures from food proteins [1–5]. However, effectively all industrial production relies on high-moisture extrusion cooking techniques, which are a form of thermo-mechanical processing. Despite the widespread use of extrusion in industry, the rationale required to control the structure of the final product is limited [3, 6]. Knowledge generation is complicated by, among others, the complex flow patterns that occur inside the extruder barrel. Therefore, formulation and process development is still based mostly on empirical knowledge.

In order to better understand the extrusion cooking process, so-called shear cells were developed [7–9]. Shear cells offer a simpler form of thermo-mechanical processing through the use of simple shear flow and heat, and can also be used to produce fibrous, meat-like structures [1, 10–12]. During shear cell processing a bio-polymer mixture is subjected to continuous shear-flow [2]. Recent investigations have yielded insights into the key process and material properties for the production of fibrous structures [13–15]. It is thought that two immiscible phases are required for fibre formation in sheared bio-polymer mixtures [16]. Tolstoguzov [17] proposed that the deformation and alignment of the dispersed phase would lead to an anisotropic structure, which implies that the dispersed phase is of importance to structure formation. Fibrous structures have been produced using various bio-polymer mixtures: soy protein and gluten [1, 3, 16, 18], soy protein and pectin[11], and pea protein and gluten [12]. For neat calcium caseinate, it was shown that air incorporation is vital to obtain a fibrous structure [14]. Also in soy-pectin mixtures, an internal air phase was found that is deformed in the shear-flow direction [11, 12]. Clearly, the knowledge base for process and formulation development is expanding rapidly, but steps still have to be taken towards the intelligent design of fibrous meat-like structures.

We have recently shown that gluten forms a continuous network when present at a sufficiently high level in (non-sheared) mixed soy protein and gluten gels [19]. Gluten protein swells to a lower level than soy protein during free swelling [1, 19, 20]. The continuous gluten network can limit the swelling of the soy protein in a mixed gel through a mechanical interaction [19]. The continuity of the gluten phase could, therefore, be deduced from the regime in which the swelling of soy (or another protein) is inhibited [19]. Grabowska et al. [1] showed that a fibrous structure can be made from soy protein-gluten mixtures with a shear cell, and suggested that gluten is the continuous phase [1]. We, therefore, hypothesise that in order to create fibrous

structures from gluten-containing protein mixtures, gluten content needs to be high enough to form a strong and continuous network.

We will test this hypothesis by studying the swelling and structure-formation of gluten in combination with protein isolates from either fababean (FPI), pea (PPI) or soy (SPI). First, the maximum swelling ratio of single-phase protein gels is studied. The swelling ratio of mixed protein gels is calculated based on the swelling of single-phase gels by assuming no mechanical interaction between the protein phases. Water partitioning between the gluten and non-gluten proteins will be taken into account by using Flory–Rehner theory. Subsequently, the actual swelling ratio of the mixed gels is measured and compared to the calculated values. Furthermore, the deformation of the non-gluten phase caused by the swelling is discussed using the neo-Hookean framework. The outcome of the swelling experiments will be mirrored against structure formation experiments with a shear cell using the same materials.

3.2 Material and methods

Vital wheat gluten (gluten; Roquette, Vitens, St. Louis, MO, USA), fababean protein isolate (FPI; supplied by Ingredion, Hamburg, Germany), pea protein isolate (PPI; NUTRALYS® F85G, Roquette, Vitens, St Louis MO, USA) and soy protein isolate (SPI; Supro 500E IP, DuPont, St. Louis, MO, USA) had protein contents of 77.9 %, 84.0 %, 78.6 % and 81.7 % respectively (Nx5.7). Sodium chloride ($NaCl$; Sigma-Aldrich, Steinheim, Germany) was of analytical grade. Mili-Q water was used for all experiments. All components were at room temperature (22°C) unless stated otherwise.

3.2.1 Preparation of single-phase gels

Single-phase gels were prepared from FPI and PPI using the protocol of Cornet et al. [19]. In short, the protein powder was dispersed in water and mixed thoroughly. The mixture was transferred to a plastic bag and freed from air by applying a vacuum of 50 mbar for 45 s. The mixtures were left overnight at 4°C to allow for hydration. The hydrated mixtures were transferred to stainless steel gelation vessels with an internal height of 5 mm and a radius of 12.5 mm. The vessels were hermetically sealed and submerged in a Julabo shaking water bath heated to 95°C. After 30 min, the vessels were cooled in water of 15°C for 15 min after which the gels were removed from the vessels. Gel edges were trimmed with a sharp razor and visually inspected for defects before use.

3.2.2 Mixed gel preparation

Mixed gels were prepared from mixtures of gluten with either FPI, PPI or SPI by using a protocol similar to that for the single-phase gels with some adaptations. After mixing the non-gluten protein (FPI, PPI or SPI) with the water, gluten was added and mixed thoroughly through the dough. Dough and gel preparation proceeded from thereon without alterations to the protocol for single-phase gels as described in Section 3.2.1.

3.2.3 Gel washing and swelling

Gels were washed and swollen to remove any ions present and to determine their maximum level of swelling using the method of Cornet et al. [19]. In short, gels were placed in excess water (1/100 wt/wt ratio) for a period of at least 48 h until a constant gel weight was reached. The water was renewed three times during this period. After swelling, the dry matter content (DMC) was determined by oven drying for 48 h at 105°C. We will express the maximum level of swelling as the ratio between the volume of water and the volume of polymer as given by:

$$Q_i = \frac{wt_w/\rho_w}{wt_{p,i}/\rho_p} \tag{3.1}$$

wt_w is the total weight of water, $wt_{p,i}$ is the weight of protein i. ρ_w and ρ_p are the densities of water and protein and taken as $1000 \, \mathrm{kg \, m^{-3}}$ and $1330 \, \mathrm{kg \, m^{-3}}$, respectively. For mixed gels containing gluten, gluten was assumed to reach a constant level of swelling, absorbing 1.5 g water $\mathrm{g^{-1}}$ protein [19]. Subtracting the contribution of gluten to the swelling enabled us to calculate the swelling of the other protein in mixed gels. Note that we have previously used 2 $\mathrm{g\,g^{-1}}$, which is the value for non-heated gluten [1, 19]. The value of 1.5 $\mathrm{g\,g^{-1}}$ corresponds to that of heated gluten [19], and was considered to be a more accurate approximation. The volumetric swelling ratio of non-gluten proteins was calculated as:

$$Q_i = \frac{(wt_w - 1.5wt_{p,glu})/\rho_w}{(wt_{p,i} - wt_{p,glu})/\rho_p} \tag{3.2}$$

with $wt_{p,glu}$ as the weight of gluten protein.

3.2.4 Dynamic vapour sorption

Water vapour sorption isotherms were determined at 25°C on an SPSX-S3-EU01508 (Project Messtechnik). Samples were dried for 24 h at a relative humidity (RH) of 0

% before increasing the RH in 10 % increments to an RH of 90 %. Equilibrium was assumed when the sample weight change was less than 0.005 % min^{-1} over a window of 10 min for a period of 120 min. The maximum step duration was set to 2000 min. Isotherms were recorded in duplicate on the protein powders.

3.2.5 High-temperature Shear Cell

Mixtures containing gluten and either FPI, PPI or SPI were prepared. Gluten protein fractions of 0, 0.167, 0.333, 0.500, 0.667 and 1 wt/wt were used. The mixtures were structured in a shear cell (Wageningen University, The Netherlands, [10]) following the protocol reported by Grabowska et al. [1] with some modifications. Mixtures containing FPI and PPI were prepared with a DMC of 0.375 wt/wt, while for the mixtures containing SPI a DMC of 0.300 wt/wt was used to ensure comparability with the results of Cornet et al. [19]. All samples contained 0.01 wt/wt $NaCl$. The $NaCl$ was dissolved in the water after which the non-gluten protein (FPI, PPI or SPI) was mixed in using a spatula. Gluten was added to the mixture, followed by further mixing. The doughs were placed in the HTSC, which was pre-heated to 140°C. The protein blends were sheared for 15 min at a constant temperature of 140°C and a rotational speed of 30 rpm, which corresponds to a shear rate of 39 s^{-1}. After shearing, the HTSC was cooled down in 5 min to below 60°C before opening and removing the samples. Sample structure was assessed immediately. All samples were produced in duplicate. For the swelling experiments, samples were taken from the outer edge of the sample.

3.2.6 Assessment of the fibrous structure

The samples were visually inspected for fibrous structure formation by bending them parallel to the shear flow direction. A wedge was cut from the circular sample. The wedge was bent by moving the sharp tip of the wedge towards the outer edge, resulting in a tear parallel to the shear flow direction. The bent piece was placed on a metal pin and the fracture surface was photographed. This technique reveals the potential orientation of the structure in the outer 4 cm of the sample and is similar to the techniques used to reveal fracture patterns in extrudates [6, 18].

3.2.7 Statistics

Values are presented as the mean± standard error of the mean. The number of duplicates, n, is reported with the data. Where applicable, significant differences were tested for using a one-way ANOVA with a significance level of p<0.05.

3.3 Theory

3.3.1 Flory–Rehner theory

Polymer content at cross-linking can affect the cross-link density of a polymer network. Hence, the water partitioning in a polymer mixture at gelation should be known to be able to make predictions about the swelling ratio of a mixed gel. We use the Flory–Rehner theory to describe the water partitioning in bio-polymer mixtures. Flory–Rehner theory describes the swelling based on the swelling pressure, Π_{swell}, which has two contributions. The first contribution accounts for the pressure due to the mixing of polymer and solvent and is captured by the mixing pressure, Π_{mix}. The second contribution describes the pressure generated due to the deformation upon swelling and is described with the elastic pressure, Π_{elas}. At equilibrium, Π_{swell} is balanced by the externally applied pressure, Π_{ext}:

$$\Pi_{ext} = \Pi_{swell} = \Pi_{mix} - \Pi_{elas} \tag{3.3}$$

Mixing pressure

We have used free volume Flory–Huggins theory to describe Π_{mix}:

$$\Pi_{mix} = \frac{RT}{v_w}\left[\ln(1-\varphi) + \varphi(1-\frac{1}{N}) + \chi\varphi^2 + F(\varphi)\right] \tag{3.4}$$

Here, R is the universal gas constant, T is the absolute temperature, v_w is the molar volume of water, φ is the polymer volume fraction, $F(\varphi)$ accounts for the additional sorption by glassy polymeric materials [21, 22] and N is the ratio of the molar volumes of water and polymer. Since the molar volume of protein is very large compared to that of water, the term $\frac{1}{N}$ is effectively zero, simplifying the equation. χ is the effective Flory–Huggins interaction parameter and captures the polymer-water affinity. χ is composition dependent and, therefore, depends on φ [23]:

$$\chi = \chi_0 + (\chi_1 - \chi_0)\varphi^2 \tag{3.5}$$

χ_0 and χ_1 are the interaction parameters under dilute and concentrated conditions respectively. Since water is a theta solvent for proteins in the limit of low protein concentrations, χ_0 is 0.5 [24]. $F(\varphi)$ was calculated based on van der Sman and Meinders [23]:

$$F(\varphi) = \begin{cases} 0 & \text{if } T \geq T_g \\ -M_w y_s^2 \frac{\Delta C_{p,w}}{RT}\frac{dT_g}{dy_s}\frac{T-T_g}{T_g} & \text{if } T \leq T_g \end{cases} \tag{3.6}$$

with

$$\frac{dT_g}{dy_s} = -\frac{\Delta C_{p,s}\Delta C_{p,w}(T_{g,w} - T_{g,s})}{(y_w\Delta C_{p,w} + y_s\Delta C_{p,s})^2} \qquad (3.7)$$

T_g was calculated according to Couchman-Karasz [25]:

$$T_g = \frac{y_w\Delta C_{p,w}T_{g,w} + y_s\Delta C_{p,s}T_{g,s}}{y_w\Delta C_{p,w} + y_s\Delta C_{p,s}} \qquad (3.8)$$

M_w represents the molar weight of water, $\Delta C_{p,i}$ is the change in heat capacity over the glass transition, $T_{g,i}$ is the glass transition temperature of the pure material, and y_i represent the weight fractions of polymer and water as denoted with subscripts s and w, respectively. $\Delta C_{p,s}$ was taken as $0.425\,\text{kJ}\,\text{K}^{-1}$, which appears to be universal for bio-polymers [23, 26, 27]. The additional term introduced by the free volume extension, $F(\varphi)$, is equal to zero in the rubbery regime ($T > T_g$). Hence, $F(\varphi)$ was equal to zero when determining the water partitioning. The water activity a_w, relates to Π_{mix} via:

$$\ln(a_w) = \frac{v_w\Pi_{mix}}{RT} \qquad (3.9)$$

Elastic pressure

We describe Π_{elas} using the phantom network model:

$$\Pi_{elas} = G_{ref}[\tilde{\varphi}^{1/3} - \frac{\tilde{\varphi}}{2}] \qquad (3.10)$$

G_{ref} is the elastic shear modulus in the reference state. The reference state refers to the composition at which the polymers in the network are relaxed, and thus experience neither compressive nor extensional stress [28]. $\tilde{\varphi}$ is a measure for network deformation relative to the reference state φ_{ref}:

$$\tilde{\varphi} = \frac{\varphi}{\varphi_{ref}} \qquad (3.11)$$

Water partitioning in a bio-polymer mixture

The elastic properties of the non-gluten protein phases depends on the moisture content at gelation. Therefore, the hydration properties of the gel also depend on the moisture content at gelation. At the moment of gelation, the water is assumed to have partitioned between the gluten and non-gluten protein according to thermodynamic equilibrium. To calculate the water partitioning, the gluten was

considered a cross-linked network [29, 30], while this was not the case for the other proteins (soy, pea, and fababean). Hence, Flory–Rehner theory was used to describe the hydration of gluten (Equation 3.10 and 3.4 [19]), while regular FH theory was used for the hydration of the other protein phase (Equation 3.4). We have recently used this approach to describe water partitioning between soy protein and gluten [19] and will use the same approach here. Thus, the water partitioning in the hydrated protein mixture before gelation can be found by solving:

$$\Pi_{mix,i}(\varphi_i) = \Pi_{mix,gluten}(\varphi_{gluten}) - \Pi_{elas,gluten}(\varphi_{gluten}) \tag{3.12}$$

with i as either SPI, FPI, or PPI. The elastic properties of gluten are taken to be $G_{ref} = 0.17$ MPa and $\varphi_{ref} = 0.023$ [19]. The composition of the gluten phase and phase i will depend on the amount of water added to the proteins at the moment of hydration. Denoting the weight fraction of water in the hydrated mix as wt_w, the protein weight fractions as $wt_{p,i}$ and the water partition coefficient as P, the polymer volume fractions of the two phases read:

$$\varphi_i \quad = \quad \frac{wt_{p,i}/\rho_p}{wt_{p,i}/\rho_p + (P \cdot wt_w)/\rho_w} \tag{3.13}$$

$$\varphi_{gluten} \quad = \quad \frac{wt_{p,gluten}/\rho_p}{wt_{p,gluten}/\rho_p + ((1-P) \cdot wt_w)/\rho_w} \tag{3.14}$$

ρ_p and ρ_w are the densities of polymer and water, and taken as 1330 kg m^{-3} and 1000 kg m^{-3}. The water partitioning coefficient P is obtained by simultaneously solving Equation 3.12 and 3.13. Equation 3.12 was solved using the bisection method and varying the partition coefficient P.

3.3.2 Neo-hookean framework

In the neo-Hookean framework, deformation is relative to a reference state. This reference state can be defined as the swelling ratio at which the polymer chains are relaxed, Q_{ref}. We point out that Q is inversely proportional to the commonly used polymer volume fraction φ; the relations are, therefore, inverse compared to when using φ. van der Sman [24] showed that for several bio-polymers, φ_{ref} is proportional to the polymer volume fraction at maximum swelling, φ_0:

$$\varphi_0 = 2/3\varphi_{ref} \tag{3.15}$$

Hence, the swelling ratio at maximum swelling, Q_0, relates to Q_{ref} via:

$$Q_0 = 1.5Q_{ref} \tag{3.16}$$

The deformation of the polymer network, ϵ, for a given swelling ratio, Q, is proportional to the ratio between Q_{ref} and Q:

$$\epsilon \propto \left[\frac{Q_{ref}}{Q}\right]^{-1/3} \tag{3.17}$$

The polymer network is stretched when Q is greater than Q_{ref}, or compressed when Q is smaller than Q_{ref}. The polymers are non-deformed or relaxed when Q equals Q_{ref}; hence the term reference state.

3.4 Results and discussion

3.4.1 Water sorption isotherms

Water sorption isotherms were determined for fababean protein isolate (FPI) and pea protein isolate (PPI) (Figure 3.1). The isotherm for soy protein isolate (SPI) was added for the sake of comparison. SPI has slightly higher water sorption than PPI and FPI when the water activity exceeds 0.7. Isotherms were fitted with Flory–Huggins free volume theory to determine the interaction parameter χ (Equation 3.9). Values for the glass transition temperature in the dry state, T_g, were taken from [31] and were 436 K for FPI and 438 K for PPI. The fitted values for χ were 0.96±0.03 and 0.90±0.02 for FPI and PPI respectively. The values are comparable to what we found previously for soy protein isolate (SPI; 0.91±0.02 [19]). The interaction parameter of gluten was determined previously as 1.16±0.04 [19]. The interaction parameters were used in Section 3.4.3 to determine the water partitioning in protein mixtures.

3.4.2 Swelling of single-phase gels

Gels were prepared from SPI, FPI, and PPI with different DMC at gelation. The gels were swollen in water until maximum swelling was achieved (Figure 3.2). Swelling decreased with increasing DMC at gelation for all tested proteins, following a power law. For SPI gels, this reduction was shown to be due to an increase in cross-link density [19]; we expect this explanation also to hold for FPI and PPI. The swelling ratios of SPI and PPI are comparable, while FPI gels swell much less. Given the similar affinity for water of the different proteins (Figure 3.1), differences in cross-link density are most likely responsible for the observed differences in swelling as follows from Flory–Rehner theory (Equation 3.3).
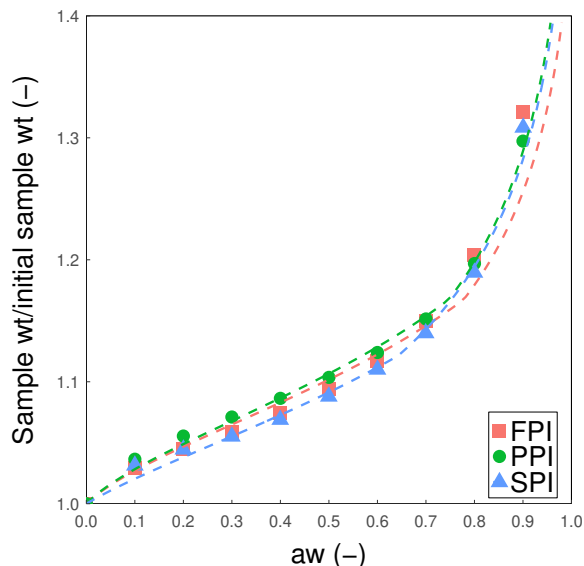
Figure 3.1: Sorption isotherms for powders of soy protein isolate (SPI), pea protein isolate (PPI) and faba bean protein isolate (FPI) as determined at 25 °C. Fitted Flory–Huggins interaction parameters for SPI, PPI and FPI were 0.91±0.02, 0.90±0.2, and 0.96±0.03 respectively. SPI data was reproduced from [19].

3.4.3 Swelling of mixed gels

Mixed gel swelling when assuming no mechanical interaction

When assuming no mechanical interaction, the expected level of swelling for the non-gluten protein follows from the relation established for the single-phase gels, as shown in Figure 3.2. Since the swelling of single-phase gels depends on the DMC at gelation (Figure 3.2), the water partitioning in the mixed gel prior to gelation must be known to determine the level of swelling of the gel. The water partitioning was calculated using Flory–Rehner theory. Equation 3.12 was solved to determine the DMC in the non-gluten protein before gelation. The expected level of swelling of the non-gluten protein is presented as the open symbols in Figure 3.3. When no mechanical interaction is assumed, all three proteins show an increase in the expected level of swelling with increasing gluten content (Figure 3.3).
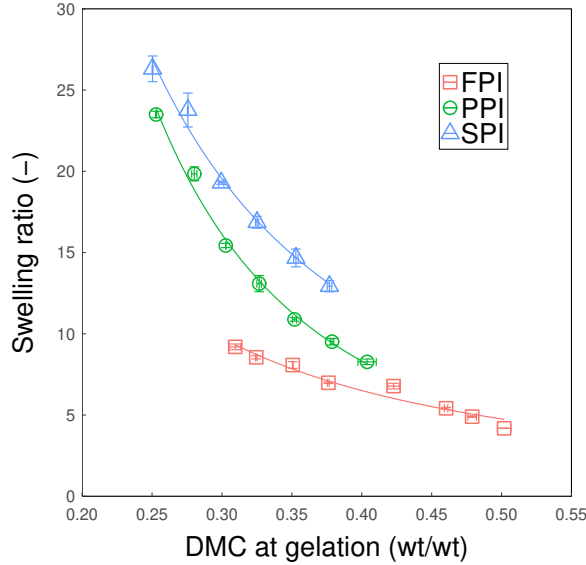
Figure 3.2: The swelling ratio of single-phase FPI, PPI, and SPI gels at maximum swelling presented as function of the dry matter content at gelation. Solid lines represent fits for $y = a(x^b)$ with $a = 1.80$, $b = -1.40$ for FPI, $a = 1.01$, $b = -2.30$ for PPI and $a = 2.35$, $b = -1.76$ for SPI. Error bars represent standard error from the mean with $n = 3$. SPI data was reproduced from [19].

Mixed gel swelling with mechanical interaction

The actual experimental swelling ratios of the non-gluten phase when mechanical interactions are taken into account are presented in Figure 3.3 (closed symbols). The actual values show an opposite trend compared to when mechanical interactions are ignored, with the swelling ratio going down instead of up. This difference is due to the mechanical interaction between the gluten and non-gluten phases, as we have previously shown for SPI-gluten mixtures [19]. The reduction in swelling was the result of the continuous gluten network present. The similar qualitative behaviour shown here for SPI, PPI and FPI suggests that there is a similar mechanical interaction between gluten and the other proteins used.

To identify any universality in the effect of gluten on mixed gel swelling, the relative swelling ratio of the non-gluten proteins was determined. The relative swelling ratio
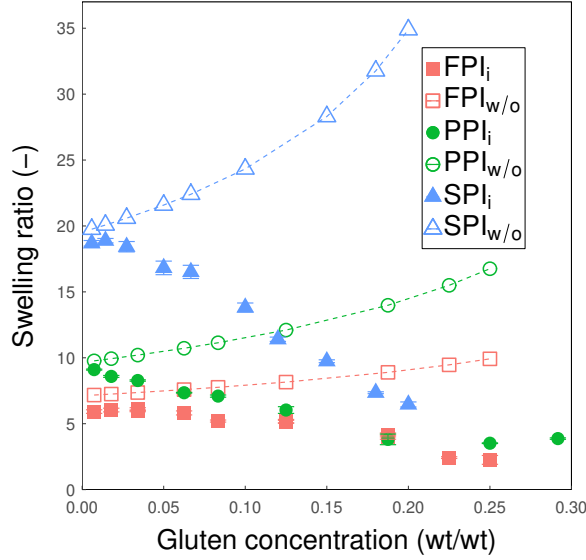
Figure 3.3: The swelling ratio of fully swollen mixed gels prepared from gluten with either FPI, PPI, or SPI as a function of the gluten concentration at gelation. Gluten swelling was subtracted used Equation 3.2 to determine the swelling ratio of the non-gluten protein phase. Open symbols represent expected swelling ratios when no mechanical interaction between phases is assumed and is based on the single-phase gels taking into account water partitioning (Figure 3.2). Closed symbols are measured values. For PPI and FPI a total initial DMC of 0.375 wt/wt was used; for SPI, 0.3 wt/wt was used. Error bars are standard errors from the mean with n = 3.

was calculated by dividing the swelling ratios with the swelling ratio of single-phase gels with the same initial total DMC (Figure 3.4). All three proteins show a similar *relative* reduction in swelling (Figure 3.4), despite the differences in absolute swelling (Figure 3.3). A linear regression led to a fit with $y = -2.436x + 0.955$ ($R^2 = 0.90$). Adding the type of non-gluten protein as an independent fit parameter did not significantly improve the fit. This suggests that gluten has a similar interaction with the three different proteins used.
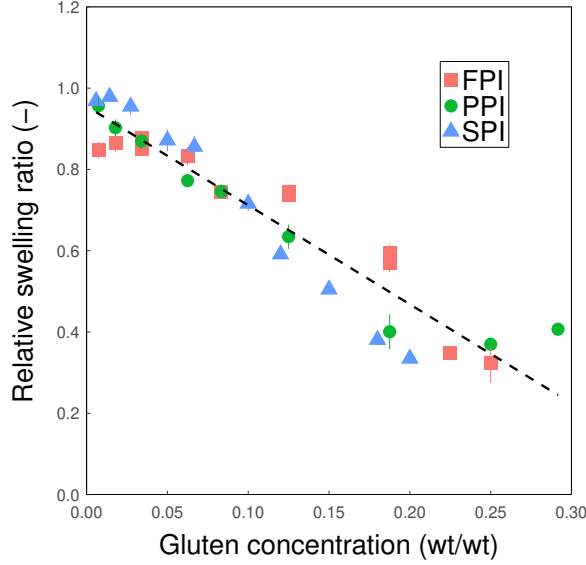
Figure 3.4: Measured levels of non-gluten swelling (FPI, PPI, and SPI; Figure 3.3) were divided by the swelling of their respective single-phase gel with the same DMC. The obtained relative swelling is expressed as function of the gluten fraction of total protein ($n = 3$). Dashed line is a linear fit ($y = -2.436x + 0.955$), with $R^2 = 0.90$.

Deformation of the non-gluten phase

The similar relative reduction in swelling ratio and clear dependence on gluten concentration suggest a universal underlying mechanism. To better understand the apparent universality of the effect of gluten content on mixed gel swelling we will discuss the deformation of the non-gluten phase. As explained in Section 3.3.2, deformation is relative to a reference state, Q_{ref}, which is related to maximum swelling ratio, Q_0 [24]. Due to the mechanical interaction with gluten, this maximum swelling ratio cannot be reached. However, since the water partitioning between the gluten and non-gluten phases before gelation was determined (Equation 3.12), the expected swelling ratio when no mechanical interactions are assumed is known (open symbols; Figure 3.3). Using Equation 3.16 we obtain the values for Q_{ref} for the different proteins and gluten concentrations. The strain on the non-gluten phase is then obtained by entering Q_{ref} and the experimental values for Q (closed symbols; Figure 3.3) into Equation 3.17.

van der Sman [24] constructed a master curve of network deformation (φ/φ_{ref} or equivalently Q_{ref}/Q) versus Π_{ext} normalized with the cross-link density of the gel and identified two distinct regimes. Furthermore, it was concluded that when $Q > Q_{ref}$ the elastic pressure dominates the swelling behaviour, and when $Q < Q_{ref}$ the mixing pressure dominates. The pressure applied by gluten, Π_{gluten}, is known to increase with increasing gluten content of the gel [19]. Gluten content can therefore be considered as proportional to the externally applied pressure, Π_{ext}. By plotting the gluten content as a function of Q/Q_{ref} we obtain an approximation of the master curve as presented by van der Sman [24] (Figure 3.5). Two different slopes can be observed, with a transition around $Q = Q_{ref}$, in line with the master curve shown by van der Sman [24]. This suggests that the same transition from elastic to mixing pressure dominated behaviour might also occur in these gels.

The pressure exerted by gluten on the non-gluten phase depends on the deformation of gluten. Since gluten forms a continuous network in the mixed gels, its deformation must be proportional to the swelling of the non-gluten phase. The apparent master curve in Figure 3.5 suggests this effect might already be captured, which can be qualitatively explained based on the effect of the elastic modulus on the swelling and deformability of polymer networks. A polymer network with a low elastic modulus will swell more but is also more easily deformed than a network with a higher elastic modulus. The greater deformability results in a larger absolute reduction in swelling compared to a network with a higher modulus, and vice versa (Figure 3.3). Due to the balance between the swelling pressure and the external pressure (or gluten pressure), these differences are limited on a relative scale (Figure 3.4). This balance may only be there for materials with a similar Flory–Huggins interaction parameter, as is the case here. Figure 3.5 also shows that gluten interacts in a similar way with the three different proteins used. This suggests that the different protein phases in the mixed gels are arranged in the same way.

Swelling of sheared samples

The gluten-containing mixtures were also swollen after processing in a shear cell. This will relate the shear structuring experiments to the swelling experiments and reveal any effect of thermo-mechanical treatment on swelling. Absolute swelling ratios of the sheared single-phase SPI and PPI gels were significantly higher than of the non-sheared gels; FPI was significantly lower (see caption to Figure 3.6). We note that the differences in swelling between the sheared and non-sheared samples are limited in absolute terms. For sheared SPI and PPI gels, the relative swelling as a function of
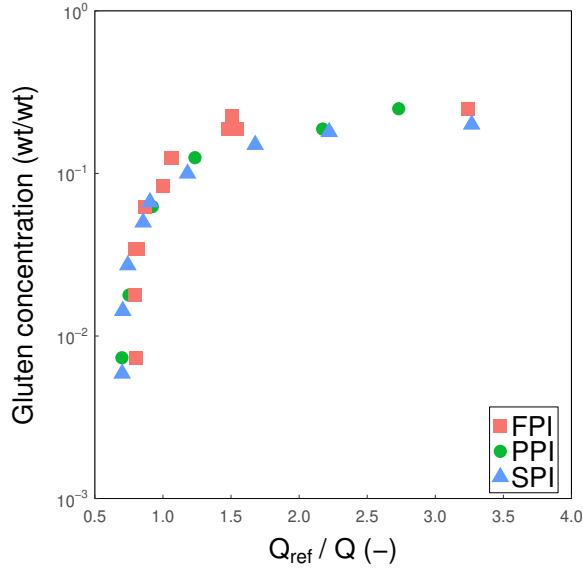
Figure 3.5: Approximation of the master curve as shown by van der Sman [24], with Q_{ref}/Q as a measure for deformation and gluten concentration as a measure for Π_{ext}. Q_{ref} follows from Equation 3.16 and Figure 3.3.

gluten content shows a negative trend, as was also found for the non-sheared samples (Figure 3.6). The gradual reduction in swelling was less extensive but suggests a similar effect of gluten for SPI and PPI. The smaller effect of gluten on swelling may be due to anisotropy in the cross-link density along the shear flow direction. However, anisotropy in swelling was not observed. The effect of gluten content on the swelling of the sheared FPI gels is different from SPI and PPI, with an increase in swelling ratio with gluten content. The sheared FPI samples suffered from skin formation while the SPI and PPI samples did (Supplementary Figure 3.8). The skin appeared to be harder than the bulk of the material. This affected the swelling ratio of the FPI sample. The values of FPI can, therefore, not be compared directly with those of the other proteins. The similar effect of gluten on the swelling of SPI and PPI is an indication that gluten also has a mechanical interaction with the non-gluten proteins after processing in a shear cell.
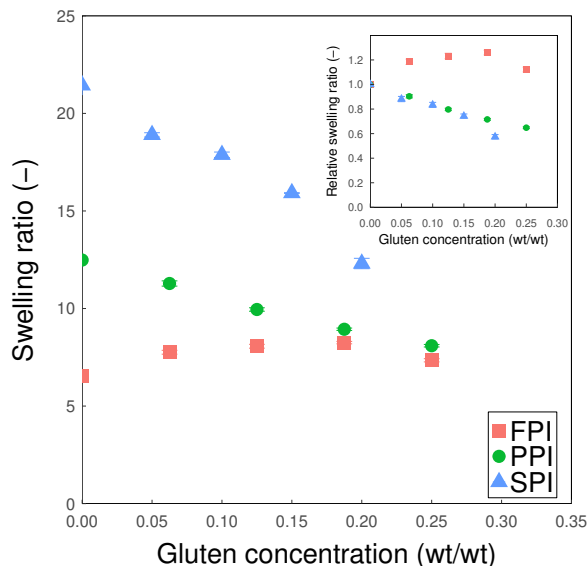
Figure 3.6: The swelling ratio of fully swollen, sheared mixed gels prepared from gluten with either FPI, PPI, or SPI as a function of the gluten concentration at gelation (main figure). Gluten swelling was subtracted used Equation 3.2 to determine the swelling ratio of the non-gluten protein phase. For PPI and FPI a total initial DMC of 0.375 wt/wt was used; for SPI, 0.3 wt/wt was used. The measured levels of non-gluten swelling of sheared samples (FPI, PPI, and SPI) were divided by the swelling of their respective single-phase sheared gel with the same DMC. The obtained relative swelling is expressed as a function of the gluten fraction of total protein (insert). Error bars are standard errors from the mean with n = 3.

3.4.4 Structure formation under shear

To study the relation between the presence of a continuous gluten network and the formation of fibrous structures, sheared gels were produced from FPI, PPI and SPI in combination with gluten using a shear cell. The same compositions were used as for the mixed gels (Section 3.4.3). Gluten content is indicated as the weight fraction of the total protein content. The sheared gels were bent in the parallel direction to the shear flow direction to visualize any fibre formation (Figure 3.7).

Shearing of pure FPI, PPI and SPI doughs without gluten resulted in visually homogeneous gels with no orientation in the shear flow direction. Addition of 0.167

Figure 3.7: Photographs of the macro-structures obtained after structuring FPI-gluten, PPI-gluten and SPI-gluten mixtures in a shear cell. The left column indicates the gluten fraction of total protein (wt/wt), while the numbers presented with the images indicate actual the actual gluten concentration (wt/wt). The shear cell was operated at 140°C for 15 min at a shear rate of 30 rpm (39 s^{-1}). Structures were prepared in duplicate; these are representative images of the structure found in the outer 4 cm of the sample. Each sample has a width of approximately 5 cm ($n = 2$).

wt/wt gluten had no effect on the structure of either the FPI or SPI sample. The PPI sample showed a rough surface after bending without visible orientation or fibres. At 0.33 wt/wt gluten both FPI and PPI mixtures showed structures orientated in the shear flow direction, but no fibres were observed. The SPI mixture showed no orientation at all. For all ingredients fibres appeared only when at least 0.5 wt/wt gluten was added. The individual fibres in the FPI samples seem to be thicker than in the PPI and SPI samples, although the fibres did become thinner as the gluten content approached 1 wt/wt.

3.4.5   General discussion

We investigated the swelling and shear cell structuring of gluten mixed with soy, pea, or fababean protein isolate (SPI, PPI, FPI). Single-phase SPI, PPI, and FPI gels were swollen until equilibrium and used to predict the swelling of the gluten-containing mixed gels. These predictions assumed no interaction between the gluten and non-gluten phases and suggested an increase in non-gluten swelling ratio with increasing gluten content (Figure 3.3). Experimental measurements of mixed gel swelling showed, however, that there was an interaction between the gluten and non-gluten phases, which resulted in a decreased swelling ratio. The absolute levels of swelling differed between protein sources. After normalization with gels of the pure secondary protein phase, seemingly universal behaviour was seen regardless of protein source and absolute swelling ratio (Figure 3.4). Based on our previous study on SPI–gluten mixtures, the interaction can be attributed to the presence of a continuous gluten network [19]. This seemingly universal behaviour indicates that gluten might interact in a similar manner with other proteins as well. Further analysis of the deformation of the polymer network suggested behaviour similar to that reported by van der Sman [24] and underlined the similarity of the interaction with gluten between the different proteins (Figure 3.5). Furthermore, the two apparent master curves obtained suggest that the gluten–non-gluten composites have similar structures for the different proteins. However, additional experiments are necessary to confirm the origin of the universality.

We initially hypothesised there to be a percolation threshold above which a continuous network would be present. This would have been indicated by a sudden reduction in swelling ratio when the gluten content surpassed this threshold. The approximately linear reduction in swelling ratio starting from low gluten contents onward does not support this hypothesis and implies that there is an interaction already at low gluten contents. Our shear cell experiments showed that when gluten is the main

proteinaceous component ($\geq$0.5 wt/wt), fibrous structures can be made with all of the proteins used (Figure 3.7). This level of similarity and interchangeability between protein sources has not been seen before in shear cell processing. Previous studies using SPI or PPI in combination with gluten also found fibres at gluten fractions of 0.5 wt/wt [12, 16]. In contrast, earlier studies reported the presence of fibres in sheared SPI–gluten gels at lower gluten fractions (>0.2 wt/wt [1, 2]). However, direct comparison with the present study is impeded by the lower DMC and processing temperatures used in the mentioned studies (0.3 wt/wt and 95°C), along with the lack of visual representations of the formed structures. Grabowska et al. [1] also reported the formation of fibres using only hydrated gluten (0.3 wt/wt). However, since this was accompanied by hysteresis, the moisture content cannot be compared directly with the current study. We note that recent studies also show an apparent shift towards higher gluten content formulations to produce fibrous structures.

A recent rheological study by Schreuders et al. [12] showed that gluten is a continuous or bi-continuous phase during shear treatment at high temperature (120-140°C) when combined with PPI or SPI. The exact structure of the composite was found to depend on the processing conditions and raw material used. Micro-graphs of mixed SPI-gluten gels taken by Dekkers et al. [16] using confocal scanning laser microscopy (CSLM) show that gluten can be present in elongated domains at relatively low concentrations (gluten fraction = 0.06 wt/wt; total DMC 0.30 wt/wt). Lucas et al. [32] studied the micro-structure of gluten networks in wheat flour doughs in more detail and developed a system to classify the different micro-structures. Some of the observed structures had very thin gluten strands. These thin gluten strands were associated with a more inter-connected and branched network. Possibly, such a continuous gluten network forms at low gluten fractions ($\leq$0.50 wt/wt) when gluten is combined with another protein. Such a low volume but interconnected gluten phase could still limit the swelling of the non-gluten phase, but might not be visible upon inspection of the macro-structure of the sheared material due to its limited volume fraction.

A dominant hypothesis on how protein systems form fibrous structures under shear flow is based on the deformation and solidification of a two-phase system [17, 33, 34]. The dispersed phase is thought to deform and align, resulting in mechanical anisotropy. Grabowska et al. [1] suggested that gluten forms the continuous phase in SPI-gluten based fibrous structures. SPI was, therefore, considered the dispersed phase, contributing to the fibre formation. In mixed (non-sheared) SPI-gluten gels, gluten is thought to form a continuous network that entraps SPI [19]. However, Schreuders et al. [15] showed that under shear flow a structure with gluten being

co-continuous with the second protein can occur, which was concluded based on their rheological behaviour. The presence of a bi-continuous network structure is not in line with the hypothesis of a dispersed and deformed phase.

Our results suggest that the non-gluten phase is not essential to fibre formation as fibres were also obtained in the absence of a second protein, as shown in Figure 3.7. Hydrated gluten could be considered a two-phase system with glutenin and gliadin making up the two respective phases [35]. Hence, hydrated gluten alone could already fulfil the requirement of a dispersed and continuous phase. This could explain why fibres can be produced from hydrated gluten alone. Furthermore, commercial gluten ingredients also contain starch residues, which could act as a second (or third) phase. Addition of limited amounts of a second protein (≥ 0.5 wt/wt) still resulted in the formation of fibres. When gluten was no longer the main component, no fibres were formed. We, therefore, propose that in gluten-containing mixtures, gluten is primarily responsible for the formation of fibres, while the second protein acts merely as a filler. Addition of a second protein can still be useful though, as our results showed that by varying the amount of second protein one can modulate the thickness of the fibres and extent of fibrillation.

We note that the formation of a fibrous structure does not only depend on formulation; process parameters such as temperature and shearing time are key and will need to be adjusted [1, 11, 12]. Nevertheless, a continuous gluten network seems essential to achieve a fibrous structure when using formulations containing gluten.

3.5 Conclusion

We have studied the swelling of single-phase gels from fababean protein, pea protein, and soy protein, as well as mixed gels in combination with gluten. Analysis of the swelling of gluten-containing mixed gels suggested that gluten applies an external pressure that limits non-gluten swelling. This was attributed to the formation of a continuous gluten network. Normalizing the level of swelling with that of a single-phase gel resulted in seemingly universal behaviour between the three studied proteins, regardless of DMC and absolute level of swelling. Shear structuring with a shear cell resulted in the formation of fibre structures when gluten was the main protein component. Hydrated gluten also forms fibres without a second protein present. This suggests that the choice of the non-gluten protein could extend beyond the used in this study. These insights could benefit future investigations into the use of novel ingredients for use in meat analogue products.

Supplementary information

(a)

(b)

Figure 3.8: Representative image of a fababean protein isolate – gluten sample after shear structuring. The darker areas had a skin (Figure 3.8a). Representative image of a sample after shear structuring, without a skin (Figure 3.8b).

References

[1] K.J. Grabowska, S. Tekidou, R.M. Boom, and A.J. van der Goot. Shear structuring as a new method to make anisotropic structures from soy-gluten blends. *Food Research International*, 64:743–751, 2014.

[2] G. Krintiras, J. Göbel, A. van der Goot, and G. Stefanidis. Production of structured soy-based meat analogues using simple shear and heat in a Couette Cell. *Journal of Food Engineering*, 160:34–41, 2015.

[3] J.H. Chiang, S.M. Loveday, A.K. Hardacre, and M.E. Parker. Effects of soy protein to wheat gluten ratio on the physicochemical properties of extruded meat analogues. *Food Structure*, 19 (September 2018):100102, 2019.

[4] M. Nieuwland, P. Geerdink, P. Brier, P. Van Den Eijnden, J.T.M.M. Henket, M.L. Langelaan, N. Stroeks, H.C. Van Deventer, and A.H. Martin. Food-grade electrospinning of proteins. *Innovative Food Science and Emerging Technologies*, 20:269–275, 2014.

[5] K.D. Mattice and A.G. Marangoni. Comparing methods to produce fibrous material from zein. *Food Research International*, 128(October 2019):108804, 2020.

[6] V.L. Pietsch, J.M. Bühler, H.P. Karbstein, and M.A. Emin. High moisture extrusion of soy protein concentrate: Influence of thermomechanical treatment on protein-protein interactions and rheological properties. *Journal of Food Engineering*, 251(August 2018):11–18, 2019.

[7] S.H. Peighambardoust, A.J. van der Goot, R.J. Hamer, and R.M. Boom. A New Method to Study Simple Shear Processing of Wheat Gluten-Starch Mixtures. *Cereal Chemistry*, 81(6):714, 2004.

[8] R.M. van den Einde, A. Bolsius, J.J. van Soest, L.P. Janssen, A.J. van der Goot, and R.M. Boom. The effect of thermomechanical treatment on starch breakdown and the consequences for process design. *Carbohydrate Polymers*, 55(1):57–63, 2004.

[9] R.M. van den Einde, M.E. van der Veen, H. Bosman, A.J. van der Goot, and R.M. Boom. Modeling macromolecular degradation of corn starch in a twin screw extruder. *Journal of Food Engineering*, 66(2):147–154, 2005.

[10] K.J. Grabowska, S. Zhu, B.L. Dekkers, N.C.A. De Ruijter, J. Gieteling, and A.J. van der Goot. Shear-induced structuring as a tool to make anisotropic materials using soy protein concentrate. *Journal of Food Engineering*, 188:77–86, 2016.

[11] B.L. Dekkers, C.V. Nikiforidis, and A.J. van der Goot. Shear-induced fibrous structure formation from a pectin/SPI blend. *Innovative Food Science and Emerging Technologies*, 36:193–200, aug 2016.

[12] F.K.G. Schreuders, B.L. Dekkers, I. Bodnár, P. Erni, R.M. Boom, and A.J. van der Goot. Comparing structuring potential of pea and soy protein with gluten for meat analogue preparation. *Journal of Food Engineering*, 261(May):32–39, 2019.

[13] B.L. Dekkers, R. Hamoen, R.M. Boom, and A.J. van der Goot. Understanding fiber formation in a concentrated soy protein isolate - Pectin blend. *Journal of Food Engineering*, 222:84–92, 2018.

[14] Z. Wang, B. Tian, A.J. van der Goot, and R. Boom. Air bubbles in calcium caseinate fibrous material enhances anisotropy. *Food Hydrocolloids*, 87:497–505, 2018.

[15] F. Schreuders, I. Bodnár, P. Erni, R. Boom, and A. van der Goot. Water redistribution determined by time domain NMR explains rheological properties of dense fibrous protein blends at high temperature. *Food Hydrocolloids*, 101, 2020.

[16] B.L. Dekkers, M.A. Emin, R.M. Boom, and A.J. van der Goot. The phase properties of soy protein and wheat gluten in a blend for fibrous structure formation. *Food Hydrocolloids*, 79: 273–281, 2018.

[17] V.B. Tolstoguzov. Thermoplastic extrusion—the mechanism of the formation of extrudate structure and properties. *Journal of the American Oil Chemists' Society*, 70(4):417–424, apr 1993.

[18] V.L. Pietsch, M.A. Emin, and H.P. Schuchmann. Process conditions influencing wheat gluten polymerization during high moisture extrusion of meat analog products. *Journal of Food Engineering*, 198:28–35, 2016.

[19] S.H.V. Cornet, A.J. van der Goot, and R.G.M. van der Sman. Effect of mechanical interaction on the hydration of mixed soy protein and gluten gels. *Current Research in Food Science*, 3: 134–145, 2020.

[20] A. Bot and D. de Bruijne. Osmotic properties of gluten. *Cereal Chemistry*, 80(4):404–408, 2003.

[21] L. Leibler and K. Sekimoto. On the Sorption of Gases and Liquids in Glassy Polymers. *Macromolecules*, 26(25):6937–6939, 1993.

[22] J.S. Vrentas and C.M. Vrentas. Sorption in Glassy Polymers. *Macromolecules*, 24(9):2404–2412, 1991.

[23] R.G.M. van der Sman and M.B.J. Meinders. Prediction of the state diagram of starch water mixtures using the Flory–Huggins free volume theory. *Soft Matter*, 7:429, 2011.

[24] R.G.M. van der Sman. Biopolymer gel swelling analysed with scaling laws and Flory-Rehner theory. *Food Hydrocolloids*, 48:94–101, 2015.

[25] P.R. Couchman and F.E. Karasz. A Classical Thermodynamic Discussion of the Effect of Composition on Glass-Transition Temperatures. *Macromolecules*, 11(1):117–119, 1978.

[26] R.G.M. van der Sman. Thermodynamics of meat proteins. *Food Hydrocolloids*, 27(2):529–535, 2012.

[27] M. Pouplin, A. Redl, and N. Gontard. Glass transition of wheat gluten plasticized with water, glycerol, or sorbitol. *Journal of Agricultural and Food Chemistry*, 47(2):538–543, 1999.

[28] M. Quesada-Pérez, J.A. Maroto-Centeno, J. Forcada, and R. Hidalgo-Alvarez. Gel swelling theories: the classical formalism and recent approaches. *Soft Matter*, 7(22):10536, 2011.

[29] G. Attenburrow, D.J. Barnes, A.P. Davies, and S.J. Ingman. Rheological properties of wheat gluten. *Journal of Cereal Science*, 12(1):1–14, 1990.

[30] T.S.K. Ng and G.H. McKinley. Power law gels at finite strains: The nonlinear rheology of gluten gels. *Journal of Rheology*, 52(2):417–449, 2008.

[31] E. Derbyshire, D.J. Wright, and D. Boulter. Legumin and vicilin, storage proteins of legume seeds. *Phytochemistry*, 15(1):3–24, 1976.

[32] I. Lucas, T. Becker, and M. Jekle. Gluten polymer networks-A microstructural classification in complex systems. *Polymers*, 8(6), 2018.

[33] V.B. Tolstoguzov, A.I. Mzhel'sky, and V.Y. Gulov. Deformation of emulsion droplets in flow.

Colloid & polymer science, 252:124–132, 1974.

[34] B.L. Dekkers, R.M. Boom, and A.J. van der Goot. Structuring processes for meat analogues. *Trends in Food Science and Technology*, 81:25–36, 2018.

[35] A. Boire, P. Menut, M. Morel, and C. Sanchez. Phase behaviour of a wheat protein isolate. *Soft Matter*, 9(47):11417, 2013.

Chapter 4

Enhancing the water holding capacity of model meat analogues through marinade composition

Abstract

Meat analogues can offer consumers a more sustainable alternative to meat. A successful meat analogue is characterized by a meat-like texture and high juiciness. Juiciness is related to the water holding capacity (WHC). To gain an understanding of how to control the WHC via external conditions, we investigate the effect of ionic strength and pH on water uptake. Model meat analogues were prepared in a shear cell and swollen in baths of known pH and ionic strength. The effect of bath composition on water uptake was determined experimentally and simulated using on Flory–Rehner theory. Experiments and simulations were in qualitative agreement. The results show that water uptake increases with an increasing difference between bath pH and the protein's iso-electric point (pI). At low ionic strengths, the internal pH is near the pI, resulting in reduced swelling. At high ionic strengths, the charge imbalance between gel and bath is limited, also resulting in reduced swelling. At intermediate ionic strengths, swelling increases with decreasing bath ionic strength. Cross-link density negatively relates to WHC and can be controlled via the addition of cross-linking and reducing agents. This work shows that by carefully choosing marinade pH and ionic strength, the WHC of meat analogues can be controlled. These advancements can help improve the sensory characteristics and yield of meat analogues and could enable the production of reduced-salt products.

4.1   Introduction

Meat products can offer consumers an excellent sensory experience. However, their production puts excessive strain on our food production system and the environment [1, 2]. Since consumers are not expected to simply stop eating meat [3, 4], an alternative is needed. Plant-based meat alternatives may offer a more sustainable alternative to meat [5]. This need has intensified the research focused on developing meat-like products from plant-based ingredients. Consumer studies indicate that consumers are most attracted to meat alternatives that accurately mimic the beloved sensory attributes of meat [6]. Several attributes of meat, including fibrousness, can already be found in structures produced with the novel shear cell technology. The shear cell can structure different combinations of bio-polymers into fibrous gels that visually and structurally resemble meat [7–10]. Together with fibrousness, juiciness is one of meat's most desirable attributes [6, 11, 12]. Taste and textural properties of meat and meat analogue products can be enhanced by marination and impregnation [13–16]. A marinade can be a carrier of salt, as well as water-soluble flavours, or fat-soluble flavours when using an emulsion. In addition to flavour, marinade composition could affect the water holding capacity (WHC) of meat and meat analogue products [17, 18].

The WHC and moisture content of meat and meat products are related to their juiciness [11, 19–21]. The WHC of meat can be described with the Flory–Rehner theory of cross-linked polymer networks [22, 23]. Flory–Rehner theory relates the WHC of the polymer network to material properties such as polymer-water affinity and cross-link density [24, 25]. We have recently shown that the Flory–Rehner theory for neutral gels can also adequately describe the WHC of simplified meat analogues made from soy protein and gluten [26]. Since proteins are polyampholytes they can carry both positive and negative charges depending on the pH. English [18] provided an extension for the Flory–Rehner theory that takes the additional swelling due to the local charge density into account [18, 27]. Variations in pH and ionic strength can, therefore, affect the WHC. It was shown that sensory juiciness is strongly affected by marinade pH, although no relationship with WHC was found for short marination times [28]. How the WHC of meat analogues is affected by marinade properties such as ionic strength and pH is currently not well understood.

We use a combination of experiments and simulations to improve our understanding of the effect of pH and ionic strength on the WHC of meat analogues. Model meat analogues prepared with a conical shear cell were swollen in marinades with different

pH and ionic strength. Ionic strength was controlled using either $NaCl$ or KCl. KCl was selected alongside $NaCl$ as it is a commonly used sodium-free alternative for $NaCl$ [29]. The effect of pH and ionic strength on swelling was also simulated using a model based on the extended Flory–Rehner theory. The simulations were aimed at qualitatively explaining the outcomes of the swelling experiments. They should provide insight into how WHC and juiciness can be controlled with pH and ionic strength, alongside cross-link density and structure.

4.2 Theory

4.2.1 Flory–Rehner theory

The water holding capacity of polymer networks can be described with Flory–Rehner theory by relating it to the swelling pressure, Π_{swell}. In the original theory for neutral gels, Π_{swell} has two contributions. The first contribution, Π_{mix}, accounts for the interaction between polymer and solvent. The second contribution, Π_{elas}, accounts for the elastic pressure generated as a result of network deformation upon swelling or de-swelling. Π_{elas} counteracts the moisture sorption due to Π_{mix} at sufficiently high moisture contents. At equilibrium, Π_{swell} is equal to the pressure applied to the gel:

$$\Pi_{ext} = \Pi_{swell} = \Pi_{mix} - \Pi_{elas} \tag{4.1}$$

Π_{ext} is thus the pressure externally applied on the gel (e.g. via centrifugation). Under free swelling conditions, such as when submerged in a bath, Π_{ext} can also be zero. In that case, Π_{swell} is also zero and thus Π_{mix} equals Π_{elas}. Flory–Rehner theory has been extended to describe the swelling as a result of different ion concentrations inside and outside the gel, as captured by the ionic pressure Π_{ion} [30]. Π_{ion} contributes to Π_{swell} as:

$$\Pi_{ext} = \Pi_{swell} = \Pi_{mix} + \Pi_{ion} - \Pi_{elas} \tag{4.2}$$

According to the Rehner hypothesis all three contributions are independent. The three contributions to the swelling pressure are described below.

4.2.2 Mixing pressure

We describe Π_{mix} with Flory–Huggins theory, which depends on the Flory–Huggins interaction parameter χ. The mixing pressure is taken as:

$$\Pi_{mix} = \frac{RT}{v_w} \left[\ln\left(1 - \varphi\right) + \varphi(1 - \frac{1}{N}) + \chi\varphi^2 \right] \tag{4.3}$$

v_w is the molar volume of water, R is the universal gas constant, T is the absolute temperature, and φ is the volume fraction of polymer. N is the ratio between molar volumes of polymer and water [31]. Because of the relatively large volume of proteins, the term $\frac{1}{N}$ is effectively zero. We have previously determined the values of χ for soy protein isolate and gluten by fitting the sorption data with the extended Free Volume Flory–Huggins (FVFH) theory [32]. χ is 0.91±0.02 for soy protein; for gluten χ is 1.16±0.04 [26]. The applicability of FVFH theory has already been demonstrated for numerous foods [23, 26, 31, 33, 34] and bio-polymer gels [35]. Note that FVFH theory includes an additional term to account for the increased sorption in the glassy regime. Since food polymers present in wet materials, such as meat analogues, are in the rubbery regime, we have omitted the free volume term our expression for Π_{mix} (Equation 4.3). The interaction parameter, χ, is composition dependent [36]:

$$\chi = \chi_0 + (\chi_1 - \chi_0)\,\varphi^2 \tag{4.4}$$

with χ as the effective Flory–Huggins interaction parameter and χ_0 and χ_1 as the interaction parameters under dilute and concentrated conditions respectively. Water is a theta solvent for proteins at very low polymer concentrations; χ_0 is therefore 0.5.

4.2.3 Elastic pressure

We describe the network deformation and resulting elastic pressure, Π_{elas}, with the affine network model:

$$\Pi_{elas} = G_{ref}[\tilde{\varphi}^{1/3} - \frac{\tilde{\varphi}}{2}] \tag{4.5}$$

$\tilde{\varphi}$ is defined as:

$$\tilde{\varphi} = \frac{\varphi}{\varphi_{ref}} \tag{4.6}$$

G_{ref} and φ_{ref} are the shear modulus and polymer volume fraction in the reference state. The reference state refers to the value of φ at which the polymer chains are neither extended nor compressed [37]. It must be mentioned that the physical meaning of φ_{ref} and the conditions at which φ_{ref} should be determined are still under debate [25, 38]. φ_0 is related to G_{ref} via [39, 40]:

$$G_{ref} \propto \varphi_0^{9/4} \tag{4.7}$$

φ_0 and φ_{ref} are related via $\varphi_0 = 2/3\varphi_{ref}$ [35]. We use the relation between G_{ref} and φ_{ref} to select reasonable values for φ_{ref} and G_{ref} in our simulations [26].

4.2.4   Ionic pressure

The approach developed by English [18] was used to describe the swelling as a result of an unequal distribution of charges between bath and gel. The bath is assumed to be in excess and is not affected by the gel. The bath is a $NaCl$ solution of known ionic strength and pH, comparable to the experimental set-up. The ionic strength is regulated by varying the salt concentration c_{NaCl}. The counter ions for the protein side-groups in the gel phase are assumed to be Na^+ and Cl^-.

When ion concentrations become sufficiently high, their activity γ can deviate from 1. The conditions used in our model simulations are in the regime where $\gamma \neq 1$ and activity coefficients should be taken into account. We initially accounted for the non-ideal behaviour using the Pitzer equations for the bath, and Debye-Hueckel for the gel phase [41]. However, accounting for the non-ideal behaviour had only a minor effect on the absolute outcome of the simulations and did not change the qualitative conclusions that could be drawn. van der Sman et al. [41] similarly showed that the qualitative outcomes of simulated swelling experiments are similar when non-ideal effects are ignored. The lengthy equations were, therefore, omitted and ideality was assumed throughout.

We first describe the equilibria in the bath, followed by the equilibria in the gel. The subscripts α and β were used to differentiate between the gel and bath respectively.

Equilibria in the bath

The bath is a $NaCl$ solution of known concentration, c_{NaCl}, and pH. $NaCl$ is assumed to be fully dissociated. The pH of the bath is regulated by the addition of HCl or $NaOH$. The bath pH depends on the concentration of protons in the bath $c_{H,\beta}$. The dissociation of water is governed by its dissociation constant K_w and the bath water activity a_w:

$$K_w = \frac{c_{H,\beta} c_{OH,\beta}}{a_w} \tag{4.8}$$

K_w is taken to be a constant with value 10^{-14}. a_w follows from Raoult's law.

Equilibria in the gel

We consider a soy protein network with both acidic and basic side-groups, capable of carrying either negative or positive charges respectively. The concentrations and pKa values of the ionizable side groups on soy protein were determined by van der Sman

Table 4.1: Concentrations and pKa values of the different ionizable protein side-groups on soy protein as determined by van der Sman et al. [41] via acid titration.

AA (three letter code)	Concentration ($\mathrm{mol\,kg^{-1}}$)	pKa
Glutamic acid (Glu)	0.10	4.25
Aspartic acid (Asp)	0.66	3.67
Histidine (His)	0.43	6.54
Lysine (Lys)	0.306	10.67

et al. [41] via acid titration on the premise that the effective charge of the protein is zero at the iso-electric point (pI; Table 4.1). We use the subscripted three letter codes to refer to the different amino acids (Table 4.1). These are Glu, Asp, His and Lys for Glutamic acid, Aspartic acid, Histidine and Lysine respectively. The ionizable groups were reported as the number of residues per gram protein n_i. By multiplying n_i with the density of protein, ρ_p, and the polymer volume fraction, φ, the concentration of ionizable groups, $C_{A,i}$, is obtained:

$$C_{A,i} = n_i \rho_p \varphi \tag{4.9}$$

(De-)protonation of the acidic (Glu, Asp) and basic side-groups (His, Lys) is indicated with the subscripts $_{AH} \longleftrightarrow _{A^-}$ and $_{A} \longleftrightarrow _{AH^+}$ respectively. The dissociation reactions of the acidic side-groups depend on $K_{A,i}$ via:

$$K_{A,i} = \frac{c_{H,\alpha} c_{A^-,i}}{c_{AH,i}} \qquad i = Glu, Asp \tag{4.10}$$

The dissociation of basic side groups His and Lys depends on $K_{A,i}$ via:

$$K_{A,i} = \frac{c_{H,\alpha} c_{A,i}}{c_{AH^+,}} \qquad i = His, Lys \tag{4.11}$$

The degree of side-group dissociation θ_i depends on the ratio of dissociated side-groups over all side-groups of species i. For Glu and Asp, θ_i is given by:

$$\theta_i = \frac{c_{A^-,i}}{c_{A,i}} = \frac{K_{A,i}}{K_{A,i} + c_{H,\alpha}} \qquad i = Glu, Asp \tag{4.12}$$

Since His and Lys are charged at low pH, θ_{His} and θ_{Lys} are given by:

$$\theta_i = \frac{c_{AH^+,i}}{c_{A,i}} = 1 - \frac{K_{A,i}}{K_{A,i} + c_{H,\alpha}} \qquad i = His, Lys \tag{4.13}$$

The conservation of ionizable side-groups is ensured by:

$$c_{A,i} = c_{AH,i} + c_{A-,i} \qquad\qquad i = Glu, Asp \qquad\qquad (4.14)$$

$$c_{A,i} = c_{AH+,i} + c_{A,i} \qquad\qquad i = His, Lys \qquad\qquad (4.15)$$

The concentration of positive and negative counter ions are c_+ and c_-. $c_{H,i}$ and $c_{OH,i}$ are assumed to be negligible compared to c_{NaCl}. Therefore, c_+ and c_- are taken as $c_+ \approx c_{Na^+}$ and $c_- \approx c_{Cl^-}$. The ionic strength is thus related to c_+ and c_- via:

$$c_+ c_- = I^2 \qquad\qquad (4.16)$$

The Donnan equilibria are:

$$\frac{c_{Na,\alpha}}{c_{Na,\beta}} = \frac{c_{OH,\beta}}{c_{OH,\alpha}} \qquad\qquad (4.17)$$

$$\frac{c_{Cl,\alpha}}{c_{Cl,\beta}} = \frac{c_{H,\beta}}{c_{H,\alpha}} \qquad\qquad (4.18)$$

Since $\frac{c_{H,\alpha}}{c_{H,\beta}} = \frac{c_{OH,\beta}}{c_{OH,\alpha}}$, we can express c_- and c_+ as the ratio between $c_{H,\alpha}$ and $c_{H,\beta}$:

$$c_+ = \frac{I c_{H,\alpha}}{c_{H,\beta}} \qquad\qquad (4.19)$$

$$c_- = \frac{I c_{H,\beta}}{c_{H,\alpha}} \qquad\qquad (4.20)$$

The electro-neutrality condition of the gel is therefore given by:

$$
\begin{aligned}
& c_{A,His}\left(1 - \frac{K_{His}}{K_{His} + c_{H,\alpha}}\right) + c_{A,Lys}\left(1 - \frac{K_{Lys}}{K_{Lys} + c_{H,\alpha}}\right) + \frac{I c_{H,\alpha}}{c_{H,\beta}} + c_{H,\alpha} \\
& = \quad \frac{c_{A,Glu} K_{Glu}}{K_{Glu} + c_{H,\alpha}} + \frac{c_{A,Asp} K_{Asp}}{K_{Asp} + c_{H,\alpha}} + \frac{K_w}{c_{H,\alpha}} + \frac{I c_{H,\beta}}{c_{H,\alpha}}
\end{aligned}
\qquad (4.21)
$$

By filling out the above equations into the electro-neutrality condition and simplifying, we arrive at a lengthy sixth-order polynomial similar to English [18]. The polynomial was omitted because of its size and poor readability.

The proton concentration inside the gel was obtained by solving the electro-neutrality condition with respect to $c_{H,\alpha}$, using a numerical solver in Python. The degrees of dissociation for the different side-groups, θ_i, are then obtained from their dissociation constants. The molar concentration of ionized groups on the protein follows from:

$$n_p = \sum_i z_i \theta_i c_{A,i} \qquad\qquad (4.22)$$

With n_p as the molar concentration of ionized side-groups and z as side-group valency. We use the expression by Horkay et al. [42] for the ionic pressure:

$$\Pi_{ion} = 2RT\left[\sqrt{I^2 + (\frac{1}{2}n_p)^2} - I\right] \tag{4.23}$$

4.3 Materials and methods

4.3.1 Materials

Soy protein isolate (SPI, Supro 500E, Solae, St Louis MO, USA; 81.7±1.1 % protein Nx5.7; 95.2±0.4wt % DMC) and vital wheat gluten (Roquette, Lestrem, France; protein 77.9±0.1 % Nx5.7; 92.5±0.7 wt% DMC) were obtained from commercial sources. The protein isolates contained 1.33±0.01 and 0.39±0.01 wt% $NaCl$ equivalents respectively [26]; this was accounted for when setting the ionic strength of the solutions. Glutaraldehyde (25 % aqueous solution), dithiothreitol (DTT; 99 %), sodium chloride ($NaCl$), potassium chloride (KCl), disodium phosphate (Na_2HPO_4), monosodium phosphate (NaH_2PO_4), and all other reagents used were of analytical grade and were obtained from Sigma-Aldrich (Steinheim, Germany). Mili-Q water was used for all experiments (IQ7000, Merck KGaA, Darmstadt, Germany).

4.3.2 Sample preparation

Fibrous model meat analogue samples were prepared from soy protein isolate (SPI), gluten, $NaCl$, and water in the weight ratio of 23 : 7 : 1 : 69 using an in-house built high-temperature shear cell (HTSC; Wageningen University and Research; [8]), resulting in a DMC of 29.4 wt%. The sample preparation procedure and the used formulation have previously been described in detail by Grabowska et al. [7]. Samples were prepared as follows. $NaCl$ was dissolved in water and the SPI added, followed by vigorous mixing with a spatula until a homogeneous paste was obtained. The paste was covered with Parafilm (Pechiney Plastic Packaging, Inc., IL, USA) to prevent water evaporation and left to hydrate for 30 min. After hydration, gluten was added, followed by further mixing. The obtained homogeneous mixture was transferred to the shear cell, pre-heated at 95°C. The shear cell was sealed hermetically by lowering the top cone and applying a sealing pressure of 2 bar. The shearing process was started immediately thereafter by applying a shear rate of 39 s^{-1} at the edge sample's edge (30 rpm) for 15 min. After shearing, the system was cooled down in 5 min

to a temperature of 50°C by connecting it to a cooling oil bath (Julabo PrestoPlus LH85, Seelbach, Germany). After opening the shear cell, the sample was immediately transferred to a hermetically sealed bag to prevent evaporative moisture loss. After the bagged samples reached room temperature (22°C) they were horizontally placed in a freezer and frozen at -18°C until use to prevent sample spoilage.

4.3.3   Vacuum impregnation and swelling

Samples were thawed at room temperature before use. Samples with a diameter of 7 mm and a height of 5 mm were taken with a sharp biopsy punch. Vacuum impregnation was carried out by placing samples in the bath solution and exposing them to a vacuum of 30 mbar for 60 min using a vacuum pump (SC 950, KNF Neuberger GmbH, Freiburg, Germany). After the vacuum was released sample containers were sealed and left to equilibrate overnight at 4 °C. Various bath compositions were used as described in the next paragraph. Some samples underwent a washing treatment by replacing the water frequently until the washing water reached a constant conductivity.

Bath composition

Bath composition was varied with respect to pH and ionic strength. The pH was varied between pH 6 and pH 8 with a step size of 0.5, and stabilized using phosphate buffers. The buffer solutions were prepared by mixing stock solutions of Na_2HPO_4 and NaH_2PO_4 in appropriate ratios. The ionic strength was adjusted to 0.002, 0.01, 0.05, 0.09, 0.15, 0.25, 0.43, or 0.8 m by adding either water or a $NaCl$ solution. Actual ionic strength were calculated afterwards for each sample separately. In some experiments, $NaCl$ was replaced with KCl. Where applicable, glutaraldehyde or DTT were diluted with buffer to achieve the desired concentrations. The buffer's ability to stabilize the pH was confirmed in preliminary tests.

4.3.4   Determination of the water holding capacity

The water holding capacity (WHC) is expressed as the swelling ratio Q and was determined using a similar method as Paudel et al. [31]. Q was determined based on the polymer volume fraction at maximum swelling, φ_0. φ_0 is based on the dry weight fraction of polymer, y_p, and the assumption that no polymer is lost during swelling. Dry weight was determined after drying at 105°C for 24 h. φ_0 was calculated

as:

$$\varphi_0 = \frac{y_p/\rho_p}{(y_p/\rho_p) + (1 - y_p)/\rho_w} \tag{4.24}$$

Swelling ratio Q relates to φ_0 via:

$$Q = \varphi_0^{-1} \tag{4.25}$$

ρ_p and ρ_w are the polymer and water densities with values 1330 $\mathrm{kg\,m^{-3}}$ and 1000 $\mathrm{kg\,m^{-3}}$ respectively. y_p was determined gravimetrically after drying at 105°C for 24h. Simulation results were normalized to the level of swelling at the pI (pH 5) to obtain a measure for Q.

4.3.5 Statistics

The number of repetitions differed between experiments and is indicated with n. Error bars indicate the 95 % confidence interval of the observation. Where applicable, significant differences were tested using a one-way ANOVA and Tukey test.

4.4 Results and discussion

We have studied the swelling of a soy protein and wheat gluten-based model meat analogue prepared. The pH and ionic strength of the bath were varied to investigate their effect on swelling. Cross-link density was varied by adding cross-linking or reducing agents to the marinades. Model simulations based on the extended Flory–Rehner theory were run alongside the experimental work and are part of the discussion.

4.4.1 Experimental results

Effect of pH and I on maximum swelling

Model meat analogues were swollen in bath solutions with different pH and ionic strength. The level of swelling was determined and is expressed as the swelling ratio Q (Figure 4.1). Bath ionic strength, I, affects Q, with low I resulting in more swelling than high I. Washing samples with water until constant conductivity, and low I, resulted in the highest level of swelling. There is an apparent plateau at $Q \approx 4.75$ when $I > 0.5$. At moderate I ($I \approx 0.01 - 0.2$), pH has a pronounced effect on Q, with an increase in pH resulting in more swelling. The effect of pH on swelling is weakened
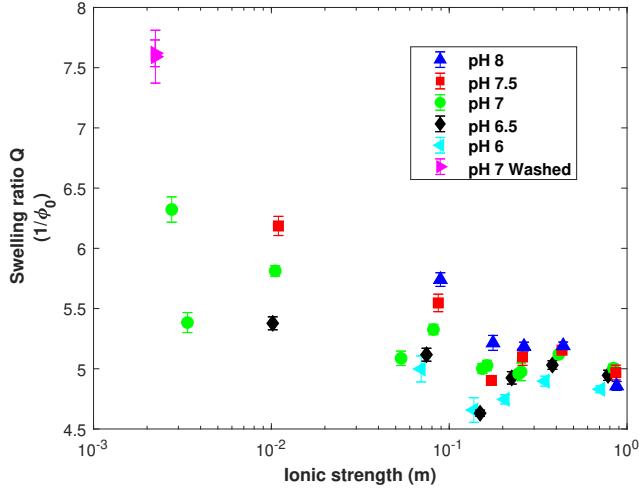
Figure 4.1: Maximum level of swelling expressed as a function of bath ionic strength and pH. The bath was a phosphate buffered saline solution, or water in the case of the lowest ionic strength. Error bars are the 95% confidence intervals with n=3.

as I increases, as indicated by the similarity in Q between samples around $I \approx 0.8$.

The effect of potassium chloride (KCl) on the WHC was also determined as KCl is a commonly used alternative to $NaCl$ (Figure 4.2). To exclude any effect of the phosphate buffer, bath solutions were prepared without a buffer. The solutions thus had a pH equal to the initial sample pH of 7. Both $NaCl$ and KCl showed a decrease in WHC as the ionic strength increased, and an apparent plateau at high ionic strength. Samples swollen in KCl solutions show similar levels of swelling compared to those swollen in $NaCl$ solutions at high ionic strengths ($I > 0.1$). A minor but significant increase in swelling is noticeable at low ionic strength when using KCl instead of $NaCl$, as indicated by the lack of overlap between confidence intervals. No significant effect was observed at higher ionic strengths (as confirmed with ANOVA; not shown). The origin of the minor increase at low ionic strength cannot be identified based on our results. We do note that commercially available meat analogue products tend to have ionic strengths over 0.1 m [43]. At such ionic strengths the effect of using KCl on WHC does not differ from that of $NaCl$.
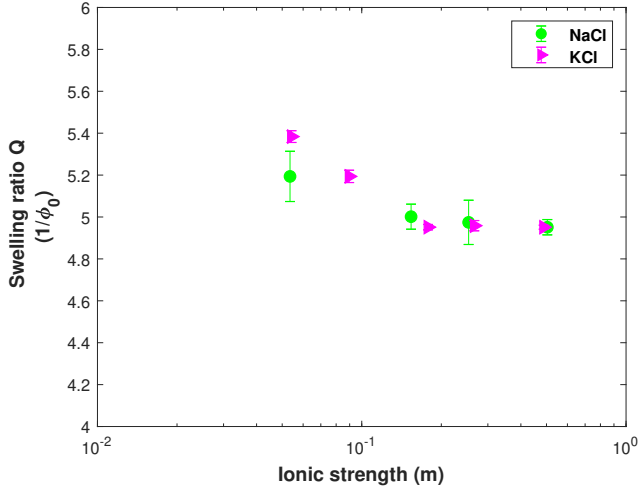
Figure 4.2: Maximum level of swelling as a function of bath ionic strength. The ionic strength was adjusted with either $NaCl$ or KCl. The pH was 7 and was not adjusted. Error bars are the 95% confidence intervals with n=3.

Salt addition before shear-induced structuring

$NaCl$ is commonly added to the hydrated soy-gluten mixture prior to shear-induced structuring [7, 9]. We have omitted the addition of $NaCl$ before shear-induced structuring and tested its effect on WHC. The samples with and without added $NaCl$ had a visually similar structure. Swelling in bath solutions of high ionic strength revealed no significant effect on the WHC (Table 4.2). Also when both samples were washed, no significant effect on the WHC was found. This suggests salt addition before structuring has no irreversible effects on WHC.

Effect of cross-link density on swelling

The cross-link density was altered through the addition of cross-linking agent glutaraldehyde and reducing agent DTT. Glutaraldehyde can form cross-links between various functional groups of proteins [44], while DTT disrupts disulfide bonds [45]. Cross-linking with glutaraldehyde had a negative effect on WHC, as indicated by the decrease in swelling ratio Q (Figure 4.3a). WHC reduced proportionally upon increasing the glutaraldehyde concentration. DTT had the opposite effect and

Table 4.2: Effect of salt addition to the soy protein - gluten mixture prior to shear-induced structuring on WHC. Standard formulation contained 1 wt% $NaCl$. All baths had pH 7. Values are presented as swelling ratio $Q \pm$ confidence interval. Letters indicate different significant groups ($p = 0.05$).

Formulation	Bath ionic strength (m)	Swelling ratio Q
Standard	0.25	4.9±0.2 [a]
No $NaCl$ added	0.25	5.1±0.1[a]
Standard	0.002	7.6±0.1[b]
No $NaCl$ added	0.002	7.6±0.1[b]

increased the WHC (Figure 4.3b). For DTT, no concentration dependence was observed. Conductivity measurements revealed no effect of glutaraldehyde or DTT addition on ionic strength (data not shown).

4.4.2 Model simulations and discussion

Model considerations

The effects of pH and I on the swelling of a simplified meat analogue were simulated using the extended Flory–Rehner theory. The bath is a $NaCl$ containing solution with a pH between 2 to 12. The cross-link density was varied by adjusting G_{ref}. The experimental results were explained based on the model simulations and their implications discussed. Gluten swelling accounts for only a minor part of mixed soy protein - gluten gel swelling [26]. However, gluten can exert an additional (mechanical) pressure on soy in mixed soy-gluten gels when present at sufficiently high concentrations [26]. Since the magnitude of this effect can not be predicted accurately at this time, a more simplified meat analogue containing solely soy protein was assumed for the simulations. Given the minor contribution of gluten to the overall swelling, our simulations can still provide meaningful qualitative information. The degree of swelling was determined by solving $\Pi_{ext} = \Pi_{swell}(\varphi) = 0$. The degree of swelling is expressed with the normalized swelling ratio Q. Q is obtained by normalizing with the degree of swelling at the pI ($Q = \phi/\phi_{pI}$).

The effect of ionic strength and pH on Q near the pI

The simulated swelling data is presented as a function of pH instead of ionic strength (like in Figure 4.1) to improve visibility of the observable effects (Figure 4.4). The
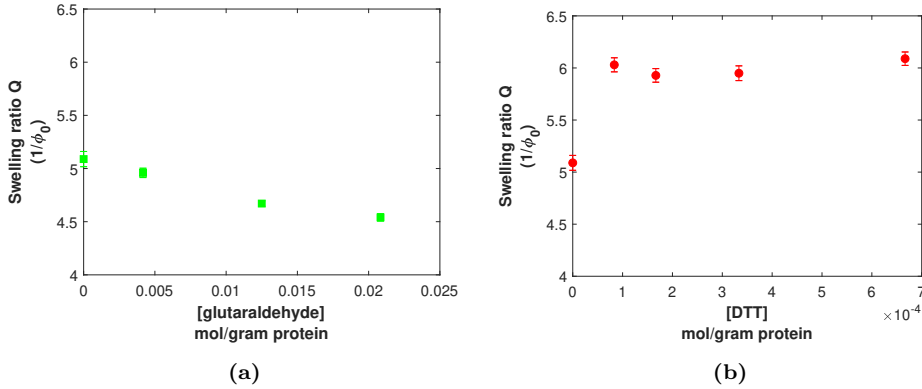
Figure 4.3: Swelling as affected by the addition of glutaraldehyde and DTT. The ionic strength was 0.03 m for all samples. The pH was 7 and was not adjusted. Error bars are the 95% confidence intervals with n=3.

insert in Figure 4.4 serves to ease comparison with Figure 4.1. The simulation results show a minimum in swelling ratio Q around the pI of soy protein (Figure 4.4; pH 5). The swelling minimum is in good agreement with the reported pI of soy protein ($pI \approx 4.5 - 5$; e.g. [46]), as van der Sman et al. [41] determined the number of lysine residues based on the pI. Swelling increases on either side of the swelling minimum as the bath pH moves away from the pI. This is a result of increased protein net charge due to additional side-group dissociation. Lowering the ionic strength results in a progressive widening of the swelling minimum (Figure 4.4 left). When the ionic strength becomes sufficiently high ($0.01 > I > 1$), ionic strength no longer affects swelling around the pI (Figure 4.4 right). As the ionic strength takes extreme values ($I > 1$), the swelling minimum widens once more. At high I, non-ideal ion behaviour could be of importance.

pH buffering by proteins near the pI

The observed widening and narrowing of the swelling minimum around the pI upon changing the ionic strength in the range $I < 1$ is a result of the ability of proteins to act as pH buffers. At the pI, net protein charge is zero. As the pH changes, side-groups dissociate while satisfying the electro-neutrality condition. When sufficient ions are present in the bath solution (moderate to high ionic strength), the electro-neutrality condition can be satisfied by taking up counter-ions from the bath.
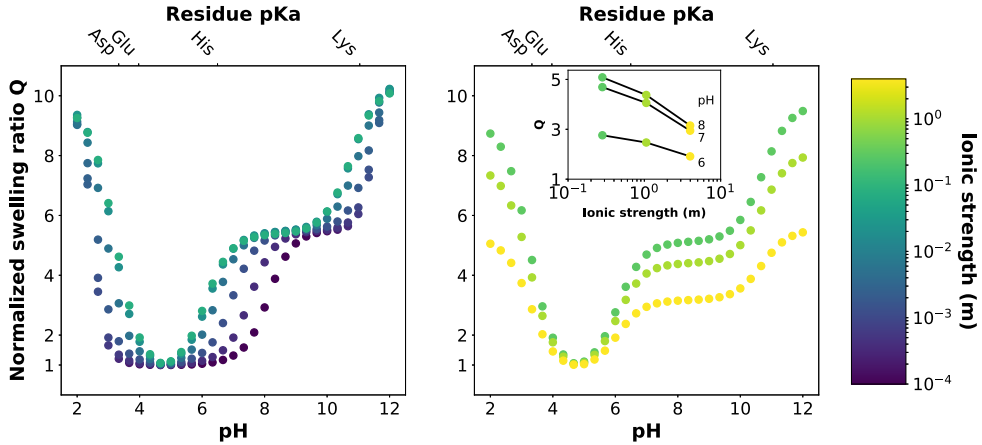
Figure 4.4: Model simulations of the level of maximum swelling, based on the extended Flory–Rehner theory with $\Pi_{ext} = 0$ for different ionic strength and pH. Low (left) and high (right) ionic strengths are presented separately for clarity. The insert serves to ease qualitative comparison with Figure 4.1. The gel's elastic properties were taken as $G_{ref} = 50\text{kPa}$ and $\varphi_{ref} = 0.091$. The used colour map should scale well with (printed) greyscale.

However, at low bath ionic strengths, counter-ion availability is limited. To achieve gel electro-neutrality, side-group dissociation must be limited to reduce the number of counter-ions required. Since this occurs near the pI, the gel's internal pH will have deviated from the bath pH and be close to the pI (Figure 4.5). The internal gel pH close to the pI thus explains the widened swelling minimum near the pI at low ionic strength.

The reduced swelling at low ionic strengths was not observed experimentally, even after simulating an infinitely large bath of low I through repeated washing with de-ionized water (Figure 4.1). A possible explanation lies in the composition of the (commercial) protein isolates used in this study. Commercial isolates can contain a considerable amount of ions. Possibly, these ions were only partially washed out during the swelling experiments, either due to slow diffusion or protein-ion binding. As shown by Borukhov et al. [47], polymer charge might also contribute to the ionic strength, and elevate the ionic strength. Both situations could result in an elevation of the gel's internal ionic strength.
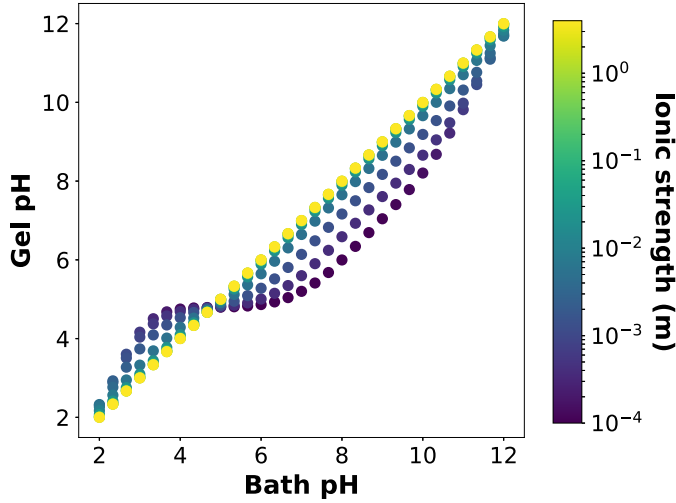
Figure 4.5: Internal gel pH as a function of the bath pH and buffer concentration, as determined by solving the electro-neutrality condition (Equation 4.21). The gel's elastic properties were taken as $G_{ref} = 50$kPa and $\varphi_{ref} = 0.091$. The used colourmap should scale well with (printed) greyscale.

The effect of pH on Q

When the pH moves from the pI, swelling ratio Q increases as a result of increased protein charge. Changes in Q occur near the pKa of the different amino acid residues. In the pH range, 7.5 - 9, an apparent plateau forms, indicating swelling is not affected by pH. At these pH values, the two acidic side-groups are deprotonated and charged, while histidine is neutral and lysine is protonated. As the pH approaches the pKa of Lysine (pH 10.7), Lysine is deprotonated. The protein net charge will have increased, which explains the additional swelling. At the limit of high and low pH, all available groups will have dissociated. Further increasing or decreasing the pH does not result in increased polymer charge and, therefore, does not affect swelling.

In reality, the pKa of an individual amino acid residue is affected by its local environment [48]. The effect of pH on swelling is, therefore, more gradual as the pH passes through the range of pKa values of a given amino acid. This explains why there was still a pronounced effect of pH on swelling in the pH range 7.5 - 9 (Figure 4.1). Increasing the ionic strength results in reduced swelling for all pH values except
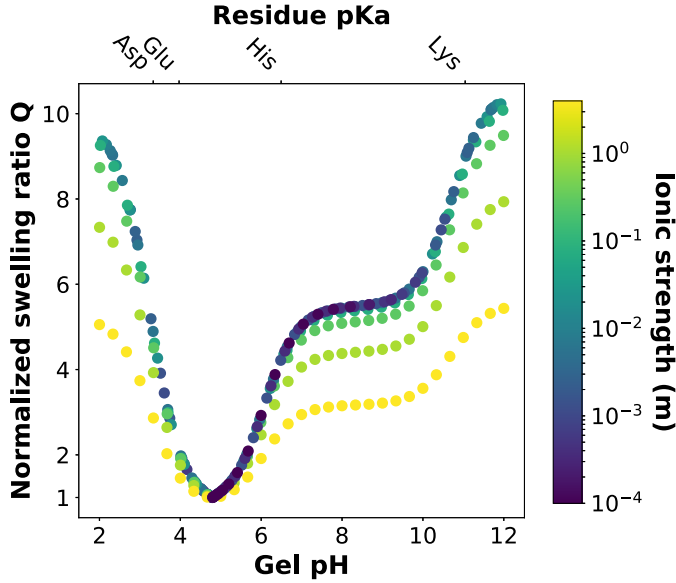
Figure 4.6: Normalized swelling ratio Q as function of the internal gel pH and bath ionic strength. The gel's elastic properties were taken as $G_{ref} = 50$kPa and $\varphi_{ref} = 0.091$. The used colourmap should scale well with (printed) greyscale.

the pI. The greater ionic strength results in a lower ionic pressure and therefore reduced swelling. This also explains the widening of the swelling minimum around the pI at high ionic strength. Since the proteins have no net charge, swelling at the pI is not affected by ionic strength. Although the experimental pH range is narrower, the same trend is observed; moving the bath pH from the pI results in additional swelling (Figure 4.1). The detrimental effect of high ionic strength on swelling as shown by the simulations is in line with our experimental observations. Plotting Q as a function of the internal gel pH, all but the highest ionic strength data points collapse onto a single curve (Figure 4.6). This shows that the main function of ionic strength is to modulate the effect of pH. Thus, the ionic strength indirectly controls swelling by affecting the internal gel pH.

The effect of cross-link density on swelling

The shear modulus, G_{ref}, is proportional to the cross-link density [49]. By varying G_{ref} we can further study the effect of the cross-link density on WHC (Figure 4.7). In our simulations, increasing the modulus resulted in reduced swelling. Similarly, reducing the modulus increased WHC. This is what would be expected based on Equation 4.1 and 4.5, which show that a greater modulus results in a greater resistance to swelling. Reducing G_{ref} thus results in a larger relative contribution of the mixing and ionic pressure to the swelling pressure, and results in more swelling.

The experimental results show a similar relation between WHC and cross-link density. Upon increasing the cross-link density with glutaraldehyde, the WHC progressively declined. Reducing the disulfide bonds with DTT did have a positive effect on WHC, but no effect of concentration was visible. Glycinin, the main protein in soy, has 2 mole disulfide bonds per mole protein (approximately $6.7\mu\text{mol g}^{-1}$) [50], which is lower than the concentrations of DTT used in the experiments. Glycinin also contains free sulfhydryl groups, which decrease upon heating [51]. This suggests additional disulfide bonds may have been present. Furthermore, gluten also contains disulfide bonds [52]. However, the lack of a concentration-dependence in the WHC suggests all disulfide bonds were already reduced at the used lowest concentration of DTT, and that the actual number of disulfide bonds is below the lowest concentration of DTT used. Peters et al. [45] also reported a positive effect of DTT on the WHC of whey protein particles and did find a concentration dependent response. This suggests that such an effect could have been visible at lower DTT concentrations. Glutaraldehyde acts on several functional groups on proteins [44], which could explain why it did show a concentration effect. Soy protein gels and extrudates are stabilized not only by disulfide bonds but also by physical interactions such as hydrogen bonds, hydrophobic interactions and ionic interactions [53, 54]. The physical bonds remaining after DTT treatment formed a sufficiently strong network to prevent further swelling. Lowering salt content prior to shear-induced structuring showed that the addition of $NaCl$ has no irreversible effects on WHC (Table 4.2). Furthermore, the fibrous structure was not affected. This suggests the importance of ionic cross-links is limited.

4.4.3   General discussion

We have shown that simulations based on Flory–Rehner theory are in good qualitative agreement with experimental observations of the swelling of model meat analogues at a range of pH values and ionic strengths. Our simulations show that low ionic strength results in reduced swelling over a wide range of pH values due to an internal gel pH
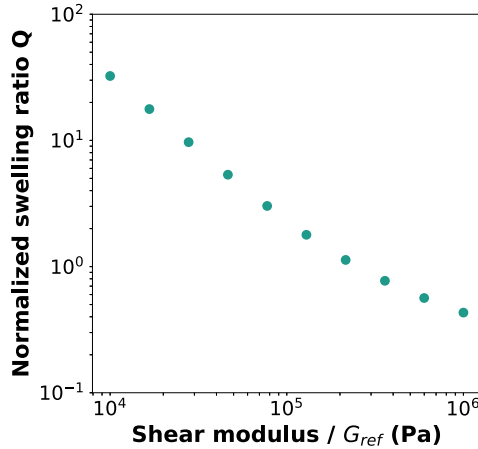
Figure 4.7: Simulations of the effect of cross-link density on swelling ratio Q. Cross-link density was altered by varying G_{ref}. The corresponding values of ϕ_{ref} range from 0.048 to 0.30. The ionic strength was 0.03 m and the pH was 7.

close to the pI. The gel minimizes side-group dissociation to achieve electro-neutrality when counter ions are limited. The presence of more ions can, therefore, be beneficial to the water uptake by meat analogues. Ions present in soybean and its derived ingredients, or added during processing, increase the gel's internal ionic strength and thereby limit the gel's buffering capacity. This could explain the experimentally observed swelling maximum at low bath (/marinade) ionic strengths. While some ions should be present to act as counter-ions, the addition of copious amounts of salt is detrimental to the WHC. The development of salt-reduced meat analogue products with improved juiciness might, therefore, be possible.

Small pH alterations can greatly improve water uptake by model meat analogues and improve product yield. Increased moisture content might be beneficial for the product's sensory properties by enhancing the juiciness. Tailoring product formulation and post-structuring process conditions can, therefore, have a substantial effect on the final product properties. We do note that pH adjustment of concentrated protein products is challenging due to the high buffering capacity of proteins. The use of concentrated acid or base might, therefore, be unavoidable.

Cross-link density can be used to modify the WHC. Increasing the cross-link density reduces WHC while reducing cross-link density results in improved WHC.

Since glutaraldehyde and DTT are by no means fit for human consumption, cross-linking and proteolytic enzymes such as trans-glutaminase [45] and papain could be considered to achieve the desired level of WHC.

Product reformulation could be an alternative path toward salt reduction. Omitting the addition of $NaCl$ to the pre-mix prior to structuring could be beneficial as it resulted in improved WHC while maintaining a fibrous appearance. Replacing $NaCl$ by another salt such as KCl also has potential for sodium reduction. KCl addition had a similar negative effect on WHC as $NaCl$ in the regime most relevant for meat analogue products. Given its similar effect on WHC, the use of KCl could help reduce the sodium content of meat analogue products [29].

4.5 Conclusions

The effect of pH and ionic strength on the WHC of soy protein - gluten-based model meat analogues were studied using both experimental data and model simulations. The experimental results and simulations are in qualitative agreement on the effect of pH. They show that a marinade pH far from the iso-electric point of the protein results in additional swelling. Minimizing the ionic strength experimentally resulted in the highest level of swelling, while our simulations showed limited swelling at low ionic strength. The simulations showed that the buffering capacity of the protein limits protein side-group dissociation at low ionic strengths. This effectively widens the iso-electric point of the protein, which in turn reduces swelling. However, the internal gel pH is decisive in setting the degree of swelling. We have shown that marinade pH and ionic strength are tools to control water uptake by simplified meat analogues. Furthermore, altering the cross-link density could be a route to alter WHC without the addition of ions. With these tools, food manufacturers can develop meat analogue products that more closely resemble real meat, and improve product yields. Low-salt marinades showed the highest water uptake, which might enable the development of salt-reduced meat analogues.

References

[1] D. Pimentel and M. Pimentel. Sustainability of meat-based and plant-based diets and the environment. *American Journal of Clinical Nutrition*, 78(3 SUPPL.), 2003.

[2] H. Aiking. Future protein supply. *Trends in Food Science and Technology*, 22(2):112–120, 2011.

[3] OECD/FAO. OECD-FAO Agricultural Outlook 2020-2029. Technical report, Rome/OECD Publishing, Paris, 2020.

[4] D. Tilman, K. Cassman, P. Matson, R. Naylor, and S. Polasky. Agircultural sustainability and intensive production practices. *Nature*, 418:671–677, 2002.

[5] S. Smetana, A. Mathys, A. Knoch, and V. Heinz. Meat Alternatives – Life Cycle Assessment of Most Known Meat Substitutes. *The International Journal of Life Cycle Assessment*, 2050: 1254–1267, 2015.

[6] A.C. Hoek. *Will Novel Protein Foods beat meat? Consumer acceptance of meat substitutes - a multidisciplinary research approach.* PhD thesis, Wageningen UR, 2010.

[7] K.J. Grabowska, S. Tekidou, R.M. Boom, and A.J. van der Goot. Shear structuring as a new method to make anisotropic structures from soy-gluten blends. *Food Research International*, 64:743–751, 2014.

[8] K.J. Grabowska, S. Zhu, B.L. Dekkers, N.C.A. De Ruijter, J. Gieteling, and A.J. van der Goot. Shear-induced structuring as a tool to make anisotropic materials using soy protein concentrate. *Journal of Food Engineering*, 188:77–86, 2016.

[9] B.L. Dekkers, C.V. Nikifordis, and A.J. van der Goot. Shear-induced fibrous structure formation from a pectin/SPI blend. *Innovative Food Science and Emerging Technologies*, 36:193–200, aug 2016.

[10] F.K.G. Schreuders, B.L. Dekkers, I. Bodnár, P. Erni, R.M. Boom, and A.J. van der Goot. Comparing structuring potential of pea and soy protein with gluten for meat analogue preparation. *Journal of Food Engineering*, 261(May):32–39, 2019.

[11] R.D. Warner. Chapter 14 – The Eating Quality of Meat—IV Water-Holding Capacity and Juiciness. In F. Toldra, editor, *Lawrie´s Meat Science*, pages 419–459. Woodhead Publishing Limited, eighth edition, 2017. ISBN 9780081006948.

[12] H. Bertram and M. Aaslyng. Pelvic suspension and fast post-mortem chilling: Effects on technological and sensory quality of pork - A combined NMR and sensory study. *Meat Science*, 76(3):524–535, 2007.

[13] R.M. Burke and F.J. Monahan. The tenderisation of shin beef using a citrus juice marinade. *Meat Science*, 63(2):161–168, 2003.

[14] C. Alvarado and S. Mckee. Marination to Improve Functional Properties. *Journal of Applied Poultry Research*, 16(1):113–120, 2007.

[15] Y.B. Lee, D.J. Sehnert, and C.R. Ashmore. Tenderization of Meat with Ginger Rhizome Protease. *Journal of Food Science*, 51(6):1558–1559, 1986.

[16] P.R. Sheard and A. Tali. Injection of salt, tripolyphosphate and bicarbonate marinade solutions to improve the yield and tenderness of cooked pork loin. *Meat Science*, 68(2):305–311, 2004.

[17] A. Lebert and J.D. Daudin. Modelling the distribution of aw, pH and ions in marinated beef

meat. *Meat Science*, 97(3):347–357, 2014.

[18] A.E. English. *Phase Transitions in Polyampholytic Polymers and Hydrogels*. Doctor of philosophy in medical engineering and medical physics, Massachusetts Institute of Technology, 1996.

[19] M.D. Aaslyng, C. Bejerholm, P. Ertbjerg, H.C. Bertram, and H.J. Andersen. Cooking loss and juiciness of pork in relation to raw meat quality and cooking procedure. *Food Quality and Preference*, 14(4):277–288, 2003.

[20] K.L. Pearce, K. Rosenvold, H.J. Andersen, and D.L. Hopkins. Water distribution and mobility in meat during the conversion of muscle to meat and ageing and the impacts on fresh meat quality attributes - A review. *Meat Science*, 89(2):111–124, 2011.

[21] E. Puolanne and M. Halonen. Theoretical aspects of water-holding in meat. *Meat Science*, 86 (1):151–165, 2010.

[22] R.G.M. van der Sman. Moisture transport during cooking of meat: An analysis based on Flory-Rehner theory. *Meat Science*, 76(4):730–738, 2007.

[23] R.G.M. van der Sman. Thermodynamics of meat proteins. *Food Hydrocolloids*, 27(2):529–535, 2012.

[24] P.J. Flory and J. Rehner. Statistical Mechanics of Cross-Linked Polymer Networks II. Swelling. *The Journal of Chemical Physics*, 11(11):521–526, 1943.

[25] M. Quesada-Pérez, J.A. Maroto-Centeno, J. Forcada, and R. Hidalgo-Alvarez. Gel swelling theories: the classical formalism and recent approaches. *Soft Matter*, 7(22):10536, 2011.

[26] S.H.V. Cornet, A.J. van der Goot, and R.G.M. van der Sman. Effect of mechanical interaction on the hydration of mixed soy protein and gluten gels. *Current Research in Food Science*, 3: 134–145, 2020.

[27] J. Rička and T. Tanaka. Swelling of Ionic Gels: Quantitative Performance of the Donnan Theory. *Macromolecules*, 17(12):2916–2921, 1984.

[28] S.M. Yusop, M.G. O'Sullivan, J.F.P. Kerry, and J.F.P. Kerry. Effect of marinating time and low pH on marinade performance and sensory acceptability of poultry meat. *Meat Science*, 85 (4):657–663, 2010.

[29] E.S. Inguglia, Z. Zhang, B.K. Tiwari, J.P. Kerry, and C.M. Burgess. Salt reduction strategies in processed meat products – A review. *Trends in Food Science and Technology*, 59:70–78, 2017.

[30] A.E. English, S. Mafé, J.A. Manzanares, X. Yu, A.Y. Grosberg, and T. Tanaka. Equilibrium swelling properties of polyamapholytic hydrogels. *Journal of Chemical Physics*, 104(21): 8713–8720, 1996.

[31] E. Paudel, R.M. Boom, and R.G.M. van der Sman. Change in Water-Holding Capacity in Mushroom with Temperature Analyzed by Flory-Rehner Theory. *Food and Bioprocess Technology*, 8(5):960–970, 2015.

[32] J.S. Vrentas and C.M. Vrentas. Sorption in Glassy Polymers. *Macromolecules*, 24(9):2404–2412, 1991.

[33] R. van der Sman, E. Paudel, A. Voda, and S. Khalloufi. Hydration properties of vegetable foods explained by Flory–Rehner theory. *Food Research International*, 54(1):804–811, nov 2013.

[34] X. Jin, R.G.M. van der Sman, J.F.C. van Maanen, H.C. van Deventer, G. van Straten, R.M.

Boom, and A.J.B. van Boxtel. Moisture Sorption Isotherms of Broccoli Interpreted with the Flory-Huggins Free Volume Theory. *Food Biophysics*, 9(1):1–9, 2014.

[35] R.G.M. van der Sman. Biopolymer gel swelling analysed with scaling laws and Flory-Rehner theory. *Food Hydrocolloids*, 48:94–101, 2015.

[36] R.G.M. van der Sman and M.B.J. Meinders. Prediction of the state diagram of starch water mixtures using the Flory–Huggins free volume theory. *Soft Matter*, 7:429, 2011.

[37] R.G.M. van der Sman. Hyperelastic models for hydration of cellular tissue. *Soft Matter*, 11: 7579–7591, 2015.

[38] A.R. Khokhlov. Swelling and collapse of polymer networks. *Polymer*, 21(4):376–380, 1980.

[39] F. Horkay and M. Zrínyi. Studies on the Mechanical and Swelling Behavior of Polymer Networks Based on the Scaling Concept. 4. Extension of the Scaling Approach to Gels Swollen to Equilibrium in a Diluent of Arbitrary Activity. *Macromolecules*, 15(5):1306–1310, 1982.

[40] P.G. De Gennes. *Scaling concepts in Polymer Physics*. Cornell University Press, Ithaca and London, 1979.

[41] R.G.M. van der Sman, S. Houlder, S.H.V. Cornet, and A. Janssen. Physical chemistry of gastric digestion of proteins gels. *Current Research in Food Science*, 2:45–60, 2020.

[42] F. Horkay, I. Tasaki, and P.J. Basser. Effect of monovalent-divalent cation exchange on the swelling of polyacrylate hydrogels in physiological salt solutions. *Biomacromolecules*, 2(1): 195–199, 2001.

[43] B.M. Bohrer. An investigation of the formulation and nutritional composition of modern meat analogue products. *Food Science and Human Wellness*, 8(4):320–329, 2019.

[44] I. Migneault, C. Dartiguenave, M.J. Bertrand, and K.C. Walrdon. Glutaraldehyde: behavior in aqueous solution, reaction with proteins, and application to enzyme crosslinking. *BioTechiques*, 5(37):790–802, 2004.

[45] J.P.C.M. Peters, H. Luyten, A.C. Alting, R.M. Boom, and A.J. van der Goot. Effect of crosslink density on the water-binding capacity of whey protein microparticles. *Food Hydrocolloids*, 44: 277–284, 2015.

[46] P.D. Virkar, M. Hoare, M.Y.Y. Chan, and P. Dunnill. Kinetics of the acid precipitation of soya protein in a continuous-flow tubular reactor. *Biotechnology and Bioengineering*, 24(4):871–887, 1982.

[47] I. Borukhov, D. Andelman, R. Borrega, M. Cloitre, L. Leibler, and H. Orland. Polyelectrolyte titration: Theory and experiment. *Journal of Physical Chemistry B*, 104(47):11027–11034, 2000.

[48] E. Alexov, E.L. Mehler, N. Baker, A. M. Baptista, Y. Huang, F. Milletti, J. Erik Nielsen, D. Farrell, T. Carstensen, M.H. Olsson, J.K. Shen, J. Warwicker, S. Williams, and J.M. Word. Progress in the prediction of pK a values in proteins. *Proteins: Structure, Function and Bioinformatics*, 79(12):3260–3275, 2011.

[49] J.M. Gosline. The temperature-dependent swelling of elastin. *Biopolymers*, 17(3):697–707, 1978.

[50] J.M.S. Renkema. *Formation , structure and rheological properties of soy protein gels*. Phd, Wageningen UR, 2001.

[51] J. Berghout, R. Boom, and A. van der Goot. Understanding the differences in gelling properties

between lupin protein isolate and soy protein isolate. *Food Hydrocolloids*, 43:465–472, 2015.

[52] J.A. Delcour, I.J. Joye, B. Pareyt, E. Wilderjans, K. Brijs, and B. Lagrain. Wheat Gluten Functionality as a Quality Determinant in Cereal-Based Food Products. *Annual Review of Food Science and Technology*, 3(1):469–492, 2012.

[53] K. Shimada and J.C. Cheftel. Determination of Sulfhydryl Groups and Disulfide Bonds in Heat-Induced Gels of Soy Protein Isolate. *Journal of Agricultural and Food Chemistry*, 36(1): 147–153, 1988.

[54] V.L. Pietsch, J.M. Bühler, H.P. Karbstein, and M.A. Emin. High moisture extrusion of soy protein concentrate: Influence of thermomechanical treatment on protein-protein interactions and rheological properties. *Journal of Food Engineering*, 251(August 2018):11–18, 2019.

Chapter 5

Water release kinetics from soy protein gels and meat analogues as studied with confined compression

Abstract

In this paper, we report on the use of confined compression to study the water release properties from food gels and model meat analogues. Confined compression is a novel method in food science that provides information on the dynamics of water release under mechanical load. Confined compression measurements are compared with numerical simulations based on Flory–Rehner theory. Simulation results for soy protein gels are in reasonable agreement with experiments, while they underestimate the water release from model meat analogues. Time-domain nuclear magnetic resonance (TD-NMR) revealed the presence of internal water-filled cavities in the meat analogues. These cavities could provide a path of low resistance for the water to travel through. However, they are not captured by our current model, which explains the higher fluxes observed experimentally. Our results indicate a relation between the water release properties of meat analogues and pore structure. Control of the pore structure might, therefore, provide new opportunities to improve meat analogue juiciness.

5.1   Introduction

Reducing the consumption of meat products and transitioning towards a more plant-based diet could be beneficial to the environment [1, 2]. To ease this transition, meat analogue products that accurately mimic the sensory characteristics of real meat should be developed [3]. Some of the most important characteristics of meat are its flavour, fibrous texture, and juicy mouthfeel. The fibrous texture can already be mimicked with reasonable accuracy by processing mixtures of plant proteins in a Shear Cell [4–7]. However, the number of studies dedicated to understanding and improving the juiciness of meat analogue products is limited [8, 9].

The juiciness of real meat is related to the water holding capacity and the juice released during mastication [10, 11]. In meat, juiciness can be considered as a multistage or time-dependent sensation and can be divided into initial and sustained juiciness [10, 12, 13]. Bertram et al. [13] showed that the spatial distribution and relative mobility of water in pork correlate with the perceived juiciness. During (over-) cooking of meat, the water distribution changes due to denaturation of muscle proteins and contraction of the muscle fibre [14]. Water is expelled from the myofibrils into the extracellular space before moving out of the meat entirely [13, 15]. The extracellular water has higher mobility and might, therefore, be more easily expelled than the water still bound to the myofibrillar proteins. The initial juiciness could, therefore, be related to water loosely held inside internal cavities, which is easily expelled during the first bite. The sustained juiciness could relate to the release of more tightly held water, which is expelled during continued mastication. The sustained juiciness is thought to be associated with the water holding capacity (WHC) and moisture content [10, 11, 16–18]. Additional factors such as fat content, flavour compounds, the presence of salts, and salivation by the consumer will probably also play a role in the sensory perception of juiciness [10].

An accurate meat analogue should also encompass the two stages of juiciness. Meat analogues can contain considerable volumes of air [19–21]. These cavities could be filled with fluid through impregnation. Water-filled cavities can affect the local resistance to flow [22], and will alter the rate of water release from meat analogues. Cavities might also collapse, leading to further expulsion of water. Hence, the cavities could contribute to the initial juiciness. This study focuses on understanding the water release properties of porous model meat analogues and non-porous soy protein gels by studying the water release rate as a function of applied pressure over time.

We have designed a confined compression cell to measure the rate of water release from

(food) hydrogels (Figure 5.1). During confined compression, a sample is deformed inside a water-permeable confined space using a texture analyser. The change in sample height is recorded and provides a direct measure for the sample volume. When it is assumed that only water is expelled, the composition and water release rate can be determined in time. The ability to accurately track the sample volume during an experiment is the main advantage of confined compression over conventional unconfined compression. Confined compression is used in other fields to study the mechanical and hydration properties of soft materials such as collagen gels [23], cartilage [24, 25], and agarose gels [26]. To our knowledge, we are the first to report on the use of confined compression to study the hydration properties of food gels. Hence, an additional purpose of this paper is to showcase the capabilities of confined compression. Furthermore, alongside the experimental work, we have developed a model to simulate the water release from a cross-linked polymer gel. The model is based on the Flory–Rehner theory of polymer gel swelling [27] and Darcy flow. The gel's local permeability is calculated based on the work by Tokita and Tanaka [22]. Using this combination of experiments and simulations we aim to improve our physical understanding of the relation between meat analogue structure and water release kinetics.

5.2   Materials and methods

Before taking samples for the confined compression tests, the gels and model meat analogues were equilibrated with pure water. This puts them in a well-defined thermodynamic state. From the swollen materials, cylindrical samples were taken and transferred to the compression cell. The sample was compressed by a piston according to the load profile in Figure 5.5 and the water release rates were determined. The evolution of the pore structure of the model meat analogues after compression was studied using time-domain nuclear magnetic resonance (TD-NMR). The water mobility distribution from TD-NMR provides insight into the mobility and the relative size of the different water populations, such as water present in the gel matrix or cavities. Model simulations of confined compression were run to better understand the water release from gels without pores.

5.2.1   Materials

Soy protein isolate (SPI; Supro 500E, Solae, St Louis MO, USA) and vital wheat gluten (gluten; Roquette, Lestrem, France) were obtained from commercial sources

and were used as received. SPI and gluten had a protein content of 81.7±1.1 % and 77.9±0.1 % (Nx5.7) on a dry matter basis respectively. Sodium chloride ($NaCl$) and all other reagents used were of analytical grade and were obtained from Sigma-Aldrich (Steinheim, Germany). Milli-Q water was used for all experiments.

5.2.2   Methods

Production of soy protein gels

Soy protein isolate (SPI) gels were prepared according to Cornet et al. [8]. SPI powder was weighed and added to water to achieve the desired final dry matter content (DMC; 25, 30, 35 wt%). The protein dispersion was vigorously mixed by hand until a dough was obtained. The doughs were placed in vacuum bags and air was removed by applying a vacuum of 50 mbar for 45 s. The vacuumed doughs were stored overnight at 4°C to allow for full hydration. The moisture content of all hydrated doughs was measured after preparation (Section 5.2.2). Hydrated doughs were transferred to stainless steel gelation vessels (12.5 mm inner diameter; 5 mm inner height) and sealed hermetically. The sealed vessels were submerged in a Julabo water bath, pre-heated at 95 °C and shaken at a frequency of 100 rpm. After 30 min, the vessels were transferred to a water bath of approximately 15°C for 15 min to cool. Vessels were then opened and the gels were gently removed. After trimming the edges the final gel was obtained. The gels were allowed to swell as explained in Section 5.2.2.

Production of model meat analogues

Fibrous model meat analogues were prepared from SPI, gluten, $NaCl$, and water using a Couette-type shearing device similar to the one described by Krintiras et al. [28]. An SPI:gluten:$NaCl$:water ratio of 15:15:1:69 was used, resulting in a DMC of 31 wt%. Samples had a height of 25 mm and were prepared as follows. $NaCl$ was dissolved in water and the SPI powder was added and mixed using a Z-blade mixer (Winkworth Machinery Ltd., Basingstoke, UK). After a hydration period of 30 min gluten was added, followed by further mixing. The obtained mixture was transferred to the Couette shearing device. The Couette device was heated, and an average shear rate of 14.1 s^{-1} was applied for 35 min, during which the sample reached a temperature of 135°C. After shearing, the system was cooled down to 50°C after which the device was opened. The sample removed immediately and stored in a hermetically sealed bag to prevent moisture loss. After the model meat analogues

reached room temperature (22 °C) they were stored at -18 °C until use to prevent spoilage.

Swelling pre-treatment

Gels and model meat analogues were swollen to equilibrium in an excess of Milli-Q water at 4°C before all confined compression experiments. A sample : water ratio of 1 : 100 (wt : wt) was used for the SPI gels. Gels were swollen for at least 24 h during which the water was exchanged three times to wash away most ions present. Due to the larger size of the model meat analogues a sample : water ratio of 1 : 20 was used, and the swelling time was extended to at least 72 h. The composition after swelling was determined by measuring the dry matter content (Section 5.2.2).

Dry matter content and maximum level of swelling determination

Dry matter content (DMC) was determined by drying at 105 °C for at least 24 h. The maximum level of swelling was determined based on the DMC in the swollen state. In our model we will use the polymer volume fraction in the fully swollen state φ_0 as a measure for swelling:

$$\varphi_0 = \frac{y_p/\rho_p}{(y_p/\rho_p) + (1 - y_p)/\rho_w} \tag{5.1}$$

y_p and $(1-y_p)$ are the dry and wet weight fractions as determined during oven drying. ρ_p and ρ_w are the density of polymer and water, respectively.

Confined compression

Description of the setup   Water release kinetics were measured using an in-house built confined compression cell (Figure 5.1; Wageningen Technical Development Studio). The setup consists of an acrylic cylinder with an inner diameter of 40 mm that screws onto an acrylic bottom compartment. The bottom compartment has a vent hole to prevent pressure build-up. A stainless steel perforated plate rests in between the bottom compartment and the cylinder. The plate is covered with a fine steel mesh to provide both mechanical support and minimal flow resistance. The piston is made of poly-ether ether ketone (PEEK) and attached to a stainless steel shaft. The piston has an outer diameter approximately 20 µm smaller than the inner diameter of the cylinder to ensure a good fit. The piston shaft was attached to an Instron 5564 system outfitted with a 2 kN load cell, which was used to apply a range of loads. The confined compression cell was submerged in water during experiments

to prevent evaporative moisture loss. A thin layer of water between the piston and cylinder walls was assumed to provide frictionless motion. Submersion in water gives a unique definition of the boundary condition, where the chemical potential of water μ_w equals zero.

The design of the confined compression setup bears a resemblance to earlier designs reported in literature [23–26]. Liu et al. [26] used a porous confinement cell and piston and thus allowed for water to leave the sample from all sides, while in the present design water could only leave the sample from the bottom of the sample. Knapp et al. [23], Roos et al. [24], and Soltz and Ateshian [25] instead used a porous piston combined with impermeable sides and base. Roos et al. [24] used both torsional and axial actuators to apply both compressive and rotational strains. All mentioned studies submerged the compression cell in water during the measurements. Furthermore, Roos et al. [24] varied the ionic strength of the bath to study its effect on the shear modulus, which led to corrosion of their setup. All mentioned studies either did not discuss friction between the piston or sample and the confinement cell [23, 25, 26] or, like the present study, assumed frictionless motion due to a lubricating film of water [24].

Experimental procedure Swollen samples were trimmed to a diameter of 40 mm using a cylindrical knife. Samples were submerged in water for at least 1 h after trimming to minimize its effect on sample water retention. The confined compression cell was submerged in water while making sure no air bubbles were entrapped inside the cell. The sample was then placed on the stainless steel plate inside the cylinder. The piston was lowered without touching the sample as observed through the transparent cylinder. The piston was attached to the load cell before starting the experiment.

To ensure the sample was properly seated, the piston was first lowered at a rate of 5 $\mathrm{mm\,min^{-1}}$ until the force exceeded 2 N. Then, a sequence of loads was applied with a deformation rate of 5 $\mathrm{N\,s^{-1}}$. A lower rate of 2.5 $\mathrm{N\,s^{-1}}$ was used for the model meat analogues to reduce excessive crosshead movement. The duration of each load step was 300 s (5, 10, 15, 20, 25, 30, 35, 50 N; Figure 5.5, right axis). The height at 3 N was taken as the initial height of the sample. Recorded parameters were time, force, and height.

Load-controlled experiments require a balance between the gain and rate of load application to prevent oscillations and (large) overshoots in the applied load. After preliminary experiments on swollen SPI gels, a gain of 0.02 $\mathrm{mm\,N^{-1}}$ was selected. This
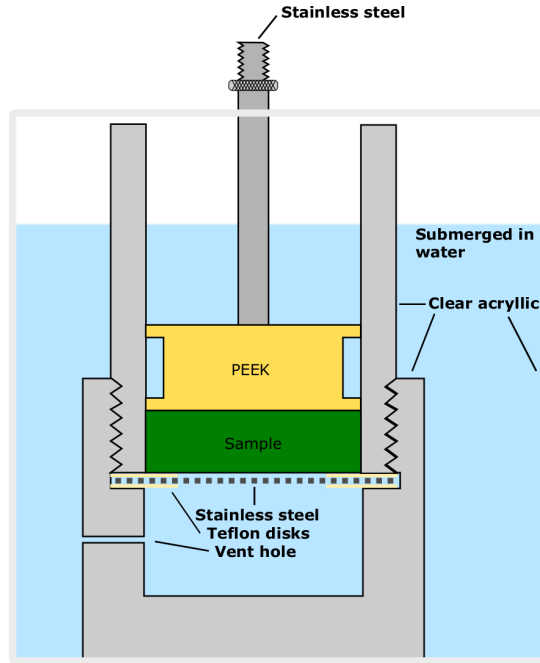
Figure 5.1: Cross-sectional representation of the confined compression cell. Materials used are indicated in the figure. The steel shaft connects to an Instron texture analyser. The setup was submerged in water during experiments. Image is not to scale; relevant dimensions are described in the text.

resulted in a limited overshoot with a duration of up to 1 s and a near-instantaneous load application (Figure 5.2). The effect of the load overshoot on the measurements will be discussed with the results. Preliminary experiments with an empty cell confirmed that the confined compression cell does not significantly deform during the experiment.

Data analysis The volumetric flux of water release, j, was deduced from the incremental volume change over time step dt:

$$-j(t) = \frac{dH}{dt} \tag{5.2}$$

The polymer volume fraction at time t $\varphi(t)$ was deduced from the initial polymer volume fraction φ_0, initial height, H_0, and actual height, $H(t)$, assuming
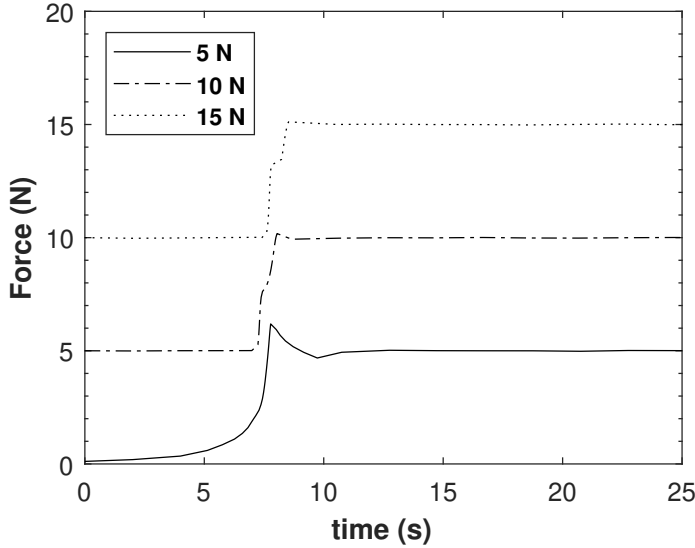
Figure 5.2: Raw force data as function time for a swollen 25 wt% SPI gel showing the increase in measured force. The 10 N and 15 N lines are offset by 300 s.

incompressibility and the absence of air:

$$\varphi(t) = \frac{H_0}{H(t)} \varphi_0 \tag{5.3}$$

The swollen soy protein gels were analysed in triplicate, which were averaged and used to calculate standard errors. For the swollen model meat analogue, two duplicates with three replicates each were recorded. Since there was some variation in the initial and final DMC of the model meat analogues, individual data sets were analysed by calculating the flux over periods of 5 s.

Time-domain nuclear magnetic resonance (TD-NMR)

Time-domain NMR (TD-NMR) experiments were performed on a Maran Ultra NMR spectrometer with a field strength of 0.72 T (30.7 MHz ^{1}H resonance frequency) and controlled with the RINMR software package (Resonance Instruments Ltd., Witney, UK). A protocol similar to Schreuders et al. [29] was used, which consisted of a Carr-Purcell-Meiboom-Gill (CPMG) echo train with 5 data points per echo and a total of 12288 echos. A sampling time of 10 µs resulted in a spectral width of 100 kHz. The

time between echos was 500 µs. 16 transients were recorded with phase cycling and a relaxation delay of 10 s, which were averaged to a single data point. All TD-NMR experiments were performed in triplicate and analysed using the IDL software package (ITT Visual Information Solutions, Boulder, CO, USA). The CONTIN fit routine was used to determine the water mobility distributions [30]. Intensities were normalized to the highest intensity within a single data set. Peak areas were determined using the trapezoidal method in Matlab.

Compression by centrifugation

Studying the effect of compression on the internal pore structure required an alternative method of compression as sampling during a confined compression experiment is not possible. Therefore, a centrifuge was used as an alternate means of applying an external pressure, Π_{ext}. The combination of centrifugation and TD-NMR has been used previously by [31]. Samples were trimmed to a diameter of 5 mm using a biopsy punch and placed inside the upper compartment of centrifugal filtration tubes. The tubes have two compartments separated by a filter (pore size 0.2 µm; Pall Centrifugal Devices, Medemblik, The Netherlands). During centrifugation in an Eppendorf bench-top centrifuge, the expelled fluid was collected in the bottom compartment. A swinging bucket rotor was used to ensure that the axis of deformation was parallel to the axis of load application. Samples were centrifuged for 1 h at different centrifuge speeds, which was long enough to reach equilibrium. Samples were transferred to NMR tubes immediately after a centrifugation step was completed and their water mobility distribution was recorded (Section 5.2.2). Furthermore, the amount of expelled water was determined by weighing. A range of external pressures was applied by returning the samples to their centrifuge tubes and increasing the centrifuge speed (50, 100, 200, 400, 800 $\times g$). Sample composition was calculated based on the moisture loss and the initial composition. By assuming a linear gradient in both φ and Π_{ext}, Π_{ext} was calculated as:

$$\Pi_{ext} = \frac{1}{2}\overline{\rho}g_{actual}H \tag{5.4}$$

$\overline{\rho}$ is the mean density of the sample, g_{actual} is the actual relative centrifugal force at the sample location, and H is the height of the sample. The amount of polymer in the sample is assumed to remain constant during centrifugation. The height of the sample is thus a direct consequence of the moisture loss and can be calculated as:

$$\varphi_{init}H_{init} = \overline{\varphi}H \tag{5.5}$$

φ_{init} is the initial polymer volume fraction, H_{init} is the initial sample height, and $\overline{\varphi}$ is the mean polymer volume fraction after centrifugation.

Statistics

Error bars indicate the 95% standard error of the observation, with n indicating the number of observations.

5.3   Model description

5.3.1   Flory–Rehner theory

Swelling of cross-linked polymer gels can be described with Flory–Rehner theory. Gel swelling is characterized by the swelling pressure, Π_{swell}. At swelling equilibrium, Π_{swell} is equal to the externally applied pressure, Π_{ext}.   In the case of free swelling in pure water, we define $\Pi_{ext} = \Pi_{swell}$ as equal to zero.   There are two independent contributions to Π_{swell}:   the mixing pressure, Π_{mix}, and the elastic pressure, Π_{elas}:

$$\Pi_{ext} = \Pi_{swell} = \Pi_{mix} - \Pi_{elas} \tag{5.6}$$

As has been shown for several types of food gels including soy protein gels, Π_{mix} can be described with Flory–Huggins theory [8, 32–34]. The Cloizeaux scaling law describes a more compact way of determining Π_{mix} in the semi-dilute regime [35], and has been shown successful at describing Π_{mix} for several bio-polymers [33, 36]. The external pressures applied in our confined compression experiments are lower than those commonly used in centrifugation experiments [8, 32, 37]. Sample compositions were therefore expected to remain in the semi-dilute regime. Hence it is deemed more appropriate to use the Cloizeaux scaling law to describe Π_{mix}:

$$\frac{\Pi_{mix}\nu_w}{RT} \propto \varphi^{\beta} \tag{5.7}$$

ν_w is the molar volume of water, R is the universal gas constant, and T the absolute temperature.   The exponent β has a value of 9/4 for dilute polymer solutions [35].

The elastic pressure, Π_{elas}, is the pressure generated upon deforming the network. We define the network deformation using the stretch parameter, λ_i, where i represents the principal directions. In the freely swollen state it holds that:

$$\lambda_x = \lambda_y = \lambda_z = \lambda_0 \tag{5.8}$$

with λ_0 as λ_i in the freely swollen sate. In uni-axial compression with lateral confinement, λ_x and λ_y are constant and remain equal to λ_0. λ_z does vary and can be expressed in terms of λ_0, the sample height H, and the height in the freely swollen state H_0:

$$\lambda_z = \lambda_0 \frac{H}{H_0} \tag{5.9}$$

Network deformation is directly related to the polymer volume fraction, φ, and the polymer volume fraction in the reference state, φ_{ref}:

$$\lambda_0 \lambda_0 \lambda_z = \frac{\varphi_{ref}}{\varphi} \tag{5.10}$$

λ_0 relates directly to the composition of the fully swollen network as follows from the incompressibility condition:

$$\lambda_0 = \frac{\varphi_{ref}}{\varphi_0}^{1/3} \tag{5.11}$$

with φ_0 as the polymer content in the freely swollen state, and φ_{ref} as the polymer content in the reference state. The reference state refers to the composition at which the polymer chains are in the relaxed state [38, 39]. There is no generally accepted method to define or determine φ_{ref} [38]. van der Sman [33] showed that for may bio-polymers φ_0 and φ_{ref} are related via:

$$\varphi_0 = 2/3\varphi_{ref} \tag{5.12}$$

with φ_0 as the polymer volume fraction at maximum swelling. We have recently found an alternative relation between φ_0 and φ_{ref} for soy protein gels [8]. However, when fitting φ_{ref} to φ as function of Π_{ext}, the value $\varphi = \varphi_0$ ($\Pi_{ext} \approx 0$) was excluded. Since in the confined compression experiments, φ remains relatively close to φ_0, it was deemed more appropriate to use Equation 5.12 to determine φ_{ref}. Swelling relative to the reference state can be expressed as $\tilde{\varphi}$:

$$\tilde{\varphi} = \frac{\varphi}{\varphi_{ref}} \tag{5.13}$$

A schematic representation of the stretches and their relation to $\tilde{\varphi}$ is presented in Figure 5.3. The mechanical stress resulting from network deformation is determined using the Neo-Hookean model for the strain energy function:

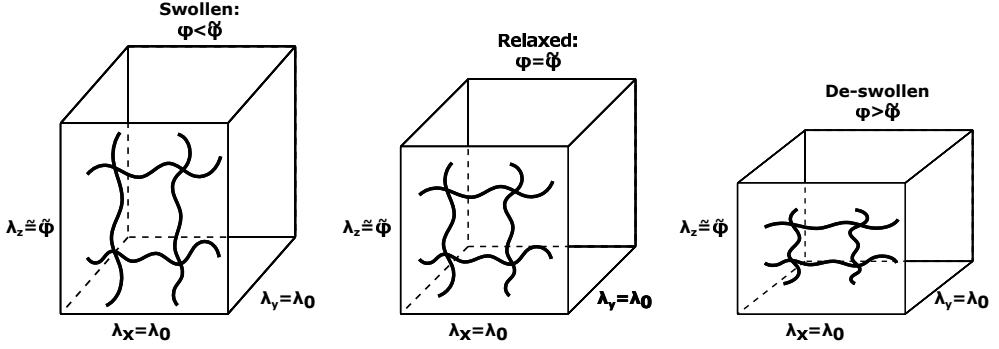$$W = \frac{1}{2} G_{ref} \left[\lambda_x^2 + \lambda_y^2 + \lambda_z^2 - 3 \right] \tag{5.14}$$

Figure 5.3: After free swelling, all three stretch parameters are equal to λ_0. During uni-axial confined compression, λ_x and λ_y remain equal to λ_0, while λ_z changes proportionally with $\tilde{\varphi}$ (Equation 5.9).

with W as the internal mechanical energy and G_{ref} as the shear modulus in the reference state. G_{ref} is related to φ_{ref} via [40]:

$$G_{ref} \propto \phi_{ref}^{\beta} \tag{5.15}$$

The stress along the axial direction is given by [39]:

$$
\begin{aligned}
\sigma_{zz} &= \tilde{\varphi}\lambda_z \frac{\delta W}{\delta \lambda_z} \\
&= G_{ref}\tilde{\varphi}\lambda_z^2 \\
&= \Pi_{elas}
\end{aligned}
\tag{5.16}
$$

5.3.2 Determination of fluxes

Local mechanical equilibrium is assumed, meaning the gradient in pressures within a volume element is zero:

$$\nabla \Pi = 0 \tag{5.17}$$

with Π as the sum of all pressures. The application of an external pressure Π_{ext} greater than the swelling pressure Π_{swell} will result in a pressure gradient $\nabla \Pi$ between the swollen gel and the exterior. The flux is then given by Darcy's law:

$$-j = D_s \frac{\nabla \Pi}{\nu_w RT} \tag{5.18}$$

where j is the flux and D_s is the self-diffusion coefficient of water. The diffusion coefficient in Equation 5.18 is proportional to the ratio between the permeability and viscosity [41]. D_s is a function of φ [22]:

$$D_s = D_{s,0}\alpha\varphi^{-\sqrt{\beta}} \tag{5.19}$$

with $D_{s,0}$ as the self-diffusion coefficient of pure water α is a constant with value 0.013 and was estimated based on Drozdov and deClaville Christiansen [42]. β is a constant with value 9/4. Note that this will diverge when φ approaches zero. It is inserted into the continuity equation:

$$\partial_t\phi = -\partial_z j \tag{5.20}$$

The following assumptions and boundary conditions complete the model:

- No friction occurs between the piston, cylinder, and gel

- The piston and all side walls are impermeable

- The plate upon which the gel rests is perfectly permeable (zero resistance)

- The chemical potential of water in the bath, μ_{bath}, equals 0

The model was solved in the Lagrangian framework, moving with the polymer network. A rectangular geometry was used with the same dimensions and initial composition as used experimentally, and consisted of 10 volume elements. Spatial derivatives were computed using Finite Differences. Time integration was done using the Euler forward method.

Simulation approaches

Two main simulation approaches were used. The first simulation approach used the experimentally measured external pressure as a model input in which case the simulation was run continuously (from $t = 0$ until $t = t_{end}$). As described in Section 5.2.2, an overshoot in the applied load occurred during the step-change in the experiments. This led to the use of a second simulation approach in which the step-change was not simulated. Instead, the average composition determined experimentally from the piston height directly after the step change was introduced to the model after each step-change. As will be discussed in Section 5.4.1, there were differences in composition between volume elements. To ensure these differences were maintained after the experimental composition was introduced, we assumed the same

gradient in φ as before the step change, but with the new averaged value of φ as determined from the new experimental piston height. The gradient in φ after the step-change was calculated for each volume element, i, as:

$$\varphi_i = \frac{V_{p,i}}{V_{p,i} + f_{w,i} \cdot ((V_p/\overline{\varphi}) - V_p)} \tag{5.21}$$

with $f_{w,i}$ as the fraction of total volume water in the gel before the step change, V_p as the total volume of protein in the gel, and $V_{p,i}$ as the volume of protein in volume element i. $\overline{\varphi}$ is the experimental polymer volume fraction after the step-change.

5.4   Results and discussion

A confined compression cell was used to apply a sequence of increasing external pressures to swollen soy protein isolate (SPI) gels and model meat analogues. The external pressures applied are shown on the right axis of Figure 5.10. The fluxes determined for the SPI gels will be discussed first, followed by the change in composition during compression. The flux and composition of the model meat analogues come next. Water mobility distributions were determined before and after swelling, and after applying an external pressure through centrifugation and will be discussed. The results are followed by a general discussion.

5.4.1   Confined compression of soy protein gels

The step-wise increase in external pressure during the confined compression of swollen SPI gels resulted in a repeating flux profile, as calculated using Equation 5.2 (Figure 5.4). The effect of dry matter content (DMC) before gelation on the flux was limited as indicated by the similarity in fluxes for gels with different DMCs. The different gels also showed qualitatively similar behaviour and will, therefore, be discussed together (Figure 5.4). The flux was high shortly after an increase in external pressure and quickly decayed. The high initial flux is partly due to the overshoot in applied pressure, as discussed in Section 5.2.2. The non-zero fluxes at the end of each step in external pressure indicate that the 5 min periods of constant external pressure were too short to achieve swelling equilibrium. Direct comparison with earlier studies on the equilibrium WHC would thus not provide meaningful insight. The expulsion of water led to an increase in polymer volume fraction, φ (Figure 5.5). The experimental composition increased in a manner that could be expected based on the determined fluxes. The change in composition was fast shortly after the applied

pressure increased, and slowed down afterwards. This fast and slow compositional change was seen for each consecutive step in external pressure for all three tested protein concentrations.

The flux was simulated using a model based on Flory–Rehner theory and the work by Tokita and Tanaka [22] (Section 5.3). The experimentally measured external pressures were used as an input for the simulation, which enables direct comparison of the simulated and experimental results (Figure 5.4; black circles). The simulated fluxes are in good agreement with the experimentally measured fluxes when the external pressure is constant. However, the model did underestimate the flux directly after an increase in external pressure despite using the experimentally measured external pressures as a model input. Due to the consecutive step-changes, the underestimations accumulated. This led to an increasing underestimation of the polymer volume fraction, as shown in Supplementary Figure 5.10. By omitting the step change, as explained in Section 5.3.2, reasonable agreement between the experimental and simulated composition was achieved (Figure 5.5). This confirms that the discrepancy between simulated and experimental fluxes during the short period after a change in load is the origin of the difference in the composition in Supplementary Figure 5.10.

There is generally good agreement between the experimental and simulated results when the external pressure is constant. This suggests that the model can provide a reasonable estimate of the flux for systems like soy protein gels. Furthermore, it indicates that the permeability based on the work by Tokita and Tanaka [22] provides a reasonable estimate of the permeability. We do note that there was only a limited effect of DMC on the flux as seen both experimentally and in the simulations. This suggests that the relative importance of the change in permeability due to the change in polymer content is limited in this regime (Equation 5.19).

The compositional change in the individual volume elements during simulated confined compression can be insightful (Figure 5.6). During the 5 min periods of constant external pressure, the moisture was primarily expelled from the area near the surface, as indicated by the relatively large changes in φ near the surface (high z) compared to the elements further from the surface (low z). As time progressed, moisture from areas further from the surface of the gel had travelled through and out of the gel, and led to more widespread compositional changes. Omitting the step-change in the simulations (as explained in Section 5.3.2) had only a minor effect on the local composition (Figure 5.6b) compared to when the simulations were run continuously (Figure 5.6a). As the local differences in φ were limited, the effect on

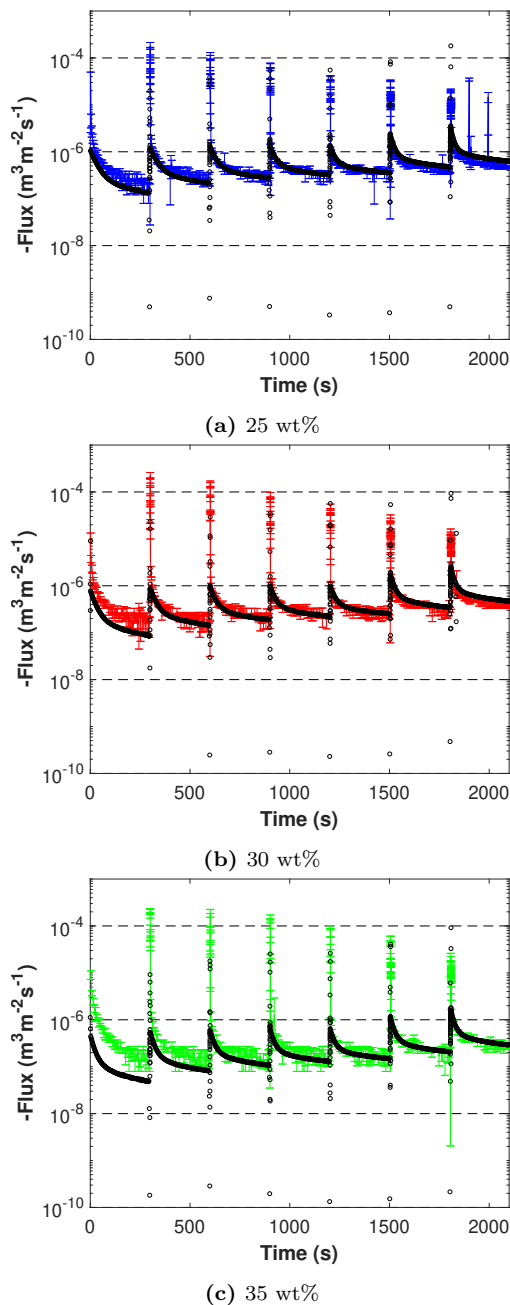**(a)** 25 wt%

(b) 30 wt%

(c) 35 wt%

Figure 5.4: Water release rates as determined with confined compression of swollen soy protein isolate gels. Compositions are presented with Figure 5.5. Black circles are model simulations assuming identical geometry and initial composition, and the experimentally measured external pressure as model input. n=3 for the experimental fluxes.
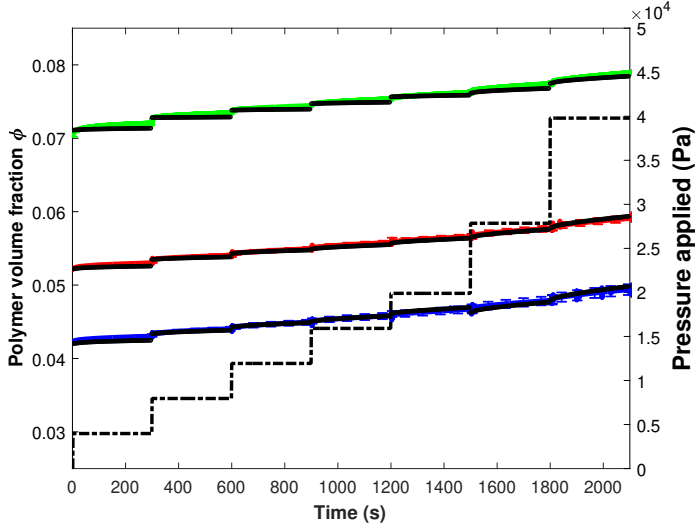
Figure 5.5: Polymer volume fractions (φ) of swollen soy protein gels during confined compression experiments (n=3). Initial levels of swelling (φ_0) were 0.042±0, 0.052±0 and 0.072±0 with initial DMCs of 25.1±0.0 wt%, 30.3±0.0 wt% 35.4±0.1 wt% (n=3). Solid black lines are model simulations. The experimental φ shortly after a load increase was used as a model input to bypass the period of high flux (Section 5.3.2). Simulated fluxes are presented in Supplementary Figure 5.12. The dash-dotted line is the applied load.

the local pressure gradients and permeability is considered to be minor. This is in line with the reasonable agreement found for both flux (Supplementary Figure 5.12) and composition (Figure 5.5).

5.4.2 Confined compression of a model meat analogue

A swollen model meat analogue was compressed using the confined compression cell. The model meat analogue swelled less than a neat soy protein gel with a comparable initial DMC. This can be explained by the lower swelling capacity of gluten and mechanical interaction between soy and gluten through which gluten limits soy's ability to swell [8]. We present a single representative data set for improved clarity; duplicates can be found in Supplementary Figures 5.11 and 5.13.

The experimentally measured flux for a model meat analogue follows a similar profile as the soy protein gels with fast and slow regimes (Figure 5.7). However, the initial
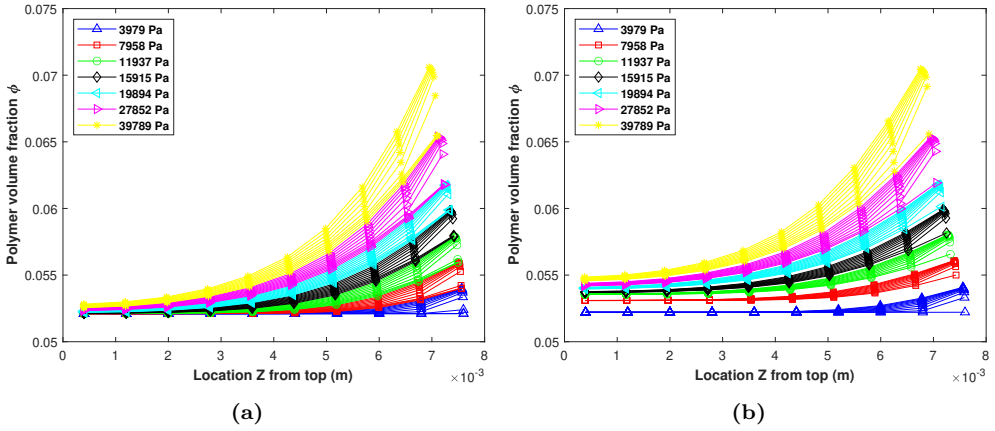
Figure 5.6: Composition during simulated confined compression from the continuous approach including the step-changes (5.6a), and the discontinuous approach omitting the step-change in external pressure (5.6b). Composition is presented at the center of each volume element relative to the top of the sample ($Z(top) = 0$) for a 30 wt% SPI gel. Data is presented at 30 s intervals.

fast regime appears to be longer compared to the soy protein gels. Furthermore, the flux is more irregular during the first three compression steps ($\Pi_{ext} \approx 4$, 8 and 12 kPa). Inspection of the raw force and deformation data suggests that the irregular flux is due to the fast release of water from the samples (Supplementary Figure 5.14). The fast water release resulted in fast dissipation of the external pressure, making it difficult for the texture analyser to maintain a constant external pressure. Stick-slip is an unlikely cause for the noise as the sample was never stationary and responded as soon as the load increased (Supplementary Figure 5.14).

The measured fluxes were generally higher than those found for the swollen SPI gels (Figure 5.4). This is interesting given the much higher polymer content of the swollen model meat analogues compared to the swollen gels ($\varphi_0 = 0.17$ versus 0.04–0.08) (Figure 5.5). The higher polymer content of the swollen meat analogue would have led to a decreased permeability based on Equation 5.19. A lower flux compared to the gels was, therefore, expected. Moreover, the flux decreased as the external pressure increased, while the opposite would be expected based on Equation 5.18 due to the greater pressure gradient. Polymer content did increase during compression (Supplementary Figure 5.11), which would have decreased the permeability by up to approximately 40 % (Equation 5.19). However, this limited
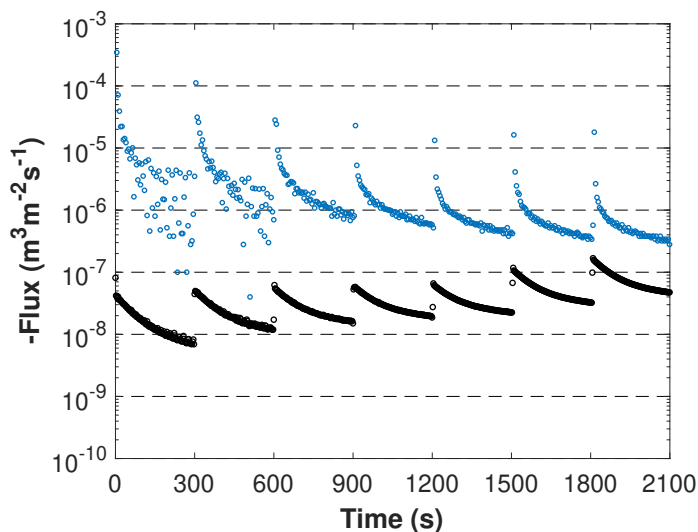
Figure 5.7: Experimental flux from a swollen model meat analogue with an initial DMC of 31 wt% (blue circles). Black circles are the simulated flux of a homogeneous gels with identical dimensions using the experimental force as a model input.

reduction in permeability cannot fully explain the reduction in flux when the applied pressure was increased.

Since the change in composition is effectively an integral of the fluxes, the qualitative change of the model meat analogue resembles that of the soy protein gels, with periods of fast change followed by a longer period of slower change (Supplementary Figure 5.11). The first three steps in external pressure have longer periods of fast change compared to the subsequent steps and the soy protein gels.

The simulations underestimated the experimentally determined fluxes by up to two orders of magnitude (Figure 5.7). As a result of the low simulated fluxes, also the compositional change was gravely underestimated (Supplementary Figure 5.11). The simulated fluxes increased as the applied load was increased, while the experimental results show an opposite trend. The discrepancy between the experimental and simulated fluxes thus decreases as the experiment progresses. For the simulations, an isotropic material was assumed, while meat analogues are anisotropic materials. Although they could be considered isotropic along a single axis, the anisotropy could have affected the permeability. Furthermore, the material was assumed to

be homogeneous and composed of soy protein alone, while the model meat analogues used in the experiments also contained gluten. The presence of gluten was expected to lead to a lower flux due to its lower swelling capacity [4, 8]. Given the higher polymer content and thus lower permeability of the model meat analogues compared to the SPI gels, a lower flux was expected. Since a higher flux was measured experimentally, the model meat analogue might have features that allow for water to be released faster by providing it with a path of low resistance. Structural features capable of channelling water are internal cavities, which are known to be present in meat analogues [7, 19, 21].

5.4.3 Time Domain Nuclear Magnetic Resonance (TD-NMR)

Time-domain NMR (TD-NMR) was used to study the different water populations present in the soy protein gels and model meat analogues. The relaxation time and relative size of the different water populations can provide information on a material's internal structure [43]. Different water populations can be identified based on their relaxation time, $T_{2,i}$, which is a measure for water mobility. A short T_2 corresponds to immobile water closely associated with proteins while a longer T_2 can correspond to water in the protein matrix, inside internal cavities, or free water outside the sample. Here, i is used to distinguish between water populations in a sample, starting with $i = 1$ for the shortest relaxation time until $i = n$ for the longest.

The non-swollen SPI gels have two main relaxation times, which can be attributed to two different water populations (Figure 5.8a). Population $T_{2,1}$ has a relaxation time of 4-6 ms and probably corresponds to protons closely associated with the protein. $T_{2,2}$ has a longer relaxation time of 20-35 ms and accounts for the rest of the signal. $T_{2,2}$ shifts to shorter relaxation times with increasing polymer concentration, which suggests this population corresponds to the water inside the polymer matrix.

After gel swelling, the relative intensity of $T_{2,1}$ (approx. 6 ms) has reduced. Since the amount of protein is taken to be constant, the reduction in relative intensity can be attributed to the increased water content. The relaxation time of $T_{2,2}$ has increased to 100-200 ms due to the increased water content of the samples. A third minor population $T_{2,3}$ was observed for the swollen SPI gels with a relaxation time of 600-1000 ms. Additional experiments indicated that population $T_{2,3}$ originated from water on the surface of the glass tube as the signal persisted after removing the sample from the tube (data not shown). $T_{2,3}$ is, therefore, considered an artefact.
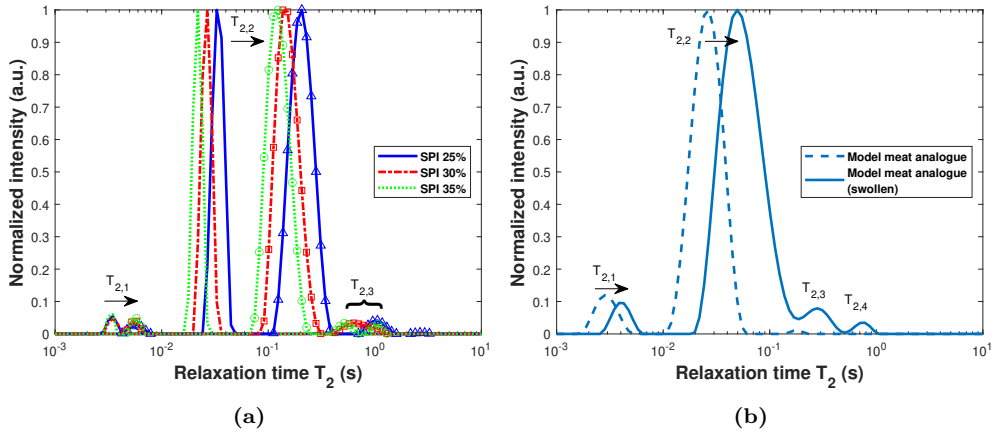
Figure 5.8: CONTIN fits of the T_2 relaxation of SPI gels (5.8a) and model meat analogues before and after swelling (5.8b). The arrows indicate the shift upon swelling. Individual representative data sets were plotted data (n=3).

The non-swollen model meat analogue has two main water populations with similar relaxation times as the non-swollen SPI gel with a similar DMC (30 wt%; Figure 5.8b). This could be expected based on their similar composition and comparable DMC. Upon swelling the water mobility distribution of the model meat analogue shows similar qualitative changes as the SPI gels. The shift towards longer relaxation times is, however, less extensive ($T_{2,1} \approx 4$ ms; $T_{2,2} \approx 50$ ms), which can be explained by the lower water uptake during swelling. In addition to the shift, also an additional population appeared in the model meat analogues. This population, $T_{2,3}$, has a markedly longer relaxation time of approximately 570 ms and is relatively intense compared to $T_{2,3}$ seen in the swollen SPI gels.

Meat analogues can contain (air-filled) cavities after production [7, 19, 21]. These cavities can be filled with water during swelling, as was found using X-Ray Tomography (voxel size 7 µm; data not shown). Given its high mobility and moderate intensity, population $T_{2,3}$ is thought to correspond to the water present inside internal cavities. Fibrous SPI-gluten based model meat analogues contain approximately 6-7 vol% of air [7], which is comparable to the intensity of the signal (Figure 5.9). There is an additional minor population $T_{2,4}$ visible. Whether this population corresponds to water in larger cavities or water on the surface of the sample or NMR tube was not confirmed experimentally.
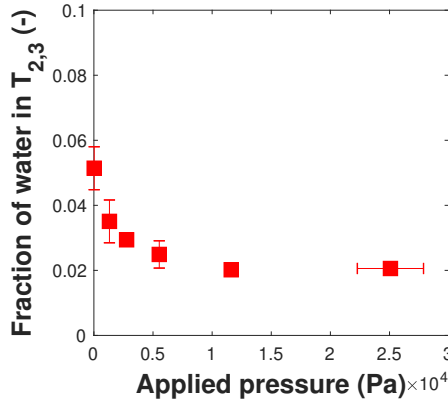
Figure 5.9: Relative contribution of water population $T_{2,3}$ to the total signal as a function of applied centrifugal load for swollen model meat analogues (n=4).

The effect of external pressure on water population $T_{2,3}$ in the swollen model meat analogues was assessed by applying a centrifugal load. Any change in the fraction of total water in population $T_{2,3}$ will provide information on whether the water from population $T_{2,3}$ is expelled at a similar pressure as population $T_{2,2}$. A range of loads was applied by increasing the centrifugal speed. Figure 5.9 shows that populations $T_{2,2}$ and $T_{2,3}$ are released at different pressures. Population $T_{2,3}$ first makes up approximately 5 % of total water, while after applying 10 kPa, this is reduced to approximately 2 %. This shows that population $T_{2,3}$, which is associated with the water in internal cavities, is released at a lower pressure than the population $T_{2,2}$. This is in agreement with Figure 5.7, where the flux reduces at pressure above 10 kPa. The remaining 2 % of water present in population $T_{2,3}$ suggests that some of the cavities did not fully collapse. The fraction appears to be constant at 2 % of total water. This suggests that the pore space is initially more easily deformed. After reaching 2 %, the pore space deforms at the same rate as the rest of the matrix.

5.4.4 General discussion

Confined compression was used to study the water release from swollen soy protein gels and model meat analogues. A range of external pressures was applied with step-change transitions between the different pressures. The confined compression cell gave reproducible results that, for homogeneous SPI gels, were in reasonable to

good agreement with the simulated fluxes when the external pressure was constant (Figure 5.4). However, slight overshoots in external pressure did lead to a discrepancy between the experimental and simulated composition results (Supplementary Figure 5.10). By omitting the step-change in the simulations, however, good agreement was achieved (Figure 5.5). The origin of the discrepancy was not identified. A reviewer suggested we compare the pressures applied during our confined compression with the pressures exerted by the molars during mastication. To our knowledge there are at present no studies where the mastication of meat analogues was reported. During the mastication of other foods of varying hardness, De Boever et al. [44] recorded an average load of approximately 13 N. When assuming a contact area of 3 cm^2, the average pressure was approximately 43 kPa, which is comparable to the maximum pressure applied during our experiments (up to 40 kPa).

Model meat analogues with a more complex structure and composition were also analysed with the confined compression cell. Although the interpretation of the results did require input from other methods such as TD-NMR, the confined compression cell did provide new insights into the water release from meat analogues. The measured fluxes were much higher than could be expected for a material with such a polymer content (Figure 5.7). This suggested that the model meat analogue has features capable of channelling the water. These features were identified as internal water-filled cavities using TD-NMR (Figure 5.8b), as indicated by the presence of a water population with a long relaxation time ($T_{2,3}$). The cavities could provide a low-resistance path for water and thus explain the high measured fluxes. Upon compression, the volume fraction of cavities reduced (Figure 5.9), rendering a more homogeneous gel as in the case of SPI. This could explain why for higher external pressures the flux reduced to a level closer to simulated result. Some cavities may persist at higher loads, which can explain why the flux remains at a higher level than the simulations. The numerical simulations of the model meat analogue showed that they do not behave as homogeneous gels, which is expected to be due to the internal cavities. A sensory study by Aaslyng et al. [12] on the juiciness of pork showed that the factors responsible for the perceived juiciness change during mastication. They concluded that meat juices are most important during the first few chews, while salivation by the consumer is also of importance during prolonged mastication. Confined compression of model meat analogues showed that the initial juice release is fast, but that it rapidly reduces. The simulated compositional gradients for the SPI gels showed that moisture is mainly released from the areas near the surface. This effect will be less pronounced in meat analogues due to the greater connectivity offered by the internal cavities. Furthermore, during mastication structural breakdown

occurs. This will reduce the distance the juice will have travel to be released, and could further increase the juice release rate. As the food breaks down, the timescale at which water release occurs therefore also becomes smaller. This suggests that different parts of the release rate curves may be relevant as mastication progresses.

Internal cavities can provide a way for water, and meat analogue juices, to be released at a higher rate. They could, therefore, be desired in a meat analogue products as they may enhance the initial juiciness. Incorporating greater quantities of air could increase this effect. Furthermore, the shape and orientation of the cavities could influence the magnitude and persistence of the effect. Elongated and highly connected channels parallel to the axis of compression may not collapse during compression and could enhance the release rate over longer periods and at higher loads. Several recent studies showed that elongated channels are present in meat analogues and that the level of elongation depends on the shear rate and temperature during processing in a shear cell [7, 19, 21]. An alternative approach to create such elongated channels is through directional freezing during post-processing [45]. Juiciness could be enhanced through the intelligent design of the meat analogue structure, although the correlation with sensory perceived juiciness is to be confirmed. The use of confined compression as an analytical tool could help in this process.

5.5 Conclusions

We have investigated the use of confined compression in food science by studying the water release from soy protein gels and meat analogues. The water release kinetics from swollen soy protein gels can be measured with confined compression and simulated with good accuracy using models based on Flory–Rehner theory and the framework proposed by Tokita when the external pressure is constant. Confined compression of model meat analogues showed much higher fluxes due to the presence of internal water-filled cavities. TD-NMR results showed that these cavities largely disappear as loads increase. Some cavities, however, persist and could explain why the experimental flux remains greater than the simulations. This study has shown that the water release from meat analogue products depends on their internal structure. By controlling the internal structure, the perception of juiciness could be enhanced. Confined compression has proven to be a promising tool to study food gels.

Acknowledgements

Supplementary Material

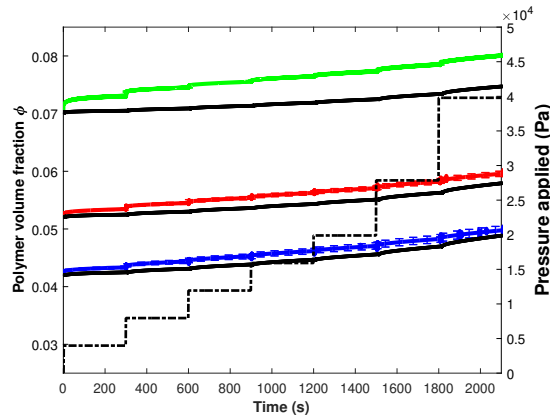**Figure 5.10:** Average polymer volume fractions (φ) of swollen soy protein gels during confined compression experiments (n=3). Solid black lines are model simulations using the experimental force data as input. Dash-dotted line is the applied load.
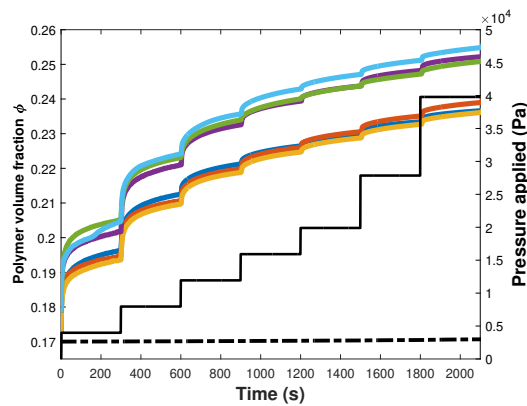
Figure 5.11: Change in composition during confined compression of a model meat analogue. Different colors are the result of different experiments.

(a) 25 wt%

(b) 30 wt%

(c) 35 wt%
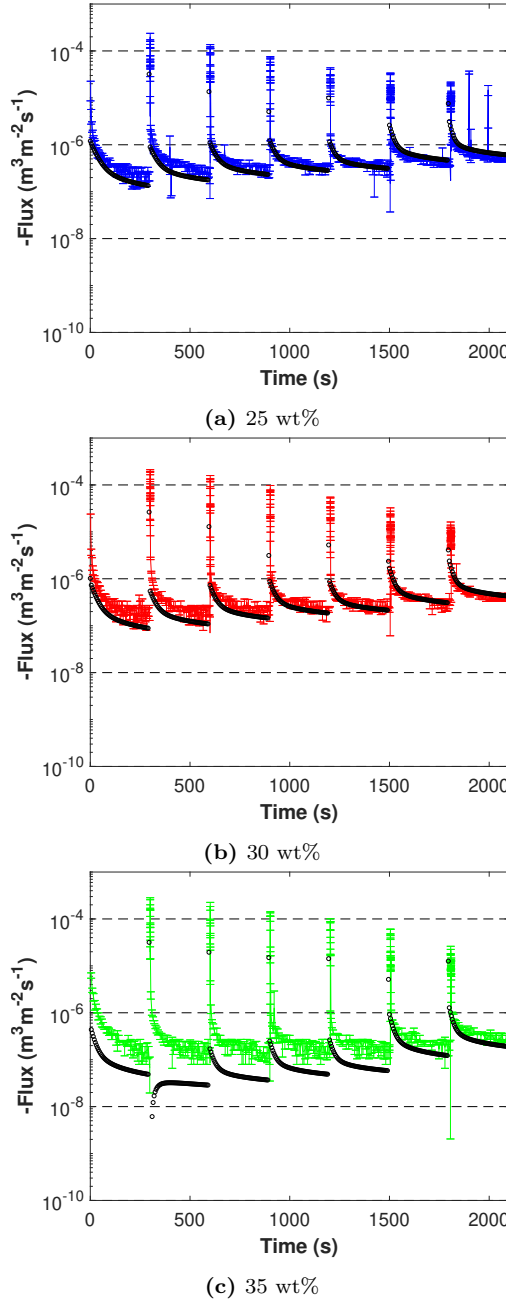
Figure 5.12: Water release rates as determined with confined compression of swollen soy protein isolate gels. Compositions are presented with Figure 5.5. The experimental φ shortly after a load increase was used as a model input to bypass the period of high flux (Section 5.3.2). Black circles are model simulations assuming identical geometry and initial composition. n=3 for the experimental fluxes.
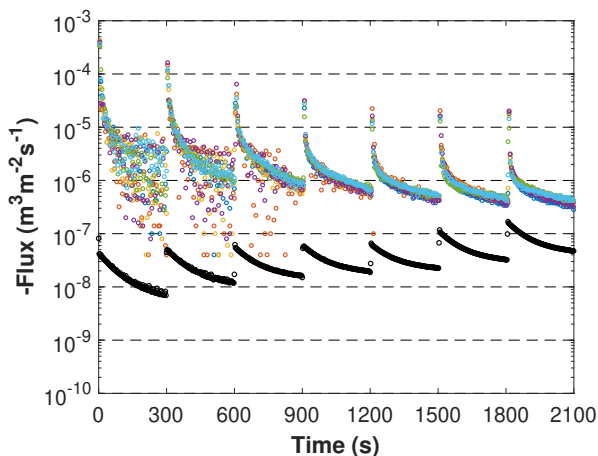
Figure 5.13: Model meat analogue experimental fluxes during confined compression. Different colors indicate different duplicate measurements; black circles are simulation results.
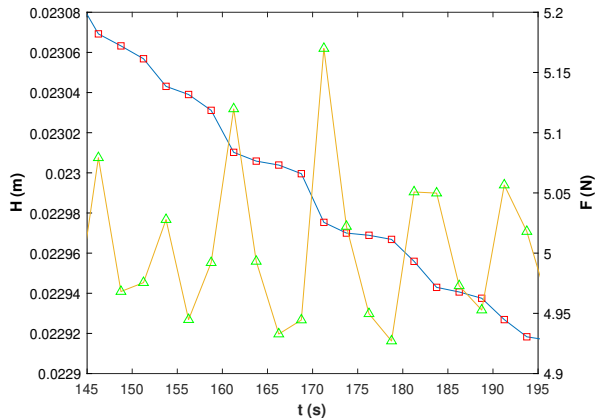

Figure 5.14: Raw force data and height data obtained during the confined compression of a swollen model meat analogue. Vertical dashed lines serve to guide the eye and show that the onset of the change in height coincides with the load increase. This shows there was no stick-slip, as otherwise a delay would be expected.

References

[1] H. Aiking. Future protein supply. *Trends in Food Science and Technology*, 22(2):112–120, 2011.

[2] S. Smetana, A. Mathys, A. Knoch, and V. Heinz. Meat Alternatives – Life Cycle Assessment of Most Known Meat Substitutes. *The International Journal of Life Cycle Assessment*, 2050: 1254–1267, 2015.

[3] A.C. Hoek. *Will Novel Protein Foods beat meat? Consumer acceptance of meat substitutes - a multidisciplinary research approach.* PhD thesis, Wageningen UR, 2010.

[4] K.J. Grabowska, S. Tekidou, R.M. Boom, and A.J. van der Goot. Shear structuring as a new method to make anisotropic structures from soy-gluten blends. *Food Research International*, 64:743–751, 2014.

[5] K.J. Grabowska, S. Zhu, B.L. Dekkers, N.C.A. De Ruijter, J. Gieteling, and A.J. van der Goot. Shear-induced structuring as a tool to make anisotropic materials using soy protein concentrate. *Journal of Food Engineering*, 188:77–86, 2016.

[6] B.L. Dekkers, C.V. Nikiforidis, and A.J. van der Goot. Shear-induced fibrous structure formation from a pectin/SPI blend. *Innovative Food Science and Emerging Technologies*, 36:193–200, aug 2016.

[7] F.K.G. Schreuders, B.L. Dekkers, I. Bodnár, P. Erni, R.M. Boom, and A.J. van der Goot. Comparing structuring potential of pea and soy protein with gluten for meat analogue preparation. *Journal of Food Engineering*, 261(May):32–39, 2019.

[8] S.H.V. Cornet, A.J. van der Goot, and R.G.M. van der Sman. Effect of mechanical interaction on the hydration of mixed soy protein and gluten gels. *Current Research in Food Science*, 3: 134–145, 2020.

[9] S.H.V. Cornet, S.J.E. Snel, J. Lesschen, A.J. van der Goot, and R.G.M. van der Sman. Enhancing the water holding capacity of model meat analogues through marinade composition. *Journal of Food Engineering*, 290:110283, 2021.

[10] R.D. Warner. Chapter 14 – The Eating Quality of Meat—IV Water-Holding Capacity and Juiciness. In F. Toldra, editor, *Lawrie´s Meat Science*, pages 419–459. Woodhead Publishing Limited, eighth edition, 2017. ISBN 9780081006948.

[11] R. Winger and C. Hagyard. Juiciness - its importance and some contributing factors. In A. Pearson and T. Dutson, editors, *Quality attributes and their measurement in meat, poultry and fish products*, chapter 4, pages 94–124. Springer Science+Business Media, Dordrecht, 1st edition, 1994.

[12] M.D. Aaslyng, C. Bejerholm, P. Ertbjerg, H.C. Bertram, and H.J. Andersen. Cooking loss and juiciness of pork in relation to raw meat quality and cooking procedure. *Food Quality and Preference*, 14(4):277–288, 2003.

[13] H.C. Bertram, M.D. Aaslyng, and H.J. Andersen. Elucidation of the relationship between cooking temperature, water distribution and sensory attributes of pork - A combined NMR and sensory study. *Meat Science*, 70(1):75–81, 2005.

[14] R.G.M. van der Sman. Moisture transport during cooking of meat: An analysis based on Flory-Rehner theory. *Meat Science*, 76(4):730–738, 2007.

[15] H.C. Bertram, H.J. Andersen, and A.H. Karlsson. Comparative study of low-field NMR relaxation measurements and two traditional methods in the determination of water holding capacity of pork. *Meat science*, 57(2):125–132, 2001.

[16] M.J. Van Oeckel, N. Warnants, and C.V. Boucqué. Comparison of different methods for measuring water holding capacity and juiciness of pork versus on-line screening methods. *Meat Science*, 51(4):313–320, 1999.

[17] L.W. Lucherk, T.G. O'Quinn, J.F. Legako, R.J. Rathmann, J.C. Brooks, and M.F. Miller. Assessment of objective measures of beef steak juiciness and their relationships to sensory panel juiciness ratings. *Journal of Animal Science*, 95(6):2421–2437, 2017.

[18] K.O. Honikel and R. Hamm. Measurement of water-holding capacity and juiciness. In A. Pearson and T. Dutson, editors, *Quality Attributes and their Measurement in Meat, Poultry and Fish Products*, chapter 5, pages 125–161. Springer Science + Business Media, Dordrecht, 1st edition, 1994.

[19] B.L. Dekkers, R. Hamoen, R.M. Boom, and A.J. van der Goot. Understanding fiber formation in a concentrated soy protein isolate - Pectin blend. *Journal of Food Engineering*, 222:84–92, 2018.

[20] B. Tian, Z. Wang, A.J. van der Goot, and W.G. Bouwman. Air bubbles in fibrous caseinate gels investigated by neutron refraction, X-ray tomography and refractive microscope. *Food Hydrocolloids*, 83:287–295, 2018.

[21] Z. Wang, B. Tian, A.J. van der Goot, and R. Boom. Air bubbles in calcium caseinate fibrous material enhances anisotropy. *Food Hydrocolloids*, 87:497–505, 2018.

[22] M. Tokita and T. Tanaka. Friction coefficient of polymer networks of gels. *The Journal of Chemical Physics*, 95(6):4613–4619, 1991.

[23] D.M. Knapp, V.H. Barocas, A.G. Moon, K. Yoo, L.R. Petzold, and R.T. Tranquillo. Rheology of reconstituted type I collagen gel in confined compression. *Journal of Rheology*, 41(5):971–993, 1997.

[24] R.W. Roos, R. Petterson, and J.M. Huyghe. Confined compression and torsion experiments on a pHEMA gel in various bath concentrations. *Biomechanics and Modeling in Mechanobiology*, 12(3):617–626, 2013.

[25] M.A. Soltz and G.A. Ateshian. Experimental verification and theoretical prediction of cartilage interstitial fluid pressurization at an impermeable contact interface in confined compression. *Journal of Biomechanics*, 31(10):927–934, 1998.

[26] Q. Liu, G. Subhash, and D.F. Moore. Loading velocity dependent permeability in agarose gel under compression. *Journal of the Mechanical Behavior of Biomedical Materials*, 4(7):974–982, 2011.

[27] P.J. Flory and J. Rehner. Statistical Mechanics of Cross-Linked Polymer Networks II. Swelling. *The Journal of Chemical Physics*, 11(11):521–526, 1943.

[28] G.A. Krintiras, J. Gadea Diaz, A.J. Van Der Goot, A.I. Stankiewicz, and G.D. Stefanidis. On the use of the Couette Cell technology for large scale production of textured soy-based meat replacers. *Journal of Food Engineering*, 169:205–213, 2016.

[29] F. Schreuders, I. Bodnár, P. Erni, R. Boom, and A. van der Goot. Water redistribution determined by time domain NMR explains rheological properties of dense fibrous protein blends

at high temperature. *Food Hydrocolloids*, 101, 2020.

[30] S.W. Provencher. Contin: A general purpose constrainded regularization program for inverting noisy linear algebraic and integral equations. *Computer Physics Communications*, 35:818–819, 1984.

[31] H.C. Bertram, S. Dønstrup, A.H. Karlsson, and H.J. Andersen. Continuous distribution analysis of T2 relaxation in meat—an approach in the determination of water-holding capacity. *Meat Science*, 60:279–285, 2002.

[32] E. Paudel, R.M. Boom, and R.G.M. van der Sman. Change in Water-Holding Capacity in Mushroom with Temperature Analyzed by Flory-Rehner Theory. *Food and Bioprocess Technology*, 8(5):960–970, 2015.

[33] R.G.M. van der Sman. Biopolymer gel swelling analysed with scaling laws and Flory-Rehner theory. *Food Hydrocolloids*, 48:94–101, 2015.

[34] J. Ubbink, M.I. Giardiello, and H.J. Limbach. Sorption of water by bidisperse mixtures of carbohydrates in glassy and rubbery states. *Biomacromolecules*, 8(9):2862–2873, 2007.

[35] J. Des Cloizeaux. The Lagrangian theory of polymer solutions at intermediate concentrations. *Journal de Physique*, 36(4):281–291, 1975.

[36] S. Mizrahi, O. Ramon, M. Silberberg-Bouhnik, S. Eichler, and Y. Cohen. Scaling approach to water sorption isotherms of hydrogels and foods. *International Journal of Food Science and Technology*, 32(2):95–105, 1997.

[37] P.N. Kocher and E.A. Foegeding. Microcentrifuge-Based Method for Measuring Water-Holding of Protein Gels. *Journal of Food Science*, 58(5):1040–1046, 1993.

[38] M. Quesada-Pérez, J.A. Maroto-Centeno, J. Forcada, and R. Hidalgo-Alvarez. Gel swelling theories: the classical formalism and recent approaches. *Soft Matter*, 7(22):10536, 2011.

[39] R.G.M. van der Sman. Hyperelastic models for hydration of cellular tissue. *Soft Matter*, 11: 7579–7591, 2015.

[40] F. Horkay and M. Zrínyi. Studies on the Mechanical and Swelling Behavior of Polymer Networks Based on the Scaling Concept. 4. Extension of the Scaling Approach to Gels Swollen to Equilibrium in a Diluent of Arbitrary Activity. *Macromolecules*, 15(5):1306–1310, 1982.

[41] M.A. Bisschops, K.C.A. Luyben, and L.A. Van Der Wielen. Generalized Maxwell-Stefan approach for swelling kinetics of dextran gels. *Industrial and Engineering Chemistry Research*, 37(8):3312–3322, 1998.

[42] A. Drozdov and J. deClaville Christiansen. A simplified model for equilibrium and transient swelling of thermo-responsive gels. *Journal of the Mechanical Behavior of Biomedical Materials*, 75:20–32, 2017.

[43] F. Mariette. Investigations of food colloids by NMR and MRI. *Current Opinion in Colloid and Interface Science*, 14(3):203–211, 2009.

[44] J.A. De Boever, W.D. McCall, S. Holden, and M.M. Ash. Functional occlusal forces: An investigation by telemetry. *The Journal of Prosthetic Dentistry*, 40(3):326–333, 1978.

[45] D. Fukushima. Soy proteins for foods centering around soy sauce and tofu. *Journal of the American Oil Chemists' Society*, 58(3):346–354, 1981.

Chapter 6

Thermo-mechanical processing of plant proteins using shear cell and high-moisture extrusion cooking

---

*These authors share first authorship

Abstract

Consumption of plant-based meat analogues offers a way to reduce the environmental footprint of the human diet. High-moisture extrusion cooking (HMEC) and shear cell processing both rely on thermo-mechanical treatment of proteins to product fibrous meat-like products. However, the mechanisms underlying these processes are not well understood. In this review we discuss the effect of thermo-mechanical processing on the physicochemical properties and phase behaviour of proteins and protein mixtures. The HMEC and shear cell processes are comparable in their basic unit operations, which are 1) Mixing and hydration, 2) Thermo-mechanical treatment, and 3) Cooling. An often overlooked part of the extruder that could be crucial to fibrillation is the so-called breaker plate, which is situated between the barrel and die sections. We found a lack of consensus on the effect of heat on protein-protein interactions, and that the experimental tools to study protein-protein interactions are limited. The different mechanisms for structure formation proposed in literature all consider the deformation and alignment of the melt. However, the mechanisms differ in their underlying assumptions. Further investigation using novel and dedicated tools is required to fully understand these thermo-mechanical processes.

6.1 Introduction

Reducing the amount of animal protein in our diet is considered essential to improving the sustainability of our diet [1–3]. One strategy towards achieving this protein transition is to offer consumers a plant-based alternative to meat. Meat-eating consumers would prefer products that strongly resemble real meat [4]. This is stimulating the development of plant-based meat analogues and the technologies used to produce them. Technologies capable of producing a fibrous, meat-like structure from plant-based ingredients are electro-spinning [5], high-moisture extrusion cooking (HMEC) [6], and shear cell technology [7, 8]. Of these three technologies, only extrusion cooking is currently used industrially for the production of meat analogues. Electro-spinning of food-grade protein fibres has recently seen several developments [5, 9–11]. However, the electro-spinning of proteins is considered notoriously difficult, uses large amounts of water or organic solvents, and upscaling poses a challenge [5, 12]. Shear cell devices were initially developed to study the extrusion process [13, 14], and were later identified as a novel structuring technique [7, 15]. The shear cell and HMEC processes both rely on thermo-mechanical stresses to create fibrous structures and are the focus of this review.

The thermo-mechanical processing of proteins is often studied for non-food products such as bio-plastics [16, 17], and food products such as meat analogues [18]. Several recent studies have explored the effect of process parameters such as specific mechanical energy (SME) [19, 20], shear rate [21], and temperature [20, 22, 23] on food product properties. Still, formulation development and ingredient screening lean heavily on empirical knowledge and trial-and-error based experimentation. Greater insight into the effect of the different processing steps would streamline product development and could lead to improved ingredient flexibility and process stability.

Although extrusion processes have been studied for several decades, the field is still at an exploratory stage. This paper provides a review of the thermo-mechanical structuring of plant-based proteins. Both the shear cell and HMEC processes will be considered. The paper is organized as follows. First the unit operations of the shear cell and HMEC processes are described. Then we go through the different unit operations step-by-step and discuss the physicochemical and phase changes that are induced by the process. The different mechanisms for structure formation posed in the literature will be discussed, and we will reflect on some of the predominant experimental approaches described in the literature. We will conclude with a general

discussion in which we identify the current knowledge gaps and provide an outlook for future research.

6.2 Process description

The high-moisture extrusion cooking (HMEC) and shear cell processes both make use of thermo-mechanical treatment to create fibrous structures. The processes are comparable in their basic unit operations and comprise of a mixing and hydration step, thermo-mechanical treatment, and a cooling step (Figure 6.1). Furthermore, the formulations that have led to a fibrous structure are similar between the two technologies (Table 6.1). Both use leguminous protein isolates or concentrates from e.g. soy, fababean or pea, often in combination with gluten or a polysaccharide (Table 6.1). Other less conventional protein sources have also led to favourable outcomes, such as peanut protein, microalgae, or non-refined soy flour (Table 6.1). Water contents used in HMEC and shear cell processing are comparable and range from approximately 50 to 70%.

6.2.1 High-moisture extrusion cooking

The application of extrusion cooking for the production of meat-like products started in the 1970s using primarily soy [24]. These meat-like products were expanded and had to be hydrated before use [25]. Expansion of the extrudate can occur due to the pressure drop upon exiting the die. This can lead to boiling and the rapid evaporation of water and results in a spongy texture [18]. The use of a long cooling die can be used to prevent the product from expanding and has enabled the extrusion of materials with a high moisture content [26]. High moisture extrusion cooking (HMEC) can be defined as extrusion with a water content exceeding 50% [27], which is also reflected by the compositions listed in Table 6.1.

Table 6.1: An overview of plant-based ingredients and combinations thereof, and process conditions used to produce fibrous structures through thermo-mechanical processing. *Abbreviations*: TSE, twin-screw extrusion; SC, shear cell; SSE, single screw extrusion; SPC, soy protein concentrate; MA, microalgae; PPI, pea protein isolate; WG, wheat gluten; PP, peanut protein; FPI, fababean protein isolate.; LPI, lupin protein isolate; SPI, soy protein isolate; CS, corn starch; SPF, soy protein fraction; SF, soy flour; WS, wheat starch; PPC, peanut protein concentrate; DPF, defatted peanut flour

Technique	Material	Moisture content (%)	Maximum temperature (°C)	References
TSE	SPC+MA	60	140	[27]
SC	PPI+WG	60	95-140	[28]
TSE	PP	55	155	[29]
SC	FPI+WG	61.5	140	[30]
TSE	SPC+WG	60	170	[6]
TSE	LPI+MA	50	140-175	[31]
TSE	SPC	60	100, 140, 160	[32]
TSE	SPI+WG+CS	70	160	[18]
SC	SPF+SF	56	140	[33]
SC	SPI+pectin	55	120-140	[23]
SC	SPC	50-65	120-140	[34]
TSE	PPI	60	140	[35]
TSE	SPI+WG	50	148	[36]
TSE	SPI	50	150	[19]
SC	SPI+WG	70	95	[7]
TSE	PPI	55	100-160	[37]
SSE	PPC+DPF	50-55	165	[38]
TSE	SPI+WG+WS	60-72	170	[39]
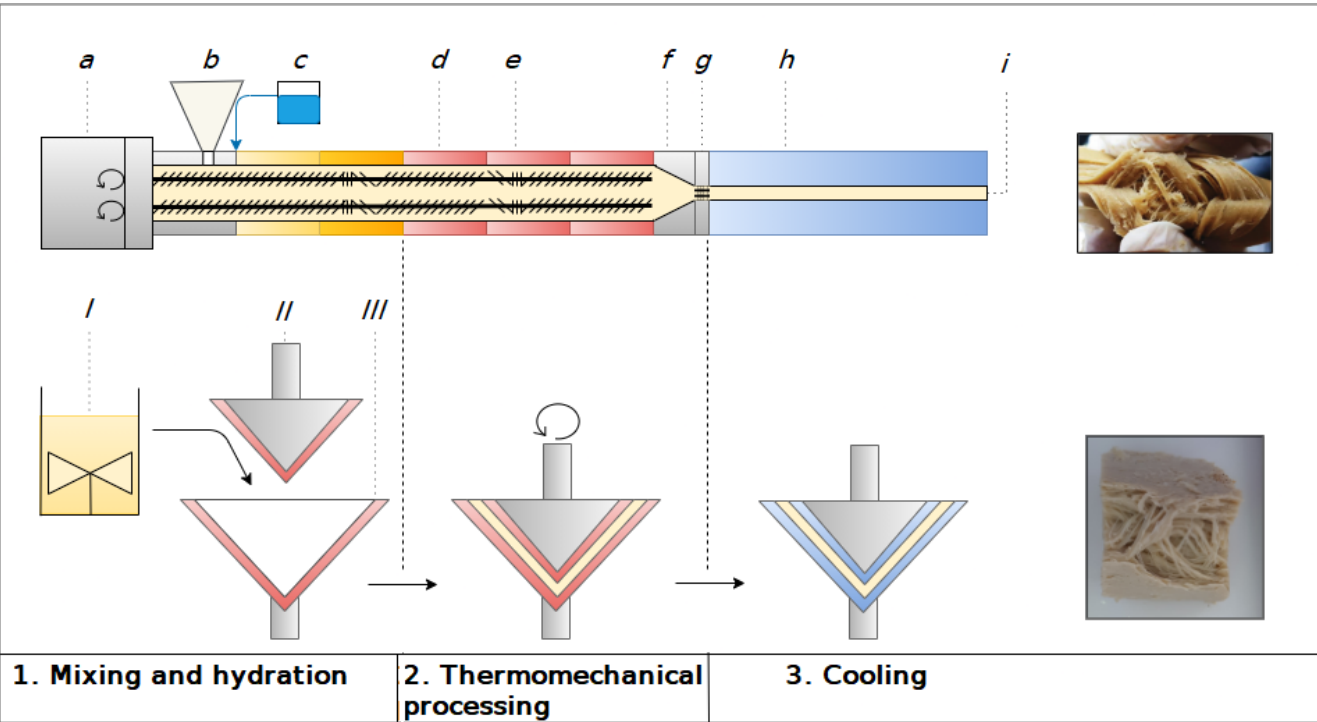
Figure 6.1: Schematic representation of an extruder and a conical shear cell. The different sections of the extruder are indicated with letters: a, motor; b, (dry) feeder; c, water pump; d, extruder barrel with screws; e, kneading blocks; f, transition zone; g, breaker plate; h, cooling die; i, die outlet. The different sections of the shear cell are indicated with roman numbers: I, external mixer for dry and wet ingredients; II, stationary top cone; III, rotating bottom cone. Extrudate picture was reproduced from [18] with permission.

An extruder consists of a heated barrel (Figure 6.1*d*) equipped with one or two screws driven by a motor (Figure 6.1*a*), a transition zone (Figure 6.1*f*), and a cooling die (Figure 6.1*h*). Twin-screw extruders with co-rotating screws are mostly used for the production of meat analogues, although some have also used single screw extruders (Table 6.1). Dry and wet ingredients are fed separately into the extruder barrel at the desired feed rates (Figure 6.1*b, c*). The extruder barrel consists of different sections that can be heated individually. The co-rotating motion of the screws provides mixing and hydration of the ingredients and conveys them towards the end of the barrel. The screws can be equipped with different screw elements that induce more thorough mixing, such as kneading blocks (Figure 6.1*e*). The continuous mixing facilitates heat transfer, while the motion along the barrel results in a pressure build-up. The approximate pressure along the extruder barrel is presented in Figure 6.2. The high pressure prevents boiling of the material and allows for high processing temperatures. The combination of high shear and high temperature makes this a thermo-mechanical process. At the end of the barrel, pressure builds to a maximum as the material is pushed out of the barrel through the cone-shaped transition zone (Figure 6.1*f*). So-called breaker plates or diffusers (Figure 6.1*g*) can be placed after the transition zone, and are an often overlooked part of the extruder. Breaker plates are perforated steel disks that ensure a homogeneous pressure distribution and are thought to align the flow before it enters the cooling die [26, 40]. The cooling die (Figure 6.1*h*) is a long rectangular channel and is cooled to a temperature of approximately 50°C to ensure cooling and to prevent expansion of the extrudate when it exits the die (Figure 6.1*i*).

6.2.2 Shear cell

Shear cells were originally used as an off-line method to study the effect of extrusion-like conditions on biopolymers such as starch or proteins [13, 14]. When the processing of calcium caseinate led to the formation of fibrils [15], the shear cell was identified as a novel structuring technology. The shear cell was later used as a new way of thermo-mechanical treatment [7]. Contrary to HMEC, the process utilizes well-defined shear flow during heating. There are two types of shearing devices with either a cone-in-cone or a Couette design. The conical device is also known as the shear cell and consists of a stationary top cone (Figure 6.1*II*) and a rotating bottom cone (Figure 6.1*III*). The Couette device is a scale-up concept of the conical device and consists of a stationary outer cylinder and a rotating inner cylinder. These cylinders will induce Couette flow over the gap, similar to the shear flow inside the conical device.

The shear cell process has the same three basic unit operations as HMEC, being mixing and hydration, thermo-mechanical treatment, and cooling (Figure 6.1). A general procedure for dough preparation was identified. Most formulations use $NaCl$, which is first dissolved in water. A protein isolate or concentrate is mixed with the water (6.1I), either by hand with a spatula or using a Z-blade mixer, depending on the scale of operation (lab or pilot scale respectively). The water-protein mixture is left to hydrate for 30 min at room temperature. After hydration, another protein or polysaccharide is added followed by further mixing to obtain a dough. The dough is transferred to the pre-heated shearing device and the shearing process is started.

Current versions of the conical shearing device rely on external heating by circulating heated water [41] or oil through the top and bottom cones [34]. The use of oil enables high-temperature processing. The Couette device is heated by a steam jacket around the concentric cylinders [8]. The shearing devices have seals and a pressurized cavity to prevent boiling and minimize moisture losses. This has enabled processing at conditions similar to extrusion cooking (Table 6.1; Figure 6.2; [23, 34]). A constant shear rate is applied to the material for 15 min while heating (conical device), resulting in thermo-mechanical treatment. The material is then cooled down by circulating cooled oil through the top and bottom cones of the shear cell. The shear cell is opened after the temperature reads 50°C, which is low enough to solidify the material and avoid expansion due to the evaporation of water when opening the device. The bottom cone of the shear cell is stationary during cooling and, therefore, no shear rate is applied during cooling. Similarly, the Couette device is stationary while cooling.

6.2.3   Comparison of process conditions

Although the HMEC and shear cell processes are comparable in their basic unit operations, some differences can be noted. The main difference between HMEC and shear cell processing is that HMEC is a continuous process, while the shear cell process is batch-operated. Furthermore, the current shearing devices rely on external mixing (Figure 6.1I) and preparation of a dough, which is transferred to the pre-heated device [7, 8, 42]. In HMEC the different ingredients are often fed to the extruder separately and mixed inside the barrel. Note that pre-mixing and hydration of ingredients can also be used in HMEC [43]. The current window of operation for HMEC appears to be wider (100-175°C) than for the shear cell (95-140°C; Table 6.1). Moreover, the residence time of the HMEC process is much shorter at 2-5 min compared to at least
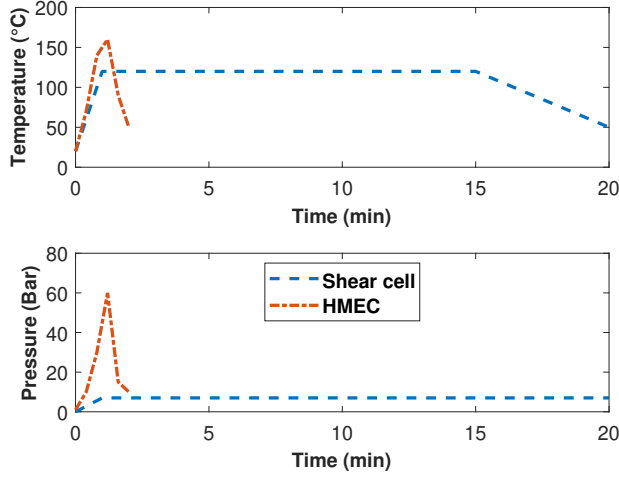
Figure 6.2: Comparison of the temperature and pressure profile during high-moisture extrusion cooking (HMEC) and shear cell processing. Values represent conventional process conditions as described by Cheftel et al. [26] for HMEC and Schreuders et al. [22] for the shear cell.

20 min for the conical shear cell (Figure 6.2).

Both during HMEC and shear cell processing a mechanical deformation is applied. Comparing the shear rates applied in both processes can be informative. The apparent shear in the shear cell is proportional to the rotation speed and is thus well defined. Although shear is applied in both the extruder barrel and the cooling die, not all shear is considered important for structure formation. The cooling die is often considered as the 'structuring zone' (Figure 6.1h). Therefore, it is deemed more informative to only consider the shear rate in the cooling die here. The shear rate inside the cooling die is proportional to the die's dimensions and the throughput, and can thus be calculated. Wall slip can occur in polymer melts when the wall shear exceeds a certain critical value [44]. The slip velocity is thought to depend on factors such as wall shear and normal stresses, temperature, and polymer properties such as the molecular weight distribution [44]. For simplicity, we have assumed a no-slip boundary in the die in our calculation of the apparent shear rate. The shear rate inside the die was calculated assuming no wall slip, after Son [45]:

$$\dot{\gamma}_{apparent} = 6 \cdot Q_{net}/(w \cdot h^2) \tag{6.1}$$

With $\dot{\gamma}_{apparent}$ as the apparent shear rate in the die, w the width and h the height of the die. The volumetric flow rate, Q_{net}, was calculated as:

$$Q_{net} = M/\rho_{melt} \tag{6.2}$$

With M as the mass feed rate. ρ_{melt} is the density of the melt and was approximated as 1087.2 kg m^{-3} by assuming a protein content of 40wt%. The residence time in the die was calculated as:

$$t = V_{die}/Q_{net} \tag{6.3}$$

With V_{die} as the volume of the die calculated with $w \cdot h \cdot l$, in which l is the length of the die. The calculated shear rate in the cooling die ranges from 1 to 45 s^{-1} (Figure 6.3). There seems to be an exponential relation between residence time and shear rate, with processing at a low residence time resulting in higher apparent shear rates. This seems intuitive as a lower apparent shear rate would require a longer residence time to achieve a similar level of structure formation. Although most extrusion trials are based on empirical knowledge, there is probably a relation between the total shear applied and structure formation which is currently not well understood. During shear cell processing, a constant shear rate of 39 s^{-1} is most often applied, which is comparable to those used in low-throughput extrusion cooking (Figure 6.3). Other shear rates have also been used, namely 7-130 s^{-1} [21]. The total shear applied ($\gamma_{total} = \dot{\gamma}_{apparent} \cdot t$) in a shear cell is 3.5×10^4 when assuming a shear rate of 39 s^{-1} and a shearing time of 15 min. This is much higher than the total shear applied in the cooling die, which ranges from 1.8×10^2 to 7.7×10^2 (Table 6.2). We note that in a shear cell device the shear rate and pressure are independent from the throughput of the process, while these parameters are related for extrusion. The shear cell might, therefore, offer more flexibility in processing conditions.

6.3   Mixing and hydration

The first step in protein structuring is the mixing of the wet and dry ingredients to obtain a dough. In HMEC the raw materials are fed into the barrel and mixed through the continuous rotating motion of the screws (Figure 6.1 *b,c*). The screws can exert high shear to the dough, especially at the screw tips where shear rates over 2430 s^{-1} were found according to the outcomes of computational fluid dynamics (CFD) simulations of starch matrices [46]. The latter study also reported that the mixing index was highest when the shear rate was below 574 s^{-1}. This suggests that mixing is not proportional to the shear rate. The mixing processes used on lab
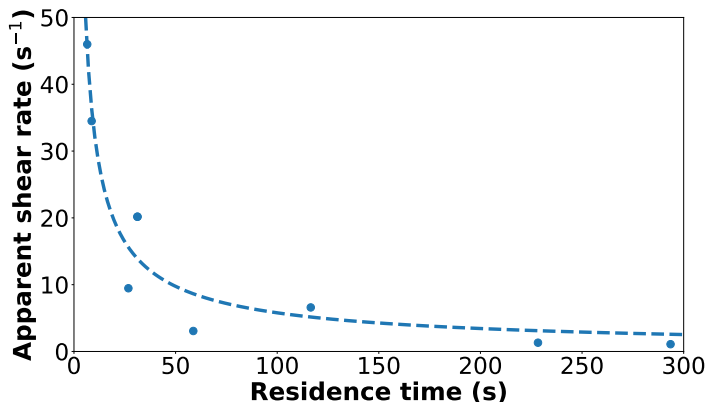
Figure 6.3: Apparent shear rate in the cooling die as calculated from the values from Table 6.2 (Equation 6.1 and 6.2) as a function of the residence time (Equations 6.2 and 6.3). The dotted line represents an exponential fit and serves to guide the eye ($\dot{\gamma}_{apparent} = 185 \cdot t^{-0.75}$; $R^2 = 0.92$).

and pilot scale versions of the shear cell may be more susceptible to lump formation due to the lower mixing intensity. Future industrial processing might cope with this by using twin-screw pre-mixers. Mixtures of different proteins, and proteins mixed with polysaccharides, do not tend to mix due to thermodynamic incompatibility [47–49]. Most HMEC and shear cell studies use moisture contents over 50% (Table 6.1). Upon hydration of a protein blend, the water will partition between the two phases. Clark et al. [50] proposed the use of Time-Domain Nuclear Magnetic Resonance (TD-NMR) to study the water partitioning between proteins. TD-NMR was used to study the water partitioning in hydrated mixtures of soy protein and gluten [51], and pea protein and gluten [28]. Both studies found that gluten binds less water than soy or pea protein. The water distribution was hardly affected after a thermo-mechanical treatment (95-140°C and sheared at 39 s^{-1} for 15 min), as measured at room temperature [28, 51]. An alternative approach to determine the water partitioning is based on Flory–Huggins theory. Flory–Huggins theory describes the free energy of mixing polymers with a solvent, in this case, water. The free energy of mixing directly relates to the water activity. When the different polymer phases are in thermodynamic equilibrium, their water activities must be equal. Hence the equilibrium water distribution is found where the free energy is equal in both

Table 6.2: Overview of cooling die dimensions, process parameters, and apparent shear rates in the cooling die as calculated with Equations 6.1 and 6.2 during high-moisture extrusion cooking.

Mass feed rate [$\mathrm{kg\,s^{-1}}$]	w [m]	h [m]	l [m]	Apparent shear rate [$\mathrm{s^{-1}}$]	Ref.
1.7×10^{-3}	7.0×10^{-2}	1.0×10^{-2}	5.0×10^{-2}	1.3	[18]
2.2×10^{-3}	5.0×10^{-2}	1.5×10^{-2}	8.0×10^{-1}	1.1	[31]
4.2×10^{-3}	3.0×10^{-2}	9.0×10^{-3}	3.8×10^{-1}	9.5	[32]
7.2×10^{-3}	6.0×10^{-2}	1.0×10^{-2}	1.3	6.6	[27]
6.7×10^{-4}	2.0×10^{-2}	2.0×10^{-3}	1.0×10^{-1}	4.6×10^{1}	[36]
5.0×10^{-4}	2.0×10^{-2}	2.0×10^{-3}	1.0×10^{-1}	4.5×10^{1}	[19]
2.8×10^{-4}	1.9×10^{-2}	2.0×10^{-3}	2.1×10^{-1}	2.0×10^{1}	[37]
3.3×10^{-3}	6.0×10^{-2}	1.0×10^{-2}	3.0×10^{-1}	3.1	[39]

phases. Some proteins, such as gluten, form a cross-linked network. Stretching of the network during hydration will result in an additional elastic contribution to the free energy and must be taken into account by using Flory–Rehner theory instead. This approach was used to describe the water partitioning in mixtures of gluten with a protein isolate from either soy [52], pea, or fababean [30]. Although the water distribution in polymer mixtures can be measured and predicted, the water distribution *during* thermo-mechanical treatment is currently unknown. This could be relevant for understanding structuring processes, as the rheological properties will be affected by the water distribution. It is still unclear whether the rheological properties of the dough are relevant for shear-induced structuring and the formation of anisotropic structures.

6.4 Thermo-mechanical treatment

The mixing and hydration step is followed by a thermo-mechanical treatment through the simultaneous application of heat and shear at elevated pressure (Figure 6.1). This combination of heat and shear is deemed essential as applying heat or shear alone does not result in a fibrous structure. The increase in temperature affects the intra- and intermolecular bonds that stabilize the protein structure. Hydrogen bonds are weakened as the temperature increases [53], while hydrophobic interactions can increase with temperature [54]. Free thiol groups will become increasingly reactive as the temperature rises [55], while pre-existing intra- and intermolecular disulfide

bonds become increasingly labile [56]. Disulfide bonds can undergo alkali-catalyzed β-elimination to form free thiol groups; this reaction also occurs at neutral pH and high temperature (100°C; [56]). Furthermore, free thiol groups and labile disulfide bonds can participate in thiol-disulfide interchange reactions to create a so-called transient or reversible network [57–59]. These thiol-disulfide interchange reactions may be promoted by shear stress [55, 60, 61]. The change in the protein's stabilizing interactions will result in a change or loss of the native protein structure, which is commonly referred to as denaturation. Most authors assume dense protein dispersions to reach a so-called molten state during thermo-mechanical treatment [16, 20, 37, 62–64] due to the weakening of intra- and intermolecular interactions at high temperature. But while the formation of a melt is widely recognized, the properties of the protein melt and the effect of thermo-mechanical treatment on protein-protein interactions are subjects of debate. The different views will be discussed.

6.4.1   Wheat gluten and the fate of the disulfide bond

The interactions between proteins will greatly affect melt properties. Especially the disulfide bond is considered to play a pivotal role in melt properties and has been extensively studied for wheat gluten proteins [39, 65–67]. Wheat gluten is a commonly used ingredient in both extruded and shear cell formulations (Table 6.1). The gluten proteins form a cross-linked network upon hydration [68, 69]. The gluten network has the remarkable ability to be reversibly deformed beyond its breaking point. Bloksma [58] proposed a mechanism to explain this behaviour by assuming disulfide bonds to act as reversible cross-links at room temperature. Disulfide bonds can undergo what are known as thiol-disulfide interchanges, suggesting they could contribute to a reversible or *transient* network [14, 70–72]. Emin et al. [73] showed that the complex modulus of gluten increases as the temperature exceeds 90°C. This was attributed to the formation of glutenin polymers via disulfide bonding. Domenek et al. [74] modelled the heat-induced aggregation of gluten proteins as a two-stage process (T < 95°C), and concluded that the protein must first unfold before aggregating. Gluten aggregation is generally attributed to the formation of disulfide bonds [66, 67, 74, 75]. Schreuders et al. [28] and Pietsch et al. [66] measured the evolution of the viscoelastic properties of gluten in time at process-like conditions (100-160°C). During iso-thermal experiments at a constant shear rate, both reported a maximum in the complex modulus and complex viscosity followed by a decrease. The maximum could hint towards cross-linking and aggregation, while the subsequent reduction could be due to a structural break-down. The magnitude of, and time until the maximum was reached decreased with increasing temperature [66], which we suggest could be due

to the weakening of the interactions with increasing temperature. This could be considered an indication of the presence of a transient network at higher temperatures. However, given the temporal evolution of the visco-elastic properties, it remains challenging to conclude what happens during thermo-mechanical processing of gluten inside the extruder barrel or shear cell. Emin et al. [73] reported the evolution of the complex modulus as function of temperature (20-170°C) for gluten hydrated to different levels (20, 30, 40%). The complex modulus decreased to a local minimum at ~80-90°C before reaching a maximum at 130-140°C, and subsequently decreasing again. The increase was attributed to aggregation, while the decrease was attributed to structural break-down due to so-called degradation reactions. Whether reducing the temperature after heating over 130-140°C restored the modulus was not reported, although it could have provided insight into the possibility of a transient network. A transient network would become permanent as the interactions become stronger at lower temperatures, leading to an increase in modulus. Interestingly, Emin et al. [73] did refer to hydrated bio-polymers at high temperatures as melts but did not consider melting as a result of weakened intermolecular interactions when interpreting the observed reduction in viscosity.

6.4.2 Disulfide bonding by non-gluten proteins

Understanding the fate of disulfide bonds in the melt is also important for other proteins. For soy protein it was shown that increasing the processing temperature over 130°C leads to softening of the material, which was attributed to the partial breakdown of disulfide bonds [76]. Dekkers et al. [77] studied the effect of temperature on soy protein isolate and showed a reduction in viscosity as the temperature exceeded 120-130°C. Interrupting a time-sweep at high temperatures (120-140°C) for 8 s resulted in a temporary increase in complex modulus, after which it returned to a similar magnitude as before the interruption. The increase in the complex modulus, ΔG^*, was lowest at 140°C and was not affected by the time before interrupting the deformation. The protein network formed during the interruption was probably broken down again as soon as the deformation resumed, suggesting the presence of a transient network. At lower temperatures, ΔG^* was higher and increased with the time before interrupting. This could indicate that the material was not fully molten below 140°C. Ralston and Osswald [17] used a capillary rheometer to study the viscosity of bio-plastics based on soy protein and corn starch at 200°C. They reported only a minor decrease in viscosity after repeatedly extruding the same sample at 200°C. Similarly, Noguchi [78] described how a fibrous soy extrudate could be cut up and extruded for a second and third time, while still resulting in a

similar microstructure and fibrous texture. Dead-stop operation during re-extrusion indicated that the material had melted and fused together in the heated section of the barrel (Figure 6.1d; [78]). O'Kane et al. [79] showed that the elastic modulus of soy protein gels followed the same trajectory during reheating and subsequent cooling between 85°C and 25°C. For pea protein, they found that this could also be achieved when using a low initial cooling rate of 0.2°C min^{-1}. This suggests that the changes made to the gel network upon cooling are thermally reversible at these relatively low temperatures. Interestingly, Pietsch et al. [66] reported no change in protein-protein interactions for soy protein isolate after processing at high temperature when compared to the raw material. Ingredient specific properties might, therefore, also be of importance. For example, the total number of cysteine residues differs between proteins and, therewith, also the number of potential disulfide bonds that can form. Gluten contains relatively large amounts of cysteine [80], while pea protein contains relatively low amounts. Berghout et al. [81] studied the role of disulfide bonds in the gelation of protein isolates from lupin and soy. Lupin protein was found to contain more disulfide bonds and free thiol groups than soy protein. However, despite the higher number of potential disulfide bonds, lupin displayed poor gelling properties compared to soy. This was attributed to the large number of disulfide bonds on a single protein, which hindered protein unfolding and prevented gel formation. The accessibility of disulfide and free thiol groups is thus also of importance to network formation. Non-covalent physical interactions will also affect melt properties, especially for materials low in thiol groups and disulfide bonds.

6.4.3   Analysis of protein-protein interactions

Numerous studies have reported on the effect of thermal or thermo-mechanical treatment on the physical and covalent interactions between proteins. However, since most protein analyses can only be performed under ambient conditions, information on proteins *during* thermo-mechanical processing is limited. Many authors have, therefore, studied the material obtained *after* processing at elevated temperatures. A commonly used method to study the change in protein-protein interactions is by measuring protein solubility in different buffer systems [6, 18, 19, 29, 32, 35, 82]. The different buffers selectively disrupt the different types of protein-protein interactions, which is assumed to solubilize them. Phosphate buffers are often used to extract soluble proteins without disrupting any specific interactions. Urea is added to disrupt physical interactions such as hydrophobic-, ionic-, and hydrogen bonds. The addition of dithiothreitol (DTT) reduces the covalent disulfide bonds to free thiol groups [82]. Several authors have agreed that the extrusion of soy and pea protein at high

temperatures leads to protein aggregation [39, 66, 83, 84]. The aggregates are thought to be due to a combination of covalent disulfide bonds and non-covalent physical bonds, although their relative importance is debated and will differ between protein sources. Interestingly, Pietsch et al. [32] found that protein solubility in different buffer systems was not affected by thermo-mechanical treatment when compared to non-treated soy protein concentrate (SPC). From this, they concluded that the polysaccharide fraction of SPC must be responsible for the observed rheological changes. An alternative interpretation could be that the number of intermolecular interactions increased at a loss of intramolecular interactions. The use of buffer systems to determine protein–protein interactions is not without controversy. Liu and Hsieh [39] showed that the buffer selection process is vital and that more conclusive results can be obtained by reversing the commonly used order of buffer addition. Instead of *adding* different reducing agents to the baseline buffer, they show that it could be better to *remove* reducing agents from a buffer system. This would allow for clearer differentiation between the relative importance of covalent and non-covalent bonds.

Another method to indirectly measure protein-protein interactions is based on the analysis of molecular weights before and after thermo-mechanical processing using sodium dodecyl sulfate–polyacrylamide gel electrophoresis (SDS-PAGE) [19, 29, 35, 83] or size exclusion chromatography (SEC) [65, 66, 74, 85]. Some authors observed a decrease in intensity of specific bands on the gel after extrusion of soy [19, 83, 86] and pea protein isolates [35]. They attributed this to the formation of large aggregates that were unable to enter the gel's pores. Chen et al. [86] also observed increased aggregation after raising the maximum temperature from 140 to 160°C and after lowering the water content from 60 to 28% during the extrusion of soy protein. Fang et al. [19] reported an increase in low molecular weight fractions after the extrusion of soy protein. This further increased after raising the SME. In another study by the same author, extruded soy protein was again found to have higher fractions of low molecular weight components after extrusion, as determined using SEC and multi-angle laser light scattering [85].

So-called dead-stop experiments are often used to collect material from the different parts of an extruder [39, 83, 87]. The extruder is simply shut-down when steady state is reached and left to cool before samples are taken. Liu and Hsieh [39] performed dead-stop experiments and concluded that disulfide bonds are formed in the barrel as a result of high temperature and high moisture and that they do not change in the cooling die. However, in a dead-stop experiment samples are taken after

cooling down the extruder and its contents. Similarly, the aforementioned studies on protein-protein interactions using buffer systems and size analysis methods have examined the material after cooling down. The findings from such studies may provide some insight into the material- and product properties, but cannot be used to elucidate the changes that occur *during* processing as the material changes upon cooling. Any changes invoked by the process can, therefore, not be attributed to a specific step in the process, be it heating, shearing, cooling, or a combination of those. Attributing specific functionality to a process step would facilitate the transition from empirical knowledge to a full understanding of thermo-mechanical structuring processes. Measurements at processing conditions are thus important and can be done either by measuring *inline* inside the extruder or shear cell, or by measuring *off-line* using dedicated analytical tools that mimic process conditions.

Barnes et al. [88] reported on the use of several spectroscopic tools to study various melt properties during the processing of non-food polymers. They used Raman and Fourier Transform Near-Infrared spectroscopy (FT-NIR) to track melt compositions during the extrusion of ethylene-vinyl acetate. Huang et al. [89] also used Raman spectroscopy to determine the ratio between polystyrene and polypropylene in the melt. Fluorescence spectroscopy was found to offer a real-time measure for the residence time during extrusion [88]. Hörmann et al. [90] reported on the use of NIR spectroscopy during the extrusion of a pharmaceutical product. A fibre-optic probe located after the die section was used to monitor the concentration of the active pharmaceutical compound in the hot melt and to determine residence times. Hansen and Vedula [91] reported on the use of NIR spectroscopy as an inline method to monitor the so-called melt index (MI) of polyethylene vinyl acetates. The MI is inversely proportional to the molecular weight and, at low stresses, also inversely proportional to the viscosity for synthetic polymers [91]. For some materials, spectroscopic tools could provide insight into both aggregation and viscosity. Although these tools have mostly been developed and used for non-food extrudates, they might also be used in food extrusion. In particular, Raman spectroscopy could prove insightful when studying protein melts. For example, disulfide bonds can be measured directly with Raman spectroscopy [92]. Furthermore, the wavenumber is thought to vary between exposed and buried thiol groups [93]. Raman spectroscopy during thermo-mechanical treatment could, therefore, provide further insight into the fate of the disulfide bond. While spectroscopic tools can provide insight at the molecular level, other tools are needed to examine the rheological properties of the melt. The use of inline and off-line methodologies to study the rheological properties of the melt will be discussed in the next section.

6.4.4   Rheological characterization of the melt

Understanding how the viscous melt transforms into a fibrous product requires in-depth knowledge of the melt's rheological properties. However, obtaining meaningful rheological information is challenging as experimentally replicating the conditions found inside an extruder or shear cell is difficult [73, 94]. Identifying the role of individual ingredients is complicated by factors such as water partitioning and changes in phase behaviour. For example, Zhang et al. [29] performed a rheological characterization of material collected from the different zones of an extruder by sampling after a dead-stop and re-dispersing the material in water at 20% (w/w). A molecular mechanism was postulated based on the viscosity curves determined at 25°C to explain the extrudate properties. Such experiments may offer insight into the behaviour of materials after processing. However, they do not necessarily relate to melt properties as they would occur during thermo-mechanical processing due to the change in temperature and moisture content. To achieve a better understanding of the phenomena during processing, well-designed experiments in which process-like conditions are used are essential. Two approaches were identified that are capable of measuring at relevant conditions. These analytical tools can either be incorporated into an extruder or shear cell to measure material properties *inline*, or they are external analytical tools that can mimic the process conditions to measure material properties *off-line*.

Inline rheological characterization

The use of inline rheometers, such as capillary or slit die rheometers, is considered the most accurate way to measure the viscosity of the melt [95]. Instead of an extrusion die, the slit die rheometer or capillary rheometer is attached to the end of the extruder. The pressure drop is measured over a section of known diameter and used to calculate the wall shear stress. The melt velocity is used to calculate the wall shear rate. By using several sections with a range of diameters in series an entire flow curve can be determined in a single run. A drawback of inline rheometers is that the change in diameter can modify back-pressure, which affects the degree of filling in the barrel. This could alter the thermo-mechanical stresses applied in the barrel [73]. Therefore, it is crucial to keep the back-pressure constant. To achieve this, Horvat et al. [96] designed an inline slit die rheometer with an adjustable geometry capable of maintaining a constant back-pressure, which ensures a constant processing history of the melt. Some studies successfully applied capillary rheometry to food materials and polymer melts [17, 97–100].

Off-line rheological characterization

While inline methods offer direct measurements of material properties during processing, they are limited in their flexibility. Furthermore, inline methods also require operating an extruder at steady-state conditions. They are, therefore, unsuitable for ingredient screening and testing large numbers of samples. Off-line methods generally offer greater experimental flexibility and require smaller sample sizes. They are, therefore, better suited for small-scale testing and generating large data-sets. There are many different rheological tools available such as oscillatory shear rheometry, capillary rheometry and viscometry. These tools can be used to characterize ingredients and obtain information on material properties such as viscosity, elastic and viscous moduli, and elongational viscosity. However, most conventional bench-top rheometers are not capable of mimicking the high pressures, high temperatures, and high shear rates found during thermo-mechanical processing. Furthermore, preventing moisture losses is challenging when temperatures exceed 100°C. Several manufacturers of bench-top rheometers do offer pressure cells for use with existing bench-top rheometers. The ability to perform rotational experiments and the greater torque sensitivity could prove advantageous as the viscosity of the protein melt is rather low [101].

Off-line capillary rheometers can also measure at high temperatures and pressure, and have been applied to study melt properties. Capillary rheometry is frequently applied in the field of plastic and bio-plastic extrusion. Klüver and Meyer [16] reported on the shear and elongational viscosities of gluten, soy protein and pea protein, plasticized with glycerol at elevated temperatures ($T = 140 - 160$°C). The different protein melts were described as thermoplastic with shear-thinning behaviour that could be approximated with power-laws with exponents of 0.31-0.40. Ralston and Osswald [17] studied the shear viscosity of mixtures of soy protein and corn starch plasticized with glycerol and water. They also found shear-thinning and power-law behaviour with comparable exponents. Extruding the material a second time resulted in a limited reduction in viscosity but did not affect the power-law exponent [17]. The limited effect of repeated thermo-mechanical treatment on the viscosity may explain why Noguchi [78] was able to make fibres after repeated extrusion of defatted soy flour [78]. Food ingredients have also been studied using capillary rheometers. Beck et al. [100] reported on the shear viscosity of hydrated pea protein isolate. They found that a longer holding time at 130°C reduced the viscosity of pea protein isolate, although this effect was not significant. They suggested that the break-down of aggregates over time could explain the observed trend. This appears to conflict with the notion that

aggregation occurs at high temperature.

Closed cavity rheometry

A recent development is the use of rheometers that were originally designed for analysing the vulcanization process of rubber compounds [102–104] for the rheological characterization of food polymers [28, 32, 33, 73, 94, 105]. This class of rheometers has a closed cavity that can withstand high pressures and temperatures without the risk of evaporative moisture losses. In the field of food science these rheometers are, therefore, often referred to as 'closed-cavity rheometers' or CCRs, as opposed to 'rubber process analysers'. CCRs can, to some degree, mimic the conditions inside a shear cell or extruder, although the accessible range of pressures and shear rates is limited. Furthermore, CCRs are not capable of rotation and can only impose an oscillatory deformation, which might limit the resemblance with the flow patterns that occur inside an extruder barrel or shear cell. By applying the Cox-Merz rule, the dynamic viscosities determined with a CCR could be used to determine the steady-state viscosities [106]. The principle of time-temperature superposition could also be used to create rheological master curves, as was demonstrated for cheese and whey proteins [107, 108]. Rheological properties measured at higher temperatures may be described using for example the Carreau model [109]. Several pioneering studies have already employed CCRs to investigate the rheological properties of food polymers during thermo-mechanical treatment [28, 32, 33, 66, 77, 105]. Some related this rheological fingerprint to the formation of a fibrous structure, as will be discussed in Section 6.6. In addition to the CCR's intended purpose as a rheometric instrument, CCRs can be used as a method to produce samples for further analysis with other analytical methods. This could be particularly helpful when trying to separate the thermal and mechanical stresses during thermo-mechanical processing. In an extruder, the residence time is affected by the rotation speed of the screw inside the barrel. This limits and complicates the control over the duration and intensity of the thermal and mechanical stresses applied to the material. This issue is not there in shear cell processing, nor in the CCR. CCR rheometers can thus be used as a way to provide thermo-mechanical treatment to samples in a controllable way, as has been done by Pietsch et al. [66]. The application of CCRs for the analysis of food polymers and food polymer melts is still in its infancy and dedicated CCRs capable of more accurately mimicking extrusion-like conditions may yet be developed.

In the context of food, some consider the extruder barrel as a chemical reactor in which thermo-mechanical stresses induce changes in the material [66, 73]. In particular,

the cross-linking of gluten has been studied extensively in this regard. Morel et al. [70] showed that shear can reduce the activation energy required to induce gluten cross-linking below 80°C. Similarly, Strecker et al. [65] used an extrusion rheometer to show that gluten polymerization speeds up with the shear rate (40-170°C). We must note that the activation energy for cross-linking reported by Strecker et al. [65] is approximately 5-10 times lower than the value found in a more recent study by Domenek et al. [74]. The lowering effect of shear on the activation energy suggests that shear can facilitate the interaction between proteins. The reduced activation energy could relate to the concept of effective temperature. This concept suggests that the viscous forces can increase the effective temperature of the system and thereby lower the energy barrier of a reaction. This might explain the importance of shear during thermo-mechanical treatment. Emin and Schuchmann [84] showed that an increase in shear rate during iso-thermal processing of gluten in a CCR reduced the complex viscosity ($T = 120$°C; $\dot{\gamma} = 0.1 - 50\mathrm{s}^{-1}$). Interestingly, in a similar experiment Pietsch et al. [66] did not find an effect of increasing the shear rate from 0.1 s^{-1} to 50 s^{-1} on the amount of SDS-soluble gluten proteins for a range of temperatures. Similarly, the processing of soy protein concentrate (SPC) in a CCR at different shear rates did not result in significant changes in protein solubility across a range of extraction buffers [32]. This suggests that food protein cross-linking may not be a thermo-mechanical but merely a thermal process at lower shear rates. At the higher shear rates cross-linking could still be affected. Noguchi [78] showed that the repeated extrusion of defatted soy progressively reduced the soluble protein fractions while getting a fibrous structure after all three passes through the extruder. They, therefore, argued that "texturization" and "reactions" such as cross-linking should be considered as separate [78].

The use of large amplitude oscillatory shear (LAOS) rheology as well as the energy dissipation ratio, which shows a simplified perspective to reveal the complex information in the Lissajous curve, have also been picked up as tools to study melt properties [101]. LAOS provides information on the rheological properties beyond the linear viscoelastic regime but is more difficult to interpret than conventional small amplitude oscillatory shear (SAOS) measurements [104]. Using LAOS methods it was found that a thermal treatment can increase the elasticity of protein networks [101]. The thermal treatment caused pea protein isolate to lose its elastic properties more quickly than soy protein isolate and gluten.

The identification of new rheological tools has enabled the determination of rheological properties of the melt. This has led to rheological fingerprinting of the melt. A next

step will be to understand and interpret these complex results and relate them to the structuring process.

6.5   Cooling

After the thermo-mechanical treatment, the melt is cooled down (Figure 6.1). Cooling leads to a strengthening of the non-covalent interactions and the labile disulfide bonds become permanent (Section 6.4). This first results in an increase in viscosity before the material fully solidifies and the structure is fixed. When assuming the presence of a transient network in the melt, this network will become permanent upon cooling. An additional purpose of cooling is to prevent the expansion of the product as it exits the die or after opening the shear cell. Since the melt is cooled from the outside a viscosity gradient will be present before the material is fully solidified, with a lower viscosity in the hot interior. The significance of this change in viscosity depends on whether shear is applied during cooling.

The solidified material will have formed a cross-linked polymer network or gel. The protein source and concentration, cooling rate and heating temperature all affect the gel's properties. For example, pea protein isolates form weaker and less elastic gels compared to soy protein isolate [79, 110]. O'Kane et al. [79] showed that a low cooling rate results in stronger gels for both pea legumin and soy glycinin by measuring the storage modulus. Transmission electron microscopy showed more branched networks for samples made with a low cooling rate. This was attributed to the proteins remaining unfolded for longer, allowing for interactions and disulphide bonds to form more optimally [79]. However, it is unclear whether these findings also apply to the gelation during thermo-mechanical processing. Liu and Hsieh [82] compared heat-induced gels with extrudates made from SPI. Extrudates were found to be around 10 times harder and to have more disulphide bonds as measured via buffer extraction. However, since the gels were prepared at a much lower temperature (95°C) than the extrudates (170°C), direct comparison of these results is difficult. Apart from the cooling rate, also the protein concentration influences the modulus of SPI gels, with a higher concentration resulting in a higher modulus [52].

6.6   Mechanisms for structure formation

Now that we have described the different unit operations commonly found in thermo-mechanical processes and the effects they have on the material, we can discuss

the mechanism behind the structure formation itself. Since HMEC has been studied for a longer time than the shear cell, it is not surprising that effectively all hypotheses on structure formation stem from HMEC. Most mechanisms consider the cooling die (Figure 6.1h) as the 'structuring zone' where the formation of the fibrous structure takes place [26, 48, 63, 111]. However, the structuring zone may extend towards other regions of the extruder as well [87, 112]. All the identified mechanisms assume the presence of multiple phases that are in relative motion. However, they differ in the assumed reason for the multi-phase system, or the origin of the relative motion. As mentioned, these mechanisms have been developed with HMEC in mind. However, the proposed mechanisms may still apply to both HMEC and shear cell processing given the similar conditions inside (the beginning of) a cooling die and a heated, rotating shear cell. An overview of the different mechanisms is presented in Table 6.3 alongside a schematic representation of the mechanisms.

6.6.1 Phase behaviour of protein mixtures

The presence of two (or more) separate phases in bio-polymer mixtures is broadly accepted and has been studied extensively using a range of experimental and theoretical tools [7, 26, 28, 47–49, 51, 52]. The group of Tolstoguzov showed that protein-polysaccharide mixtures generally tend to phase-separate [47, 48], and that protein-protein blends do not mix at concentrations relevant to extrusion and shear cell processing [49]. Some do consider the hot melt as homogeneous, with separation occurring upon cooling down [111, 113]. However, the presence of two separate phases in bio-polymer mixtures was confirmed experimentally for hydrated mixtures of soy protein and gluten. The use of TD-NMR and rheological methods led to the insight that at both 25°C [51] and 140°C two separate phases are present [28].

Dekkers et al. [94] studied the rheological properties of soy protein and gluten. They suggested that to create fibrous structures the two phases in a bio-polymer mixture must have similar rheological properties during processing at high temperature. Schreuders et al. [28] later showed that pea protein and gluten have rather different rheological properties but can still be fibrillated. The similarity in rheological properties of the two phases, therefore, does not seem to be a universal requirement. Grabowska et al. [7] showed that gluten alone can form fibrous structures in the shear cell. Adding up to 50% of another protein (soy, pea, fababean) still resulted in the formation of fibres [30]. It was suggested that gluten should be a continuous phase, and is primarily responsible for fibre formation in gluten-containing mixtures. The second protein may act merely as a filler and may thus be easily replaced.

Protein isolates are multi-protein ingredients but are often assumed to behave as a single-phase when molten. This suggests that multiple ingredients are needed to obtain a two-phase system. Interestingly, the formation of fibrous structures from a single-ingredient has also been reported, such as through extrusion of hydrated pea protein isolate [35] or soy protein isolate [19]. Arêas [114] proposed that single-ingredient systems can still behave as a two-phase system. They described in an earlier study that insoluble and non-melting components in a protein isolate could act as a second phase and induce structure formation. Indeed, the polysaccharides in protein concentrates can also act as a second phase [34]. Hydrated gluten is also thought to form a two-phase system due to partitioning based on the molecular weight [115]. This might explain why processing hydrated gluten in a shear cell results in a fibrous product [7, 30]. Despite the predominant thought that protein melts are multi-phase systems, a recent paper by Sandoval Murillo et al. [111] posed that the hot melt is a homogeneous single-phase system of hydrated bio-polymers. They hypothesized that a melt of pea protein isolate and water decomposes into water-rich and protein-rich domains upon entering the cooling die due to *spinodal decomposition*. The spinodal decomposition of the melt in the die section was simulated using the Cahn-Hilliard equation. Phase separation was assumed to be temperature-driven through a temperature-dependent free-energy. The notion of a homogeneous, single-phase melt seems to conflict with the often assumed thermodynamic incompatibility of proteins. Protein isolates are always mixtures of different proteins despite originating from the same crop, in this case, pea. Different phases could, therefore, still be a possibility. Furthermore, as also stated by Sandoval Murillo et al. [111], some of the used model parameters such as the chosen interfacial tension, may not have been appropriate. Regardless, they provide an interesting hypothesis for structure formation in the die.

6.6.2 Flow-induced structuring mechanisms

All the identified hypotheses for structure formation consider the importance of the flow behaviour of the melt. The Reynolds number, Re, can give insight into flow behaviour by providing an indication of whether laminar (low Re) or turbulent flow (high Re) could be expected. When assuming a rectangular duct, the Reynolds number can be calculated as [116]:

$$Re = \frac{\rho_{melt} \cdot u \cdot D_H}{\mu} \tag{6.4}$$

With ρ_{melt} as the melt density (1087.2 kg m^{-3}), u as the average melt velocity, and μ as the melt dynamic viscosity. The hydraulic diameter, D_H, was calculated as $D_H = \frac{4 \cdot A}{C}$ with A as the cross-sectional area and C as the circumference of the die. When assuming a melt viscosity of 1 kPa s, the Reynolds numbers for the processes in Table 6.1 range from 2 to 73. At such low Reynolds numbers, it is reasonable to assume laminar flow [116]. The *laminar flow* profile in the cooling die is often considered to be responsible for structure formation [31, 37, 63, 64, 111]. However, the type of laminar flow is most often not specified, although some have assumed shear flow at the entrance of the die and plug flow towards the end of the die [111]. Shear flow has been shown to induce alignment in dilute polymer solutions when flowing through a rectangular or circular die [117]. Cheftel et al. [26] and later Akdogan [63] discussed a mechanism where the melt would solidify as it passes through the cooling die. The material closest to the die wall would be cooled down first and, therefore, increase in viscosity. The interior would remain hotter and, therefore, of lower viscosity. The difference in viscosity would enhance the velocity gradient in the cooling die. This was suggested as the origin of fibre formation. While the mechanism hypothesised by Cheftel et al. [26] and Akdogan [63] is commonly considered reasonable, direct proof in support of the hypothesis is limited to visual observations of the extrudate [26]. Future research could combine rheological measurements with modeling to test this hypothesis further.

The group of Tolstoguzov showed that the dispersed phase in emulsions can be deformed by shear flow. The degree of droplet deformation was found to depend on the viscosity ratio between the two phases [118]. They also studied the extrusion of bio-polymer mixtures [47–49]. The mechanism they proposed for the deformation of emulsion droplets was also used to explain structure formation inside the cooling die during low-moisture extrusion [48]. It was assumed that droplets of the dispersed phase *deform and align* in the shear flow direction (Table 6.3). Individual droplets could coalesce and result in both long and short fibres. The low interfacial tension between phases in water-in-water emulsions would facilitate the generation of the additional interface and facilitate phase deformation and alignment [48]. The formed structure could be fixed through cooling. This mechanism has been applied by Dekkers et al. [23] to explain the formation of a fibrous structure obtained after processing soy protein isolate and citrus pectin in a shear cell. Soy can also act as a co-continuous or dispersed phase when combined with gluten [28, 30]. The continuous phase may thus depend on the combination of ingredients used. If the mechanism posed by Tolstoguzov [48] would apply to a bi-continuous system is unclear.

6.6.3 Barrel to die transition zone

While most authors have focused on the cooling die when studying structure formation, the section between the barrel and the cooling die could also be of importance to the structure formation process. Yao et al. [87] used dead-stop experiments to study structure formation inside the barrel using soy protein, gluten and starch. Their results showed that fibre formation may start at the end of the barrel as indicated by both an increase in anisotropy and visual inspection of the structure. However, as also mentioned in the original study, the dead-stop approach could have affected the structure.
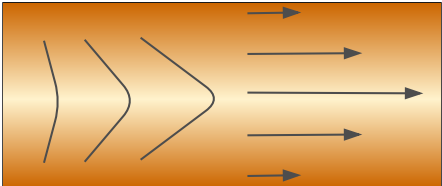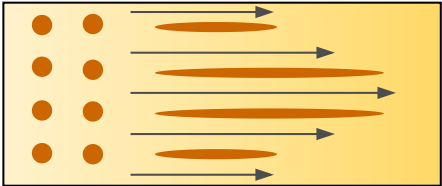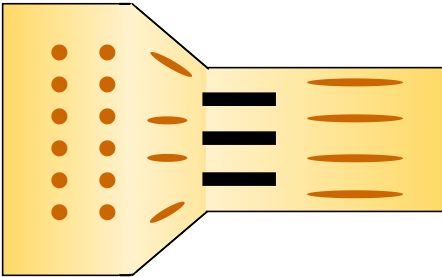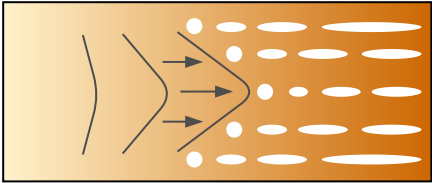
In the transition zone between the barrel and the cooling die, a so-called breaker plate can be present (Figure 6.1g). The breaker plate can homogenize the pressure and pre-align the flow before the melt enters the cooling die. Hine et al. [40] studied the effect of removing the breaker plate on the alignment of glass fibre in reinforced polypropylene extrudates. The use of a breaker plate resulted in more alignment of the glass fibres, which was attributed to the pre-alignment of the fibres by the breaker plate. Lin and Cheung [112] reported the presence of strands inside the extrudates when extruding blends of polyoxymethylene (POM) and polypropylene (PP). The location and positioning of the strands matched the holes of the breaker plate. Probably, the spherically shaped dispersed phase experienced *elongational flow* when passing through the breaker plate. This could have stretched the dispersed phase into elongated strands, resulting in the observed structure. Local concentrations of the two polymers varied, with the outer strands higher in polypropylene. Although one of the main purposes of a breaker plate is to stabilize and align the flow, their potentially significant role in structure formation has to our knowledge not yet been picked up in the field of food science.

6.6.4 Shear-induced structuring in some non-food systems

Foods can be considered highly complex in both composition and behaviour. This complexity can hinder the elucidation of the underlying mechanisms by impeding direct measurements and obscuring the behaviour. It can, therefore, be of interest to study systems that are simpler in terms of composition. Shear-induced structure formation is also seen in particle suspensions and two-phase polymer systems. We will discuss some of the findings from these fields and discuss their potential implications for the thermo-mechanical processing on foods.

Flow-induced structure formation is frequently observed in suspension rheology in

Table 6.3: Schematic representation of different structuring mechanisms that could be responsible for the structuring potential of plant-proteins, HMEC, High-Moisture Extrusion Cooking, SC, Shear Cell.

Mechanism	Applicability	Schematic representation
Laminar flow results in a velocity gradient, which induces fiber formation parallel to the deformation. Velocity gradients can be enhanced by temperature-induced viscosity gradients [26, 63]	HMEC	
Phase deformation and alignment, the dispersed phase in the melt is deformed in the flow direction [48]	HMEC, SC	
Elongational flow in the breaker plate, the dispersed phase is deformed in the flow direction while passing through the breaker plate [40]	HMEC	
Spinodal decomposition, the homogeneous melt undergoes spinodal deformation into a water-rich and water-poor phase as a result of shear and a critical cooling temperature [111]	HMEC	

the form of shear-bands [119–124]. Van Loon et al. [121] systematically investigated the importance of several rheological characteristics of the continuous phase for the occurrence of shear bands and identified shear-thinning behaviour of the continuous phase as essential for the formation and stability of shear-bands. As two particles approach each other, the local shear rate will increase. This would locally reduce the viscosity of the shear-thinning fluid, and limit the hydrodynamic coupling between particles. This, they argue, would enable each particle on the chain to satisfy the zero-torque condition, and thus keep the chain as a whole from tumbling and breaking up. The resemblance between a shear-thinning fluid with dispersed rigid particles and a two-phase polymer melt may be limited. Polymer melts are generally shear-thinning, which suggests that both the continuous and dispersed phases of the melt will have similar properties. However, the properties of the dispersed phase may not be comparable to those of the relatively rigid colloidal particles used in the aforementioned studies. Although approximating the dispersed phase as rigid particles may be an over-simplification, some of the physics may still apply. Whether shear-thinning of the continuous phase is decisive for structure formation in HMEC or shear cell processing thus remains unclear.

The formation of shear-bands has also been observed in sheared polymer solutions [125–128]. Caserta et al. [127] showed that a mixture of two immiscible polymer solutions can form shear-bands [127]. Shear-band formation was associated with a reduction in overall viscosity of the system and is, therefore, thought to be an effort of the system to reduce the viscous energy dissipation [127]. The droplets present in solutions of two immiscible polymers can also align on a string parallel to the flow direction [127, 128]. When the viscosity ratio was reduced to 0.01, droplets formed 'pearl-necklace' structures parallel to the vorticity direction superimposed to those in the flow direction [127]. The dimensionless size of the droplets was shown to scale with the dimensionless shear rate, until a transition from droplets to string formation occurred as the shear rate went below 2.5 s^{-1} [128]. Moving through this transition induces a change in micro-structure from individual droplets to elongated strings through alignment and coalescence of the individual droplets.

Most of these studies use semi-dilute polymer solutions (10% v/v); much lower concentrations than commonly used in food extrusion ($> 30wt\%$). Still, some similarities can be identified. The observations by Migler [128] for dilute two-phase polymer solutions are comparable to the mechanism proposed by Tolstoguzov [48] for extrudates.

6.7 General discussion

We have reviewed the thermo-mechanical processing of plant-proteins through high-moisture extrusion cooking (HMEC) and shear cell processing for the production of plant-based meat analogues. The HMEC and shear cell processes were found to be comparable in their basic processing steps. These steps are mixing and hydration, thermo-mechanical treatment, and cooling (Figure 6.1). We noticed a lack of understanding of the physical changes that are induced by the process, most notably the effect of thermo-mechanical treatment on protein-protein interactions. Furthermore, the mechanism by which fibrous structures are made remains unclear.

The effect of thermo-mechanical treatment on proteins has been studied extensively. However, many studies focused on the product obtained *after* processing. While this may provide insight into product properties, it does not provide conclusive information on protein behaviour *during* processing. Indeed, direct measurement of for example protein-protein interactions at processing conditions is challenging with the currently available machinery. However, it is our opinion that thermo-mechanical processes can only be fully understood by learning the nature of protein-protein interactions at the relevant processing conditions. The use of inline spectroscopic methods such as NIR and Raman spectroscopy could greatly improve our understanding of the behaviour of proteins during thermo-mechanical processing.

We identified several hypotheses to explain the formation of fibrous structures. These hypotheses are all based on flow-induced deformation (Table 6.3). Due to the lack of shear during cooling in the shear cell process, structure formation in shear cell processing is expected to be completed as soon as the shear is stopped. The mechanisms that assume shear during cooling (spinodal decomposition and deformation; temperature-induced viscosity gradients; Table 6.3), therefore, cannot apply to the shear cell. The mechanism of a deformed dispersed phase could apply to both structuring processes. However, the amount of direct evidence supporting the different mechanisms is limited and keeps us from selecting a universal mechanism for the thermo-mechanical structuring of plant proteins. Furthermore, we found that the often overlooked breaker plates found in extruders could play an important role in structure formation by providing elongational flow. Moreover, the fact that fibrous structures can be made from ingredients with different properties suggests that different mechanisms may result in a similar fibrous product. Therefore, more direct and indirect measurements of material properties inside the cooling die and shear cell

are necessary to confirm the mechanism underlying structure formation. For example, the shear cell developed by Velichko et al. [129] combined with (ultra-) small-angle neutron and X-ray scattering (SANS/SAXS) could provide insight into the micro- and nano-scale structure of flowing two-phase systems. Doppler Velocimetry [130] could prove useful by providing an inline measurement of the flow profile. Furthermore, the extensive body of work on flow-induced structuring in non-food suspensions and polymer mixtures and future studies using simplified model systems could provide further insight.

Off-line methodology will also play an important role due to their flexibility and ease of operation. The use of sophisticated closed-cavity rheometers (CCRs) could mark the start of a revolution in protein structuring as they enable measuring rheological properties at high temperatures and pressures. However, the currently available CCRs cannot match all of the relevant process conditions such as pressure and shear rate. Therefore, the development of CCRs dedicated to protein melt analysis may be necessary. These devices should include the ability to perform rotational experiments in addition to oscillatory experiments to improve the resemblance with thermo-mechanical processing. The additional insight into material properties during processing could be used as an input for physical model simulations. Accurate model inputs are essential to the validity of simulation results. While models are always simplifications of reality, they could help in identifying the relevant process parameters and could limit the number of extrusion or shear cell trials needed to answer a specific research question.

In conclusion, we have found that thermo-mechanical processing still has many open questions. These questions will need to be answered through the use of online and off-line methods to obtain better control over the process, and to ultimately acquire predictive power concerning ingredient–product relationships.

Acknowledgements

References

[1] H. Aiking and J. de Boer. The next protein transition. *Trends in Food Science and Technology*, pages 512–522, 2020.

[2] A. Chaudhary, D. Gustafson, and A. Mathys. Multi-indicator sustainability assessment of global food systems. *Nature Communications*, 9(1), 2018.

[3] D. Pimentel and M. Pimentel. Sustainability of meat-based and plant-based diets and the environment. *American Journal of Clinical Nutrition*, 78(3 SUPPL.), 2003.

[4] A.C. Hoek. *Will Novel Protein Foods beat meat? Consumer acceptance of meat substitutes - a multidisciplinary research approach*. PhD thesis, Wageningen UR, 2010.

[5] M. Nieuwland, P. Geerdink, P. Brier, P. Van Den Eijnden, J.T.M.M. Henket, M.L. Langelaan, N. Stroeks, H.C. Van Deventer, and A.H. Martin. Food-grade electrospinning of proteins. *Innovative Food Science and Emerging Technologies*, 20:269–275, 2014.

[6] J.H. Chiang, S.M. Loveday, A.K. Hardacre, and M.E. Parker. Effects of soy protein to wheat gluten ratio on the physicochemical properties of extruded meat analogues. *Food Structure*, 19(September 2018):100102, 2019.

[7] K.J. Grabowska, S. Tekidou, R.M. Boom, and A.J. van der Goot. Shear structuring as a new method to make anisotropic structures from soy-gluten blends. *Food Research International*, 64:743–751, 2014.

[8] G.A. Krintiras, J. Gadea Diaz, A.J. Van Der Goot, A.I. Stankiewicz, and G.D. Stefanidis. On the use of the Couette Cell technology for large scale production of textured soy-based meat replacers. *Journal of Food Engineering*, 169:205–213, 2016.

[9] I. Kutzli, M. Gibis, S.K. Baier, and J. Weiss. Electrospinning of whey and soy protein mixed with maltodextrin – Influence of protein type and ratio on the production and morphology of fibers. *Food Hydrocolloids*, 93(January):206–214, 2019.

[10] R. Leidy and Q.C. Maria Ximena. Use of electrospinning technique to produce nanofibres for food industries: A perspective from regulations to characterisations. *Trends in Food Science and Technology*, 85(May 2018):92–106, 2019.

[11] A.C. Mendes, K. Stephansen, and I.S. Chronakis. Electrospinning of food proteins and polysaccharides. *Food Hydrocolloids*, 68:53–68, 2017.

[12] J.M. Manski, A.J. van der Goot, and R.M. Boom. Advances in structure formation of anisotropic protein-rich foods through novel processing concepts. *Trends in Food Science and Technology*, 18(11):546–557, 2007.

[13] R.M. Van Den Einde, A.J. Van Der Goot, and R.M. Boom. Understanding Molecular Weight Reduction of Starch during Heating-shearing Processes. *Journal of Food Science*, 68(8): 2396–2404, 2003.

[14] S.H. Peighambardoust, A.J. van der Goot, R.J. Hamer, and R.M. Boom. A New Method to Study Simple Shear Processing of Wheat Gluten-Starch Mixtures. *Cereal Chemistry*, 81(6): 714, 2004.

[15] J.M. Manski, A.J. van der Goot, and R.M. Boom. Formation of fibrous materials from dense calcium caseinate dispersions. *Biomacromolecules*, 8(4):1271–1279, 2007.

[16] E. Klüver and M. Meyer. Thermoplastic Processing, Rheology, and Extrudate Properties of Wheat, Soy, and Pea Proteins. *Polymer Engineering & Science*, 55(8):1912–1919, 2015.

[17] B. Ralston and T. Osswald. Viscosity of soy protein plastics determined by screw-driven capillary rheometry. *Journal of Polymers and the Environment*, 16(3):169–176, 2008.

[18] S. Samard, B.Y. Gu, and G.H. Ryu. Effects of extrusion types, screw speed and addition of wheat gluten on physicochemical characteristics and cooking stability of meat analogues. *Journal of the Science of Food and Agriculture*, 99(11):4922–4931, 2019.

[19] Y. Fang, B. Zhang, and Y. Wei. Effects of the specific mechanical energy on the physicochemical properties of texturized soy protein during high-moisture extrusion cooking. *Journal of Food Engineering*, 121(1):32–38, 2014.

[20] V.L. Pietsch, M.A. Emin, and H.P. Schuchmann. Process conditions influencing wheat gluten polymerization during high moisture extrusion of meat analog products. *Journal of Food Engineering*, 198:28–35, 2016.

[21] B.L. Dekkers, R. Hamoen, R.M. Boom, and A.J. van der Goot. Understanding fiber formation in a concentrated soy protein isolate - Pectin blend. *Journal of Food Engineering*, 222:84–92, 2018.

[22] F.K.G. Schreuders, B.L. Dekkers, I. Bodnár, P. Erni, R.M. Boom, and A.J. van der Goot. Comparing structuring potential of pea and soy protein with gluten for meat analogue preparation. *Journal of Food Engineering*, 261(May):32–39, 2019.

[23] B.L. Dekkers, C.V. Nikifioridis, and A.J. van der Goot. Shear-induced fibrous structure formation from a pectin/SPI blend. *Innovative Food Science and Emerging Technologies*, 36:193–200, aug 2016.

[24] G. Puski and A.H. Konwinski. Process of making a soy-based meat substitute, 1976.

[25] M.F. Campbell. Processing and product characteristics for textured soy flours, concentrates and isolates. *Journal of the American Oil Chemists' Society*, 58(3):336–338, 1981.

[26] J. Cheftel, M. Kitagawa, and C. Queguiner. New Protein Texturization Processes by Extrusion Cooking at High Moisture Levels. *Food Reviews International*, 8(2):235–275, 1992.

[27] M.P. Caporgno, L. Böcker, C. Müssner, E. Stirnemann, I. Haberkorn, H. Adelmann, S. Handschin, E.J. Windhab, and A. Mathys. Extruded meat analogues based on yellow, heterotrophically cultivated Auxenochlorella prototheecoides microalgae. *Innovative Food Science and Emerging Technologies*, 59(December 2019):102275, 2020.

[28] F. Schreuders, I. Bodnár, P. Erni, R. Boom, and A. van der Goot. Water redistribution determined by time domain NMR explains rheological properties of dense fibrous protein blends at high temperature. *Food Hydrocolloids*, 101, 2020.

[29] J. Zhang, L. Liu, Y. Jiang, S. Faisal, Y. Xu, and Q. Wang. High-moisture extrusion of peanut protein-/carrageenan/sodium alginate/wheat starch mixtures: Effect of different exogenous polysaccharides on the process forming a fibrous structure. *Food Hydrocolloids*, 99(August 2019):105311, 2020.

[30] S.H.V. Cornet, J.M. Bühler, R.C. Goncalves, M. Bruins, R.G.M. van der Sman, and A.J. van der Goot. Apparent universality in swelling and fibre formation by mixtures of gluten and leguminous proteins. *Submitted*, 1(1):1, 2020.

[31] M. Palanisamy, S. Töpfl, R.G. Berger, and C. Hertel. Physico-chemical and nutritional

properties of meat analogues based on Spirulina/lupin protein mixtures. *European Food Research and Technology*, 245(9):1889–1898, 2019.

[32] V.L. Pietsch, J.M. Bühler, H.P. Karbstein, and M.A. Emin. High moisture extrusion of soy protein concentrate: Influence of thermomechanical treatment on protein-protein interactions and rheological properties. *Journal of Food Engineering*, 251(August 2018):11–18, 2019.

[33] M.E. Geerts, B.L. Dekkers, A. van der Padt, and A.J. van der Goot. Aqueous fractionation processes of soy protein for fibrous structure formation. *Innovative Food Science and Emerging Technologies*, 45(September 2017):313–319, 2018.

[34] K.J. Grabowska, S. Zhu, B.L. Dekkers, N.C.A. De Ruijter, J. Gieteling, and A.J. van der Goot. Shear-induced structuring as a tool to make anisotropic materials using soy protein concentrate. *Journal of Food Engineering*, 188:77–86, 2016.

[35] R. Osen, S. Toelstede, P. Eisner, and U. Schweiggert-Weisz. Effect of high moisture extrusion cooking on protein-protein interactions of pea (Pisum sativum L.) protein isolates. *International Journal of Food Science and Technology*, 50(6):1390–1396, 2015.

[36] B. Zhang, Y. Zhang, J. Dreisoerner, and Y. Wei. The effects of screw configuration on the screw fill degree and special mechanical energy in twin-screw extruder for high-moisture texturised defatted soybean meal. *Journal of Food Engineering*, 157:77–83, 2015.

[37] R. Osen, S. Toelstede, F. Wild, P. Eisner, and U. Schweiggert-Weisz. High moisture extrusion cooking of pea protein isolates: Raw material characteristics, extruder responses, and texture properties. *Journal of Food Engineering*, 127:67–74, 2014.

[38] D. Rehrah, M. Ahmedna, I. Goktepe, and J. Yu. Extrusion parameters and consumer acceptability of a peanut-based meat analogue. *International Journal of Food Science and Technology*, 44(10):2075–2084, 2009.

[39] K. Liu and F.H. Hsieh. Protein-protein interactions during high-moisture extrusion for fibrous meat analogues and comparison of protein solubility methods using different solvent systems. *Journal of Agricultural and Food Chemistry*, 56(8):2681–2687, 2008.

[40] P.J. Hine, S.W. Tsui, P.D. Coates, I.M. Ward, and R.A. Duckett. Measuring the development of fibre orientation during the melt extrusion of short glass fibre reinforced polypropylene. *Composites Part A: Applied Science and Manufacturing*, 28(11):949–958, 1997.

[41] J.M. Manski, E.E. van der Zalm, A.J. van der Goot, and R.M. Boom. Influence of process parameters on formation of fibrous materials from dense calcium caseinate dispersions and fat. *Food Hydrocolloids*, 22(4):587–600, jun 2008.

[42] G. Krintiras, J. Göbel, A. van der Goot, and G. Stefanidis. Production of structured soy-based meat analogues using simple shear and heat in a Couette Cell. *Journal of Food Engineering*, 160:34–41, 2015.

[43] F.E. Giezen, W.W.J.T. Jansen, and J.H. Willemsen. Method of making structured protein composites, 2014.

[44] S.G. Hatzikiriakos. Wall slip of molten polymers. *Progress in Polymer Science (Oxford)*, 37 (4):624–643, 2012.

[45] Y. Son. Determination of shear viscosity and shear rate from pressure drop and flow rate relationship in a rectangular channel. *Polymer*, 48(2):632–637, 2007.

[46] M.A. Emin and H.P. Schuchmann. Analysis of the dispersive mixing efficiency in a twin-screw

extrusion processing of starch based matrix. *Journal of Food Engineering*, 115(1):132–143, 2013.

[47] V.Y. Grinberg and V.B. Tolstoguzov. Thermodynamic incompatibility of proteins and polysaccharides in solutions. *Food Hydrocolloids*, 11(2):145–158, apr 1997.

[48] V.B. Tolstoguzov. Thermoplastic extrusion—the mechanism of the formation of extrudate structure and properties. *Journal of the American Oil Chemists' Society*, 70(4):417–424, apr 1993.

[49] V.I. Polyakov, V.Y. Grinberg, and V.B. Tolstoguzov. Thermodynamic incompatibility of proteins. *Food Hydrocolloids*, 11(2):171–180, 1997.

[50] A. Clark, R. Richardson, S. Ross-Murphy, and J. Stubbs. Structural and Mechanical Properties of Agar/Gelatin Co-gels. Small-Deformation Studies. *Macromolecules*, 16(8):1367–1374, 1983.

[51] B.L. Dekkers, D.W. de Kort, K.J. Grabowska, B. Tian, H. Van As, and A.J. van der Goot. A combined rheology and time domain NMR approach for determining water distributions in protein blends. *Food Hydrocolloids*, 60:525–532, 2016.

[52] S.H.V. Cornet, A.J. van der Goot, and R.G.M. van der Sman. Effect of mechanical interaction on the hydration of mixed soy protein and gluten gels. *Current Research in Food Science*, 3: 134–145, 2020.

[53] F. Cordier and S. Grzesiek. Temperature-dependence of protein hydrogen bond properties as studied by high-resolution NMR. *Journal of Molecular Biology*, 317(5):739–752, 2002.

[54] E. van Dijk, A. Hoogeveen, and S. Abeln. The Hydrophobic Temperature Dependence of Amino Acids Directly Calculated from Protein Structures. *PLoS Computational Biology*, 11 (5):1–17, 2015.

[55] E. Evans. Probing the relation between force - lifetime - and chemistry in single molecular bonds. *Annual Review of Biophysics and Biomolecular Structure*, 30:105–128, 2001.

[56] D.B. Volkin and A.M. Klibanov. Thermal destruction processes in proteins involving cystine residues. *Journal of Biological Chemistry*, 262(7):2945–2950, 1987.

[57] A.P. Ryle and F. Sanger. Disulphide interchange reactions. *The Biochemical journal*, 60(4): 535–540, 1955.

[58] A.H. Bloksma. Thiol and disulfide groups in dough rheology. *Cereal Chemistry*, 52(3):170–183, 1975.

[59] J.D. Schofield, R.C. Bottomley, M.F. Timms, and M.R. Booth. The effect of heat on wheat gluten and the involvement of sulphydryl-disulphide interchange reactions. *Journal of Cereal Science*, 1(4):241–253, 1983.

[60] H. Choi, K. Aboulfatova, H.J. Pownall, R. Cook, and J.F. Dong. Shear-induced disulfide bond formation regulates adhesion activity of von Willebrand factor. *Journal of Biological Chemistry*, 282(49):35604–35611, 2007.

[61] P. Nagy. Kinetics and mechanisms of thiol-disulfide exchange covering direct substitution and thiol oxidation-mediated pathways. *Antioxidants and Redox Signaling*, 18(13):1623–1641, 2013.

[62] D.J. Van Zuilichem. Extrusion Cooking: Craft or Science ? *PhD Thesis Wageningen University*, pages 1–189, 1992.

[63] H. Akdogan. High moisture food extrusion. *International Journal of Food Science and Technology*, 34(3):195–207, 1999.

[64] J. Zhang, L. Liu, H. Liu, A. Yoon, S.S.H. Rizvi, and Q. Wang. Changes in conformation and quality of vegetable protein during texturization process by extrusion. *Critical Reviews in Food Science and Nutrition*, 59(20):3267–3280, 2019.

[65] T.D. Strecker, R.P. Cavalieri, R.L. Zollars, and Y. Pomeranz. Polymerization and Mechanical Degradation Kinetics of Gluten and Glutenin at Extruder Melt-Section Temperatures and Shear Rates. *Journal of Food Science*, 60(3):532–537, 1995.

[66] V.L. Pietsch, H.P. Karbstein, and M.A. Emin. Kinetics of wheat gluten polymerization at extrusion-like conditions relevant for the production of meat analog products. *Food Hydrocolloids*, 85(July):102–109, 2018.

[67] B. Lagrain, B.G. Thewissen, K. Brijs, and J.A. Delcour. Mechanism of gliadin-glutenin cross-linking during hydrothermal treatment. *Food Chemistry*, 107(2):753–760, 2008.

[68] T.S.K. Ng and G.H. McKinley. Power law gels at finite strains: The nonlinear rheology of gluten gels. *Journal of Rheology*, 52(2):417–449, 2008.

[69] G. Attenburrow, D.J. Barnes, A.P. Davies, and S.J. Ingman. Rheological properties of wheat gluten. *Journal of Cereal Science*, 12(1):1–14, 1990.

[70] M.H. Morel, A. Redl, and S. Guilbert. Mechanism of Heat and Shear Mediated Aggregation of Wheat Gluten Protein upon Mixing. *Biomacromolecules*, 3:488–497, 2002.

[71] D. Peressini, S.H. Peighambardoust, R.J. Hamer, A. Sensidoni, and A.J. van der Goot. Effect of shear rate on microstructure and rheological properties of sheared wheat doughs. *Journal of Cereal Science*, 48(2):426–438, 2008.

[72] N.M. Edwards, D. Peressini, J.E. Dexter, and S.J. Mulvaney. Viscoelastic properties of durum wheat and common wheat dough of different strengths. *Rheologica Acta*, 40(2):142–153, 2001.

[73] M.A. Emin, M. Quevedo, M. Wilhelm, and H.P. Karbstein. Analysis of the reaction behavior of highly concentrated plant proteins in extrusion-like conditions. *Innovative Food Science and Emerging Technologies*, 44(June):15–20, 2017.

[74] S. Domenek, M.H. Morel, J. Bonicel, and S. Guilbert. Polymerization kinetics of wheat gluten upon thermosetting. A mechanistic model. *Journal of Agricultural and Food Chemistry*, 50(21):5947–5954, 2002.

[75] B. Lagrain, K. Brijs, and J.A. Delcour. Reaction Kinetics of gliadin-glutenin cross-linking in model systems and in bread making. *Journal of Agricultural and Food Chemistry*, 56(22):10660–10666, 2008.

[76] K. Shimada and J.C. Cheftel. Determination of Sulfhydryl Groups and Disulfide Bonds in Heat-Induced Gels of Soy Protein Isolate. *Journal of Agricultural and Food Chemistry*, 36(1):147–153, 1988.

[77] B.L. Dekkers, R.M. Boom, and A.J. van der Goot. Viscoelastic properties of soy protein isolate - pectin blends: Richer than those of a simple composite material. *Food Research International*, 107(February):281–288, 2018.

[78] A. Noguchi. Extrusion Cooking of High-Moisture Protein foods. In C. Mercier, P. Linko, and J.M. Harper, editors, *Extrusion Cooking*, chapter 11, pages 343–370. American Association of Cereal Chemists, St. Paul Minnesota, 1st edition, 1989.

[79] F. O'Kane, R. Happe, J. Vereijken, H. Gruppen, and M. Van Boekel. Heat-induced gelation of pea legumin: Comparison with soybean glycinin. *Journal of Agricultural and Food Chemistry*, 52(16):5071–5078, 2004.

[80] P.R. Shewry and A.S. Tatham. Disulphide bonds in wheat gluten proteins. *Journal of Cereal Science*, 25(3):207–227, 1997.

[81] J.A.M. Berghout, P. Venema, R.M. Boom, and A.J. van der Goot. Comparing functional properties of concentrated protein isolates with freeze-dried protein isolates from lupin seeds. *Food Hydrocolloids*, 51:346–354, 2015.

[82] K.S. Liu and F.H. Hsieh. Protein-protein interactions in high moisture-extruded meat analogs and heat-induced soy protein gels. *JAOCS, Journal of the American Oil Chemists' Society*, 84(8):741–748, 2007.

[83] F.L. Chen, Y.M. Wei, and B. Zhang. Chemical cross-linking and molecular aggregation of soybean protein during extrusion cooking at low and high moisture content. *LWT - Food Science and Technology*, 44(4):957–962, 2011.

[84] M.A. Emin and H.P. Schuchmann. A mechanistic approach to analyze extrusion processing of biopolymers by numerical, rheological, and optical methods. *Trends in Food Science and Technology*, 60:88–95, 2017.

[85] Y. Fang, B. Zhang, Y. Wei, and S. Li. Effects of specific mechanical energy on soy protein aggregation during extrusion process studied by size exclusion chromatography coupled with multi-angle laser light scattering. *Journal of Food Engineering*, 115(2):220–225, 2013.

[86] F.L. Chen, Y.M. Wei, B. Zhang, and A.O. Ojokoh. System parameters and product properties response of soybean protein extruded at wide moisture range. *Journal of Food Engineering*, 96(2):208–213, 2010.

[87] G. Yao, K.S. Liu, and F. Hsieh. A New Method for Characterizing Fiber Formation in Meat Analogs during High-moisture Extrusion. *Food Engineering and Phyiscal Properties*, 69(7): 303–307, 2004.

[88] S.E. Barnes, M.G. Sibley, H.G. Edwards, and P.D. Coates. Process monitoring of polymer melts using in-line spectroscopy. *Transactions of the Institute of Measurement & Control*, 29 (5):453–465, 2007.

[89] X. Huang, Y. Lei, M. Wang, and G. Jin. In-line monitoring of component content of polypropylene/polystyrene blends during melt extrusion using Raman spectroscopy. *Journal of Raman Spectroscopy*, 49(3):513–519, 2018.

[90] T.R. Hörmann, J. Rehrl, O. Scheibelhofer, L.M. Schaden, A. Funke, C. Makert, and J.G. Khinast. Sensitivity of a continuous hot-melt extrusion and strand pelletization line to control actions and composition variation. *International Journal of Pharmaceutics*, 566(February): 239–253, 2019.

[91] M.G. Hansen and S. Vedula. In-line fiber-optic near-infrared spectroscopy: Monitoring of rheological properties in an extrusion process. Part I. *Journal of Applied Polymer Science*, 68 (6):859–872, 1998.

[92] C.H. Wang, C.C. Huang, L.L. Lin, and W. Chen. The effect of disulfide bonds on protein folding, unfolding, and misfolding investigated by FT–Raman spectroscopy. *Journal of Raman Spectroscopy*, 47(8):940–947, 2016.

[93] Y. Ozakisj, A. Mizunolt, and K. Iriyamas. Inter- and Intramolecular Disulfide Bond Formation and Related Structural Changes in the Lens Proteins. *Journal of Biologic*, 262 (32):15545–15551, 1987.

[94] B.L. Dekkers, M.A. Emin, R.M. Boom, and A.J. van der Goot. The phase properties of soy protein and wheat gluten in a blend for fibrous structure formation. *Food Hydrocolloids*, 79: 273–281, 2018.

[95] Y.L.N. Thadavathi, S. Wassén, and R. Kádár. In-line rheological and microstroctural characterization of high moisture content protein vegetable mixtures in single screw extrusion. *Journal of Food Engineering*, 245(April 2018):112–123, 2019.

[96] M. Horvat, M. Azad Emin, B. Hochstein, N. Willenbacher, and H.P. Schuchmann. A multiple-step slit die rheometer for rheological characterization of extruded starch melts. *Journal of Food Engineering*, 116(2):398–403, 2013.

[97] G.M. Corfield, M.J. Adams, B.J. Briscoe, P.J. Fryer, and C.J. Lawrence. A critical examination of capillary rheometry for foods (exhibiting wall slip). *Food and Bioproducts Processing: Transactions of the Institution of of Chemical Engineers, Part C*, 77(1):3–10, 1999.

[98] W. Aichholzer and H.G. Fritz. Rheological characterization of thermoplastic starch materials. *Starch/Staerke*, 50(2-3):77–83, 1998.

[99] A. Ponrajan, T. Tonner, M. Okos, O. Campanella, and G. Narsimhan. Comparing inline extrusion viscosity for different operating conditions to offline capillary viscosity measurements. *Journal of Food Process Engineering*, 43(March):1–11, 2019.

[100] S.M. Beck, K. Knoerzer, J. Sellahewa, M.A. Emin, and J. Arcot. Effect of different heat-treatment times and applied shear on secondary structure, molecular weight distribution, solubility and rheological properties of pea protein isolate as investigated by capillary rheometry. *Journal of Food Engineering*, 208:66–76, 2017.

[101] F. Schreuders, L. Sagis, I. Bodnár, P. Erni, R. Boom, and A. van der Goot. Small and large oscillatory shear properties of concentrated proteins. *Food Hydrocolloids*, 110, jan 2021.

[102] J.L. Leblanc. Nonlinear viscoelastic characterization of molten thermoplastic vulcanizates (TPV) through large amplitude harmonic experiments. *Rheologica Acta*, 46(8):1013–1027, 2007.

[103] A. Mongruel and M. Cartault. Nonlinear rheology of styrene-butadiene rubber filled with carbon-black or silica particles. *Journal of Rheology*, 50(2):115–135, 2006.

[104] K. Hyun, M. Wilhelm, C.O. Klein, K.S. Cho, J.G. Nam, K.H. Ahn, S.J. Lee, R.H. Ewoldt, and G.H. McKinley. A review of nonlinear oscillatory shear tests: Analysis and application of large amplitude oscillatory shear (LAOS). *Prog. Polym. Sci.*, 36(12):1697–1753, 2011.

[105] M. Pommet, M.H. Morel, A. Redl, and S. Guilbert. Aggregation and degradation of plasticized wheat gluten during thermo-mechanical treatments, as monitored by rheological and biochemical changes. *Polymer*, 45(20):6853–6860, 2004.

[106] W.P. Cox and E.H. Merz. Correlation of Dynamic and Steady Flow Viscosities. *Journal of Polymer Science*, 28(118):619–622, 1958.

[107] C.T. Udyarajan, D.S. Horne, and J.A. Lucey. Use of time-temperature superposition to study the rheological properties of cheese during heating and cooling. *International Journal of Food Science and Technology*, 42(6):686–698, 2007.

[108] K. Katsuta and J.E. Kinsella. Effects of Temperature on Viscoelastic Properties and Activation Energies of Whey Protein Gels. *Journal of Food Science*, 55(5):1296–1302, 1990.

[109] A. Allmendinger, S. Fischer, J. Huwyler, H.C. Mahler, E. Schwarb, I.E. Zarraga, and R. Mueller. Rheological characterization and injection forces of concentrated protein formulations: An alternative predictive model for non-Newtonian solutions. *European Journal of Pharmaceutics and Biopharmaceutics*, 87(2):318–328, 2014.

[110] A.C.Y. Lam, A. Can Karaca, R.T. Tyler, and M.T. Nickerson. Pea protein isolates: Structure, extraction, and functionality. *Food Reviews International*, 34(2):126–147, 2018.

[111] J.L. Sandoval Murillo, R. Osen, S. Hiermaier, and G. Ganzenmüller. Towards understanding the mechanism of fibrous texture formation during high-moisture extrusion of meat substitutes. *Journal of Food Engineering*, 242(November 2019):8–20, 2019.

[112] X.D. Lin and W.L. Cheung. Effect of single screw extrusion through a round die on the morphology of POM/PP blends. *Journal of Materials Processing Technology*, 63(1-3):476–480, 1997.

[113] D.A. Ledward and R.F. Tester. Molecular transformations of proteinaceous foods during extrusion processing. *Trends in Food Science and Technology*, 5(4):117–120, 1994.

[114] J. Arêas. Extrusion of Food Proteins. *Critical Reviews in Food Science and Nutrition*, 32(4):365–392, 1992.

[115] A. Boire, P. Menut, M. Morel, and C. Sanchez. Phase behaviour of a wheat protein isolate. *Soft Matter*, 9(47):11417, 2013.

[116] A.B. Metzner and J.C. Reed. Flow of Non-Newtonian Fluids-Correlation of the Laminar , Transition , and Turbulent-flow Regions. *AIChE Journal*, 1(4):434–440, 1955.

[117] E. Mitsoulis. Extrudate swell of Boger fluids. *Journal of Non-Newtonian Fluid Mechanics*, 165(13-14):812–824, 2010.

[118] V.B. Tolstoguzov, A.I. Mzhel'sky, and V.Y. Gulov. Deformation of emulsion droplets in flow. *Colloid & polymer science*, 252:124–132, 1974.

[119] R. Scirocco, J. Vermant, and J. Mewis. Effect of the viscoelasticity of the suspending fluid on structure formation in suspensions. *Journal of Non-Newtonian Fluid Mechanics*, 117(2-3):183–192, 2004.

[120] R. Pasquino, F. Snijkers, N. Grizzuti, and J. Vermant. The effect of particle size and migration on the formation of flow-induced structures in viscoelastic suspensions. *Rheologica Acta*, 49(10):993–1001, 2010.

[121] S. Van Loon, J. Fransaer, C. Clasen, and J. Vermant. String formation in sheared suspensions in rheologically complex media: The essential role of shear thinning. *Journal of Rheology*, 58(1):237, 2014.

[122] I.S. Santos De Oliveira, A. Van Den Noort, J.T. Padding, W.K. Den Otter, and W.J. Briels. Alignment of particles in sheared viscoelastic fluids. *Journal of Chemical Physics*, 135(10), 2011.

[123] T. Divoux, M.A. Fardin, S. Manneville, and S. Lerouge. Shear Banding of Complex Fluids. *Annual Review of Fluid Mechanics*, 48:81–103, 2016.

[124] J. Vermant and M.J. Solomon. Flow-induced structure in colloidal suspensions, 2005.

[125] S. Caserta and S. Guido. Vorticity banding in biphasic polymer blends. *Langmuir*, 28(47): 16254–16262, 2012.

[126] M. Cromer, M.C. Villet, G.H. Fredrickson, and L.G. Leal. Shear banding in polymer solutions. *Physics of Fluids*, 25(5):1–7, 2013.

[127] S. Caserta, M. Simeone, and S. Guido. Shear banding in biphasic liquid-liquid systems. *Physical Review Letters*, 100(13):1–4, 2008.

[128] K.B. Migler. String formation in sheared polymer blends: coalescence, breakup, and finite size effects. *Physical Review Letters*, 86(6):1023–1026, 2001.

[129] E. Velichko, B. Tian, T. Nikolaeva, J. Koning, J. van Duynhoven, and W.G. Bouwman. A versatile shear cell for investigation of structure of food materials under shear. *Colloids and Surfaces A: Physicochemical and Engineering Aspects*, 566(October 2018):21–28, 2019.

[130] H. Münstedt and F.R. Schwarzl. *Deformation and flow of polymeric materials*, volume 9783642554. Springer, 2014.

Chapter 7

General discussion

7.1   Introduction

Plant-based meat analogues are being developed to provide omnivorous consumers with a more sustainable alternative to real meat. To persuade consumers, these meat analogues should accurately mimic the relevant properties of meat, such as the fibrous texture, flavour and juiciness. The water holding capacity (WHC) is associated with the juiciness of real meat and is expected to be of similar importance to the juiciness of meat analogues. Therefore, the main aim of this thesis was to understand and control the WHC of meat analogues comprising two protein phases. To achieve this, we approached the WHC as a thermodynamic property rather than an empirical value through the use of Flory–Rehner theory. First, we will briefly describe the main findings presented in this thesis. Since Flory–Rehner theory played such an important role in this thesis we will then provide a discussion of the theory and its underlying assumptions. This is followed by a reflection on our findings in a broader context, and some suggestions for future research.

7.2   Main findings

In **Chapter 2** we studied the effect of the ratio between gluten and soy protein isolate (SPI) on the WHC of two-phase gels. By first studying the WHC of single-phase gels using Flory–Rehner theory we were able to describe the WHC of the two-phase gels. Gluten was found to reduce the WHC of SPI. This was hypothesized to be the result of a mechanical pressure exerted by the continuous gluten network on the SPI phase (Figure 7.3c). This pressure can be viewed as an additional term in Flory–Rehner theory, which is added to the external pressure. When using protein isolates from pea or fababean (PPI, FPI) a similar mechanical interaction with gluten was found (**Chapter 3**). This suggests that gluten also forms a continuous network when combined with other leguminous proteins. The WHC did differ in absolute terms between gels prepared from the different proteins. However, after normalization of the WHC an apparent master curve was obtained. This underlines the similarity of the mechanical interaction with gluten. Gluten had the same negative effect on the WHC after processing in a shear cell, although the relative reduction in WHC was smaller than was found for non-sheared gels. Shear cell experiments indicated that gluten must be the main protein source ($\geq$50 %) in order to form fibres. Below this concentration, gluten may still form a continuous network, as indicated by the reduced WHC, but its strands might be too thin to be observed as fibres. The role of the non-gluten protein phase in fibre formation is unclear, although the observed

interchangeability suggests that fibre formation does not depend on the specific properties of this phase. These findings show that there is a strong link between gel structure and the WHC.

In **Chapter 4** we studied the effect of marinade composition on the WHC of meat analogues. Our experiments showed that varying the pH of the marinade offers some control over the WHC. Simulations based on Flory–Rehner theory indicated that the increase in WHC is due to an increased protein charge density. Furthermore, the pH inside the gel was found to deviate from that of the marinade. The WHC was found to be affected by the distance between the gel's internal pH and the iso-electric point (pI). Experiments and simulations also showed that the WHC is positively affected by a reduction in ionic strength. However, the simulations also suggested that the gel's internal pH approaches the pI for very low ionic strengths (<0.01 m), resulting in a reduction of the WHC. The effect of the ionic strength on the WHC appears to be based on modulating the effect of pH on the WHC. Experiments and simulations also showed that the WHC can be increased or decreased by respectively decreasing or increasing the cross-link density.

Juiciness can be regarded as a sensation with different timescales due to the temporal release of juice. In **Chapter 5**, the rate of juice release from SPI gels and meat analogues was studied during uniaxial compression using a confined compression cell and numerical simulations based on Flory–Rehner theory and Darcy flow. The dynamic release rates for swollen SPI gels were in reasonable agreement with the simulation results. However, the release rates for swollen sheared meat analogues were greatly underestimated. Furthermore, the measured release rates from the meat analogues decreased as the applied pressure increased. Time domain nuclear magnetic resonance (TD-NMR) experiments indicated the presence of internal water-filled cavities in the meat analogues. Water passing through these cavities would experience less resistance compared to when passing through the protein matrix, which could explain the higher measured release rates. TD-NMR results indicated that the internal cavities collapse upon compression. This could explain the observed reduction in release rate as the external pressure increased. The porous structure of meat analogues can facilitate juice release and could offer further tools to control the juiciness.

In **Chapter 6** we reviewed the literature on high-moisture extrusion cooking (HMEC) and shear cell processes. These thermo-mechanical structuring processes were found to be comparable in their basic unit operations. Knowledge gaps were identified concerning the effect of thermo-mechanical processing on proteins and the formation of the fibrous structure. These gaps are in part due to the limited number of

measurements at process conditions. Therefore, further study will require the use of more appropriate inline and off-line methods. Only then can sufficient understanding be acquired to control these thermo-mechanical structuring processes and their products.

7.3   Applicability   of   Flory–Rehner   theory   to protein-based networks

Flory–Rehner theory has played an important role in this thesis. However, its applicability for protein-based networks can be debated on the grounds of the theory's underlying assumptions. These assumptions are listed below and will serve to guide the discussion on the validity of these assumptions for protein-based networks, such as meat analogues.

- The polymers are Gaussian chains
- The polymer network is homogeneously cross-linked
- The polymers are neutrally charged
- Swelling is isotropic
- Deformations are purely elastic
- The different contributions to the swelling pressure are independent

The protein isolates used in our studies contain primarily globular proteins, which have a compactly folded structure. Upon heating, globular proteins can unfold due to a weakening of the inter- and intra-molecular bonds, although not all secondary structure is lost upon heating dilute solutions of soy proteins [1]. Kohn et al. [2] measured the radius of gyration of fully unfolded proteins with different chain lengths in dilute solution and found that they behave like Gaussian chains. Fitzkee and Rose [3] argued that this does not necessarily mean that all their segments behave as such. They illustrated this with the analogy of a rigid steel beam which, when made long enough, could also be considered flexible. Similarly, a protein chain with rigid segments and flexible joints could still behave as a random coil with a Gaussian length distribution when the chain is much longer than the length of a single segment. Fitzkee and Rose [3] performed Monte-Carlo simulations of such semi-rigid proteins, which resulted in the same Gaussian distribution of end-to-end distances as found by Kohn et al. [2]. This indicates that partially unfolded proteins could also behave as Gaussian

chains. Although these findings might not relate directly to concentrated protein mixtures, it could be considered plausible for proteins to behave as Gaussian chains during thermal gelation. After cross-linking, the protein polymers will have been fixed in position. When the distance between cross-links is sufficient, the chain segment in between cross-links can still be considered Gaussian. The elastic modulus, E, relates to the molecular weight between cross-links, M_c, via $E/RT = \rho_p/M_c$ [4]. For a gel with a modulus of 100 kPa, this would mean there are approximately 300 amino acids between cross-links. Eichenbaum et al. [5] suggested that a non-Gaussian model should be used below 20 monomers between cross-links. Therefore, it is plausible to consider the protein network as Gaussian.

Protein gels can either have a homogeneous 'fine-stranded' network or an inhomogeneous 'coarse' network, depending on factors such as pH and ionic strength. Li et al. [6] studied the WHC of gels made from the primarily globular whey protein. They suggested that Flory–Rehner theory applies for all fine-stranded gels, but not for coarse gels. For homogeneous polymer networks composed of linear chains, the mixing pressure is given by the des Cloizeaux scaling law as $\Pi_{mix} \propto \varphi^\beta$ [7]. The exponent β is a function of the fractal dimension d_f of the polymer network: $\beta = 1 + \frac{5d_f}{2(3-d_f)}$ [8]. For homogeneous networks of linear polymers, d_f equals 1 and thus β equals 2.25 [7]. van der Sman [9] showed that the des Cloizeaux scaling law yields a similar approximation of Π_{mix} for bio-polymers as Flory–Huggins theory. Their analysis of the mixing pressure of various food and bio-polymers, including globular whey protein, resulted in an exponent of $\beta = 2.3$ [9]. This value of β suggests a fractal dimension of approximately 1.03 and thus approximately homogeneous networks. Since Π_{mix} varies with the fractal dimension, local inhomogeneities would alter Π_{mix} locally. Coarse gels are composed of individual aggregates and thus have domains rich in either protein or water. The swelling of a coarse gel, therefore, depends on the properties of the individual aggregates and the network formed by the different aggregates. Coarse gels could be considered homogeneous at the length scale of an individual aggregate; individual aggregates could, therefore, adhere to Flory–Rehner theory. However, since observations of the WHC are made at the scale of the gel they are practically inhomogeneous and would not follow Flory–Rehner theory.

The assumption of a homogeneously cross-linked network has also been a subject of debate for non-food polymers. Vilgis et al. [8] showed that networks composed of linear polymers can be inhomogeneous due to fractal inhomogeneities. Their simulation of the random cross-linking of linear polymers resulted in a fractal dimension over 1 (1.15; [8]). When fitting Flory–Rehner theory to the WHC data

of SPI gels we also found indications that the network formed by SPI might not be homogeneous (Chapter 2). The fitted elastic properties correlated linearly with direct experimental measurements but the proportionality was not as expected. These discrepancies were attributed to network inhomogeneities that could have affected the WHC. However, the high protein fractions used in our experiments (0.25-0.40 wt/wt) make the presence of separate domains rich in either protein or water unlikely. This is in line with the TD-NMR data in Chapter 5, which indicated the presence of just two proton populations. These populations were attributed to protons closely associated with the protein and water within the swollen network. This suggests a fine-stranded network, although fast proton exchange between water populations could have obscured the presence of a possible third population [10]. A fine-stranded SPI network seems plausible, although the possibility of inhomogeneity cannot be excluded. An alternate explanation for the observed discrepancy in the elastic parameters relates to the effect of charge on the WHC.

Proteins can only be considered neutrally charged when the pH is at the iso-electric point (pI). The internal pH of a protein network approaches the pI at low ionic strengths, resulting in a deviation from the external pH (Chapter 4). When proteins do carry a net charge, the ionic pressure term must be included in Flory–Rehner theory to account for the change in WHC. In Chapter 2, the effect of charge on the WHC was assumed to be constant and negligible. Since the used swelling protocol included a washing step to remove ions, this assumption seems reasonable. However, not all ions may have been readily washed out (Chapter 4), suggesting that charge effects could have played a role in Chapter 2. The ionic pressure depends linearly on φ when the polymer charge density is greater than the ionic strength, which is a reasonable assumption when the internal pH is not at the pI. In the relevant regime of φ, the elastic pressure can also be approximated as a linear function of φ. Therefore, the fitted elastic properties may have inadvertently included the ionic pressure. The discrepancy between the fitted and experimentally determined elastic properties in Chapter 2 might, therefore, have been due to the charge effects that were not accounted for, rather than network inhomogeneities.

Charge effects can pose a threat to the assumed independence of the different contributions to the swelling pressure. Polyelectrolytes, such as proteins, can form bonds through electrostatic interactions. Vilgis and Wilder [11] argued that this voids the assumed independence of the different contributions to the swelling pressure as the elastic modulus would be composed of both covalent cross-links and electrostatic bonds. This would make the modulus dependent on the pH. The range of electrostatic

interactions is given by the Debye screening length, which reduces upon increasing the ionic strength [11]. For very high ionic strengths, electrostatics would, therefore, not affect the elastic modulus. However, this regime is of little interest for food applications as very high salt contents would render them inedible. Considering that electrostatic bonds do contribute to the elastic modulus, one could argue that the elastic modulus should remain constant as long as the ionic strength does not change. However, while the range of the interactions may be constant, the distance between polymers will vary during a swelling or de-swelling experiment. This would not only affect electrostatic interactions but also other non-covalent bonds. The distance between two polymer chains in a network scales with $\varphi^{-1/3}$. The changes in φ achieved during our experiments are, therefore, expected to have had only a minor effect on the distance between polymers and, consequently, on the elastic modulus.

Deformations as a result of swelling and de-swelling are generally assumed to be purely elastic. This means that no bonds form or break upon deformation. In Chapter 2, some gels did fracture at high external pressures, indicating the widespread breaking of bonds. This was dealt with by excluding these data points from further analysis. However, one could imagine the number of bonds to be affected by deformation without this immediately resulting in a fracture (Figure 7.1). A change in the number of bonds would affect the relationship between stress and strain. Furthermore, bonds could break and re-form in another location. This would change the undeformed length, L_0, which serves as a reference for elastic deformations and can be considered equivalent to the reference composition φ_{ref} (Figure 7.2). Both cases would lead to visco-elastic rather than purely elastic behaviour. Non-covalent bonds are expected to be more prone to breaking than covalent bonds due to their comparatively low bond strength.

Li et al. [6] studied the swelling of globular whey protein isolate (WPI) gels, which are largely stabilized by non-covalent bonds [12]. They found that non-covalent bonds continue to stabilize the gel at swelling ratios up to 40, which is higher than those achieved with SPI ($\sim$30). The quantitative agreement between their findings from experiments and simulations indicates that the cross-link density and L_0 were not affected by swelling. The actual strains and resulting stresses will depend on the polymer content at cross-linking and will, therefore, differ between studies. Li et al. [6] did find indications that the non-covalent bonds were affected when their gels were swollen in highly alkaline solutions (pH$\geq$11.5). Since our swelling experiments were performed between pH 6 and 8, it is considered reasonable to assume purely elastic behaviour.
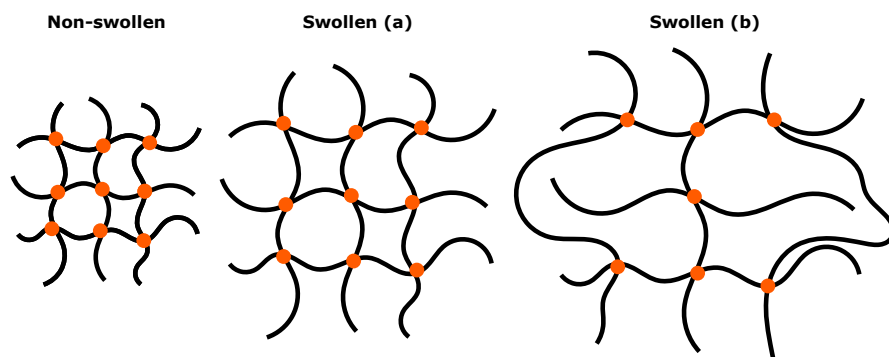
Figure 7.1: Schematic representation of a cross-linked polymer network before and after swelling. Swollen situation (a) depicts the maximum level of swelling, φ_0, when the number of cross-links is not affected by swelling. If the number of cross-links changes as a result of swelling another maximum level of swelling would be found as depicted in the swollen situation (b).

Earlier studies that applied Flory–Rehner theory to foods only considered single-phase materials. Meat analogues have multiple phases with different compositions. As shown in Chapter 2, materials with multiple phases can be described with Flory–Rehner theory by considering the different phases separately. This approach introduced the assumption that the constituents of the different phases, in this case gluten and non-gluten proteins, are present in their own respective phases and do not mix intimately. Proteins are considered thermodynamically incompatible [13]. The level of incompatibility can be expressed with their affinity for the solvent, as indicated by the Flory–Huggins interaction parameter χ. SPI, PPI, and FPI have interaction parameters that differ from that of gluten (Chapter 2), which would support the notion that they form separate phases. Furthermore, a study on solutions of the soy protein glycinin and wheat gluten found that these proteins do not cross-link upon heating [14], further supporting the notion of incompatibility. Although it is likely for some mixing to have taken place, the assumption of two immiscible phases is deemed a reasonable approximation.

Meat analogues also contain an air phase in the form of internal cavities. These cavities can be filled with water during marinating (Chapter 5) and can, therefore, also contribute to the WHC. Since the cavities lack a polymer network, they cannot be described with Flory–Rhener theory. In our studies on gels, any air was removed prior to gelation to ensure there were no air cavities in the final gel. For meat analogues,
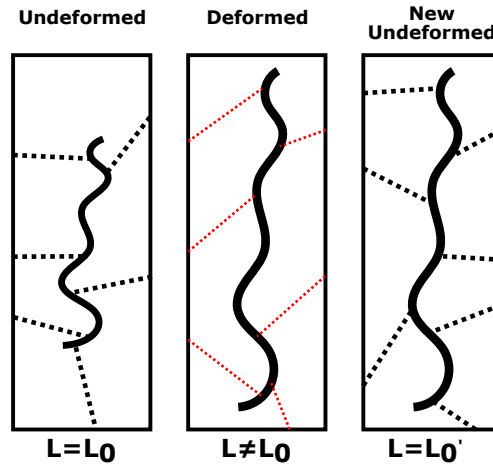
Figure 7.2: Schematic representation of how breaking and reforming of bonds upon swelling could alter the undeformed state. Bonds are depicted as dashed lines in either black or red to indicate the stressed and non-stressed situation respectively.

however, the air is an important part of the material and might even contribute to its fibrous structure [15, 16]. Future studies on the WHC of meat analogues should further explore the role of cavities. Internal cavities may deform with the matrix under external pressure, but could also collapse through creasing or buckling [17]. The capillary pressure might also be relevant for cavities that protrude through the surface of the meat analogue. Modeling such phenomena would require more sophisticated modeling approaches that can deal with these complex geometries, such as finite-element methods in 2 or even 3 dimensions.

The assumption of isotropic swelling is accurate for freely swollen homogeneous networks. In line with several recent studies [9, 18, 19], isotropic deformation was also assumed during de-swelling via centrifugation (Chapter 2). However, this may not be the most accurate approximation of the deformation as the external pressure is applied from a single direction during centrifugation, which could have led to aniostropic deformation. In Chapter 5, network deformations in the different directions were considered separately to get a better approximation of the elastic pressure during uniaxial compression. Such an approach would yield more accurate approximations for centrifugation experiments. As new insights are obtained, so too must models continuously evolve to ensure their usefulness.

Most of the underlying assumptions of Flory–Rehner theory were found to be plausible for protein-based networks, although the origin of the discrepancy between the fitted and measured elastic properties of soy was not confirmed. The amount of physical meaning that can be attributed to the fitted parameters is, therefore, limited. Nevertheless, the concept of Flory–Rehner theory is considered a meaningful approximation of the WHC of protein-based networks like meat analogues. As such, Flory–Rehner theory is useful to obtain qualitative insight into underlying mechanisms. This thought is strengthened by the fact that we were able to control the WHC of protein-based gels and meat analogues based on the tools suggested by Flory–Rehner theory. These tools are the polymer-water affinity, the cross-link density, and the charge density.

7.4 The effect of cooking on the water holding capacity and juiciness

Cooking whole-cut meats, such as steak, results in heat-induced denaturation of the meat proteins [20–22]. The denaturation of meat proteins reduces their affinity for water, as indicated by an increase of the interaction parameter, χ [4, 23]. The increase of χ causes the magnitude of the mixing pressure to decrease and triggers a reduction in the WHC. But while the WHC may be reduced, the excess water is not immediately expelled during cooking due to the limited permeability of meat [23]. The water content can, therefore, exceed the WHC of the meat. van der Sman [23] simulated the moisture transport in a beef roast during cooking using Flory–Rehner theory. They reported that the early onset of protein denaturation in the outer regions of the meat resulted in an inward pressure gradient. This caused some of the meat juices to migrate inwards. Searing meat can result in the formation of a crust and is commonly thought to limit cook losses and result in a juicier product. However, despite popular belief, searing a steak to 'seal the juices in' does not have a significant effect on juiciness or cooking losses [24, 25]. Meat has so-called drip channels which, based on our findings for meat analogues (Chapter 5), could facilitate moisture transport and thereby circumvent the relatively dry crust. Still, the thought of sealing the juices in does have some merit as the water content of the interior of a cooked steak will exceed its WHC due to the inward migration of water. When biting into such a steak, the applied pressure further lowers the WHC. As the meat is chewed its structure breaks down. This jointly results in the sudden release of juice and the experience of juiciness. The amount of juice available for release is thus set by the excess in moisture and the

pressure applied during chewing.

The production of meat analogues generally involves processing at high temperatures through a thermo-mechanical process. This will render the proteins fully denatured in the uncooked product. Moreover, industrial protein isolates may already be partially or fully denatured due to the intensive processes used during ingredient manufacturing. We experimentally confirmed that the commercial SPI used in this thesis was already denatured, as indicated by the lack of change in the interaction parameter χ upon gelation at 95°C (Chapter 2). Since the proteins are already denatured, no large change in WHC is to be expected during the final preparation by the consumer. The high temperature during cooking might weaken non-covalent bonds, which could actually increase the WHC due to a reduction in cross-link density. This is in line with a recent study on vegan pet food, which showed that thermal sterilization of canned meat analogues in a liquid medium can result in an increase in moisture content of up to 60% [26]. Therefore, unlike meat, the water content of a meat analogue product will not drastically exceed its WHC upon cooking. The amount of juice available for release will, therefore, primarily be the result of the pressure applied during chewing. Although the amount of juice available for release could be lower than in real meat, that does not necessarily mean that the sensation of juiciness will be less pronounced. Cavities could enhance the juice release rate, while flavour compounds could induce salivation to compensate for the lack of juice.

7.5 Post-processing with a marinade

Marinades can be used to change the WHC of meat analogues without affecting the water content during thermo-mechanical structuring. This would decouple the water content of the final product from the structuring process and allow for water contents beyond the window of operation of the structuring process. A marinade generally contains flavour compounds, salt ions, water and, in some cases, oil or fat. Our experimental and simulation results both indicated that the WHC of meat analogues can be improved by increasing the charge density inside the product while maintaining a low charge density in the marinade (Chapter 4). The effect of pH on the WHC, therefore, strongly depends on the amino acid composition of the protein, which determines the concentration and properties of the ionizable groups. The total concentration of ionizable groups and the ratio between positively and negatively charged amino acids will determine the highest attainable charge density. To maximize the marinade uptake by the product, the net charge should be highest

at the pH of the final product. The effect of pH on the WHC could be controlled by adjusting the amino acid composition of the swelling protein network. Direct control over the amino acid composition may not be possible without using genetic engineering or selective breeding. However, tailored ingredients could still be made by carefully adjusting the extraction and precipitation pH during protein isolate production [27]. The development and production of such ingredients would require intimate collaboration between ingredient manufacturers and food producers.

7.6   Juiciness: a structure-function relationship

Our findings show that control over the WHC and water release properties of meat analogues will require control over their structure. The fibrous, meat-like structures used in our studies were prepared through a thermo-mechanical treatment in a shear cell. We found that the shear cell process is in many ways comparable with that of the more commonly used high moisture extrusion cooking (HMEC; Chapter 6). This suggests that the insights presented in this thesis might also be applicable to meat analogues produced with HMEC. However, the thermo-mechanical processing of proteins remains poorly understood as many of the questions raised almost 30 years ago still have not been answered satisfactorily today [28]. In particular, the effect of thermo-mechanical treatment on proteins and protein aggregation is unclear. Samples are most often analysed *after* rather than *during* thermo-mechanical processing, which may have obscured the relation between cause and effect regarding protein aggregation. This may hinder further elucidation of the mechanism behind structure formation.

The formation of the fibrous structure is thought to depend on the deformation of the different phases in flow (Figure 7.3b). The rheological properties of the hot melt are generally considered important for the formation of fibrous structures. Since rheological properties depend on water content, the water partitioning between the different protein phases should be well understood. In Chapters 2 and 3 we applied Flory–Rehner theory to describe the partitioning of water between different proteins at ambient temperature (Figure 7.3a). This approach should work equally well at higher temperatures when accounting for possible changes in polymer–water affinity due to denaturation, and changes in cross-link density. Since Flory–Rehner theory requires only a few parameters to describe the water partitioning, it could offer a simple and fast way of approximating water partitioning compared to the more common and experimentally intensive approaches that rely on rheometric or NMR methods
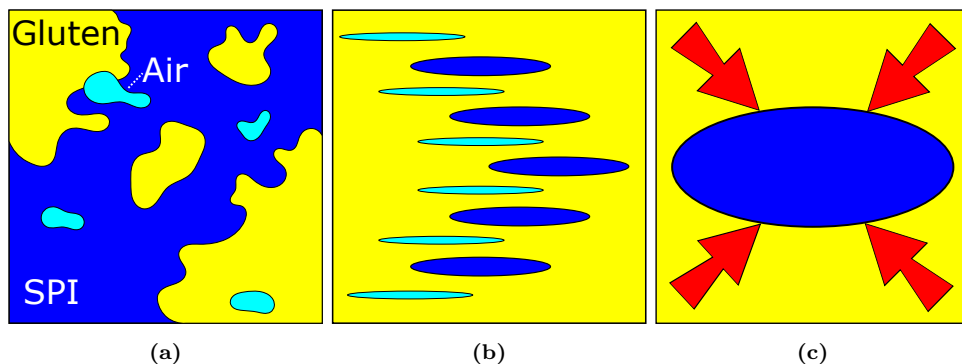
Figure 7.3: A schematic representation of a hydrated mixture of soy protein isolate (SPI) and gluten with air inclusions before shear structuring (7.3a), the mechanism proposed by Tolstoguzov [31] for structure formation based on deformation and alignment of the different phases (7.3b), and the mechanical interaction by which gluten can limit the WHC of another protein (7.3c).

[29, 30]. Air cavities might also contribute to the fibrous appearance and mechanical anisotropy of meat analogues [15, 16]. The deformation of the air phase can be controlled by varying the shear rate. Since the air cavities can improve the water release rate, the shear rate might not only affect the fibrousness but also the juiciness of meat analogues (Chapter 5).

We found that gluten content should be $\geq 50\%$ to create a fibrous structure with gluten-based formulations (Chapter 3). The WHC of the product is greatly reduced at these high gluten concentrations due to the mechanical interaction between gluten and non-gluten proteins (Chapter 2). However, this is not necessarily a bad thing for the final product properties. For example, fully swollen SPI gels are brittle and do not resemble a meat-like product, despite their high WHC. When gluten contributes $\geq 50\%$ to the total protein content, the material gets a more meat-like texture by going from a brittle to a more tough texture. After processing in a shear cell, these materials strongly resemble the fibres found in meat. Clearly, one cannot simply maximize the WHC to produce the 'most juicy' product. Since the WHC is directly related to the meat analogue's structure, an optimum must be found by balancing the different relevant attributes, including juiciness, fibrousness, and toughness, while also taking into account factors such as flavour, smell and appearance. Analytical methods should be used to objectively quantify these parameters, although they will need to be compared and correlated with sensory evaluations to confirm their validity.

Correlating objective measures with sensory data is a great challenge and should be included in future studies. A wider research scope and interdisciplinary approach will be required to understand the relative importance of the different contributors to the sensation of juiciness.

7.7　Suggestions for the production of a juicy meat analogue

Product development would greatly benefit from having an established relationship between a sensory attribute and a product property as it would limit the need for sensory panels. However, the importance of the WHC to the sensory perception of juiciness is yet to be confirmed. Despite this lack of confirmation, we can still make some suggestions on how to formulate and produce a juicy meat analogue product by assuming the relationship is there. As discussed in Section 7.4, the WHC of a meat analogue is not expected to change during final preparation. Consequently, the juiciness of an uncooked meat analogue product should mirror that of a cooked piece of meat, or even exceed it when considering cooking losses.

The hypothetical product that we will discuss is produced in a shear cell and is composed of water and two proteins, one of which is gluten. Gluten should make up at least 50 % of the total dry matter content to ensure the final product has a fibrous structure. The choice of the second protein has large implications for the final WHC of the product; by selecting a high swelling protein (e.g. soy) a higher final WHC will be reached compared to when a low swelling protein (e.g. fababean) is used. The water content during processing should be maximized as a high water content will result in a high WHC. However, the water content must stay within that specific ingredient's window of operation to ensure a firm and fibrous product. The shear rate and temperature during the shearing process offer control over the degree of deformation of the internal cavities [16, 32]. Long, elongated cavities are expected to improve the juice release rate. The channels could be parallel to the direction in which the consumer would bite into the product to keep them from collapsing. However, since the food might rotate during chewing, randomly oriented cavities might be more successful at preventing total collapse. Furthermore, chewing will break down the structure, which could limit the period during which the cavities can have a noticeable effect. The product could be frozen after shear structuring as this might enhance the fibrous texture [33]. Ice crystal growth could also enhance the formation of channels by compressing the surrounding protein matrix. After

thawing, the product is submerged in a marinade. The marinade should have a pH far from the iso-electric point of the non-gluten protein. Since proteins have a high buffering capacity, the amount of marinade should be high or the marinade itself should be pH-buffered to ensure a constant pH. A marinade with a low ionic strength is desirable for high marinade uptake. The marinade could contain proteolytic enzymes to increase the WHC by reducing the cross-link density. The marinade should also contain flavour compounds that provide taste and induce salivation to enhance the sensation of juiciness. Additional ingredients such as fats could further enhance the juiciness. The marinade could be introduced through tumbling, soaking, or via injection. We note that the relation between the WHC and juiciness is probably not linear and will have an optimum. However, due to the interconnectedness of the WHC with the meat analogue structure, a trade-off must be made between the juiciness and product properties such as fibrousness and toughness. Therefore, lower juiciness than physically possible may be desired when considering the product as a whole.

7.8 Suggestions for future research

We have identified several tools to control the WHC and water release of meat analogues in an effort to improve their juiciness. However, the importance of the WHC to the juiciness still needs to be validated through sensory evaluation. The juiciness of meat analogues is not expected to solely depend on the WHC; factors such as flavour, fat, and texture will also contribute to the sensation. Understanding the relative importance of the different contributions to the juiciness would allow for more targeted research. However, the high interconnectedness between the different contributors could limit the amount of direct insight that can be obtained from sensory evaluations. Differentiating between the different contributors will require a very methodical approach and a high level of control over product properties. Such control can only be obtained through a better understanding of the thermo-mechanical production process and the relation between ingredient and product properties. This ingredient–process–product triangle could be better understood through process simulations with physical models. We expect Flory–Rehner theory to play an important role here. Flory–Rehner theory could be applied to describe the water partitioning between protein phases during thermo-mechanical processing, although the effect of processing on the elastic properties should first be better understood. We do note that for such uses the quantitative outcome of the simulations will be of great importance to the validity of the simulation results. The assumptions underlying Flory–Rehner theory should, therefore, first be validated before undertaking such

(semi-)quantitative simulations. For example, network homogeneity could be studied by using small angle neutron scattering methods [34, 35]. The importance of charge effects should be explored systematically to get better approximations of the ionic pressure, and to determine whether the modulus is affected by the pH.

The effect of mechanical interaction between two protein phases and the WHC could also be investigated further. Through the use of so-called cavitation rheology, the gluten pressure could be measured directly [36, 37]. In cavitation rheology, a needle is inserted into a soft material and pressure is applied through the needle, for example by pumping in water. By monitoring the amount of water that can be pumped into the gluten at a certain pressure, the gluten pressure itself could be determined. This would provide direct validation of our findings from Chapter 2 and 3.

7.9   Concluding remarks

We set out to improve our understanding of the juiciness of meat analogues by studying their WHC. The use of Flory–Rehner theory enabled us to understand some of the complexity of the WHC of these multi-phase materials. Although the relation between the WHC and juiciness is yet to be confirmed, we found that the WHC has much wider implications than just juiciness. Structure formation and WHC both appear to depend on the formation of a continuous gluten network. The structure of meat analogues, therefore, has a large influence on the WHC of the product. Despite the complexity, we also found signs of universal behaviour in both swelling and structuring behaviour. This suggests that food structures might be independent of their molecular building blocks.

References

[1] K.S. Kim, S. Kim, H.J. Yang, and D.Y. Kwon. Changes of glycinin conformation due to pH, heat and salt determined by differential scanning calorimetry and circular dichroism. *International Journal of Food Science and Technology*, 39(4):385–393, 2004.

[2] J.E. Kohn, I. Millett, J. Jacob, B. Zagrovic, T. Dillon, N. Cingel, R. Dothager, S. Seigert, P. Thiyagarajan, T. Sosnick, M. Hasan, V. Pande, I. Ruczinski, S. Doniach, and K. Plaxco. Random-coil behavior and the dimensions of chemically unfolded proteins. *Proc. Natl. Acad. Sci. USA*, 101(34):12491–12496, 2004.

[3] N.C. Fitzkee and G.D. Rose. Reassessing random-coil statistics in unfolded proteins. *Proceedings of the National Academy of Sciences*, 101(34):12497–12502, 2004.

[4] R.G.M. van der Sman. Thermodynamics of meat proteins. *Food Hydrocolloids*, 27(2):529–535, 2012.

[5] G.M. Eichenbaum, P.F. Kiser, A.V. Dobrynin, S.A. Simon, and D. Needham. Investigation of the swelling response and loading of ionic microgels with drugs and proteins: the dependence on cross-link density. *Macromolecules*, 32(15):4867–4878, 1999.

[6] H. Li, L. Zhao, X.D. Chen, and R. Mercadé-Prieto. Swelling of whey and egg white protein hydrogels with stranded and particulate microstructures. *International Journal of Biological Macromolecules*, 83:152–159, 2016.

[7] J. Des Cloizeaux. The Lagrangian theory of polymer solutions at intermediate concentrations. *Journal de Physique*, 36(4):281–291, 1975.

[8] T.A. Vilgis, J.U. Sommer, and G. Heinrich. Swelling and fractal heterogeneities in networks. *Macromolecular Symposia*, 93(1):205–212, 1995.

[9] R.G.M. van der Sman. Biopolymer gel swelling analysed with scaling laws and Flory-Rehner theory. *Food Hydrocolloids*, 48:94–101, 2015.

[10] F. Mariette. Investigations of food colloids by NMR and MRI. *Current Opinion in Colloid and Interface Science*, 14(3):203–211, 2009.

[11] T. Vilgis and J. Wilder. Polyelectrolyte networks: elasticity, swelling, and the violation of the Flory-Rehner Hypothesis. *Computational and Theoretical Polymer Science*, 8(1):61–73, 1998.

[12] P. Havea, A.J. Carr, and L.K. Creamer. The roles of disulphide and non-covalent bonding in the functional properties of heat-induced whey protein gels. *Journal of Dairy Research*, 71(3): 330–339, 2004. doi: 10.1017/S002202990400024X.

[13] V.I. Polyakov, V.Y. Grinberg, and V.B. Tolstoguzov. Thermodynamic incompatibility of proteins. *Food Hydrocolloids*, 11(2):171–180, 1997.

[14] M.A. Lambrecht, I. Rombouts, and J.A. Delcour. Denaturation and covalent network formation of wheat gluten, globular proteins and mixtures thereof in aqueous ethanol and water. *Food Hydrocolloids*, 57:122–131, 2016.

[15] Z. Wang, B. Tian, A.J. van der Goot, and R. Boom. Air bubbles in calcium caseinate fibrous material enhances anisotropy. *Food Hydrocolloids*, 87:497–505, 2018.

[16] B.L. Dekkers, R. Hamoen, R.M. Boom, and A.J. van der Goot. Understanding fiber formation in a concentrated soy protein isolate - Pectin blend. *Journal of Food Engineering*, 222:84–92,

2018.

[17] S. Cai, K. Bertoldi, H. Wang, and Z. Suo. Osmotic collapse of a void in an elastomer: breathing, buckling and creasing. *Soft Matter*, 6(22):5770, 2010.

[18] R. van der Sman, E. Paudel, A. Voda, and S. Khalloufi. Hydration properties of vegetable foods explained by Flory–Rehner theory. *Food Research International*, 54(1):804–811, nov 2013.

[19] E. Paudel, R.M. Boom, and R.G.M. van der Sman. Change in Water-Holding Capacity in Mushroom with Temperature Analyzed by Flory-Rehner Theory. *Food and Bioprocess Technology*, 8(5):960–970, 2015.

[20] L. Christensen, H. Bertram, M. Aaslyng, and M. Christensen. Protein denaturation and water-protein interactions as affected by low temperature long time treatment of porcine Longissimus dorsi. *Meat Science*, 88(4):718–722, 2011.

[21] N. Ishiwatari, M. Fukuoka, and N. Sakai. Effect of protein denaturation degree on texture and water state of cooked meat. *Journal of Food Engineering*, 117(3):361–369, 2013.

[22] B.I. Zielbauer, J. Franz, B. Viezens, and T.A. Vilgis. Physical Aspects of Meat Cooking: Time Dependent Thermal Protein Denaturation and Water Loss. *Food Biophysics*, 11(1):34–42, 2016.

[23] R.G.M. van der Sman. Moisture transport during cooking of meat: An analysis based on Flory-Rehner theory. *Meat Science*, 76(4):730–738, 2007.

[24] C. Broz and N. Barber. The meat searing process: Is sealing in juices fact or fiction? *Journal of Culinary Science and Technology*, 9(2):99–105, 2011.

[25] J. Yoo, J. Kim, H. Yong, K. Baek, H. Lee, and C. Jo. Effects of searing cooking on sensory and physicochemical properties of beef steak. *Food Science of Animal Resources*, 40(1):44–54, 2020.

[26] A.M. Wehrmaker, G. Bosch, and A.J. van der Goot. Effect of sterilization and storage on a model meat analogue pet food. *Animal Feed Science and Technology*, In press:114737, 2020.

[27] B. Kuipers, G. van Koningsveld, A. Alting, F. Driehuis, A. Voragen, and H. Gruppen. Opposite contributions of glycinin- and β-conglycinin-derived peptides to the aggregation behavior of soy protein isolate hydrolysates. *Food Biophysics*, 1(4):178–188, 2006.

[28] J. Arêas. Extrusion of Food Proteins. *Critical Reviews in Food Science and Nutrition*, 32(4): 365–392, 1992.

[29] B.L. Dekkers, D.W. de Kort, K.J. Grabowska, B. Tian, H. Van As, and A.J. van der Goot. A combined rheology and time domain NMR approach for determining water distributions in protein blends. *Food Hydrocolloids*, 60:525–532, 2016.

[30] F. Schreuders, I. Bodnár, P. Erni, R. Boom, and A. van der Goot. Water redistribution determined by time domain NMR explains rheological properties of dense fibrous protein blends at high temperature. *Food Hydrocolloids*, 101, 2020.

[31] V.B. Tolstoguzov. Thermoplastic extrusion—the mechanism of the formation of extrudate structure and properties. *Journal of the American Oil Chemists' Society*, 70(4):417–424, apr 1993.

[32] F.K.G. Schreuders, B.L. Dekkers, I. Bodnár, P. Erni, R.M. Boom, and A.J. van der Goot. Comparing structuring potential of pea and soy protein with gluten for meat analogue preparation. *Journal of Food Engineering*, 261(May):32–39, 2019.

[33] D. Fukushima. Soy proteins for foods centering around soy sauce and tofu. *Journal of the*

American Oil Chemists' Society, 58(3):346–354, 1981.

[34] D. Renard, M.A. Axelos, F. Boue, and J. Lefebvre. Small angle neutron scattering and viscoelasticity study of the colloidal structure of aqueous solutions and gels of a globular protein. *Journal de Chimie Physique et de Physico-Chimie Biologique*, 93(5):998–1015, 1996.

[35] E. Gilbert. Small-angle X-Ray and neutron scattering in food colloids. *Current Opinion in Colloid and Interface Science*, 42:55–72, 2019.

[36] J. Zhu, T. Li, S. Cai, and Z. Suo. Snap-through expansion of a gas bubble in an elastomer. *Journal of Adhesion*, 87(5):466–481, 2011.

[37] J. Zimberlin, N. Sanabria-Delong, G. Tew, and A. Crosby. Cavitation rheology for soft materials. *Soft Matter*, 3(6):763–767, 2007.

About the author

Steven Cornet was born on December 1st 1992 in Houten, The Netherlands. He attended high school at College de Heemlanden with a major in Nature and Health.

In 2011, Steven enrolled in the BSc program Biotechnology at Wageningen University, with a minor in Food Science. For his BSc thesis, Steven studied the properties of lupin proteins at the Food Process Engineering department. He continued his studies in Food Science at Wageningen University, specialising in Ingredient Functionality. His MSc thesis was on the structure formation in oleic acid–sodium oleate oleogels. This project was a collaboration between the department of Food Physics and the Australian Nuclear Science and Technology Organization (ANSTO). He visited ANSTO in 2015 to use their small angle scattering instruments, and again in 2018. After completing his MSc thesis, Steven did an internship at the Fraunhofer Institute for Process Engineering and Packaging (IVV) in Freising, Germany. While there, he worked on the fractionation of plant proteins.

After completing his MSc degree, Steven continued his studies as a PhD candidate in the project Plant Meat Matters. This project is a collaboration between Wageningen Food and Biobased Research, the department of Food Process Engineering and several industrial partners.

List of publications

This dissertation

S.H.V. Cornet, A.J. van der Goot, R.G.M. van der Sman (2020). Effect of mechanical interaction on the hydration of mixed soy protein and gluten gels. *Current Research in Food Science, 3,* 134-145.

S.H.V. Cornet, S.J.E Snel, J. Lesschen, A.J. van der Goot, R.G.M. van der Sman (2021). Enhancing the water holding capacity of model meat analogues through marinade composition. *Journal of Food Engineering, 290,* 1-9

S.H.V. Cornet, D. Edwards, A.J. van der Goot, R.G.M. van der Sman (2020). Water release kinetics from soy protein gels and meat analogues as studied with confined compression. *Innovative Food Science and Emerging Technologies, 66,* 1-11.

S.H.V. Cornet, J.M. Bühler, R. Goncalves, M. Bruins, R.G.M. van der Sman, A.J. van der Goot (Under review). Apparent universality in swelling and fibre formation by mixtures of gluten and leguminous proteins.

S.H.V. Cornet, S.J.E. Snel, F.K.G Schreuders, R.G.M. van der Sman, M. Beyrer, A.J. van der Goot (2020). Thermo-mechanical processing of plant proteins using shear cell and high-moisture extrusion cooking, Critical Reviews in Food Science and Technology, ahead of print, 1-18.

Other scientific publications

R.G.M. van der Sman, S. Houlder, **S.H.V. Cornet**, A. Janssen, (2020). Physical chemistry of gastric digestion of proteins gels. *Current Research in Food Science, 2,* 45-60.

Overview of completed training activities

Discipline specific activities
Courses
Modeling and Simulation in Food and Bio-Processing, Seiano, Italy (2017)
Physical Chemistry Han-sur-Less, Han-sur-Less, Belgium, (2018)
Food Proteins, Wageningen, The Netherlands (2018)
Physical Chemistry Han-sur-Less, Han-sur-Less, Belgium, (2019)
Rheology school, Leuven, Belgium (2019)

Conferences
Food Colloids, Leeds, UK (2018)*
Food Structure and Functionality Forum, Montreal, Canada (2018)*
Science and technology for meat analogues, Wageningen, The Netherlands, (2018)*
Neutrons and Food, Sydney, Australia (2018)*
International Congress on Engineering and Food, Melbourne, Australia (2019)*
Effost conference, Rotterdam, The Netherlands (2019)*

General courses
VLAG PhD Week, Baarlo, The Netherlands (2017)
Workshop Carousel, Wageningen, The Netherlands (2018)
Getting things done, Wageningen, The Netherlands (2018)
Introduction to *R*, Wageningen, The Netherlands (2019)
Applied Statistics, Wageningen, The Netherlands (2019)
Scientific Writing, Wageningen, The Netherlands (2019)
Agile Project Management, University of Maryland, online via EDX (2020)

Optional activities
Preparation of research proposal
PhD trip to Canada*
Weekly group meetings at Food Process Engineering
Biweekly journal club on Food Structuring
Organizing committee of the Young EFFoST Day 2019

---

*Oral and/or poster presentation